THE ROLE OF ER STRESS IN THE PATHOGENESIS OF KENNEDY'S DISEASE

KARLI MONTAGUE

WELLCOME TRUST 4-YEAR NEUROSCIENCE PHD

2011

Acknowledgments

I wish to express my gratitude to my supervisors, Prof. Linda Greensmith and Dr Gyuri Szabadkai who offered me invaluable assistance, support and guidance throughout my PhD. I would also like to express my gratitude to members of the Greensmith Laboratory, particularly Dr Bilal Malik and Mr James Dick for all of their advice and patience over the last three years.

I would also like to thank my mother Jacqueline, my brother Joel and my partner Sean for their love and support throughout my studies.

The experiments in this Thesis were funded by the MRC

This Thesis is dedicated to my beloved Father, Grandfather and Grandmother, who probably wouldn't have read this, but would have been extremely proud anyway!

Abstract

The fundamental function of the Endoplasmic Reticulum (ER) is to process nascent membrane and secretory proteins in a calcium-dependent manner. Disruption of ER function by the depletion of ER calcium results in ER stress, which triggers apoptosis if prolonged. ER stress has been shown to play a role in the pathogenesis of Motor Neuron Diseases (MNDs) and CAG-repeat disorders. Kennedy's Disease (KD) is an X-linked neurodegenerative disease that is classified as both a MND and CAG-repeat disorder. In this Thesis I investigate whether ER Stress also plays a role in the pathogenesis of KD.

Using a mouse model of KD, primary motoneuron cultures from both KD and wild-type (WT) embryos were established. Confocal microscopy was used to infer ER calcium levels, and markers of ER stress and ER stress-induced apoptosis were examined using western blot analysis and immunocytochemistry.

KD motoneurons were found to have reduced levels of ER calcium and elevated levels of markers of ER stress and ER stress-induced apoptosis relative to WT controls. ER stress-induced apoptosis appears to contribute to the motoneuron death observed in KD mice, since inhibition of ER stress with Salubrinal increases ER Ca^{2+}, decreases ER stress-induced apoptosis and consequentially improves KD motoneuron survival.

Examination of markers of ER stress in the spinal cord of KD mice revealed higher expression levels compared to WT controls, with the most significant increase detected between E13 and 3 months of age i.e. pre-symptomatically. Mitochondrial dysfunction and impaired mitochondrial biogenesis was also observed in KD motoneurons. However, increasing mitochondrial biogenesis was not as effective as inhibition of ER stress in improving KD motoneuron viability.

These results show that ER stress may play an early, causal role in the pathogenesis of KD and suggest that inhibition of ER stress may be a potential therapeutic strategy for the treatment of KD.

THE ROLE OF ER STRESS IN THE PATHOGENESIS OF KENNEDY'S DISEASE

Abbreviations

ALS = Amyotrophic Lateral Sclerosis

APP = Amyloid Precursor Protein

AR = Androgen Receptor

ATF4 = Activating Transcription Factor

BDNF = Brain-Derived Neurotrophic Factor

BiP = Binding Immunoglobulin Protein

BSA = Bovine Serum Albumin

CaMK = Calmodulin-Dependent Kinase

CaN = Calcineurin

CHOP = CCAAT/enhancer-binding protein homologous protein

CK = Creatine Kinase

CNB= Complete Neurobasal Medium

CNTF= Ciliary Neurotrophic Factor

CREB = cAMP responsive element binding protein

DAPI = 4',6-diamidino-2-phenylindole

DBD = DNA-Binding Domain

DHT = Dihydrotestosterone

DIV = Days in Vitro

DLN = Dorsolateral Nucleus

eIF2a = Eukaryotic Initiating Factor 2 a

ERAD = ER-associated degradation

ETC = Electron Transport Chain

FCCP = carbonyl cyanide-trifluoromethoxyphenyl hydrazone

GDNF= Glial cell line-derived Neurotrophic Factor

GRP = Glucose-Regulated Protein

HD = Huntington's Disease

HRE = Hormone Response Element

HSP = Heat Shock Protein

IRE1 = Inositol Requiring Enzyme 1

JNK3 = c-Jun N-terminal protein kinase 3

KD = Kennedy's Disease

LBD = Ligand-Binding Domain

LMP2/7 = Low Molecular Mass Polypeptide 2/7

MAPK = Mitogen Activated Protein Kinase

MND = Motor Neuron Disease

NI = Nuclear Inclusion

NTD = Amino (N) – Terminal Domain

PERK = Pancreatic ER Kinase–like Kinase

PGC1a = Peroxisome Proliferator-activated receptor Co-activator-1a

PLC = Phospholipase C

SAL = Salubriunal

SERCA= Sarco/Endoplasmic Reticulum ATPase

SIRT1 = Silent Mating Type Information Regulation 2 Homolog 1

SOC = Store-operated Calcium Influx

SOD1= Superoxide Dismutase 1

SODH = Mice overexpressing the WT human SOD1 protein

STIM = Stromal Interacting Molecule 1

T= Testosterone

TG = Thapsigargin

TM = Tunicamycin

TMRM = Tetramethylrhodamine methylester

TRAF2 = TNF receptor-associated factor 2

UPR = Unfolded Protein Response

WT = Wild-Type

XBP1 = X box-binding protein 1

YAC = Yeast Artificial Chromosome

List of Figures

CHAPTER 1: INTRODUCTION

1.1. Kennedy's disease

1.1.1 Introduction

Kennedy's Disease (KD), otherwise known as Spinal and Bulbar Muscular Atrophy (SBMA), is an adult onset, X-linked neurodegenerative disease that can be classified as both a Motor Neuron Disease (MND) and Polyglutamine (CAG-repeat) disorder (Gallo 2001). The prevalence of KD varies in different parts of the world. In regions of Italy for example, the prevalence of KD is 3.3 in 100,000 (Guidetti et al, 2001), which is lower than the prevalence of other inherited MNDs such as Amyotrophic Lateral Sclerosis (ALS). In regions of Finland however, the prevalence of KD is 13 in 85,000, which exceeds that of ALS (Udd et al, 1998).

1.1.2 History

Although Kennedy's Disease was first described by William R Kennedy in 1968 following a study of 11 patients from two families (Kennedy, 1968), the precise genetic defect underlying the disease was not identified for another 23 years. The initial suggestion that the underlying cause of KD was genetic came in 1982 (Fischbeck, et al, 1982), however it wasn't until nine years later, in 1991, that a CAG-repeat expansion in the Androgen Receptor (AR) gene was identified as the genetic trigger (La Spada et al, 1991). Advances in our understanding of KD pathogenesis progressed quite rapidly following the discovery of the AR mutation. Within a year, a correlation between the CAG repeat number and the severity and onset of symptoms had been identified (Igarashi et al, 1992) and within three years, the first mouse model of Kennedy's Disease had been developed, which has been a critical tool in identifying cellular processes that are impaired in the disease (Bingham et al, 1995).

1.1.3 Etiology & Genetics of Kennedy's Disease

Kennedy's Disease is thus caused by a Polyglutamine (CAG-repeat) expansion in exon 1 of the AR gene on chromosome Xq-11-12 (La Spada et al, 1991). Repeat numbers of

greater than 40 result in disease manifestation, although there is some variation between individuals (Sinclair et al, 2007). Various aspects of the disease are modulated by the CAG-repeat number. It is generally accepted that the greater the number of CAG-repeats, the earlier the onset of disease symptoms (Katsuno et al, 2008). It has also been suggested that a higher repeat number increases the likelihood of future generations possessing a greater number of CAG-repeats (Katsuno et al, 2008). Dominant symptom type and symptom severity also appear to be dependent on the CAG repeat number (Suzuki et al, 2008). Motor-related symptoms for example, appear to be more severe in individuals possessing a higher repeat number, whereas sensory symptoms are thought to be more pronounced in patients with a lower number of CAG-repeats (Suzuki et al, 2008).

At a protein level, the CAG-repeat is located in the N-terminal of the AR (Chamberlain et al, 1994). In normal individuals, the repeat number ranges between 9 and 36 (Sulek et al, 2005). A repeat number of greater than 40 however, results in a gain-of-function, mis-folded protein toxicity, accompanied by loss of normal protein function (Palazzolo et al, 2008).

1.1.4 Histopathology

1.1.4.1 Neuronal histopathology

A fundamental feature of KD is the loss of spinal and bulbar motoneurons, particularly those originating from the anterior horn of the spinal cord and the brainstem nuclei (Sobue et al, 1989). Cranial nerves III (Oculomotor), IV (Trochlear) and VI (Abducens), which innervate extraocular muscles (Chilton and Guthrie, 2004) however, appear to remain unaffected in the disease (Sobue et al, 1989). An important feature of KD is that upper motoneurons appear to remain unaffected, although this suggestion has recently been challenged following electrophysiological studies of KD patients, which

suggest sub-clinical involvement of upper motoneruons (Pachatz et al, 2007, Eisen, 2007).

At a cellular level, a hallmark of all CAG-repeat diseases is the presence of mutant protein Nuclear Inclusions (Yamada et al, 2000). KD is no exception to this, with Nuclear Inclusions (NIs) containing the mutant AR present in residual brainstem and anterior horn motoneurons (Figure 1.1) and testes of KD patients (Suzuki et al, 2007, Adachi et al, 2007). Structural information about the NIs found in KD tissue has come from the use of antibodies that are targeted to specific areas of the AR. When the antibodies used are targeted to the N-terminal of the AR as well as the CAG-repeat region specifically, NI staining is positive (Tahiri et al, 2001). However, when antibodies are targeted to the C-terminal of the AR, the NIs are no longer detectable (Tahiri et al, 2001). This indicates that the formation of NIs either leads to the truncation of the C-terminal or physically conceals it, which suggests that the normal ligand-binding function of the AR C-terminal (discussed in Section 1.3.1.4) is impaired in KD.

The precise nature of the role of NI formation in disease pathology has yet to be determined. Although their presence is a key feature of Polyglutamine Diseases and their suggested structure implies that protein function is impaired, NIs containing the mutant AR are observed in cells in areas that remain unaffected in KD. For example, both the Basal Ganglia and Hypothalamus, which are not affected in KD, appear to contain NIs (Adachi et al, 2005).

As well as the accumulation of the mutant AR protein, the accumulation of phosphorylated- and non-phosphorylated neurofilament proteins and synaptophysin is also observed in distal motor axons of KD mice, which could reflect a defect in axonal trafficking (Katsuno et al, 2006). However, as discussed below (Section 1.4.2), it has recently transpired that axonal transport defects may not play a substantial role in KD pathogenesis (Malik et al, 2011).

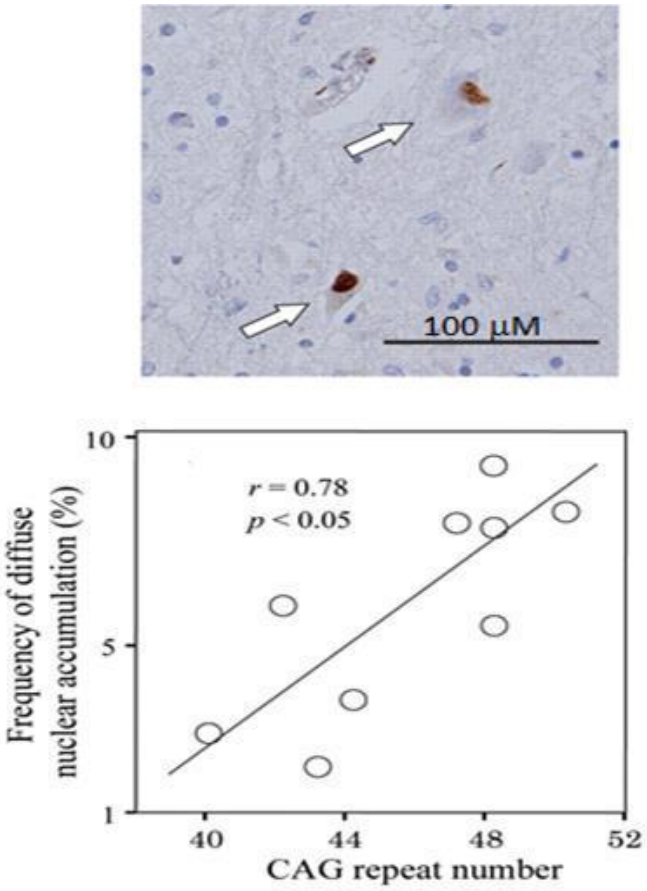

Figure 1.1: Nuclear Inclusions are observed in the anterior horn of KD patient spinal cord

Nuclear Inclusions are a histopathological feature of Kennedy's Disease. (A) Immunohistochemical analysis of the accumulation of the Androgen Receptor protein, using an anti-CAG-repeat antibody, shows aggregation in the motoneuron nuclei (white arrows) of the anterior horn of KD patients. The image is taken from Suzuki et al, 2007). When the relationship between CAG repeat number and nuclear accumulation of the AR protein is observed, as shown in the graph (B), taken from Adachi et al, 2005, there appears to be a positive correlation.

1.1.4.2 Muscle histopathology

Characteristic myogenic histopathology has also been observed in KD patients and skeletal muscle from mouse models of KD.

It has been suggested that myogenic events may be as important as neuronal events in KD pathogenesis. For example, in an animal model of KD in which the mutant AR protein is expressed in muscle tissue *exclusively*, the same neuromuscular phenotype was apparent as that observed in animal models expressing the mutant AR in *both* motoneurons and muscle even though no motoneuron degeneration was observed (Dupuis et al, 2010). This suggests that myogenic events play a pivotal role in KD neuromuscular pathology.

In some respects the muscle histopathology that is associated with KD is not typical of MNDs because the severity of the myogenic histology does not appear to directly correlate with the duration of the disease (Soraru et al, 2008). In a study based on 8 KD patients in which muscle biopsies were examined, it was found that 6 out of 8 patients possessed myogenic anomalies including fibre splitting and scattered basophilic fibres (Soraru et al, 2008). There also appeared to be variation amongst patients with respect to muscle histology, with the fibre size varying significantly (Soraru et al, 2008). The abnormalities however, did not appear to correlate with disease duration, despite appearing to be more prominent with increasing patient disability (Soraru et al, 2008). Myogenic pathology also appears to be wide-spread in KD, with progressive atrophy of all three types of muscle fibre (Type 1, 2a and 2b) being observed (Greenland & Zajac 2004).

As is the case with motor axons, the accumulation of phosphorylated and non-phosphorylated neurofilaments and synaptophysin also appears to occur in skeletal muscle of AR97Q KD mice and KD patients, as shown by immunohistochemistry, suggesting that axonal transport could be impaired in this cell type (Katsuno et al, 2006). However it appears unlikely that the presence of the mutant AR directly disrupts

cellular transport. Indeed, when α-bungarotoxin was used to label neuromuscular junctions, it was found that neurofilaments and synaptophsyin accumulated at the most distal end of the motor axon in both mice and KD patients whereas the mutant AR accumulated in the nucleus. Thus a physical association between the mutant AR and these proteins seems unlikely and therefore it is also unlikely that the mutant AR directly disrupts axonal transport (Katsuno et al, 2006, Malik et al, 2011).

1.1.5 Clinical Features of KD

1.1.5.1 Manifestation in affected males

The symptoms that are associated with KD can be classified as motor, sensory, or endocrine. Motor symptoms arise as a result of spinal and bulbar motoneuron degeneration (Suzuki et al, 2008). The most common motor symptoms include weakness and wasting of bulbar, facial and limb muscles (for review see Greenland & Zajac, 2004). Symptoms tend to begin in male carriers of the mutant AR gene between the third and fifth decade of life (Suzuki et al, 2008), although some mild symptoms, such as muscle weakness and hand tremors, have been reported by patients in their teenage years (Greenland & Zajac, 2004). The first disease manifestations include postural tremor, flexor muscle cramps and a hanging jaw (Larsen et al, 2005). Proximal flaccid weakness also occurs, usually in lower limbs before upper limbs. In approximately one third of KD patients, rapid muscle fatigability is also reported to be an early clinical manifestation (Lee et al, 2005). All of these initial symptoms remain throughout the disease and deteriorate with disease progression (Larsen et al, 2005). With time, bulbar symptoms also appear, for example, difficulty swallowing, which occurs as a result of wasting of the tongue, jaw and throat muscles (Greenland & Zajac, 2004).

KD progresses relatively slowly compared to other MNDs. In a study of 223 patients, motor symptom progression was observed and found to deteriorate over a period of 10 years (Atsuta et al, 2006). For example, the median age at which patients required the

assistance of a handrail to climb stairs was found to be 49 years of age, however it wasn't until the age of approximately 61 that most patients had such severe motor defects that they were confined to a wheelchair (Atsuta et al, 2006). Kennedy's Disease does not appear to directly affect the life-span of patients, although sufferers are more prone to complications that increase the risk of mortality, such as aspiration pneumonia and choking as a result of severe bulbar effects (Larsen and Smith, 2005).

Sensory symptoms that often accompany these motor symptoms were initially thought to be relatively minor in severity. However, it now appears that in some cases, sensory symptoms can be just as severe as motor symptoms and the original concept that sensory symptoms were mild in KD patients was a result of relatively insensitive diagnostic tools as well as incorrectly identifying the peak time at which such symptoms occur (Polo et al, 1996). Indeed, a small-scale electrophysiological study of both male patients and female carriers revealed that sensory deficits peak at earlier stages of the disease (Polo et al, 1996). A larger scale, electrophysiological study of over 100 patients showed pathological lesions in the Dorsal Root Ganglion (DRG). Furthermore, the F-wave latency was significantly longer in patients than in controls and the maximum F-wave conduction velocity was significantly lower in patients, most predominantly in upper limbs, indicating that cervical neurons that innervate upper limbs could be affected more severely than lumbar neurons innervating lower limbs (Suzuki et al, 2008). Other studies have also revealed that in a small number of patients, the tendon reflex is absent and the trigeminal reflex is severely abnormal (Antonini et al, 2000).

It has been suggested that such sensory symptoms are more dominant in patients with lower CAG-repeat numbers (Adachi et al, 2005). This could be due to the effect that the CAG-repeat length appears to have on the distribution of the mutant AR within the neuron (Adachi et al, 2005). For example, ARs containing a longer CAG-repeat tend to exist relatively diffusely in the nucleus, whilst AR proteins containing shorter CAG-repeats, associated with dominant sensory symptoms, tend to form cytoplasmic

aggregations (Adachi et al, 2005). Thus this difference in localization within neurons could account for variations in symptom type dominance.

Endocrine symptoms that are present prior to and alongside neurological symptoms include androgen resistance, gynacomastia and decreased fertility, as well as elevated levels of testosterone and progesterone in the bloodstream. Such symptoms however, are variable and do not occur in *all* cases of KD (Li et al, 2007). In a study of 22 KD patients for example (Dejager, 2002), it was found that 80% of subjects presented with gynacomastia that occurred post-puberty but prior to the presentation of muscle weakness, whilst just over half of the patients monitored experienced alterations in testicular function (Dejager, 2002). The majority of patients (86%) developed androgen resistance at later disease stages, whilst 68% of patients possessed elevated blood levels of testosterone. Thus there is variation in the presentation of endocrine symptoms between patients. As is the case with neurological symptoms, a correlation between CAG-repeat length and endocrine symptoms has also been observed. It appears that the longer the length of the CAG repeat, the weaker the transactivation of the AR, which is consistent with the presentation of more severe symptoms (Dejager, 2002).

1.1.5.2 Symptom manifestation in female carriers

Females carrying the mutant AR gene do not usually show clinical signs of KD (Schmidt et al, 2002). On the rare occasion that they do, symptoms are very mild relative to those of male carriers (Karaer et al, 2005). The presentation of symptoms in females is thought to occur as a result of skewed inactivation of one the X chromosomes according to the Lyon Hypothesis (Paradas et al, 2008), so that one of the two X chromosomes is randomly inactivated resulting in the mutant AR gene being expressed in the absence of a dominant wild-type AR gene. Symptoms reported in female carriers include minimal distal muscle weakness, cramps and fasciculations

(Soraru et al, 2008). Electrophysiological data and muscle biopsies from female carriers also revealed very mild neurogenic and myopathic alterations such as a reduction of sensory action potentials and calf hypertrophy (Soraru et al, 2008), whilst electrophysiological studies revealed that signs of mild, chronic denervation of muscle groups including the Tibialis Anterior muscle and the Orbicularis Oris muscle appear to be the most common symptoms apparent in heterozygous females (Mariotti et al, 2000). Motor and sensory conduction velocities however, usually appear to be within the normal range in heterozygous females, indicative of an absence of neuropathy (Mariotti et al, 2000).

1.1.6 Diagnosis of Kennedy's Disease

There are various ways in which Kennedy's Disease is diagnosed and distinguished from other MNDs and myopathies such as Amyotrophic Lateral Sclerosis (ALS) and Inclusion Body Myositis (IBM), respectively. The diagnosis of KD is partially based on family history of the patient, i.e. whether or not other family members have suffered from the disease. However this approach alone is not sufficient to make a reliable diagnosis (Domitrz et al, 2001).

The gold standard when diagnosing KD is genetic analysis, which is used to assess the AR CAG-repeat number in patients (Georgiou et al, 2001). DNA samples are taken from patients using non-invasive techniques such as peripheral blood extraction (Atsuta et al, 2006) and amplified using primers flanking the CAG-repeat. Genetic analysis allows a precise diagnosis of individuals to be made and is thus essential when diagnosing a disease such as KD, which phenotypically resembles other diseases.

To compliment genetic analysis, other diagnostic tools are utilised. Neurological examinations such as electrophysiological recordings are used to identify the presence of the symptoms discussed above (Section 1.1.5.1). Compound muscle action

potentials for example, are measured in potential KD patients. It has been found previously that the magnitude of muscle action potentials decreases in KD, which is indicative of axonal degeneration (Suzuki et al, 2008). This decrease in compound action potential is often more noticeable in upper limbs than lower limbs (Suzuki et al, 2008). Evoked action potentials tend to have more prolonged peak latencies in KD patients than in healthy individuals. Transcranial Magnetic Stimulation (TMS) also reveals that the motor threshold for evoked potentials, that is, the TMS voltage needed to stimulate action potentials and evoke movement, is higher in KD patients (Lai et al, 2007).

Biopsies from both muscle and scrotal tissue are also used to assist in the diagnosis of KD. In muscle tissue, neuropathic and myopathic alterations are present (as discussed above), particularly in severely affected muscle, whilst in scrotal tissue nuclear accumulation of the mutant AR is observed (Soraru et al, 2008, Adachi et al, 2007).

In addition, plasma levels of Creatine Kinase (CK) can be measured. CK has been previously shown to increase in the plasma of male carriers of the mutant AR gene (Sorenson et al, 2008). However, the identification of elevated plasma CK levels alone is not enough to confirm a case of KD, as CK levels are elevated in other neurological disorders, such as Alzheimer's Disease (Fassbender, 2001).

1.2. Models of KD

Since the identification of the CAG-repeat expansion in KD, several animal models have been developed in an attempt to establish and understand the pathogenic mechanisms underlying the disease further.

The challenges that are faced when developing animals models of KD include: slow disease progression, limited life-span of animals, maintaining disease specificity, developing a disease time course that is amenable with drug testing and accounting for

the fact that KD is predominantly a lower motoneuron and gender-specific disease (Merry, 2005, Sobue et al, 1989). Early attempts at developing a model of KD included the use of several cell lines expressing an AR protein with 44 CAG-repeats (Bingham et al, 1995). An interferon-inducible antiviral Mx promoter and a neuron-specific enolase (NSE) promoter were used to introduce a human cDNA AR fragment with 44 CAG-repeats into neuronal cell lines. However, in such cell lines, there was no detectable neuronal phenotype or repeat instability (Bingham et al, 1995), making these models unsuitable for the investigation of KD pathogenesis.

A transgenic mouse model was later developed by La Spada (La Spada, 1998), in which a mouse line containing 45 CAG-repeats in the AR protein was developed using a Yeast Artifical Chromosome (YAC). The methodology for the generation of a YAC transgenic model is described in more detail below. This model was again relatively unsuccessful at modelling KD, as no neuronal phenotype was detected in AR45 mice, even at 18 months of age. Furthermore, the expression of the AR45 transgene was not detectable in all tissues of interest, suggesting that the genetic manipulation alters the expression pattern of the gene. Other models of KD that failed to recapitulate the KD phenotype were also developed using 65 CAG-repeats (Merry et al, 1996).

Some models have been developed that *do* produce a neurological phenotype, but not one that accurately recapitulates KD. In 2001 for example, a truncated construct of the AR was used to develop of transgenic KD mouse (Abel, 2001). The phenotype of this mouse varied with the promoter used to generate the model. For instance, when a prion promoter was used, severe neurological symptoms were present as early as 2 months of age followed by an early death. However when a neurofilament (NF-L) promoter was used instead, motor-specific symptoms appeared at approximately 8 months of age (Abel et al, 2001). However, neither of these models had lower motoneuron-dominant pathology, a key characteristic of KD.

The features of the above models, in combination with the apparent inverse correlation between CAG-repeat size and time of symptom onset, lead to the idea that expanding the length of the CAG-repeat and using the most suitable promoter would improve the animal model and thus the transgenic mouse that was developed will now be discussed.

The AR100 mouse model of KD that was examined in the experiments described in this Thesis was developed by Albert La Spada in the US and has been obtained through collaboration with his lab. The AR100 transgenic mouse was created using a Yeast Artifical chromosome (YAC) as a transgene. A human AR gene, containing 100 CAG repeats in exon 1, was introduced to a YAC using the 'pop-in, pop-out' method (La Spada et al, 1998). Resultant YAC-bearing yeast cells were then fused with embryonic stem (ES) cells. Real-Time (RT) PCR was used to confirm the presence of the human AR transcript and human AR-positive ES cells were injected into C57BL/6J mouse blastocysts to create chimeric mice, whose identity was confirmed using Western blot analysis (Sopher et al, 2004).

AR100 mice have been extensively characterized by both Professor La Spada's group and our own and have been found to exhibit a progressive motor deficit. The first symptom to manifest in AR100 mice is growth retardation, which occurs at approximately 8 months of age (Sopher et al, 2004). By 10 months of age, AR100 mice appear to be smaller than Wild-Type (WT) littermates and have a lower body mass. This decrease in body mass in AR100 mice is shortly followed by proximal muscle weakness, which gives rise to curvature of the spine, giving the mice a kyphotic appearance. By 11 months of age, there is a difference in stride length between AR100 mice and WT controls and by 14 months of age mobility is impaired in the diseased mice. At this time point, AR100 mice also start to have difficulty in walking and hindlimb atrophy is observable, which eventually leads to hindlimb paralysis. Between the ages of 15-24 months, mortality is higher in AR100 mice and is usually the result of an unknown cause that requires euthanasia. Importantly, by 18 months AR100 mice have

lost a significant number of motoneurons, and only an average of 60% of motoneurons survive (Malik et al, 2011). Thus the symptoms, which manifest in AR100 mice, resemble KD patient symptom manifestation. Furthermore, female AR100 mice fail to express the full KD phenotype – in keeping with the fact that KD manifests solely in male patients.

1.3. Androgens and the Androgen receptor

In order to determine how a mutation in the androgen receptor could give rise to KD, it is important to understand both the normal functions of androgens, which will give an indication of *which* processes are most likely to be affected, and the locations at which androgen receptors are highly expressed, which will give an indication of *where* disease pathology is likely to occur.

The majority of androgens are secreted into the bloodstream in the form of testosterone (Lin et al, 1997). Testosterone is cell permeable and is metabolized in the cytosol by 5α-reductase into dihydrotestosterone (DHT). It is generally accepted that Testosterone and DHT both activate the same AR, although their downstream effects are thought to vary to some extent, with testosterone appearing to regulate the anabolic effects of androgens, whilst DHT appears to regulate androgenic effects (Sundaram et al, 1995).

1.3.1 Androgen receptor structure and expression

The AR is a ligand-activated transcription factor that belongs to group 1 of the nuclear receptor super family (Centenera et al, 2008). The AR is a modular protein that contains functionally separate domains; the amino-terminal domain (NTD), which contains the CAG repeat that is expanded in Kennedy's Disease, the DNA-binding domain (DBD), a hinge region and the ligand (androgen)-binding domain (LBD). A schematic representation of the structural domains in shown in Figure 1.2. Post-

translational modification of the receptor in the form of phosphorylation – both basal and ligand-activated (Gioeli et al 2002), acetylation, ubiquitilation and sumoylation can have varying effects on receptor activity (reviewed by Faus & Haendler 2006). The effects of modification of each of the AR protein domains will be considered in more detail below.

1.3.1.1 The amino terminal domain (NTD)

The NTD, otherwise known as activation function -1 (AF-1) in the case of the AR, is not well conserved amongst nuclear receptors. Indeed, within group 1, there is only 15% homology in the NTD sequence (McEwan et al, 2007). A major role of the NTD is receptor activation. Within AF-1, two transcription activation units, (Tau-1 and -5), have been identified (Jenster et al, 1995). Both units appear to be necessary and sufficient for the full activity of the AR, with mutations in either unit resulting in the AR protein becoming completely inactive (Callewaert et al, 2006).

The NTD contains a polymorphic glutamine (CAG) repeat and changes in length of the repeat have been associated not only with KD, but also with prostate cancer (Sinclair et al, 2007). The CAG repeat appears to mediate various aspects of androgen receptor activity such as the magnitude of response. AR proteins containing fewer CAG repeats, for example, appear to be more potent transcription factors (Callewaert et al, 2003a). As well as a poly-glutamine repeat, the NTD also contains a poly-glycine repeat. Changes in the length of this glycine expansion have also been associated with prostate cancer (Ding et al, 2005).

Post-translational modification of the NTD has various effects on AR activity (Faus & Haendler 2006). Dephosphorylation of the domain by Protein Phosphatase 2A for example, has been found to result in a decrease in activity (Yang et al 2005). Likewise, binding of the E3 ligase; C-terminus of Hsc70-interacting protein (CHIP) to the NTD also results in repression of AR activity (He et al 2004). However, the monoubiquitilated

form of the AR is suggested to have enhanced transcriptional activity (Burgdorf et al 2004).

1.3.1.2 The DNA-binding domain (DBD)

The DBD is involved in receptor dimerization that occurs following ligand activation of the receptor. In all nuclear receptors the DBD is a highly conserved region consisting of three α-helices that contain cysteine-rich zinc fingers, and a C-terminal extension (CTE) of at least 12 residues in length (Schoenmakers et al, 1999). The zinc fingers, which interact with DNA, are essential for the function of the receptor and its structural integrity (Glass, 1994), whilst the CTE is involved in dimerization of the receptor. It is not well conserved and varies with different nuclear receptors, resulting in receptor specificity.

1.3.1.3 The Hinge domain

The hinge domain of the AR is thought to have various functions. It is a poorly conserved, flexible domain that separates the DBD and LBD that is involved in DNA binding, nuclear translocation and transcriptional activity of the receptor (Verrijdt et al, 2003, Zhou et al, 1994). For example, deletion of residues specific to the region, result in prolonged androgen responses, suggesting that the hinge domain mediates the duration of androgen-induced transcription (Tanner et al, 2004).

The Hinge domain has been found to be subject to post-translational acetylation (Fu et al 2000). Acetylation of the domain is modulated by enzymes such as P300/CBP-associated factor (P/CAF) and appears to be essential for normal AR function. Indeed, mutations of the modulation site have been found to result in functional impairment of the receptor (Fu et al 2000).

1.3.1.4 The Ligand-Binding Domain (LBD)

The LBD regulates the activity of the AR. Its basic structure is a twelve α-helical 'sandwich' with a central ligand-binding region (Matias et al, 2000). Androgen activation of the receptor involves the closure of the ligand-binding pocket by movement of the twelfth helix of the LBD (Moras & Gronemeyer, 1998). The re-structured LBD is then thought to behave as a docking site for co-activators of the AR (Claessens et al, 2008). As well as interacting with AR ligands i.e. testosterone and DHT, the LBD also interacts with agonists and antagonists of the AR, such as mibolerone and Flutemide, respectively (Kemppainen et al, 1999, Gao & Dalton, 2007).

1.3.1.5 Androgen Receptor expression

The AR is expressed predominantly in 'androgen target' tissues including skeletal muscle, the prostate, liver, skin, and the central nervous system (CNS). RT-PCR has revealed that expression is at its highest in the adrenal gland, epididymis and prostate (Keller et al, 1996). Thus androgen effects are wide spread and involved in a vast number of essential processes.

In the context of this study, the most interesting location of the AR protein is in the CNS, specifically in motoneurons. The expression of ARs in motoneurons has been suggested to be regulated downstream of BDNF signalling (Hussein et al, 1997, Yang et al, 2000). When BDNF availability was prevented by axotomy in bulbar motoneurons, androgen receptor number appeared to decrease. This decrease was then rescued by BDNF application (Yang et al, 2000).

Although the precise role of androgen-mediated pathways in motoneurons has yet to be fully established, the most likely function of androgens in motoneurons is to provide essential trophic support to aid synaptic organization during development (Cary & La Spada, 2008, Fargo et al, 2009). For example, testosterone has been shown to mediate the survival of sexually dimorphic motoneuron populations such as the dorsolateral nucleus (DLN).

Figure 1.2

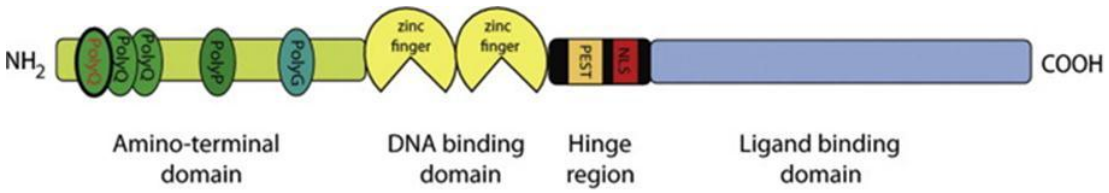

Adapted from Parodi & Pennuto 2011

This Figure depicts a schematic representation of the AR protein, compose of 4 domains. The amino-terminal domain (encoded by exon 1), contains the poly-CAG tract mutated in KD. The DNA-binding domain (encoded by exons 2 and 3), is formed by two zinc fingers, and the hinge region, which contains the PEST sequence and the nuclear localization signal (NLS). The ligand-binding domain is encoded by exons 4-8.

Indeed, when female rats were treated with testosterone prenatally, there was reduced DLN motoneuron death compared to untreated female controls (Breedlove et al, 1981). Conversely, males possessing a loss-of-function mutation in the androgen receptor gene possess a 'female' number of DLN motoneurons in adulthood (Breedlove et al, 1981). Androgens also exert trophic effects on motoneurons indirectly. For instance, they have been suggested to regulate the survival of bulbar motoneurons indirectly via their actions on target muscle, which include the enhancement of myogenic cell commitment and satellite cell proliferation (for review see Maclean & Handlesman, 2009) Androgen treatment in rats during late prenatal development appears to reduce bulbar motoneuron death despite bulbar motoneurons not expressing ARs until the second postnatal week (Jordan et al, 1997).

Androgens have also been suggested to maintain the morphology of motoneurons during adulthood, with manipulation of androgens affecting motoneuron soma size in adult rats. For example, the castration of male rats and the consequential decrease in androgen availability results in shrinkage of bulbar motoneurons, which is prevented by testosterone treatment (Kurz et al, 1991). In a recent study, it has also been suggested that androgens may play a crucial role in mediating axonal transport in motoneurons (Kemp et al, 2011). When live cell imaging was used to monitor endosomal trafficking in sciatic nerve axons from both a knock-in model and a myogenic transgenic model of KD, a deficit in both the flux and run length of retrogradely-transported endosomes was impaired (Kemp et al, 2011). However, using the AR100 mouse model examined in this Thesis, our group did not detect any axonal transport deficits in either embryonic or adult AR100 motoneurons (Malik et al, 2011). The role of axonal transport deficits in KD pathogenesis is discussed in more detail on Section 1.4.2.

1.3.2 Genomic actions of Androgens

The genomic actions of androgens, which result in the transcription of various downstream target genes, occur within minutes to hours of androgen receptor activation. Upon binding of Testosterone or DHT to the androgen receptor, the receptor dissociates from a cytoplasmic chaperone complex and the AR-ligand complex dimerizes at a consensus sequences of 5'-TGTTCT-3' (Glass, 1994). The homodimer then translocates to the nucleus. Once the AR dimer enters the nucleus it binds to sequences of DNA known as Androgen Response Elements (AREs) and recruits cofactors that are required for the execution of target gene transcription. Such cofactors include histone acetyltransferase proteins such as CREB-binding protein (CBP), which is involved in modulating oestrogen signalling, and methyltransferase proteins such as Co-activator-associated arginine methyltransferase 1 (CARM1), which is required for the anabolic effects of androgens that occur during development (Baek et al, 2006). Figure 1.3 summarizes AR activation.

Genes that are transcribed downstream of androgen receptor activation include cystatin-related protein genes (crps). Crps are involved in various sexual functions such as spermatogenesis. Rhox genes, which are transcription factors involved in embryogenesis and gametogenesis, are also transcribed downstream of AR activation (MacLean & Wilkinson, 2010). Thus genomic androgen effects are vital for sexual development, which is the process most commonly associated with androgens (Ho et al, 2011).

Other genes that are transcribed downstream of AR activation have other functions that are not immediately associated with androgens. One such function is the maintenance of normal cellular Ca^{2+} handling.

Figure 1.3: Androgen receptor activation and genomic actions

Genomic actions of androgens are elicited by a well characterized chain of events, which are depicted in this Figure. Initially, Testosterone diffuses into the cytosol where it is reduced to dihydrotestosterone (DHT) by 5α-reductase (1). Upon binding of DHT to the androgen receptor (AR), the AR-DHT complex dissociates from the heat shock protein complex that normally stabilizes the AR (2). The receptor-ligand complex then diffuses into the nucleus where it dimerizes (3) and binds to sequences of DNA referred to as androgen response elements (ARE). Genes containing this sequence of DNA are transcribed downstream of AR activation. When the AR-DHT complex binds to the ARE, cofactors are recruited along with RNA polymerase II, allowing mRNA to be transcribed (4). This chain of events occurs over a period of minutes to hours.

T = Testosterone

DHT = Dihydrotestosterone

5α-R = 5α-Reductase

AR = Androgen receptor

Hsp 70/90 = Heat Shock Protein 70/90

ARE = Androgen Response Element

ARA 70= Androgen receptor co-activator 70-Kd (Miyamoto 1998)

SRC-1= Steroid Receptor Coactivator -1 (Ye 2005)

CBP= CREB Binding Protein (Frønsdal 1998)

SP-1= Specificity Protein 1- an ubiquitous transcription factor (Dame 1997)

Figure 1. 3

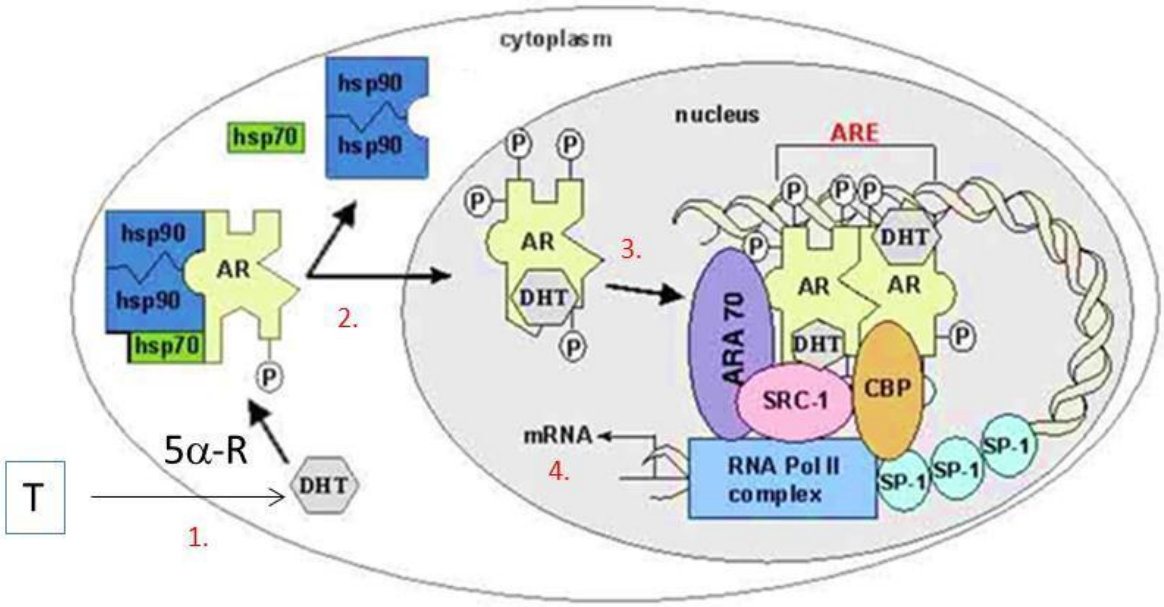

Adapted from Meehan & Sadar 2003

For example, following AR activation, the Sarco/Endoplasmic Reticulum ATPase 2 (SERCA2) pump gene is one of the target genes transcribed (Foradori et al, 2008). The SERCA2 pump, which is the SERCA pump isoform that is expressed specifically in neurons, is located in the ER membrane. It sequesters Ca^{2+} from the cytosol and actively pumps it into the ER lumen against its concentration gradient. This decreases cytosolic Ca^{2+} and facilitates refilling of ER calcium, both of which are protective to cells (see Chapter 3 for more detail). Real Time (RT) PCR has been used to show that activation of the androgen receptor in hippocampal neurons results in an increase in the level of SERCA2 mRNA, causing an increase in ER Ca^{2+}, which is required for normal cellular function (Foradori et al, 2008).

As well as cellular Ca^{2+} handling, genes transcribed downstream of AR activation also include essential cytoskeletal genes that are involved in cell division and intracellular transport. For instance, the expression of β-actin and β-tubulin mRNA in male rat motoneurons was found to decrease following castration, which effectively decreases androgen availability (Matsumoto et al, 1994). Furthermore, this apparent decrease in transcription was counteracted by the administration of testosterone, indicating that transcription of these genes is a direct result of AR activation (Matsumoto et al, 1994).

1.3.3 Non-genomic actions of androgens

It has only been in recent years that the rapid, 'non-genomic' actions of androgens have received more attention. These androgen-mediated actions have a relatively short latency and occur within seconds to minutes of AR activation. Interestingly, such responses have been shown to be evoked by non-permeable forms of Testosterone and DHT (for example, BSA-bound DHT), which suggests that, as well as intracellular receptors, plasma membrane-associated ARs with extracellular ligand-binding domains also exist (for review see Li & Al-Azzawi, 2009).

Although the precise mechanism by which rapid androgen-mediated actions are elicited has yet to be fully established, it is accepted that the responses occur either at

the plasma membrane or within the cytosol, but *not* in the nucleus or rough ER as they are insensitive to inhibitors of transcription and translation (Heinlein et al, 2002).

One of the most frequently observed consequences of Androgen-mediated, non-genomic actions in various cell types, including neurons, is a rapid increase in cytosolic calcium. There are several possible mechanisms by which the increase in calcium could be elicited so rapidly following AR activation. One suggestion is that the plasma membrane-associated androgen receptor is a G-protein coupled receptor that is linked to Phospholipase C (PLC) and thus Inositol trisphosphate (IP_3)-mediated Ca^{2+} release form the ER is induced downstream of AR activation. Ca^{2+} influx via voltage-gated and ligand-activated Ca^{2+} channels, as an indirect effect of AR activation, is also thought to accompany this (Foradori et al, 2009, Michels & Hoppe, 2008). Alternatively it has been suggested that rapid increases in intracellular Ca^{2+} following AR activation occur as a direct inhibitory effect on plasma membrane Ca^{2+} ATPases (PMCAs), which expel Ca^{2+} from the cytosol (Zylinska et al, 2009).

As well as the generation of rapid Ca^{2+} signals, rapid androgen-mediated effects are also thought to include the activation of the MAP Kinase pathway as well as Protein Kinases A and C, both of which are enhanced by the elevation of intracellular Ca^{2+} and thus could occur downstream of the Ca^{2+} signalling discussed above (Kousteni et al, 2001, Ricote et al, 2006). The activation of Protein Kinases A and C and MAP Kinase is upstream of various cellular processes such as Glucose metabolism, actomyosin assembly contraction and the activation of transcription factors such as NF-κB. Thus rapid androgen effects potentially mediate a wide variety of essential processes.

1.4. Kennedy's Disease pathogenesis

The precise mechanism underlying KD pathogenesis has yet to be established and as with many other neurodegenerative diseases, it is notoriously multifactorial and is likely to occur as the result of a combination of pathogenic mechanisms. Furthermore,

because of the progressive nature of the disease, it is difficult to determine which phenomena are causative in disease pathology, and which occur as a secondary effect. Some of the pathogenic mechanisms that have been suggested to play a role in KD pathology and other similar MNDs and CAG-repeat diseases will be discussed here.

1.4.1 Alterations in transcription

Considering the majority of AR-mediated actions result in alterations in gene transcription, it is not surprising that the N-terminal CAG repeat expansion mutation in the AR has been found to result in alterations in transcription that could contribute to KD pathogenesis. For example, the transcription of Nicotinamide Adenine Dinucleotide (NADH) dehydrogenases 1 and 5 is found to decrease as a consequence of mutant AR expression (Ranganathan et al, 2009). NADH dehydrogenases 1 and 5 are vital subunits of complex I of the electron transport chain. Their decrease in expression appeared to occur in both cell lines transfected with a mutant androgen receptor and in a transgenic mouse model of KD (Ranganathan et al, 2009). As a result, the mitochondrial membrane is depolarised and thus one consequence of mutation-mediated changes in transcription is mitochondrial function impairment, which will be examined in more detail in Chapter 5. Because there are so many transcriptional changes that occur as a result of the AR mutation (Mo et al, 2010, Slagsvold et al, 2000, Koochekpour, 2010), it is important to identify the largest and most consistent changes, i.e. those that are likely to have the greatest impact on cellular processes.

One of the most effective ways to assess the most prominent changes in transcription is to perform microarray analysis. This has recently been carried out in both skeletal muscle (Mo et al, 2010) and embryonic motoneurons (Malik et al, personal communication) from transgenic mouse models of Kennedy's Disease. In skeletal muscle, the largest and most consistent changes in transcription, which occurred in all animal models tested, included genes that are involved in cell adhesion, energy

balance, myogenesis and muscle atrophy (Mo et al, 2010). VEGFα and Integrin beta 1 binding protein 3 (Itgb1bp3), which is also known as MIBP, and is involved in the inhibition of myocyte adhesion to laminin, were also reduced. Increases in the expression of some genes were also found to occur in the skeletal muscle of all mouse models tested, including, Ankyrin repeat domain 1 (Ankrd 1), which is involved in many aspects of muscle development such as structural fixation of the contractile machinery (Tee, 2010).

Microarray analysis of primary motoneurons from the AR100 mouse model of Kennedy's disease has also revealed changes in transcription of over 400 genes (Malik et al, personal communication). Although there appears to be a larger number of genes that decrease in AR100 motoneurons, the largest magnitude of change is found in genes whose expression increases. Thus microarray analysis does not reveal a single, underlying trigger, but confirms the likely multifactorial nature of KD pathology.

1.4.2 Axonal transport

Although the role of axonal transport changes in Kennedy's Disease remains controversial (Kemp et al, 2011, Malik et al, 2011), the involvement of this cellular malfunction in both MNDs and CAG-repeat disorders has been clearly established.

Axonal transport dysfunction has been found to occur in MNDs such as Amyotrophic lateral Sclerosis (ALS) prior to symptom onset in vitro (Keiran et al, 2005) in embryonic motoneurons and in vivo in adult SOD1 mice (Bilsland et al, 2010, Williams & Cleveland, 1999), indicating that the disruption of axonal transport not only occurs as part of ALS pathology, but may be a disease trigger. Indeed in $SOD1^{G93A}$ mice, deficits in retrograde transport not only occurred prior to disease onset but also worsened with disease progression (Bilsland et al, 2010). When an in vivo assay was developed to assess the retrograde transport of endosomes and mitochondria in axons of the sciatic nerve of SOD^{G93A} mice it was found that deficits occurred as early as post-natal day 36

(Bilsland et al, 2010). Furthermore, this early axonal transport impairment appeared to be specific to fast motoneurons, which are vulnerable in ALS (Hegedus et al, 2008). In slower motoneurons, which appear to be more resistant to ALS pathology, transport deficits did not appear until 120 days of age (Bilsland et al, 2010). This indicates that defects in axonal transport can be correlated with susceptibility to disease pathology in the SOD^{G93A} model of ALS.

Evidence for axonal transport deficits in CAG-repeat disorders, such as Huntington's Disease (HD) has also been obtained from transfected cell lines, transgenic mouse models and HD patient hippocampal autopsy tissue. For example, evidence suggests that the mutant Huntingtin protein inhibits fast axonal transport via JNK3 activation in a mouse model of HD (Morfini et al, 2009). Increased JNK3 activation subsequently leads to the phosphorylation of Kinesin – a motor protein that plays a pivotal role in anterograde axonal transport. This results in decreased association of Kinesin with microtubules, thus impairing axonal transport. In another set of experiments, the fast transport of amyloid precursor protein (APP) and Brain-derived neurotrophic factor (BDNF) was monitored in both a mouse model of HD, in which the Huntingtin protein contains 150 CAG repeats, and in mutant Huntingtin - transfected retinoblastoma cells (Morfini et al, 2009). It was found that the transport of APP and BDNF was impaired in striatal neurons from pre-symptomatic HD mice. Furthermore, the transport of APP and BDNF appeared to be accelerated in cell lines in which the wild-type (WT) Huntingtin protein was over-expressed, yet disrupted in cells transfected with the mutant Huntingtin protein (Her & Goldstein, 208). This suggests that the loss of normal Huntingtin function as opposed to protein over-expression could be the cause of axonal transport defects.

Since axonal transport deficits have been detected in both MND and CAG-repeat disorders it is possible that such deficits may also play a role in the pathogenesis of KD. Indeed some evidence does suggest that fast axonal transport is impaired in KD. For example, as is the case with HD, JNK activation appears to increase in cell lines

expressing the mutant androgen receptor, resulting in impaired binding of Kinesin to microtubules (Morfini et al, 2006). Evidence for axonal transport impairment in KD pathogenesis has also been obtained from a knock-in mouse model of the disease, in which the mutant AR contains113 CAG repeats (Kemp et al, 2011). Live cell confocal imaging of CT-AF_{488}-labelled endosomes revealed that expression of the mutant AR induced severe retrograde trafficking defects in axons of the sciatic nerve (Kemp et al, 2011), Specifically, the run length of endosomes appeared to be significantly reduced in AR113Q mice compared to WT controls, as demonstrated by a significantly greater number of endosomal stalls and the transport flux was five times lower in KD mice, as demonstrated by a depletion of endosomal retrograde transport over time (Kempt et al, 2011). However, such findings should be considered with caution as the model of KD used in this study does not recapitulate KD as accurately as other models of the disease, such as the YAC AR100 model used in this Thesis and importantly do not exhibit any motoneuron degeneration (Sopher et al, 2004). Indeed, AR113Q mice have a rapidly progressing phenotype, dying by approximately 20 weeks of age (Yu et al, 2006), whereas KD a slow, progressive disease (Suzuki et al, 2008).

Indeed, a recent study from our lab has shown that, contrary to expectations, axonal transport is not impaired in motoneurons of the AR100 mouse model of KD (Malik et al, 2011). When the levels of the microtubule-associated motor protein Tau, and the motor protein Kinesin were measured using Western blot analysis of both the sciatic nerve and spinal cord of WT and KD mice at various ages, no significant difference in expression levels was detected between the genotypes. Furthermore, no axonal transport deficits were detected either in vitro in embryonic primary motoneurons or in vivo, in the intact sciatic nerve of anaesthetized AR100 mice when the kinetics of both anterograde and retrograde transport of $TeNTH_C$ were examined (Malik et al, 2011). This study suggests that whilst impaired axonal transport is implicated in the pathology of both MNDs and CAG-repeat disorders, it does not appear to play a significant role in Kennedy's Disease.

1.4.3 Proteasome dysfunction

The ubiquitin proteasome system (UPS) is a major degradation pathway for damaged and short-lived proteins. UPS function is vital for the removal of unwanted proteins and thus is essential for a variety of processes such as lysosomal degradation, normal synaptic function and cellular plasticity (Bingol et al, 2006, Tai & Schuman, 2008).

At present there is much debate as to whether or not proteasome dysfunction plays a role in KD pathogenesis. In other MNDs, such as ALS, both decreases and increases in proteasome function have been reported. In neuro2a cells proteasome inhibition is induced by the expression of the mutant SOD1 protein (Urushitani et al, 2002). Reduced proteasome function has also been reported in $SOD1^{G93A}$ mice (Kabashi et al, 2004). However its importance in disease pathology remains controversial. In $SOD1^{G93A}$ mice crossed with mice lacking the LMP2 proteasome subunit, motor function and survival is no different to that observed in $SOD1^{G93A}$ mice (Puttaparthi et al, 2007). Therefore impairment in proteasome function via the knock-out of a vital proteasome subunit has no effect on disease, suggesting that the pathological mechanism underlying ALS pathology is independent from proteasome function.

Conversely, some reports have shown that the presence of the mutant SOD1 protein results in an increase in proteasome function as shown by the induction of proteasome subunits such as LMP2, LMP7 and MECL-1 in astroglia and microglia of $SOD1^{G93A}$ mice compared to WT controls (Puttaparthi & Elliot 2005). Thus evidence for both increases and decreases in proteasome activity in ALS has been obtained.

Similarly, the role of proteasome dysfunction in HD is also unclear, despite the initial assumption that the proteasome would be overwhelmed by CAG-repeat expansions (reviewed by Ciechanover 2003). Decreased UPS activity has been reported in cell lines that have been transfected with mutant Huntingtin, as demonstrated by a decrease in chymotrypsin-like, trypsin-like and peptidylglytamyl-like activity (Seo et al, 2007). Decreases in proteasome function have also been implicated from experiments

using animal models of HD. In the R6/2 mouse model of HD, Congo red was used to inhibit oligomerization of the mutant Huntingtin protein at 9 weeks of age, thus aggregation was inhibited (Sanchez et al, 2003). In a set of parallel experiments it was found that Congo red also increased proteasome activity in mutant cells but not in control cells, suggesting that inhibition of Huntingtin aggregation rescues proteasome activity (Sanchez et al, 2003).

However, increases in proteasome activity in HD have also been reported, and for example, enzymatic assays for the three types of proteasome activity reveal an increase in proteasome function in HD94 transgenic mice, (Diaz-Hernandez et al, 2003). Furthermore, Western blot analysis of striatal neurons from these mice reveal an increase in expression of the proteasome subunits LMP2 and 7, which is consistent with an increase in function.

Because the role of the proteasome in MND and CAG-repeat disorder pathogenesis remains controversial, it is difficult to predict the role of the proteasome in Kennedy's Disease. Initial suggestions that proteasome dysfunction plays a role in the pathogenesis of KD came from the observation that AR aggregates sequester proteasome components, as demonstrated by electron microscopy and immunohistochemistry (Stenoien et al, 1999). To date, most research into the role of the proteasome in KD pathogenesis has been limited to cell lines such as mutant AR-transfected HeLa and HEK cells (Stenoien et al, 1999, Mandrusiak et al, 2003). For example, when a mutant AR protein containing 48 CAG repeats is introduced into HeLa cells, it can be detected when labelled with an antibody against the P31/PA700 proteasome cap (Stenoien et al, 1999). This suggests a direct interaction between the mutant AR protein and components of the proteasome. When transglutaminase was used to encourage AR aggregation in HEK cells, proteasome function appeared to be impaired in an AR ligand-dependent manner. This was demonstrated by the accumulation of an unstable green fluorescent protein that is normally broken down by the proteasome (Mandrusiak et al, 2003). Furthermore, Cystamine-mediated inhibition

of Transglutaminase and thus inhibition of mutant AR protein aggregation resulted in an improvement in proteasome function. This could indicate that protein aggregation itself results in proteasome function impairment. However the improvement in proteasome function could also be a result of other downstream effects of Cystamine application, such as the prevention of apoptosis and oxidative stress (Igarashi et al, 1998, Dedeoglu et al, 2002). Therefore the beneficial effects of Cystamine may not be due to the prevention of protein aggregation specifically and thus protein aggregation may not play a role in proteasome dysfunction.

1.4.4. Endoplasmic Reticulum (ER) stress

1.4.4.1 ER function and dysfunction

The fundamental function of the endoplasmic reticulum (ER) is to process newly synthesized membrane and secretory proteins. Proteins, which are not folded correctly, do not progress to the next stage of the secretory pathway – the Golgi Complex - and in this respect, the ER is often referred to as a point of protein quality control in the cell (Brodsky 1999). An important aspect of ER function is its dependence on levels of ER Ca^{2+} (Pachen 2000), which will be discussed and examined in detail in Chapter 3. ER Ca^{2+} depletion, as well as other events such a change in cell redox state and ATP depletion, result in ER impairment, which is often referred to as ER stress (Kuznetsov et al, 1996, Tsai et al, 1994, Ikesugi et al, 2006). ER stress results in the activation of the Unfolded Protein Response (UPR) and Store-operated Calcium (SOC) influx, which aim to restore ER homeostasis and ER Ca^{2+}, respectively (see Chapter 3, Section 3.1.2). Measurements of these two responses can be used to infer levels of ER stress and will form the basis of some of the experimental techniques used in this study. ER stress in neurodegenerative disease pathogenesis will therefore be discussed briefly here, and in more detail in Chapter 3.

ER stress has been implicated to play a role in both MNDs and CAG-repeat disorders such as ALS and HD, respectively (Saxena et al, 2009, Reijonen et al, 2008). Evidence

for the involvement of ER stress is ALS and HD is discussed briefly here, but is also described in more detail in Chapter 3.

1.4.5 ER stress in Amyotrophic Lateral Sclerosis and Huntington's Disease

In the mutant $SOD1^{G93A}$ mouse model of ALS, markers of the ER stress-induced Unfolded Protein Response (UPR) have been detected as early as P5 – prior to symptom onset (Saxena et al, 2009). This suggests that ER stress is not a secondary effect of other pathological mechanisms, and is more likely to play a causal role in ALS pathogenesis. Furthermore, inhibiting ER stress pharmacologically, with Salubrinal, results in an improvement in motor function and an increase in survival of $SOD1^{G93A}$ mice (Saxena et al, 2009). Markers of ER stress have also been found to be present in ALS patient tissue, and markers such as Binding Immunoglobulin Protein (BiP) are elevated in ALS patient spinal cord (Ilieva et al, 2007).

There is also strong evidence to suggest that ER stress plays a major role in HD pathogenesis. In cell lines transfected with a mutant Huntingtin protein for example, there is an increase in cell death compared to control cells (Duennwald et al, 2008), which is prevented by treatment with Salubrinal (Duennwald et al, 2008). Furthermore, the level of ER stress appears to increase with the length of the CAG repeat, which is reflected in more severe symptoms (Reijonen et al, 2008). Thus, the severity of ER stress, as determined by expression levels of BiP, has been shown to correlate with symptom severity (Reijonen et al, 2008).

1.4.6. Mitochondrial dysfunction

Mitochondrial abnormalities are known to play a major role in the pathogenesis of several neurodegenerative diseases including Parkinson's Disease (Murphy, 2009) as well as MNDs and CAG-repeat disorders including ALS and HD, respectively (Shi et al, 2010, Mochel & Haller, 2011). The role of mitochondrial dysfunction in MNDs and HD will be discussed briefly here and in more detail in Chapter 5, where the role of mitochondrial dysfunction in KD is examined.

In the case of ALS, various mitochondrial abnormalities have been found in various cell-line and animal models of the disease as well as in anterior horn motoneurons from ALS patients (for review see Shi et al, 2010). Initial indications of mitochondrial dysfunction in ALS came from observations of abnormal mitochondrial morphology (Saski and Iwata 1992). In sporadic ALS patient spinal cord for example, dense conglomerates of mitochondria have been observed (Saski and Iwata 1992), whilst degenerating mitochondrial vacuoles are present in axons and dendrites of motoneurons from pre-symptomatic SOD1 mutant mice (Del Canto and Gurney 1995). Further investigations have confirmed that mitochondrial dysfunction accompanies the observed morphological abnormalities. In motoneurons from pre-symptomatic $SOD1^{G93A}$ for example, the Ca^{2+} loading-capacity of mitochondria was found to increase compared to WT controls (Damiano et al, 2006). The consequential increase in mitochondrial Ca^{2+} is accompanied by potentially pathological events such as reactive oxygen species generation and oxidative stress (Kruman et al, 1999). As well as functional impairment, mitochondrial-mediated processes also appear to be affected by alterations in mitochondrial transport. Unlike other organelles and cell cargo, mitochondria do not have a defined destination and instead, are transported according to the energy requirements of the cell (Goldstein et al, 2000), which is particularly vital in synapses that require tightly regulated supplies of Ca^{2+} and ATP (Rowland et al, 2000). In primary motoneurons from the $SOD1^{G93A}$ mouse model of ALS, anterograde transport of mitochondria was found to be impaired, implicating that the mitochondrial supply to synapses is jeopardized both in vitro and in vivo (De Vos et al, 2007, Bilsland et al, 2010). Furthermore, in NSC34 cells, which over-express mutant SOD1, both anterograde and retrograde transport of mitochondria was found to be altered (Magrane & Manfredi, 2009). These results suggest that mitochondrial and thus energy supply is impaired in motoneurons in ALS.

Evidence also strongly suggests that mitochondrial dysfunction also plays an important role in the pathogenesis of HD. Indeed the Ca^{2+} loading capacity of mitochondria was

found to be altered in three different mouse models of HD (Oliveira et al, 2007). In the R6/2 and YAC 128 models, Ca^{2+} loading capacity was found to increase under basal conditions compared to control littermates, whilst the striatal neurons from Hdh-150 knock-in model appeared to be vulnerable to NMDA receptor challenges and failed to restore Ca^{2+} homeostasis (Oliveira et al, 2009). In lymphocytes from HD patients however, the Ca^{2+} loading capacity was found to decrease (Panov et al, 2002). Nonetheless, regardless of the direction of change, mitochondrial Ca^{2+} loading capacity is consistently altered in HD.

As well as changes in Ca^{2+} loading capacity, impaired energy production has also been found to be involved in HD pathogenesis (for review see Chen 2011). For example, reduced cAMP and an ATP/ADP ratio have been observed in the Htt mouse model of HD and lymphoblastoid cells of HD patients (Gines et al, 2003).

Abnormalities in the opening of the mitochondrial permeability transition pore (mPTP) have also been observed in HD (Panov et al, 2002). Electron microscopy has revealed that the mutant Huntingtin protein accumulates on the mitochondrial membrane, directly interacting with the mPTP and leading to mitochondrial depolarization (Panov et al, 2002). Furthermore, neurons from a knock-in model of HD containing a Huntingtin protein with 150 CAG repeats exhibited increased sensitivity to Ca^{2+}-induced mPTP opening and subsequent mitochondrial swelling (Choo et al, 2004).

Consistent with findings in other MNDs and CAG-repeat disorders, mitochondrial abnormalities have also been implicated in the pathogenesis of KD. Expression of the mutant AR protein in the motoneuron-like cell line, MN-1, resulted in a decreased mitochondrial membrane potential, which is indicative of mitochondrial dysfunction (Ranganathan et al, 2009). Furthermore, the expression of Peroxisome Proliferator-activated receptor Co-activator-1 (PGC-1), which is an inducer of mitochondrial biogenesis, also decreased in these cells (Ranganathan et al, 2009). This suggests that mitochondrial biogenesis is decreased in these cells, resulting in a deficit in

mitochondria number. Indeed, both mitochondrial mass and number were found to be lower mutant AR-expressing cells compared to controls (Ranganathan et al, 2009).

Evidence for mitochondrial abnormalities has also been obtained from KD patients. For example, the mitochondrial DNA copy number is lower in KD patients compared to healthy controls and the magnitude of the decrease in number is inversely correlated with the CAG-repeat length (Liu et al, 2003). Furthermore, both asymptomatic mutant AR carriers and symptomatic patients displayed higher levels of the oxidative biomarker, $mtDNA^{4977}$, which indicates increased mitochondrial DNA damage, compared to healthy controls (Lui et al, 2003).

1.5 Current treatment strategies for KD

Despite the identification of the genetic cause of KD, there is currently no effective disease-modifying treatment for KD. Instead, only symptomatic relief is offered to patients in the form of B vitamins, vitamin E and physiotherapy.

Initial attempts at developing disease-modifying therapies have used animal models of KD and have been designed on the basis that the disease involves a toxic gain-of-function of the androgen receptor. Attempts at modifying KD have therefore aimed to lower AR activation in the hope that this will decrease its toxic effects. One study has observed the effects of Leuprorelin treatment in the AR97Q mouse model of KD (Katsuno et al, 2003). Leuprorelin is a Leutenizing Hormone-Releasing Hormone (LHRH) agonist that decreases testosterone levels and therefore lowers AR activation and subsequent translocation of the activated receptor into the nucleus (Katsuno et al, 2004). Following the administration of Leuprorelin to AR97Q mice, decreases in nuclear accumulation of the mutant androgen receptor, as demonstrated by immunohistochemistry and western blot analysis, were observed (Katsuno et al, 2003). Furthermore, treated mice have a longer life-span, larger body size and a more improved motor performance compared to control mice that had been treated with a

control vehicle alone. Based on these findings, the effectiveness of treatment in patients has been investigated. Initial findings suggest that within 2-3 weeks of initiating Leuprorelin treatment, testosterone levels decrease to those seen following castration. However the disease phenotype is not rescued (Katsuno 2003).

The androgen receptor inhibitor Flutemide has also been considered as a possible therapeutic agent for KD. However, results suggest that Flutemide is not as effective as Leuprorelin. When AR97Q mice are treated with Flutemide at 13 weeks of age, symptoms are not alleviated and pathological features does not appear to improve (Katsuno et al, 2006). This has been suggested to be due to the fact that Flutemide may actually facilitate translocation of the mutant androgen receptor into the nucleus rather than lower AR activation.

One problem when investigating possible KD treatments is the fact that suitable and specific markers for KD severity and progression have yet to be established so that even if candidate agents are identified, there is no good outcome measure to determine efficacy within the time frame of a viable clinical trial. Although it has been suggested that muscle strength, muscle volume and bulbar function could be used as reasonable markers for Kennedy's disease when investigating therapies (Katsuno et al, 2004), they may not be the ideal markers for assessing treatment effectiveness and more rhobust indicators of disease severity and progression at a cellular level are needed. Therefore the purpose of identifying KD-specific pathogenic mechanisms is two-fold; to establish treatment targets and to identify the ideal disease marker to assess the effectiveness of new therapies.

1.6 Thesis aims

The aims of this thesis are:

1. To establish if ER stress plays a role in the pathogenesis of KD.
2. To examine whether markers of ER stress are present in the spinal cord of KD mice and change during disease progression.

3. To determine if ER stress is related to motoneuron degeneration in KD.
4. To investigate whether mitochondrial dysfunction is an early pathological feature of KD.

The experiments described in this Thesis will determine whether ER stress and mitochondrial dysfunction are early pathological features of KD. The results may therefore identify new targets for the development of novel therapeutic approaches for KD.

CHAPTER 2: MATERIALS & METHODS

2.1 Transgenic mouse colonies

In this study the AR100 mouse model of Kennedy's Disease (KD) will be used, which has been used previously by the Greensmith lab to investigate the pathogenesis of KD.

2.1.1 AR100 colony

The generation and characterization of the AR6 YAC CAG100 (AR100) transgenic mice model is described in detail by Sopher et al, 2004 and is discussed in Chapter 1 (Section 1.2). This mouse model was developed using a yeast artificial chromosome (YAC) containing the 450 kb Androgen Receptor (AR) gene with 100 CAG repeats in the N-terminal (as opposed to the normal range of 8-31). The YAC containing the mutant AR gene was then transfected into mouse embryonic stem cells. This type of cell is able to differentiate as normal in the germline hence the AR100 protein is incorporated in the same way that the Wild-Type AR protein would be (Sopher et al, 2004). Mice containing this mutation develop late onset and progressive neuromuscular symptoms that recapitulated the symptoms of KD, for example, proximal muscle weakness, hind limb atrophy and difficulty in walking, developing from about 8 -12 months of age (Sopher et al, 2004) in addition to progressive motoneuron degeneration in the spinal cord (Malik et al, 2011). Male AR100 transgenic mice were obtained from Prof. La Spada's laboratory in Seattle and a colony was established and maintained at UCL by mating male AR100 mice with C57 black 6 wild-type (WT) females (Harlan Laboratories, England). The genotype of each embryo was determined as described in Chapter 2, Section 2.5. All experiments were carried out under the Animals (Scientific Procedures) act of 1986 and following ethical approval from the Ethical Review Panel of UCL, IoN.

2.1.2 SOD1^{G93A} and SODH colonies

Transgenic mice over-expressing the G93A mutant SOD-1 gene [(TgN(SOD1G93A)1Gur] (SOD1^{G93A}) were maintained by breeding heterozygous males with female F_1 hybrids. The genotype of embryos used was determined using the

protocol described in Chapter 2, Section 2.5.5 (Gurney et al, 1994). In addition a colony in which the human Wild-Type SOD-1 protein (SODH) was over-expressed was also used as a control for protein over-expression (Li et al, 2004).

2.2 Experimental groups

The following experimental groups were examined in this Thesis:

A) WT motoneurons – derived from WT mice
   a. – DHT:- model normal female motoneurons
   b. + DHT:- model normal male motoneurons

B) KD motoneurons – derived from AR100 mice
   a. – DHT:- model unaffected female carriers with the expanded CAG repeat
   b. + DHT:- model affected males with the expanded CAG repeat i.e. diseased motoneurons

2.3 Primary ventral horn motoneuron culture

2.3.1 Preparation

Circular glass coverslips were autoclaved and then coated with Poly-Ornithine (diluted 1 in 1000 in *sterile* water) and left at 37^{o}C and 5% CO_2 overnight in sterile multi-well plates (FALCON). This results in the coverslips being coated with a negative charge. The Poly-Ornithine solution was then aspirated and coverslips were coated with Laminin (diluted at 1 in 200 in L-15 medium) and incubated at 37^{o}C for a minimum of 2.5 hours. The diameter of the coverslip required and hence the size of the multi-well plate used varied according to the experiment; For confocal experiments, 22 mm coverslips placed in 6-well plates were used; For Western blot analysis, 16 mm

coverslips in 12-well plates were used and for Immunofluorescence experiments, either 16 mm coverslips in 12 well plates or 13mm coverslips in 24 well plates were used.

Complete Neurobasal (CNB) medium was made up the day before culturing (see Appendix) and was kept at 4^{o}C for no longer than 2 weeks. All other solutions were made up fresh for each culture.

2.3.2 Embryonic ventral spinal cord dissection

Female C57/B6 Harlan mice at gestation day 12-14 were sacrificed by a Schedule 1 method and a hysterectomy performed. Each embryo-containing yolk sack was removed and the top of the yolk sack was carefully pierced and peeled away, revealing the embryo intact. Initially the tail and hind limb paws were removed and stored at 4^{o}C for subsequent genotyping. The embryo was decapitated and the liver, intestines and stomach were removed so that the embryo could be laid flat, with the spinal column exposed and facing upwards. At this point the spinal column is already visible as an opaque white line down the centre of the back. Forceps were used to gently score along either side of the spinal cord and the skin was carefully peeled off. The tip of the forceps was then run under the dorsal meninges, and then used to score along the cord in a rostral-to-caudal direction, thus releasing the meninges and exposing the cord. The spinal cord was then released from underlying tissue and prised away from the body, with the ventral surface facing up. The meninges were then peeled away and the dorsal column of the cord removed using a scalpel. The meninges and dorsal column were then discarded leaving the ventral column. The ventral column was then stored in approximately 300-400 μL 1 % Penstrep in HBSS at 4^{o}C for a maximum of 6 hours.

2.3.3 Dissociation of ventral motoneurons

In some cases, genotyping was carried out prior to dissociation and in this case up to five ventral columns of the same genotype were pooled and dissociated together as one sample. When genotyping was carried out post-dissociation however, ventral

columns were dissociated individually and plated in separate wells. When ventral columns were dissociated separately, all volumes used during the protocol described were halved.

Each ventral column was cut into small fragments of approximately 1 mm or smaller in length. The fragments were then transferred into a new 15 ml falcon tube using a 1 ml pipette and were left to settle and form a loose pellet for approximately 2-3 minutes before excess HBSS was carefully removed. 1 ml of fresh HBSS (+ 1% Pen/Strep) was then added to the ventral column fragments along with 10 μl of 2.5% Trypsin. The resulting solution was then incubated at 37^{o}C for 10 minutes and was gently agitated after the first 5 minutes.

During the Trypsin incubation period the following solution was prepared (for each falcon tube in incubation):

800 μl L-15 medium

100 μl 4% BSA (in L15)

100 μl DNAse (1 mg/ml)

Immediately after incubation, the resulting clump of ventral column tissue was transferred to this solution and was gently triturated twice and left to stand for approximately 2 minutes or until the tissue had settled and formed a loose pellet at the bottom of the flacon tube. The supernatant (containing motoneurons) was then transferred to a new 15 ml falcon tube. To the remaining pellet the following was added:

900 μl CNB

100 μl 4% BSA (in L15)

20 μl DNAse (1 mg/ml)

The suspension was then triturated more vigorously 8 times and was left to stand for approximately 3 minutes. The supernatant was then transferred to the tube containing the first supernatant. To the remaining pellet the same combination of CNB, BSA and DNAse was added again.

The suspension was then triturated vigorously 10 times and allowed to settle for 3 minutes. The new supernatant was then added to the supernatants that had been collected previously and the pellet was discarded.

1 ml of 4% BSA in L15 was then carefully added to the bottom of the supernatant tube to form a cushion and the pooled supernatants were spun at 1500 rpm at room temperature for 5 minutes.

The resultant supernatant was then removed and the pellet was re-suspended in 1 ml of CNB and 20 μl of DNAse in L15 and was triturated 6 times before being plated at the required density (see Section 2.3.5). In this final step, the volumes of CNB and DNAse were kept constant, regardless of whether spinal cords were pooled or dissociated separately. This technique results in mixed ventral horn cultures that are comprised of approximately 40% primary motoneurons.

2.3.4 Purification of dissociated ventral horn motoneurons

In some experiments, additional steps were undertaken to purify the cultures further, so that they contained a higher proportion of motoneurons. Instead of plating the re-suspended pellet as described in the protocol above, 1 ml of clear L15 was added to the cell suspension and the solution was mixed gently. 3ml of 10.4% Optiprep (a density gradient solution) was gently added to this suspension to form a cushion at the bottom, producing a clear, sharp interface (see Figure 2.1). The mixture was then centrifuged at room temperature at 760 rotations per minute (rpm) for 15 minutes. The break of the centrifuge was set to zero to minimize the deceleration of the centrifuge and thus eliminate vibration. Following centrifugation, a thin white interface (Figure 2.2) containing motoneurons was transferred into a new 15 ml falcon tube and re-

suspended in 2 ml of CNB. Approximately 8 ml of clear L15 was then added to make the volume of solution up to 10 ml. 2 ml of BSA was then carefully applied to the bottom of the suspension to form a cushion though which the cells could spin through, and the resulting suspension was spun at room temperature for 5 minutes at 1500 rpm. The pellet was then re-suspended in 1 ml of CNB and plated at the required density. This technique resulted in primary motoneuron cultures that were consistently over 90% pure.

2.3.5 Cell counts & culture plating density

In order to determine the number of cells in 1 ml of cell suspension and hence the required plating volume, a 10 μl sample of the suspension was added to 10 μl of tryphan blue (Sigma). The resultant solution was then pipetted onto a haemocytometer and the number of cells in 5 random squares of the grid was counted using a light microscope. An average of both sides of the haemocytometer was calculated and then multiplied by 50,000 to calculate the number of cells in 1 ml of the suspension. The volume needed for the required density was then calculated. In the case of imaging experiments for example, a density of 50,000 cells per cm^2 was sufficient, whilst approximately 300,000 cells per cm^2 and greater was used for cultures that were to be analysed using western blot

2.3.6 Culture Maintenance

Cultures were kept for 7 days at 37^{o}C and 5% CO_2 in sterile conditions. They were examined on a daily basis to check for motoneuron development and signs of infection. The medium was changed as required, which was usually once during the 7 day in vitro (DIV) period. Cultures were treated with 5 μM DHT diluted in PBS at 4 DIV. The appropriate volume of DHT was added to make a final concentration of 50 nM DHT. Cultures were imaged, fixed or homogenized on 7 DIV.

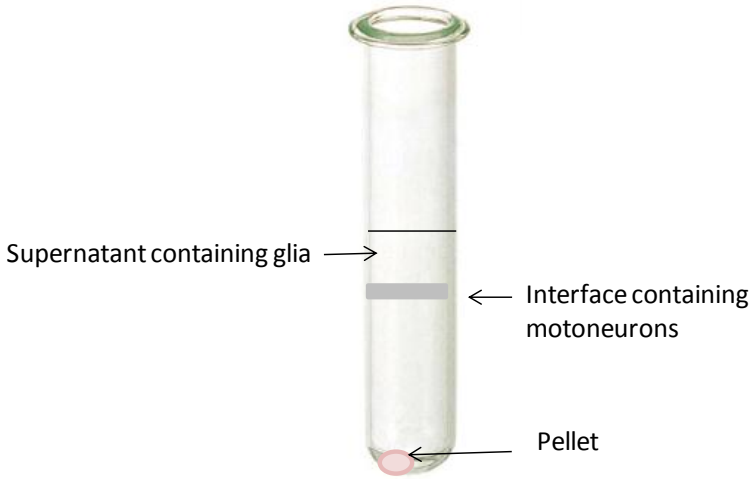

Figure 2.1: Purification of ventral horn motoneurons using Optiprep

The image shows a schematic representation of the different layers obtained following centrifugation of a ventral horn cell/Optiprep suspension. After being spun at 760 rotations per minute for 15 minutes, motoneurons were separated into a layer that was visible as an off-white interface between the supernatant and pellet. This interface was then carefully transferred into a new falcon tube.

2.3.7 Culture Homogenization

When cultures were required for Western blot analysis, approximately 750 μl of homogenization buffer at room temperature was added to each well and cells were agitated at 110 rpm in a shaker at 37°C for approximately 30 minutes. The contents of each well was then transferred to a new 1.5 ml eppendorf tube and stored at -20°C until processed. Protein content was analysed as described in Section 2.7.2.

2.4 Preparation of spinal cord tissue

Spinal cords from WT and KD mice at 3, 12 and 18 months of age were perfused with fixative (4% paraformaldehyde) by Dr B. Malik. Spinal cords from P5 mice were prepared by me. The mice were culled by decapitation, the tails were removed for genotyping and the spinal columns were dissected free of the body. Lumbar spinal cords (between L2-L6) were carefully removed and snap frozen in liquid nitrogen and stored at -80°C until they were processed for Western blot analysis and Immunohistochemistry.

2.5 Genotyping

2.5.1 Rapid digestion of embryonic tissue

The tail and/or foot were removed from E12-E14 embryos and placed in a 1.5 ml eppendorf tube. 48 μl of rapid digestion buffer was added to the samples followed by 2 μl of Proteinase K and the samples were vortexed for about five seconds. Samples were then incubated at 55°C for approximately 15 minutes, vortexed for approximately five seconds, and subsequently incubated at 95°C for a further 10 minutes. The samples were vortexed again and then spun at 14,000 rpm for 2 minutes at room temperature. 2.5 μl of each supernatant was used in a 25 μl PCR reaction (see Section 2.5.3).

2.5.2 Digestion of P5 tail biopsies

To 0.5cm of fresh or thawed tail from each P5 pup, 120 μl of 0.5M EDTA (pH 8) and 500 μl of Nuclei Lysis Solution were added. 17.5 μl of Proteinase K (20mg/ml stock) was then added and the resulting mixture was vortexed. The tails were then incubated at 55^{o}C overnight or for 4 hours, in which case they were vortexed every 30-45 minutes. Once the samples had been allowed to cool down to room temperature, 200 μl of protein precipitation solution was added and the resulting mixture was vortexed for approximately 20 seconds. Samples were then incubated for 10 minutes at -20^{o}C and subsequently centrifuged for 6 minutes at 14000g at room temperature, with the precipitated protein forming a white pellet. The DNA-containing supernatant was then carefully transferred to a clean 1.5 ml eppendorf tube and 600 μl of Isopropanol at room temperature was added. The solution was gently mixed by inversion until white thread-like strands of DNA could be seen. The solution was then centrifuged at 14000g at room temperature, for 3 minutes. The DNA-containing pellet was collected and the supernatant was discarded. The DNA was then washed in 600 μl of ethanol (EtOH) at room temperature and centrifuged again at 14000g for 3 minutes. The EtOH was then aspirated and the pellet was left to air dry for approximately 5 minutes. Samples were then stored in 200 μl distilled H_2O at - 20^{o}C and were vortexed prior to use.

2.5.3 AR100 tissue PCR

The primers used for the PCR reaction (Invitrogen) were as follows:

Forward Primer: 5'- CAT CTG AGT CCA GGG GAA CAG C -3'

Reverse Primer: 5'- GCC CAG GCG CTG CCG TAG TCC -3'

These primers amplified both the mutant human fragment and the inherent mouse gene, which are both approximately 450 base pairs (bp) in length.

The PCR conditions and PCR mix were as follows:

PCR condition	PCR reaction	
		Per sample (□l)
-Lid temperature: 105 °C	Sterile water	18.15
-95°C for 10 minutes	PCR buffer	2.5
-Cycle:	MgCl2	0.75
• 95°C for 30 secs • 68°C for 30 seconds • 72 °C for 30 seconds - repeated 34 times	dNTP	0.5
	Forward Primer	0.25
- 72°C for 5 minutes	Reverse Primer	0.25
- Hold at 4 °C	Taq polymerase	0.1
Total time = 1 hour and 34 minutes		
	Total Volume	22.5
	DNA	2.5

2.5.4 AR100 Restriction enzyme digestion

β glucosidase 1 (Bgl 1) was used to digest the human fragment of the AR gene whilst leaving the inherent mouse fragment intact allowing identification of AR100 Vs. WT samples. To 12.5 μl of each PCR product, 1 μl of Bgl1 (New England Biolabs) and 1.5 ml of PCR buffer (Invitrogen) was added and the resulting mixture was incubated at 37°C for 1.5-2.5 hours. The resulting positive transgene products produced bands at 450 bp, 350 bp and 100 bp when run on a 3% agarose gel at 90 volts for 25 minutes. Transgene negative products i.e. WT, produced only the 450 bp band (Figure 2.2).

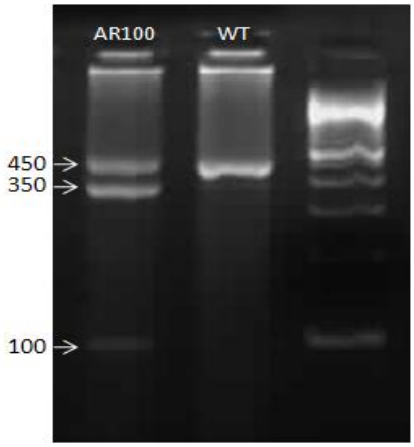

Figure 2.2: AR100 PCR products

Samples were run on a 3% agarose gel at 90 volts for 25 minutes. AR100 samples produced bands at 450 base pairs (bp), 350 bp and 100 bp. Transgene-negative products i.e. WT, produced only the 450 bp band

2.5.5 SOD1^{G93A} Genotyping

The primers used for SOD1^{G93A} PCR were as follows:

IMR0042 5'- CTA GGC CAC AGA ATT GAA AGA TCT -3'

IMR0043 5'- GTA GGT GGA AAT TCT AGC ATC ATC -3'

IMR0113 5'- CAT CAG CCC TAA TCC ATC TGA -3'

IMR0114 5'- CGC GAC TAA CAA TCA AAG TGA -3'

The PCR conditions and PCR mix were as follows:

PCR condition	PCR reaction	
-Lid temperature: 105 ^{o}C -95^{o}C for 3 minutes -Cycle: • 95^{o}C for 30 secs • 60^{o}C for 30 seconds • 72 ^{o}C for 30 seconds - repeated 35 times - 72^{o}C for 2 minutes - Hold at 4 ^{o}C		Per sample (□l)
	Sterile water	17.65
	PCR buffer	2.5
	MgCl2	0.75
	dNTP	0.5
	All primers (x 4)	0.25
	Taq polymerase	0.1
	Total Volume	22.5
	DNA	2.5

15 μl of each sample along with 3 μl of bromophenol blue was then loaded into a 2% gel and run at 50 V for 30 minutes. SOD1^{G93A} positive products produced bands at 324 bp and 236 bp, whilst WT products produced one band at 324 bp (Figure 2.3).

2.5.6 SODH PCR

The PCR conditions and mix were identical to those used for SOD1^{G93A} PCR. SODH-positive samples produced a band at 236 bp. WT products produced a band at 324 bp.

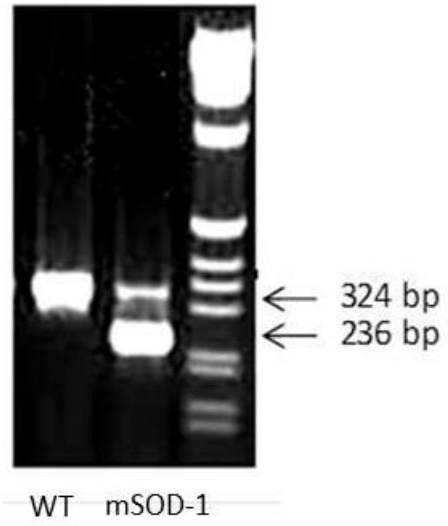

Figure 2.3: PCR products for SOD1^{G93A} genotyping

PCR products were run on a 2% gel at 50 V for 30 minutes. Wild type products produced only one band that was 324 base pairs (bp) in length. Mutant SOD1^{G93A} (mSOD1) -positive products however produced a smaller band as well, which was 236 bp in length.

2.5.7 Identification of embryo sex by genotyping

In the same experiments, motoneuron cultures of each sex were prepared. Therefore for these experiments the genotyping of individual embryos was established by PCR according to the method described by McClive and Sinclair, 2001, see Figure 2.4)

The primers used for PCR-sexing were as follows:

SrY (Y chromosome): 5' TCA TGA GAC TGC CAA CCA CAG 3'

5' CAT GAC CAC CAC CAC CAC CAA 3'

Myogenin (control): 5' TTA CGT CCA TCG TGG ACA GC 3'

5' TGG GCT GGG TGT TAG TCT TA 3'

The SrY gene is a male sex-determining gene found exclusively on the Y chromosome whilst the Myogenin (Myog) gene acts as a control, being present on both the X and Y chromosomes. The PCR conditions and PCR mix were as follows:

PCR condition	PCR reaction	
		Per sample (□l)
-Lid temperature: 105 ^{o}C	Sterile water	16.095
-94^{o}C for 5 minutes	PCR buffer	2.0
-Cycle:	MgCl2	0.57
• 94^{o}C for 5 secs • 67^{o}C for 40 seconds - repeated 30 times	dNTP	0.095
	All primers (x 4)	0.04
- 72^{o}C for 1 minutes	Taq polymerase	0.08
- Hold at 4 ^{o}C		
	Total Volume	19.0
	DNA	1.0

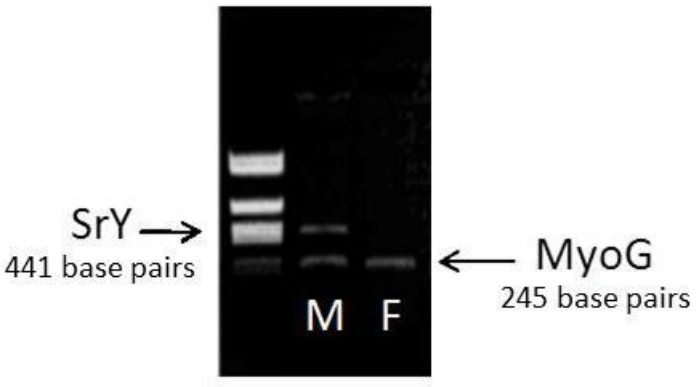

Figure 2.4: Sex-determination PCR using the Y chromosome-specific SrY gene

PCR products were run on a 0.75% gel at 120 V for 15 minutes. Male samples produced bands at 441 and 245 bp, representing SrY and MyoG, respectively, whilst female sample produced only the MyoG band, which is 245 bp.

2.5.8 Minigel preparation

10ml of 10 X TBE was diluted in 90 ml of double distilled water. 50 ml of the resulting solution was then used to make the agarose gel, the percentage of which varied with the PCR being carried out (AR100 requires a 3% gel, SOD1 requires a 2% gel, and SrY requires a 1.5% gel). The agarose was boiled for 2 minutes and 5 μl of ethidium bromide was added once the gel had cooled to approximately 70^{o}C. The agarose was then poured into the minigel apparatus and left to set for a minimum of 20 minutes. The combs and frames were then removed and the remaining 50 ml of TBE was poured over the set gel. 8 μl of a DNA ladder (Invitrogen) was loaded into the first well followed by 15 μl of each sample along with 3 μl of Bromophenol Blue into subsequent wells. The gel was then run as required.

2.6 Confocal Experiments

ER Ca^{2+} can be measured in cells in vitro indirectly by measuring the increase in cytosolic Ca^{2+} that occurs following the application of drugs that deplete the ER of Ca^{2+}, in a Ca^{2+}-free external environment. A Ca^{2+}-free environment ensures that the ER is the only source of the observed cytosolic Ca^{2+} elevation following drug application. The magnitude of this elevation can therefore be assumed to reflect ER Ca^{2+} levels (see Chapter 3).

One way in which a read out of cytosolic Ca^{2+} can be obtained is by using confocal microscopy in combination with drugs that alter cellular Ca^{2+} handling.

2.6.2 Ratiometric Vs. non-ratiometric Ca^{2+} indicators

Fluo 4-AM is a commonly used non-ratiometric, or single wave (SW) dye that measures free cytosolic Ca^{2+}. In choosing Fluo 4-AM for this study, it is important to be aware of its limitations and disadvantages and control for them by conducting the same experiments using Fura 2- a ratiometric dye. One disadvantage of using a SW dye such as Fluo 4-AM is the fact that the intensity of the emission and excitation spectra

varies with levels of free cytosolic Ca^{2+}. This makes measurements sensitive to confounding variables other than Ca^{2+} concentration. Such factors include leakage of the dye out of cells, uneven dye loading and photobleaching (destruction of the dye upon exposure to light). Ratiometric dyes such as Fura 2 however, overcome this problem. Because they are excited at two different wavelengths depending on whether the dye is Ca^{2+}-bound or Ca^{2+}-free, a ratio between the two maxima can be calculated, which minimizes the effects of the confounding variables that create problems when using SW dyes (Barreto-Chang and Dolmetsch 2009). Table 1 summarizes the key features of the two types of dye. The problem with ratiometric dyes such as Fura 2 however is the fact that they are excited by UV light. This is not ideal because exposure to UV excitation for prolonged periods can lead to cell death, with the phototoxic effects of UV rays causing depletion of the cellular NAD(P)H pool. Furthermore, Fura 2 is more prone to compartmentalization than Fluo 4-AM. Fluo 4-AM also has a greater Kd value then Fura 2, meaning that it is more suitable for monitoring larger changes in ER Ca^{2+}. Based on this characteristic, Fluo 4-AM appears to be more suitable for this study, although, precautions need to be made when analysing data, and carrying out control experiments using Fura 2 are essential.

2.6.2 Fluo 4-AM as a Ca^{2+} indicator

Confocal images were obtained using a Zeiss 510 confocal laser scanning microscope (Oberkocken, Germany) using a 40 x oil-objective lens. Cells were kept at 37^{o}C using a heated stage. 22 mm coverslips were loaded with 500 μl of 5 μM Fluo 4-AM (Molecular Probes, Invitrogen) and 0.005% pluronic acid diluted in confocal recording medium (see Appendix). Coverslips were incubated in the dark for approximately 30 minutes at 37^{o}C. Fluo 4-AM was excited at 488 nm and the emission fluorescence was measured at 518 nm. A ‘z stack’ scan was taken once a second for 800 seconds (to avoid the bias of sampling from a single plane) and background fluorescence was subtracted from the selected motoneurons. Motoneurons were selected using specific criteria as discussed below (Section 2.6.8).

The fluorescence values that were obtained were then calibrated into a Ca^{2+} concentration in nM using the following equation (Maravall et al, 2000):

$$[Ca^{2+}] = \frac{Kd \times (F/Fmax - 1/Rf)}{(1 - F/Fmax)}$$

For Fluo 4-AM: Kd = 350nM, Fmax = maximum fluorescence post – Ionomycin application, Rf = 100

2.6.3 Fura 2 as a Ca^{2+} indicator

In the case of Fura 2 experiments, the ORCA system (Hamamatsu) was used, although the cells were still viewed using a 40 x oil objective at 37^{o}C. Coverslips were incubated with 500 μl of 5 μM Fura 2 (Molecular probes, Invitrogen) and 0.005% pluronic acid diluted in confocal recording medium. Again, coverslips were incubated for approximately 30 minutes at 37^{o}C and 5% CO_2 in the dark. Fura 2 was excited at 340 nm and 380 nm and the emission fluorescence was measured at 505 nm. A ratio between to two maxima at the different wavelengths was calculated by dividing the 340 nm fluorescence value at a given time point by the 380 nm fluorescence value. Because of the mechanics of scanning via two channels, one image could only be taken approximately every 4 seconds.

2.6.4.1 Pharmacological induction of ER calcium depletion: Thapsigargin

There are various pharmacological agents that can be employed to manipulate and measure cellular Ca^{2+}. One such agent is Thapsigargin (TG), which non-competitively inhibits the SERCA pump in the ER membrane. In doing so, it prevents the ER from replenishing lost calcium, which results in a net loss of ER Ca^{2+}. One problem when using TG however is that it may not completely deplete the ER of Ca^{2+} and hence the

consequential rise in cytosolic Ca^{2+} may be an underestimation of ER Ca^{2+} levels. Indeed there is evidence to suggest that the application of TG results in depletion of a subset of TG-sensitive ER Ca^{2+} pools exclusively, which account for approximately 85% of total ER Ca^{2+} (Poulsen et al, 1995, Verma et al, 1990). However, in this study it is the difference between WT and KD motoneurons with respect to ER Ca^{2+} that is important, as opposed to absolute levels.

Another problem when using TG is the fact that there is some evidence to suggest that TG can directly lead to the influx of Ca^{2+} through the plasma membrane. For example, calcium influx was found to occur following the application of TG to human platelets, as indicated by a rise in free Ca^{2+}. This occurred in the presence of intracellular BAPTA – suggesting the calcium source was external, hence influx had occurred (Voster & Shafer 1996). This 'artefact' means that the observed level of SOC influx may be an overestimation of the actual level of SOC influx if calcium is present in the external medium at the time of TG application. Therefore, when using TG, it is vital to exclude Ca^{2+} from the external medium and to only introduce it at the time at which SOC influx is measured.

2.6.4.2 Fluorescence calibration: Ionomycin

Ionomycin is a common pharmacological tool used to investigate cellular Ca^{2+}. It is a neutral ionophore derived from the bacterium Streptomyces conglobatus. It is used to completely deplete all intracellular stores of Ca^{2+} and thereby achieve a maximum level of cytosolic Ca^{2+}. This is required for the calibration of confocal fluorescence.

2.6.5 Determination of ER Ca^{2+} levels: Measurement of cytosolic Ca^{2+}

Figure 2.5 shows an example of the protocol used to determine ER Ca^{2+} levels. Immediately prior to the start of the protocol, the Ca^{2+}-containing imaging media was

replaced with a Ca^{2+}-free medium. A basal of level of cytosolic fluorescence (Figure 2.7 A) was obtained and 1 μM Thapsigargin (TG) was then introduced approximately 45 seconds later (Figure 2.5 B); any increase in cytosolic Ca^{2+} measured would reflect ER Ca^{2+} as there is no external Ca^{2+} which could act as a source of increased cytosolic Ca^{2+}. The actions of TG are complete within 300 seconds and so the cells were left untouched for this time. Following ER Ca^{2+} depletion, Ca^{2+} was reintroduced into the external medium (Figure 2.5 C), allowing SOC influx to occur. Therefore, SOC influx was considered to be the subsequent increase in cytosolic Ca^{2+} following the reintroduction of Ca^{2+} to the external medium. 5 μM Ionomycin was then added approximately 60 seconds later (Figure 2.5 D) so that the maximum cytosolic Ca^{2+} fluorescence could be obtained, which was necessary for the calibration of fluorescence into Ca^{2+} concentration in nM (see Section 2.6.2 for the calibration procedure).

In experiments using Fluo 4-AM, cytosolic Ca^{2+} was analysed using LSM software (Carl Zeiss GmbH in association with EMBL, Heidelberg, Germany). In experiments using Fura 2, the concentration was analysed using AQM software (Tech Direct). In all experiments background fluorescence was deducted prior to calibration.

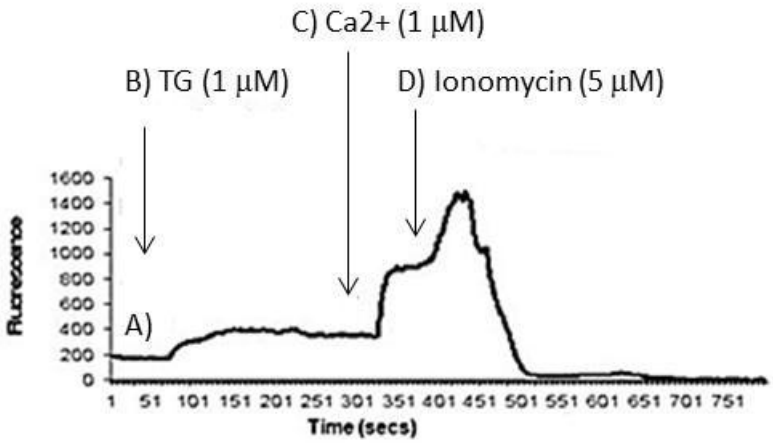

Figure 2.5: ER Ca^{2+} levels: Measurement of cytosolic Ca^{2+} concentration

Untreated and DHT-treated WT and KD primary motoneurons were imaged using confocal microscopy at 7 DIV. Cultures were incubated for approximately 30 minutes at 37 ^{o}C with 500 µl of 5 µM Fluo 4-AM and 0.005% pluronic acid diluted in confocal recording medium. Throughout the experimental period cultures were maintained at 37^{o}C using a heated stage. The image shows an example trace of cytosolic fluorescence.

2.6.6 Measurement of cytosolic Ca^{2+}: Protocol inclusion criteria

Many confounding variables affect the measurements obtained from confocal imaging experiments, such as temperature, age of drug solutions, drug concentration and length of exposure to drugs. These confounding variables are therefore kept as constant as possible. If a condition is altered, the experiment is rejected.

Even if all conditions are kept constant however, the measurements obtained still need to fit certain criteria in order to be included in the analysis. Traces are rejected for example, if a stable basal cytosolic Ca^{2+} concentration is not apparent. If the level of Ca^{2+} is fluctuating even in the absence of drug application, the effects of the drugs cannot be determined. Traces are also rejected if there is no increase in cytosolic Ca^{2+} in response to the application of Ionomycin. Ionomycin acts by depleting all internal stores of Ca^{2+}, as described above, resulting in a maximum cytosolic Ca^{2+} concentration. This maximum level of Ca^{2+} is required for calibration of the Fluo 4-AM fluorescence signal and thus if it is not obtained, fluorescence cannot be converted into a concentration and a comparison between different cells cannot be made. Finally, traces are rejected if the background noise is so large that it could conceal effects of drug application.

2.6.7 Tetramethylrhodamine methylester (TMRM)

Confocal images were obtained using a Zeiss 510 confocal laser scanning microscope (Oberkocken, Germany) using a 40 x oil-objective lens. 22 mm coverslips were loaded with 50 nM TMRM (Invitrogen) in confocal recording medium (see Appendix). Coverslips were incubated in the dark for approximately 30 minutes at room temperature. TMRM was excited at 543 nm and the emission fluorescence was measured above 560 nm. A ‘z stack’ scan was once every 4 seconds for 800 seconds and background fluorescence was subtracted. Motoneurons were selected using specific criteria (Section 2.6.8). Carbonyl cyanide p-trifluoromethoxyphenyl hydrazone

(FCCP, 1 μM) treatment was used as a control for mitochondrial membrane depolarization.

2.6.8 Motoneuron selection criteria

Most of the in vitro experiments described in this Thesis involved the use of primary mixed ventral horn cells, so it was important to use a consistent set of criteria to identify primary motoneurons. Motoneurons were identified on the basis of strict visual criteria that allowed them to be differentiated from interneurons; namely, a cell body diameter of greater than 15mm, and possessing more than 2 neuritic processes. Motoneurons also tend to grow in the upper focal plane of the culture (Bilsland et al, 2008).

2.7 Western Blot

2.7.1 Selection of time points for Western blot analysis

Markers of ER stress were examined in tissues at various key stages of disease by Western blot analysis at E13, P5, and 3, 12 and 18 months of age. Embryonic motoneurons were investigated in order to establish whether or not ER stress occurs at the earliest time point possible and thus is likely to be an early pathological feature of disease as opposed to a secondary effect.

2.7.2 Protein content determination assay for Western blot analysis

For primary ventral horn cultures, at 7 DIV, the medium was removed from the wells and was replaced with 750 μl of homogenizing buffer (see Section 2.1.5). Cells were incubated with homogenizing buffer as described above and a homogenate was obtained. 10 μl of each mixture was then pipetted into a new 96 well plate, and the top row was left free for the BSA controls (see Appendix).

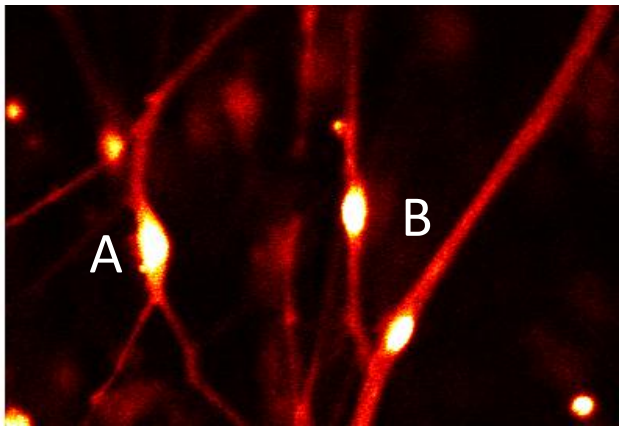

Figure 2.6: Motoneurons imaged using a confocal microscope

The image in this figure was obtained using a Zeiss Confocal microscope and analysed using LSM software. It shows an example of a cell that is considered to be a motoneuron (A) and one that is not (B) according to the criteria described previously (Bilsland et al, 2008). Although both cells were in the same focal plane and have very similar sized cell bodies, cell A) possessed 3 processes whereas cell B possessed only 2 and is therefore discounted when regions of interest were selected.

25 μl of Reagent 'A' followed by 200 μl of Reagent 'B' (BIO-RAD, Dc Protein assay reagents) was then added to each well and the plate was left to incubate at room temperature in the dark for 15-30 minutes. The concentration was then determined using the spectrophotometer at 750 nm. The value obtained for each sample was then calibrated using the values obtained for the BSA controls. In the case of spinal column tissue, homogenizing buffer was added to a sample of the cord in a 2:1 ratio.

2.7.3 Western Blot Protocol

Plates were assembled according to manufacturer's instructions and the resolving gel mixture was pipetted into the chambers, leaving approximately 2 cm at the top for stacking gel. A layer of water saturated-butanol was pipetted on top of the resolving gel to ensure that the gel would not evaporate before setting. It was then left to set at room temperature for 1 hour. During this period, transfer buffer, running buffer and the first part of the stacking gel were prepared. Samples were prepared by adding sample buffer in a 1:1 ratio. The sample volume varied so that the same amount of protein was present in each sample. The volume needed was determined using the protein content assay described above. On average, 40 μg of protein was loaded per well, although this varied between experiments (but not within the same experiment). The samples were then boiled at 95 ^{o}C for 5-10 minutes and left at room temperature until needed.

Once the resolving gel had set, the water-saturated butanol was decanted. The stacking gel was then completed and pipetted on top of the resolving gel. Combs were inserted immediately and the stacking gel was left to set. The plates were then loaded into the tank and the space between the plates was filled with running buffer. The combs were removed and 5 μl of Western Standard Marker (Bio-RAD) was loaded into a well. 20-30 μl of each sample was then loaded into each consecutive well and the remainder of the running buffer was poured into the tank. The gel was then run at 160 V for 1 hour, or until the samples had run to the bottom of the gel. Filter paper and

nitrocellulose blotting membrane were then soaked in ice cold transfer buffer and the blotter was set up.

The blotter was then placed in the tank, which was filled with ice cold transfer buffer and was run at 90 V for approximately 70 minutes. It was stirred continuously. The membrane was then removed and soaked in Ponceau solution for 2 minutes to test whether or not the transfer was successful. The membrane was washed in PBS and stored at 4^{o}C in PBS for up to 48 hours.

The blotting membrane was blocked at room temperature for 1 hour, and was gently agitated throughout this period. 10 ml of the required primary antibodies diluted in blocking solution was then applied and the blot was incubated overnight at 4^{o}C. The blot was then washed six times in PBS-Tween and was incubated at room temperature for 2 hours with suitable HRP-conjugated secondary antibodies, along with streptactin (a secondary antibody for the marker), both diluted in blocking solution. The blot was kept in the dark and gently agitated throughout this period. The blot was again washed six times before being incubated for 5 minutes at room temperature with approximately 1 ml each of solutions A and B (Supersignal West Pico, Thermo Scientific). The blot was imaged using a chemiluminescence camera and FluorChem software (Cell Biosciences, California).

2.8 Immunocytochemistry

2.8.1 Protocol

For cell cultures, at 7 DIV, the medium was removed from wells and cells were fixed in 4% PFA for 15-20 minutes at room temperature. The PFA was then carefully removed and coverslips were washed three times in PBS (Oxoid BR14) for 5 minutes each time.

For the analysis of spinal cord tissue, fresh spinal cords were removed from terminally anaesthetized WT and AR100 mice at P5, 3, 12 and 18 months, placed in an

eppendorf tube and stored at -80^{o}C until processed. Transverse spinal cord sections were cut serially at 10 μm on a cryostat onto glass slides.

Coverslips or spinal cord sections were incubated at room temperature for one hour in blocking solution, which consisted of 5% milk and 3% serum in PBS-0.1% Triton X-100 (Sigma T8787). The type of serum used varied with the secondary antibody host, for example, for goat secondary antibodies sections were blocked in goat serum. The blocking solution was aspirated and the slides were incubated at 4^{o}C overnight in the primary antibody diluted in blocking solution. The primary antibody was removed and the slides were washed three times in PBS for 10 minutes each time. The appropriate secondary antibody diluted in blocking solution to the required concentration, was then applied and the slides were incubated at room temperature, in the dark for 2 hours. The slides were then washed three times and then if required (i.e. if the secondary antibody used was a biotinylated antibody as opposed to a fluorescently conjugated antibody), an Avadin tertiary antibody (diluted in PBS) was applied and again, the slides were incubated in the dark at room temperature for 2 hours. Following a further 3 washes, the slides were then incubated with DAPI (1 in 2000 in PBS) in the dark at room temperature for 10 minutes. The slides were washed in PBS before being mounted using fluorescent mounting medium (DakoCytomation Fluorescent mounting medium S3023).

In all experiments a negative control (incubated overnight in blocking solution only, with no primary antibody) was included to test the specificity of the secondary antibody.

2.8.2 Microscopy

Spinal cord sections and motoneuron cultures were imaged using the Leica (DFC420 C) fluorescent microscope using a 40 X and 20 X objective lens.

2.8.3 Primary motoneuron counts

All counts were undertaken blind by concealing the identity of the slides using labels placed on the slide by a fellow lab member. Fields were selected systematically so that the whole coverslip was represented. The number of motoneurons in a field was measured by counting the number of nuclei (positive DAPI staining), which were β-III tubulin positive cells and which also fitted the criteria for identifying motoneurons (see Section 2.6.5). The number of motoneurons in each culture was established and expressed as a percentage of the DAPI-positive cells.

2.9 Statistical Analysis

Statistical analysis was performed using SPSS v15. To test for significance, non-parametric data analysis was performed using the KruskalWallis test and for parametric data, one-way ANOVA with Tukey's HSD and Bonferoni post-hoc tests carried out for pairwise comparison between all groups within the experiment. A p value of < 0.05 was considered statistically significant.

CHAPTER 3: RESULTS 1 – ER CALCIUM DEPLETION AND ER STRESS IN KD MOTONEURONS

3.1. Introduction

ER stress has been implicated in the pathogenesis of Motor Neuron Diseases (MNDs) and CAG-repeat disorders such as Amyotrophic Lateral sclerosis (ALS) and Huntington's Disease (HD), respectively (Saxena et al, 2009, Reijonen et al, 2008). Kennedy's Disease is classified as both an MND and CAG-repeat disorder and so this Chapter will investigate the role of ER stress in its underlying pathogenesis. The function of the ER is Ca^{2+}-dependent, with the depletion of ER calcium (Ca^{2+}) resulting in ER stress. This Chapter will therefore establish whether ER Ca^{2+} depletion occurs in KD ventral motoneurons and results in ER stress as early as E13, making it an early disease trigger. The presence of ER stress will also be monitored at various disease stages in order to further understand its role in KD pathogenesis.

3.1.1 Endoplasmic Reticulum (ER) function and Ca^{2+} dependence

3.1.1.1 Endoplasmic reticulum structure and function

The Endoplasmic Reticulum (ER) is a eukaryotic organelle that is composed of an interconnected network of tubules, cisternae and vesicles. The ER exists as two forms – rough and smooth. The rough ER is studded with ribosomes on its surface, giving the ER a rough appearance and hence its name. Ribosomes are the site at which proteins that are destined for the secretory pathway are synthesized. Indeed, the rough ER is the first cellular compartment that is involved in the secretory pathway. In general terms, its function is to process nascent membrane and secretory proteins, ensuring that they are folded correctly. The smooth ER however, which lacks ribosomes, is the site of synthesis of steroids, cholesterol and other lipids.

The ER is often considered to be the point of protein 'quality control' in cells – proteins that are not folded correctly do not progress to the next stage of the secretory pathway – the Golgi complex. Protein folding is relatively easy to disrupt, and it is often impaired in diseases. In order to understand why protein folding is so easily disrupted, an

appreciation for the thermodynamics and kinetics of protein folding in the ER is needed.

Different protein conformations have a different amount of free energy. The 'native' conformation of a protein is the conformation, which possesses the lowest amount of free energy (Dobson et al, 1998). This conformation is determined by the amino acid sequence of the protein. Therefore, disease-related mutations that result in changes in amino acid sequences will alter the native conformation of the protein.

Another reason why protein folding can be easily disrupted is because it occurs at a relatively fast pace. Small proteins are folded in less than 50 μset al, whilst mRNA translation is much slower, at 4-6 amino acids per second (Mayor et al, 2003). This means that for relatively long periods of time, preceding amino acid residues in the ER are kept in a folding-competent state until more residues can be translated and added. This makes the process of protein folding vulnerable to disturbances.

There are also many ways in which the folding capacity of the ER can be compromised. These include ATP depletion, changes in the cell's redox state and glucose deprivation (Kuznetsov et al, 1996, Tsai et al, 1994, Ikesugi et al, 2006). However, the focus of this study will be the way in which depletion of Ca^{2+} from the ER lumen disrupts ER function and results in what is known as 'ER stress'.

3.1.1.2 ER Ca^{2+} homeostasis

A key feature of ER function is that it is Ca^{2+}-dependent (for review see Pachen, 2000). Unlike the cytosol, which, under normal conditions, has a Ca^{2+} concentration of 0.1 μM, the ER has a relatively high level of Ca^{2+}, at approximately 0.3-1 mM (Jafri et al, 1992). Ca^{2+} is essential for protein folding as it participates in poly-peptide electrostatic interactions and is also necessary for the function of various ER chaperone proteins (Ostwald & MacLennan 1974, Roy et al, 1996). ER chaperone proteins are imperative to the protein folding capacity (for review see Ma & Hendershot 2004). As well as

actively promoting protein folding, they bind to unfolded proteins in order to prevent aggregation. The majority of ER chaperones are either members of the Glucose-Regulated Proteins (GRP) family, such as GRP78, otherwise known as Binding immunoglobulin Protein (BiP), or lectin-like proteins such as Calreticulin and Calnexin (Demaurex et al, 2000). These chaperones have a high binding capacity for luminal Ca^{2+} (Milner et al, 1992). Their expression and activity levels are partly determined by ER Ca^{2+} concentration – with decreases in ER Ca^{2+} resulting in increased expression but decreased activity (Vassilakos et al, 1998, Ivessa et al, 1995).

Under normal circumstances the ER tightly regulates luminal levels of Ca^{2+}. It achieves this through receptor channels and pumps in the ER membrane that control the movement of Ca^{2+} into and out of the ER lumen (Verkhratsky 2004). The release of Ca^{2+} from the ER is mediated through two channel receptors; the Inositol trisphosphate (IP_3) receptor and the Ryanodine receptor, whilst the uptake of Ca^{2+} from the cytosol into the ER is mediated by the Sarco/Endoplasmic Reticulum ATPase (SERCA) pump (Verkhratsky 2004). These ER membrane proteins form a dynamic equilibrium that regulates the amplitude and duration of Ca^{2+} signals in the cytosol.

3.1.1.3 ER Ca^{2+} release

Ca^{2+} release from the ER plays a vital role in a variety of signal transduction pathways. The IP_3 receptor is activated by plasma membrane receptors that are coupled to Phospholipase C (PLC), such as Adrenergic, Serotonergic and Cholinergic receptors (Shi et al, 2006, Feng et al, 2001, de Sevilla et al, 2008). PLC stimulation results in the production of the second messenger Inositol Trisphosphate (IP_3), which is required, along with Ca^{2+}, for the activation of IP_3 receptors (Yuan et al, 2005). Ca^{2+} release that occurs as a consequence of IP_3 receptor activation is involved in various processes such as synaptic plasticity and cell proliferation and is therefore essential for normal cellular function (for review see Berridge et al, 2008). Ca^{2+} release from the ER also occurs via the Ryanodine receptor, which is one of the major mediators of Ca^{2+}-

induced Ca^{2+} release (CICR). CICR is the process by which Ca^{2+} triggers the release of further Ca^{2+} from the ER and is essential for excitation of contractile machinery in cardiac and skeletal muscle cells (Collier et al, 2000, Endo 2009).

As well as being a necessary component of signal transduction and normal cell function, the release of Ca^{2+} from the ER can be detrimental to cells and has been suggested to play a role in triggering apoptosis (Nakano et al, 2006). Release of Ca^{2+} via IP_3 receptors for example, has been suggested to result in the release of the pro-apoptotic protein Cytochrome C, from mitochondria, which triggers the apoptotic pathway (Wozniak et al, 2006). This process will be discussed in more detail in Chapter 5.

3.1.1.4 ER Ca^{2+} uptake

Since elevated cytosolic Ca^{2+} can be toxic to cells, a mechanism by which Ca^{2+} is sequestered from the cytosol and into the ER needs to be in place and tightly regulated in order for normal cellular function to be maintained.

The SERCA pump is a 110 KDa ATPase that is present in the ER membrane that actively transports Ca^{2+} ions against a steep concentration gradient into the ER. It exists as various isoforms: SERCA1a and b, SERCA2a-c and SERCA3a-f. These isoforms are tissue specific, with motoneurons expressing the SERCA2b isoform exclusively (Van den Bosch et al, 1999). The SERCA pump lowers cytosolic Ca^{2+} whilst increasing ER Ca^{2+}. Because ER Ca^{2+} levels are a major determinant of cellular Ca^{2+} signals and plasma membrane channel activity (see below), the SERCA pump is a direct modulator of cellular Ca^{2+} signalling.

Under normal circumstances, SERCA2b expression is elevated in response to increased cytosolic Ca^{2+} concentration (Wu et al, 2000), presumably as a defence mechanism by which excess Ca^{2+} is sequestered from the cytosol into the ER. As well as elevated cytosolic Ca^{2+}, SERCA2b pump expression is also elevated downstream of Androgen Receptor (AR) activation (Foradori et al, 2008). For instance, following

treatment of primary hippocampal neurons with the AR ligand, dihydrotestosterone (DHT), SERCA2 expression is up-regulated and consequentially, ER Ca^{2+} levels increase (Foradori et al, 2008).

The SERCA pump can therefore be considered as a modulator of cellular Ca^{2+} signals that sequesters Ca^{2+} from the cytosol resulting in lower cytosolic Ca^{2+} levels and elevated ER Ca^{2+}, both of which are considered to serve a protective function to cells.

3.1.2 Consequences of ER Ca^{2+} depletion

In response to Ca^{2+} depletion – induced ER stress, the ER attempts to tackle both the source of ER stress (Ca^{2+} depletion) and the consequence of ER stress (functional impairment).

3.1.2.1 Store-operated Ca^{2+} influx – ER Ca^{2+} replenishment

Store-operated Ca^{2+} (SOC) influx is a phenomenon that is triggered as a result of ER Ca^{2+} depletion (Parekh et al, 2005). As discussed briefly in Chapter 1 (Section 1.3.5.1), SOC influx can be used to confirm the occurrence of ER Ca^{2+} depletion. Investigating SOC influx in greater detail can reveal more information about the mechanism by which the ER attempts to tightly regulate levels of Ca^{2+}.

The concept of SOC influx is relatively new and the precise mechanism by which it occurs has yet to be widely accepted. The proposed mechanism is shown in Figure 3.1. Despite the concept being relatively new, the key proteins that are involved in the process have been identified (as discussed briefly in Chapter 1). The key ER-associated protein that has been identified is Stromal Interacting Molecule 1 (STIM1), which is responsible for sensing the depletion of luminal Ca^{2+} (Williams et al, 2001). STIM1 is anchored to the ER via a single transmembrane domain and possesses key regions that have vital functions in the execution of SOC influx. The EF hand for example, which refers to a Ca^{2+}-binding motif composed of two helices – E and F, faces the ER lumen, is responsible for sensing the depletion of Ca^{2+} (Zhang et al,

2005), whilst the alpha-motif domain, which is referred to as SAM (Sterile Alpha Motif), appears to have a role in the oligomerization of STIM1 monomers – a key event in SOC influx (Cai 2007). Upon oligomerization, STIM1 has been shown to translocate to punctuate areas of the plasma membrane (Rao et al 2010). This is made possible by the fact that STIM1 contains microtubule plus ends, which associate with the microtubule end–binding protein, EB1 (Grigoriev et al, 2008). Translocation of STIM1 then leads to the dimerization of proteins in the plasma membrane, which consequentially form functional Ca^{2+} channels through which Ca^{2+} influx can occur (Kiviluoto et al, 2011). The suggested plasma membrane protein component of this pathway, which has been identified using RNAi screening, is Orai1 (Feske et al, 2006). Orai1 channels do not appear to bear any structural similarity to other Ca^{2+} channels. For example, there is evidence, which suggests that, unusually, both the N and C terminal are cytoplasmic. Many findings indicate that Orai1 is still the strongest SOC channel candidate (for review see Authi 2009). For example, co-expression of Orai1 and STIM1 in HEK293 cells produced a SOC entry current that was 10-100 times greater than the current observed in non-transfected cells (Peinelt et al, 2006). Furthermore, Orai1 is able to act as a Ca^{2+} channel despite its unusual structure. For instance, a point mutation (glutamate to alanine) near the extracellular emergence of the first transmembrane region of the protein, gives rise to non-functional channels (Yeromin et al, 2006). Furthermore, channel activity was selectively altered when the mutation made was more conservative – indicating that Orai1 forms a pore that permits Ca^{2+} entry (Prakriya et al, 2006).

As well as Orai1, Transient Receptor Potential (TRP) channels have also been identified as a possible candidate for the plasma membrane component of SOC influx (Perez et al, 2003), since they possess features that resemble those of the SOC influx channel, such as current, amplitude and latency (Perez et al, 2003).

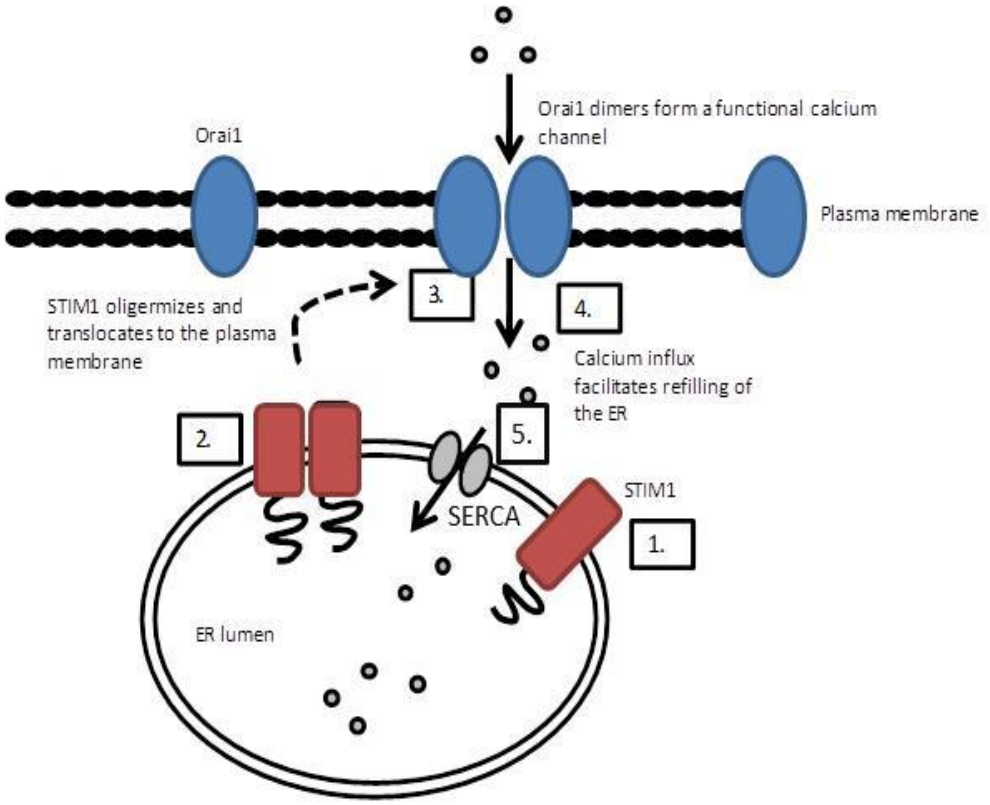

Figure 3.1: Proposed mechanism for Store-Operated Ca2+ (SOC) influx

Although the mechanism by which SOC influx occurs has yet to be established, the most accepted mechanism at present is summarized in the diagram below. Depletion of Ca^{2+} from the ER lumen is sensed by the luminal EF hands of STIM1 (1). This results in the oligomerization of STIM1 monomers (2). This then leads to the translocation of the STIM1 oligomer to punctate areas of the membrane that are associated with the protein Orai1 (3). Orai 1 monomers can then dimerize and in doing so form functional Ca^{2+} channels that permit Ca^{2+} entry in the cell (4). As a result, cytosolic Ca^{2+} levels increase, which facilitates refilling of the ER (5).

Indeed, the inhibition of TRPC (the C isoform of the TRP channel) channel transcription by the introduction of antisense TRP sequences results in a dramatic decrease in SOC influx (Zhu et al, 1996). Inhibition of TRPC4 (isoform 4 of TRPC) transcription produces the same results, suggesting that TRPC4 is the main TRPC homologue that contributes to SOC influx (Phillip, et al, 2000). However, the fact that SOC influx is not *completely* inhibited suggests that other channels may also be involved. Furthermore, Orai1 silencing appears to *completely* inhibit SOC influx, at least in vascular smooth muscle cells, although TRPC4 silencing has no observable effect (Potier et al, 2009). These findings make Orai1 a stronger candidate for the predominant plasma membrane component of SOC influx.

3.1.2.2 The Unfolded Protein Response

In conditions of ER stress the Unfolded Protein Response (UPR) is activated (for review see Lai et al, 2007). The UPR is a well conserved homeostatic mechanism that consists of three converging pathways, all of which attempt to restore ER function. The three pathways are activated sequentially (Figure 3.2), beginning with the dissociation of Binding immunoglobulin Protein (BiP), from the ER membrane protein Pancreatic ER Kinase–like Kinase (PERK), which is the first of three core stress transducers of the UPR. Dissociation of BiP from PERK results in the phosphorylation of eukaryotic Initiating Factor 2α (eIF2α). This results in the arrest of global protein translation, which alleviates the protein load of the ER. UPR proteins however, are exempt from this translation arrest and the translation and translocation of Activating Transcription Factor 4 (ATF4) into the nucleus follows. Upon translocation of ATF4 to the nucleus, the transcription of genes encoding both pro-survival and pro-apoptotic proteins occurs.

The second UPR pathway to be activated begins with the dissociation of BiP from another UPR transducer in the ER membrane – Activating Transcription Factor 6 (ATF6). Upon dissociation of BiP, ATF6 is cleaved in the Golgi complex, resulting in liberation of the transcriptionally active domain of the protein (Lai et al, 2007).

Figure 3.2: The Unfolded Protein Response (UPR)

The diagram below summarizes the UPR pathway. Following the aggregation of unfolded proteins, BiP dissociates from three different ER stress receptors and in doing so triggers three different, yet converging pathways. Following dissociation of BiP from Pancreatic ER Kinase (PERK) (1), eIF2α is phosphorylated (2) and global translation is inhibited. ATF4 is exempt from this translational block and is therefore translated. ATF4 translocates to the nucleus and activates the transcription of pro-survival genes, required to restore ER homeostasis, as well as pro-apoptotic genes. (3)The second ER stress receptor from which BiP dissociates is activating transcription factor 6 (ATF6). This dissociation leads to the cleavage of ATF6 (4) and its subsequent translocation to the nucleus, where it also activates the transcription of both pro-survival and pro-apoptotic genes. (5) The final ER stress receptor to be activated is Inositol-requiring enzyme 1 (IRE1). This leads to splicing of X box-binding protein 1 (XBP1), which then translocates to the nucleus leading to the transcription of more proteins required to restore ER function and degrade misfolded proteins (6). $P58^{IPK}$ is also transcribed downstream of IRE1 activation and provides negative feedback for the PERK pathway of the UPR by preventing eIF2α phosphorylation (7).

Thus all three sequentially activated pathways converge to restore the function of the ER by decreasing the load of the ER and by enhancing the capacity of the cell to restore ER function and degrade misfolded proteins.

Figure 3.2

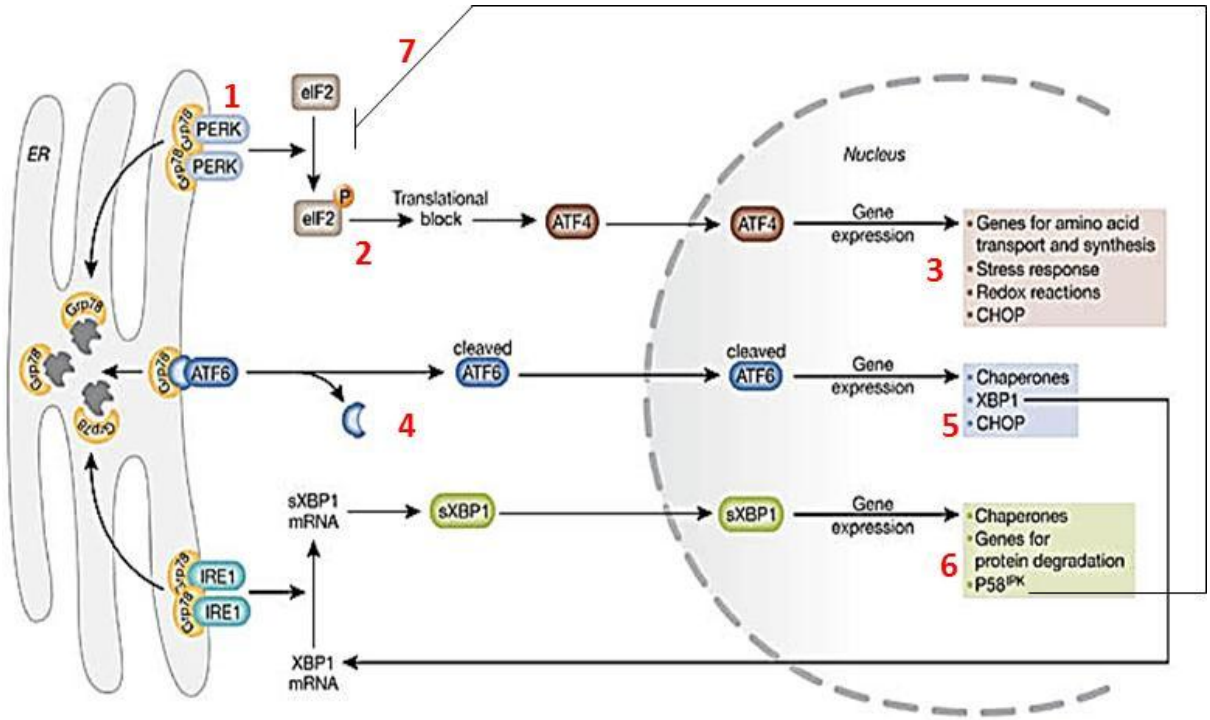

Adapted from 'Mediators of endoplasmic reticulum stress-induced apoptosis'. Eva Szegezdi et al (2006).

Cleaved ATF6 then translocates to the nucleus, which leads to the transcription of a variety of proteins that aid ER function restoration such as Chaperone proteins and X-box binding protein 1 (XBP1). XBP1 is spliced as part of the third pathway of the UPR (Lai et al, 2007). This third pathway involves the ER membrane protein Inositol-Requiring enzyme 1 (IRE1). Upon dissociation of BiP from IRE1, it mediates the splicing of XBP1. Spliced XBP1 then translocates to the nucleus and activates the transcription of chaperone proteins and proteins involved in protein degradation. $P58^{IPK}$ is also transcribed and down-regulates eIF2α activity (Huizen et al, 2003). The third UPR pathway therefore provides negative feedback that regulates activity of the PERK pathway of the UPR.

As well as increasing the expression of chaperone proteins, the UPR also controls ER-associated degradation (ERAD), which degrades misfolded polypeptides that cannot be processed by the ER (Lai et al, 2007). In general terms, ERAD involves dislocation of the misfolded poly-peptide from the ER to the cytosol, where it undergoes proteolysis as part of the ubiquitin-proteasome system (Meusser et al, 2005).

Thus the three pathways activated as part of the UPR have the convergent effects of reducing the rate of protein synthesis and increasing the transcription of genes that encode proteins involved in the UPR, protein handling and protein degradation (Lai et al, 2007, Szegezdi et al, 2006).

Although the UPR has a protective function, prolonged activation and continuous exposure to conditions that cause ER stress can be detrimental to cell survival, because the UPR also results in the expression of pro-apoptotic proteins. One such protein is CCAAT/enhancer-binding Protein Homologous Protein (CHOP), which is activated downstream of both the PERK and IRE1 pathways of the UPR (Lai et al, 2007). In general terms, CHOP inhibits anti-apoptotic mediators. This process is discussed in more detail below (Section 3.1.4.4). CHOP also acts as a feedback inhibitor of the phosphorylation of eIF2α as it activates expression of GADD34, which

directs the protein phosphatase PP1 to eIF2α thus dephosphorylating it (Novoa et al, 2001).

Another example of a pro-apoptotic protein that is upregulated as a result of the UPR is the Proapoptotic BH3-only protein, PUMA (Reimertz et al, 2003). Expression of PUMA results in the release of Cytochrome C from the mitochondria as well as activation of Caspase-3 and Caspase-9 (Reimertz et al, 2003). Thus if ER stress is prolonged and the UPR is not arrested, ER stress-induced apoptosis will ensue. This process is discussed in more detail in Chapter 4.

3.1.3 ER stress in neurodegenerative disease

ER stress has been implicated in the pathology of both MNDs and CAG-repeat disorders (Saxena et al, 2009, Reijonen et al, 2008). It has been found to occur pre-symptomatically and is present at symptom onset and progression. Because Kennedy's Disease is both a MND and CAG-repeat disorder, it is therefore likely that ER stress plays a role in the underlying pathology of this neurodegenerative disorder.

3.1.3.1 ER stress and Motor Neuron Disease (MND)

Amyotrophic Lateral Sclerosis (ALS) is the most common form of adult MND (Eisen et al, 1998). It is characterized by the progressive degeneration of spinal and cranial motoneurons. ER stress has been implicated in the pathology of ALS and has been found to occur in mouse models of the disease (Saxena et al, 2009) as well as ALS patient tissue (Atkin et al, 2008), both pre-symptomatically and after symptom manifestation (Saxena et al, 2009).

Several markers of ER stress have been found to increase in motoneurons in a number of mouse models of ALS including BiP, eIF2α, ATF4 and CHOP (Saxena et al, 2009). ER stress has been observed in spinal motoneurons of the G93A mutant SOD1 mouse ($SOD1^{G93A}$) as early as P5, well before symptom onset and motoneuron degeneration (Saxena et al, 2009). These markers are up-regulated in the $SOD1^{G93A}$ mouse spinal

cord in a subset of motoneurons that appear to be more vulnerable to the disease (Saxena et al, 2009). In addition evidence suggests that there is the same correlation between the presence of ER stress and disease progression. For instance, an increase in BiP expression is detected at an early age (P5) in the $SOD1^{G93A}$ mouse, which has a relatively early symptom onset and rapid disease progression, compared to the less aggressive $SOD1^{G85R}$ mouse (Bruijn et al, 1998), in which an abrupt increase in BiP expression is observed in spinal motoneurons just prior to muscle denervation (Saxena et al, 2009).

Markers of ER stress are also found in spinal cord biopsies from ALS patients and correlate well with the findings from mouse models. CHOP expression for example, was found to be higher in ALS patient spinal cord tissue than in control samples, which typically expressed low levels of CHOP (Ito et al, 2009).

In $SOD1^{G93A}$ mice, the presence of the $SOD1^{G93A}$ protein not only results in ER stress but also appears to prevent one of the mechanisms that is protective against ER stress, ER associated degradation (ERAD). The $SOD1^{G93A}$ protein has been found to interact with Derlin-1 and as a result, retro-translocation of the misfolded protein is impaired, thereby preventing ERAD. This leads to ER stress-activation of Apoptosis Signal-regulating Kinase 1 (ASK1), which results in apoptosis (Nishitoh et al, 2008).

To summarize, ER stress appears to play an important and early role in the pathology of ALS. In the $SOD1^{G93A}$ mouse model of ALS ER stress appears to be present as early as P5 and remains throughout disease progression until end-stage, suggesting that ER stress could play a causal role in disease pathology. Furthermore, sharp increases in ER stress marker levels appear to correlate with symptom onset.

3.1.3.2 ER stress and CAG-repeat disorders

As well as ALS, ER stress has also been suggested to play a role in the underlying pathology of CAG-repeat disorders such as Huntington's Disease (HD). In cell lines transfected with mutant N-terminal Huntingtin proteins of varying CAG-repeat lengths,

RT-PCR revealed that levels of BiP, eIF2α and CHOP were greater in cells transfected with the mutant Huntingtin proteins compared to EGFP-transfected controls (Reijonen et al, 2008). Furthermore, the level of BiP appeared to increase with an increasing number of CAG repeats, suggesting a correlation between CAG-repeat number and ER stress. In the same cells, death and protein aggregation were also found to occur. This was counteracted however by the administration of Salubrinal, which inhibits ER stress, suggesting that ER stress has a major role in cell death in this disease model (Reijonen et al, 2008).

As is the case in ALS, expression of the mutant Huntingtin protein also appears to impair ERAD. This has been shown in vitro in both PC12 and striatal cells that were transfected with a mutant Huntingtin protein containing 103 CAG repeats. In these transfected cells, the toxic CAG-expansion mutation appeared to entrap proteins that are vital for ERAD, such as Ufd1 and p97 (Duennwald et al, 2008). Furthermore, application of low levels of Tunicamycin (an ER stressor) affected these cells more than cells containing a control protein with just 25 CAG repeats, suggesting that the presence of the CAG repeat expansion sensitizes the cells to ER stressors (Reijonen et al, 2008).

As well as entrapping proteins involved in ERAD, another way in which the mutant Huntingtin protein has been suggested to inhibit ERAD is by preventing the interaction of ER chaperone proteins with ERAD-associated proteins. For example, the mutant Huntingtin protein was found to interact with BiP and in doing so it is thought to sterically block the interaction between BiP and p97, which is essential for the initiation of ERAD (Yang et al, 2010).

3.1.4 Examination of ER stress markers

A number of markers can be used to investigate ER stress. The experiments in this Chapter will focus on the 'PERK branch' of the UPR and will measure the expression of the markers BiP, phospho-eIF2α, ATF4 and CHOP (Figure 3.3). These markers have

been selected for examination in this study as they have been previously shown to be elevated in both motoneuron diseases and CAG-repeat disorders (as discussed in Section 3.1.3), and represent various UPR events.

3.1.4.1 BiP

Since BiP senses misfolded proteins, it represents the first event involved in signal transduction in response to ER stress. BiP consists of an N-terminal ATPase and a C-terminal substrate binding domain (Chevalier et al, 1998). The ADP-bound form of BiP has a high affinity for protein substrates. Upon binding of proteins to BiP, the proteins become locked in their current conformation and the ATPase activity of BiP is activated. When ADP is exchanged with ATP, the protein is released from BiP. ATP hydrolysis occurs subsequently and BiP again exists in its ADP-bound, high protein affinity form. Thus BiP undergoes a constant protein binding-unbinding cycle in which it is very sensitive to changes in protein conformation (Chevalier et al, 1998).

BiP resides in the ER as both monomeric and oligomeric forms (Freiden et al, 1992). The monomeric form is suggested to interact with unfolded proteins in the ER, whilst the oligomeric form, is suggested to be subject to posttranslational modification, such as phosphorylation (Freiden et al, 1992). Oligomeric BiP is suggested to form a BiP 'storage pool' in the ER from which monomeric BiP is recruited (Zu et al, 2005).

3.1.4.2 Phosphorylated eIF2α

eIF2α is a 65 kDa translation initiation factor protein that is present in the cytosol (Kimball 1999). It functions by forming a ternary complex with both initiator tRNA and GTP (Fels & Koumeris 2006). This complex binds to the 40s ribosome subunit followed by the binding of mRNA. As a result, a 43S pre-initiation complex is formed, which moves along mRNA towards to 3' end in order to find the start codon and commence translation.

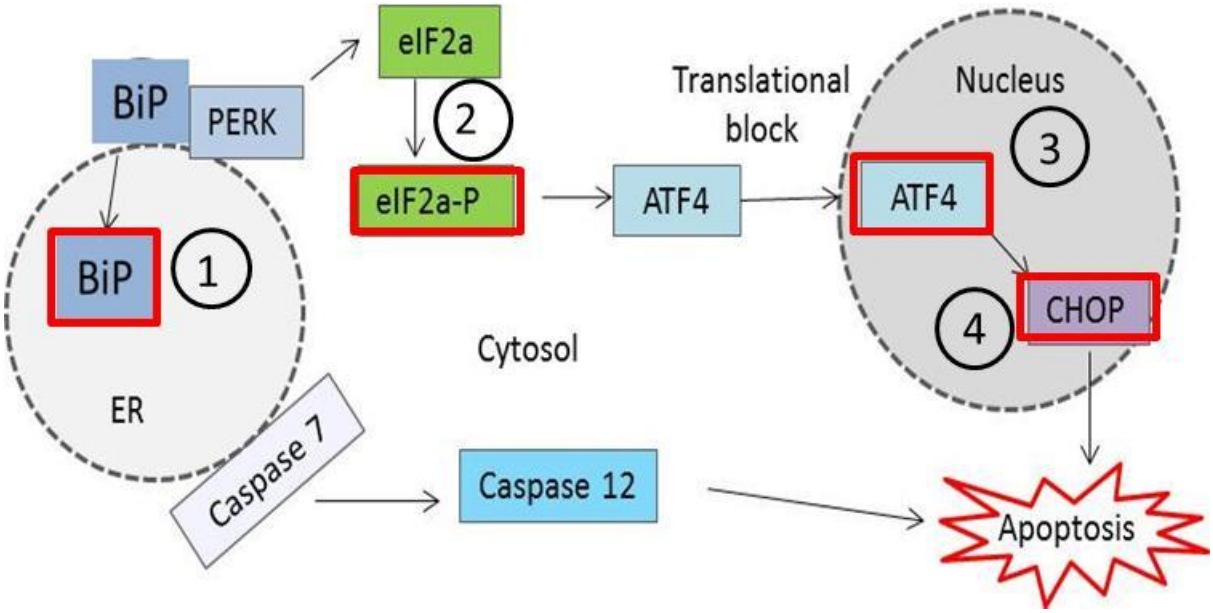

Figure 3.3: The PERK branch of the UPR

The PERK branch of the UPR has been shown to be elevated in other MNDs and CAG-repeat disorders. The diagram illustrates this pathway and highlights the markers that are examined in the experiments described in this thesis (red boxes). They include: 1) BiP, a misfolded protein sensor that is transcribed downstream of the PERK branch of the UPR; 2) phospho-eIF2α, a marker of translational arrest; 3) ATF4, a transcription factor that is exempt from global arrest; and 4) CHOP, a pro-apoptotic marker that is transcribed downstream of ATF4.

Conversion of the 43S complex into the 80S complex, which is required for completion of translation, requires hydrolysis of GTP that is bound to eIF2α (Fels & Koumeris 2006). This GDP/GTP exchange allows eIF2α to be recycled between different rounds of translation. What prevents this recycling, and hence inhibits translation, is the phosphorylation of eIF2α at its serine 51 residue by various kinases such as PERK (Fels & Koumeris 2006). By measuring the levels of phospho-eIF2α specifically, the occurrence of PERK activation and subsequent translation inhibition in response to ER stress can be inferred.

3.1.4.3 ATF4

Although global translation is inhibited by the phosphorylation of eIF2α, the translation of ER stress response genes is *elevated*. One of these genes is Activating Transcription Factor 4 (ATF4). ATF4 is a member of the cAMP responsive element binding protein (CREB) family and is a transcription factor that translocates into the nucleus following translation (Steiger et al, 2004). Upon entering the nucleus ATF4 forms a complex with its nuclear co-activator, phosphorylated CREB1, and binds to the promoter sequences of a variety of pro-survival and pro-apoptotic genes including BiP and CHOP, respectively. Measuring levels of ATF4 therefore represents the transduction of ER stress into changes in gene transcription.

3.1.4.4 CHOP

CHOP, also known as GADD53, is a transcription factor that is activated downstream of various events of ER stress such as ATF4 translation. The elevated expression of CHOP can be indicative of the initial ER stress-induced apoptosis and therefore is the connection between prolonged activation of the UPR and apoptosis. Indeed, deletion of the CHOP protein is enough to protect cells against Tunicamycin treatment, which normally results in ER stress-induced apoptosis (Marciniak et al, 2004).

One way in which CHOP results in cell death is via the down-regulation of the anti-apoptotic protein, B-cell lymphoma 2, or Bcl2 (Yamaguchi and Wang 2004). CHOP transcription also leads to the induction of the tribbles ortholog 3 (TRB3) protein, which is thought to bind to a serine/threonine-specific protein kinase referred to as Akt. This prevents the phosphorylation of Akt, which in turn prevents its anti-apoptotic actions (Ohoka et al, 2005).

Measuring CHOP is useful because in combination with the above ER stress markers, it gives an indication of the balance between the expression of pro-survival and pro-apoptotic proteins that are transcribed downstream of the UPR.

3.2 Results

3.2.1 Summary

In this Chapter Wild-Type (WT) and KD primary E13 motoneuron cultures were prepared and changes in cytosolic Ca^{2+} in response to pharmacological agents were determined using confocal microscopy in order to establish if ER Ca^{2+} depletion was present in KD motoneurons. In addition, markers of ER stress were examined in vitro and in spinal cords from WT and KD mice at various stages of disease. These stages include postnatal day 5 (P5), 3, 12 and 18 months of age. These ages represent, respectively, the earliest time point at which ER stress has been detected in the $SOD1^{G93A}$ model of ALS (Saxena et al, 2009); a pre-symptomatic stage; the time of symptom onset; and disease end stage.

Throughout this thesis four experimental groups are examined:

1) Untreated WT motoneurons
2) 72 hour DHT-treated WT motoneurons
3) Untreated KD motoneurons
4) 72hour DHT-treated KD motoneurons

These four groups are used to model affected males (DHT-treated KD motoneurons) and unaffected females (untreated KD motoneurons) as well as non-disease controls (untreated and treated WT motoneurons).

3.2.2 Fluo 4-AM fluorescence remains stable during the recording period

Prior to carrying out any experiments it was important to establish whether or not the fluorescence intensity of Fluo 4-AM changes during the recording period independently of pharmacological manipulation e.g. due to dye leakage or photobleaching, which would produce confounding results.

In order to control for this, the fluorescence of Fluo 4-AM was measured over a period of 10 minutes – twice the length of time of the recording period used in the protocol in this study. As shown in Figure 3.4 over the course of 10 minutes there is no significant change in fluorescence. This observation is reproducible (n = 30, from 3 different cultures).

3.2.3 50 nM DHT does not affect normal Ca^{2+} handling in motoneurons

The basal cytosolic Ca^{2+} level in WT motoneurons was assessed following treatment of cultures for 72 hours with a range of DHT concentrations (Figure 3.5).

The results indicate that there is a negative correlation between the concentration of DHT applied and basal cytosolic Ca^{2+} concentration. When cells are treated with 0.1 nM DHT, the average basal cytosolic Ca^{2+} concentration is approximately 580 nM (+/- 26.8 nM SEM, n=7). This then decreases to 500 nM (+/- 29.4 nM SEM, n=6) after 72 hour treatment with 1 nM. The average basal Ca^{2+} levels decrease further to approximately 420 nM (+/- 29.0 nM SEM, n=8) when cultures are treated with 10 nM DHT and the basal concentration then levels off at approximately 250 nM (+/- 22.3 nM SEM, n=5) following treatment with 50 nM DHT.

3.2.4 Motoneuron Ca^{2+} handling

3.2.4.1 Basal cytosolic Ca^{2+} in primary KD motoneurons

3.2.4.1.1 Cytosolic Ca^{2+} in a Ca^{2+}-free recording medium

As shown in Figure 3.6A, when cultures are imaged in a Ca^{2+}-free medium there is very little difference in cytosolic Ca^{2+} levels between the WT and KD motoneurons. The highest basal cytosolic Ca^{2+} is found in DHT-treated KD motoneurons, which have a mean concentration of 110 nM (+/- 5.59 nM SEM, n=35).

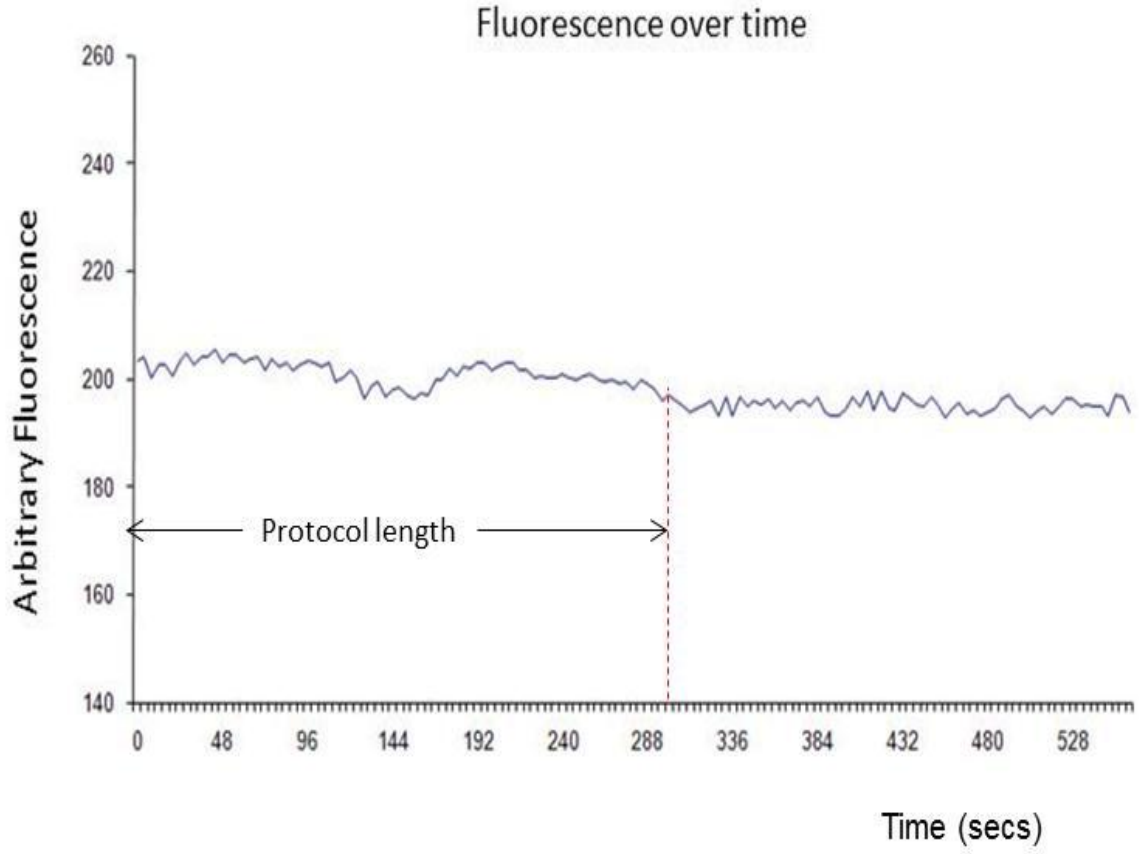

Figure 3.4: Fluo 4-AM fluorescence does not change during the protocol

At 7 days in vitro (DIV) primary motoneurons were incubated with Fluo 4-AM for 30 minutes at 37^{o}C. Cultures were then imaged for at least 10 minutes in the absence of any pharmacological manipulation. The fluorescence of selected motoneurons was measured and background fluorescence deducted. A representative trace of recordings during the 10 minute period is shown here. There is no change in Fluo 4-AM fluorescence over time. This finding is reproducible (n = 30 motoneurons from 3 different cultures).

Figure 3.5: DHT reduces basal cytosolic [Ca^{2+}] in WT motoneurons

Primary WT motoneuron cultures were treated at 4 DIV with a range of concentrations of DHT between 0.1 nM – 50 nM. Cultures were incubated with Fluo 4-AM at 7 DIV and baseline fluorescence in selected motoneurons was obtained. Ionomycin was then applied to obtain a maximum fluorescence value for calibration purposes. Background fluorescence was deducted and the resulting fluorescence values were converted into basal cytosolic Ca^{2+} concentrations. The average basal Ca^{2+} concentration was calculated by taking the average of all values prior to Ionomycin application. The schematic diagram (A) illustrates this procedure.

There is a negative correlation between basal Ca^{2+} concentration and DHT concentration as shown in the graph (B) so that as the concentration of DHT is increased, the level of cytosolic Ca^{2+} decreases.

(Error Bars = standard error of mean)

Figure 3.5

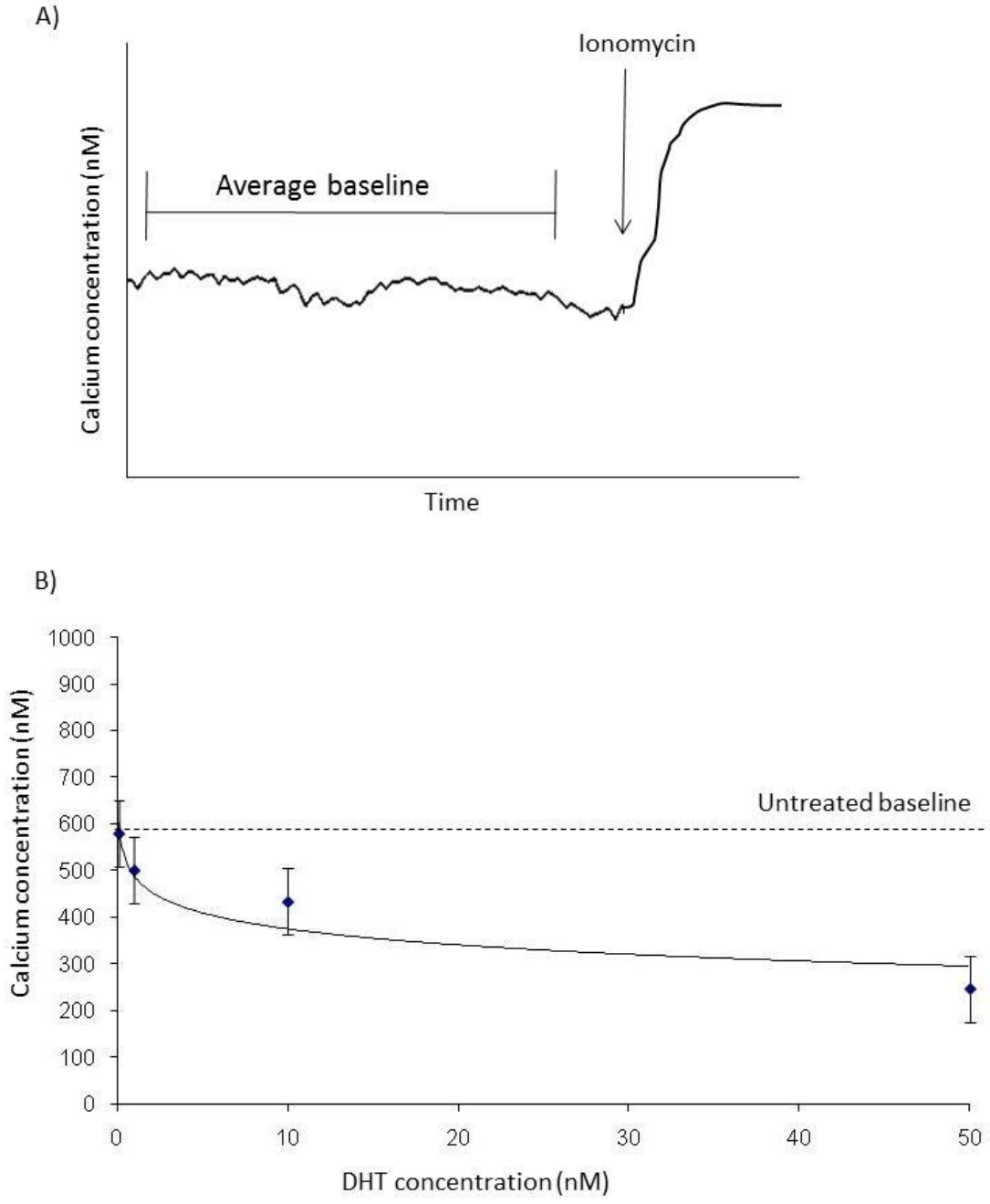
A)
Ionomycin
Average baseline
Calcium concentration (nM)
Time
B)
1000
900
800
700
600
500
400
300
200
100
0
Untreated baseline
Calcium concentration (nM)
0
10
20
30
40
50
DHT concentration (nM)

The lowest level of basal cytosolic Ca^{2+} however is found in DHT-treated WT motoneurons, which have a Ca^{2+} concentration of 97 nM (+/- 4.67 nM SEM, n=31). There is only a negligible difference of 3 nM in the average basal cytosolic Ca^{2+} concentration between untreated WT and untreated KD motoneurons, which have a Ca^{2+} concentration of 100 nM (+/- 2.12 nM SEM, n=32) and 103 nM (+/- 6.43 nM SEM, n=28), respectively.

3.2.4.1.2 Cytosolic Ca^{2+} in a 1 μM Ca^{2+} recording medium

As shown in Figure 3.6B, when cultures are imaged in a recording medium containing 1 mM Ca^{2+}, the highest cytosolic Ca^{2+} level is present in DHT-treated KD motoneurons, which have an average concentration of 275 nM (+/- 7.60 nM SEM, n=35). The lowest level of cytosolic Ca^{2+} is present in DHT-treated WT motoneurons, which have an average concentration of 110 nM (+/- 7.18 nM SEM, n=31). The difference between DHT-treated WT and DHT-treated KD motoneurons is significant (p= 0.002). There is also a significant difference (p=0.02) between untreated WT and untreated KD motoneurons, which have an average basal cytosolic Ca^{2+} concentration of 130 nM (+/- 3.71 nM SEM, n=32) and 240 nM (+/- 6.43 nM SEM, n=28), respectively.

3.2.4.2 Inferred ER Ca^{2+} in KD motoneurons

ER Ca^{2+} levels are inferred by treating the cultures with Thapsigargin (TG), which causes the release of Ca^{2+} from the ER lumen into the cytosol, where changes in cytosolic Ca^{2+} can be determined.

3.2.4.2.1 Average ER Ca^{2+} values in motoneurons

The lowest level of inferred ER Ca^{2+}, as indicated by the lowest rise in cytosolic Ca^{2+} following TG application, is observed in DHT-treated KD motoneurons, which have an TG-induced increase in cytosolic Ca^{2+} of 10 nM (+/- 5.07nM SEM, n=35).

Figure 3.6: Basal cytosolic Ca^{2+} concentration in WT and KD primary motoneurons

Primary WT and KD motoneuron cultures were imaged at 7 DIV. Cultures were either left untreated or were treated with 50 nM DHT at 4 DIV. Cultures were incubated at 37^{o}C with Fluo 4-AM, diluted in a 1 mM Ca^{2+} recording medium, prior to imaging. After 30 mins of incubation cultures were washed with, and subsequently imaged in, recording medium. In some cases however, cultures were imaged in a Ca^{2+}-free recording medium to ensure that there was no extracellular source of Ca^{2+}. In all cases cultures were kept at 37^{o}C throughout the protocol. The Bar Charts summarize basal cytosolic Ca^{2+} in untreated and DHT- treated WT and KD motoneuron cultures in the absence of external Ca^{2+} (A) and in medium containing 1 μM Ca^{2+} (B).

(Error Bars = standard error of mean)

Figure 3.6

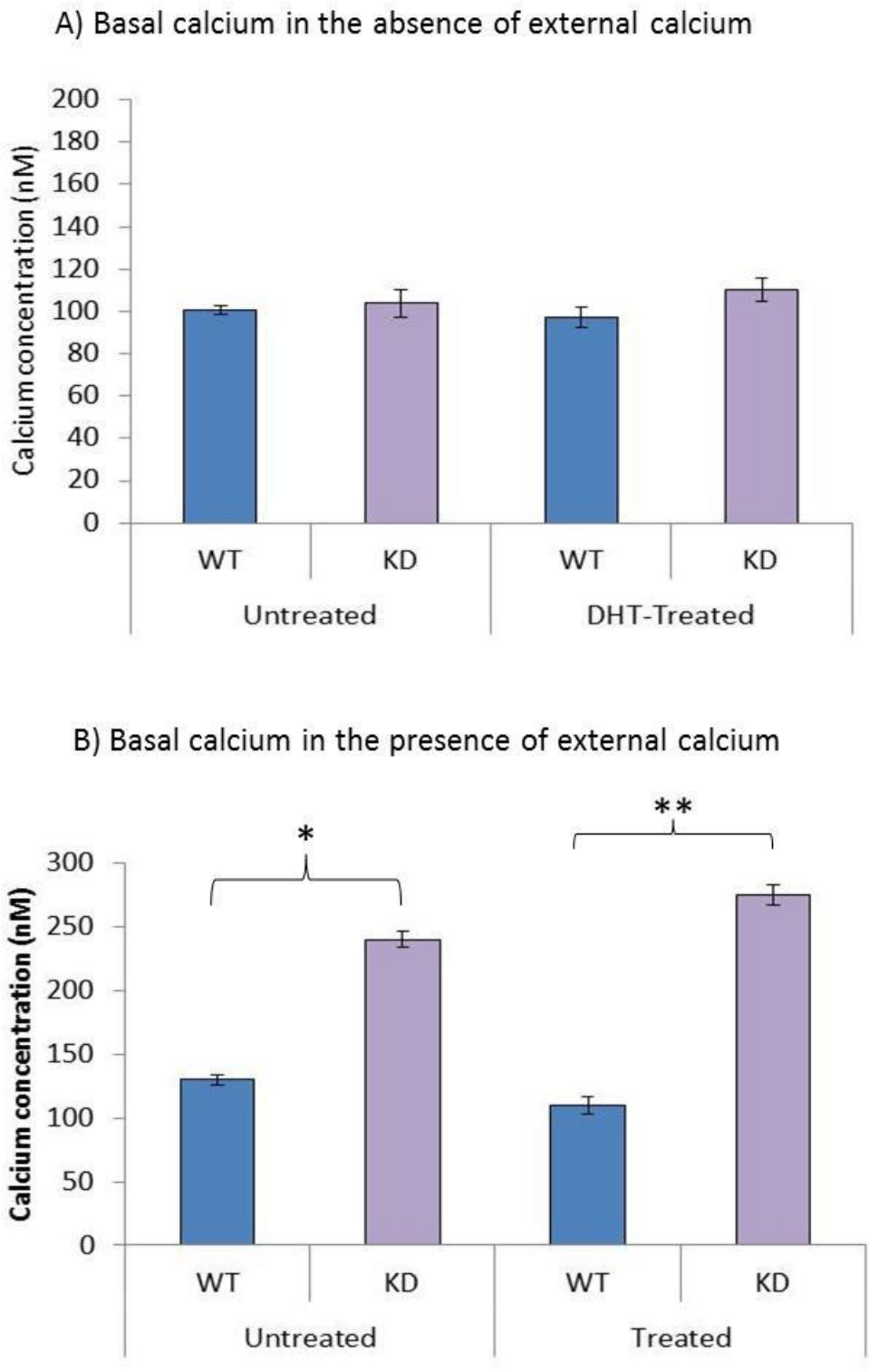

* P < 0.05
*** p < 0.005

This is significantly lower (p=0.002) than the response observed in DHT-treated WT motoneurons, which have the highest level of TG-induced increase in cytosolic Ca^{2+} at 140 nM (+/- 3.41 nM SEM, n=31). Thus steady state ER Ca^{2+} appears at least an order of magnitude lower in DHT-treated KD motoneurons than in DHT-treated WT controls (Figure 3.7). In the absence of DHT, there is only a 2.5 nM difference in TG induced increase in the cytosolic Ca^{2+} concentration between WT and KD motoneurons, (60nM (+/- 5.30 nM SEM, n=32) and 57.5 nM (+/- 4.82 nM SEM, n=28), respectively).

3.2.4.2.2 Effects of DHT treatment on ER Ca^{2+} levels

In WT motoneurons, DHT treatment causes an increase in inferred ER Ca^{2+} of 60 nM and in KD motoneurons DHT causes a decrease of approximately 40 nM (Figure 3.7).

3.2.4.2.3 The kinetics of changes in cytosolic Ca^{2+} in response to TG treatment

Examination of the TG-induced cytosolic Ca^{2+} response reveals a difference in the response kinetics between WT and KD motoneurons (Figure 3.7Ai & Aii). The Ca^{2+} response to TG appears to be of similar onset latency in WT and KD motoneurons, regardless of whether or not they have been treated with DHT. In all cases, the response to TG application is immediate and reaches a peak within 40-50 seconds. However, in WT motoneurons (both untreated and DHT-treated), the response to TG is more prolonged than the response in KD motoneurons and cytosolic Ca^{2+} only falls to a negligibly lower concentration than the peak TG-induced response during the protocol. In KD motoneurons, the response to TG appears to have more of a transient nature and the level of Ca^{2+} falls by 10 nM in the case of untreated KD motoneurons, and back to basal levels in the case of DHT-treated KD motoneurons, within 130 seconds.

Figure 3.7: Inferred ER Ca^{2+} levels in WT and KD motoneurons

ER Ca^{2+} can be inferred by the rise in cytosolic Ca^{2+} that occurs following drug-induced ER Ca^{2+} depletion in a Ca^{2+}-free recording medium. Removal of external Ca^{2+} ensures that any elevation in cytosolic Ca^{2+} can only be the result of Ca^{2+} release from the ER. Following determination of basal Ca^{2+} in a Ca^{2+}-free medium, ER Ca^{2+} depletion was induced by treatment with Thapsigargin and the resultant increase in cytosolic Ca^{2+} was measured. A value for inferred ER Ca^{2+} was calculated by taking an average of the Ca^{2+} concentration values at ten time points around the peak of the response. The traces shown in A & B show the typical response to TG treatment in untreated (Ai) and DHT-treated (Aii) cultures. These traces illustrate the kinetics of this response and show that although the onset of the TG-induced response is similar in WT and KD motoneurons, the response is relatively prolonged in WT motoneurons and of a more transient nature in KD motoneurons. The Bar Chart (B) summarizes the mean elevation in cytosolic Ca^{2+} in response to TG (inferred ER Ca^{2+}) in untreated and DHT-treated WT and KD motoneurons.

(Error Bars = standard error of mean)

Figure 3.7

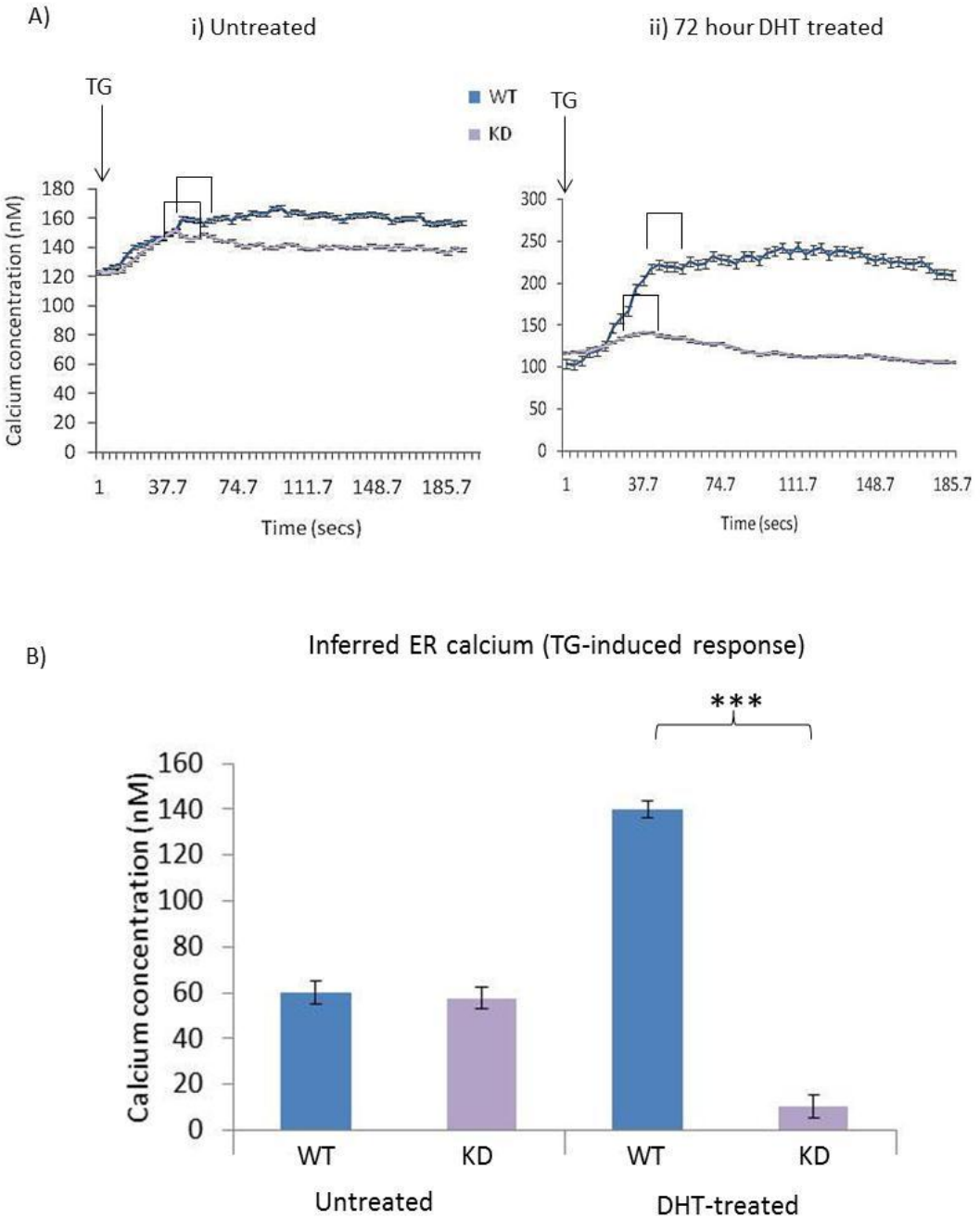

*** $p < 0.005$

3.2.4.3 Inferred Store-operated Ca^{2+} influx in WT and KD motoneurons

3.2.4.3.1 Average values of inferred SOC influx in WT and KD motoneurons

Traces illustrating the typical store-operated Ca^{2+} (SOC) influx in WT and KD motoneurons (+/-DHT) are shown in Figures 3.8Ai (WT) and 3.8Aii (KD). SOC influx can be inferred from the increase in cytosolic Ca^{2+} that occurs following introduction of Ca^{2+} into the recording medium following treatment with TG. As shown in Figure 3.8C, the highest level of SOC influx is observed in DHT-treated KD motoneurons at 1.3 μM (+/- 34.63 nM SEM, n=35). This is significantly higher (p=0.027) than the level observed in DHT-treated WT motoneurons, which have the lowest inferred level of SOC influx at approximately 300 nM (+/- 34.11 nM SEM, n=31).

3.2.4.3.2 Effects of DHT treatment on SOC influx

DHT treatment appears to have opposing effects on WT and KD motoneurons (Figure 3.8B). In KD motoneurons, DHT treatment results in a significant increase in SOC influx of approximately 350 nM (p=0.0012). In WT motoneurons however, DHT treatment results in a significant decrease in SOC influx of 400 nM (p=0.05).

3.2.4.3.3 The kinetics of cytosolic Ca^{2+} changes in response to Ca^{2+} introduction

The traces showing the responses to Ca^{2+} introduction into the recording medium reveal that both DHT treatment and genotype affect the response kinetics (Figure 8A & B). In both genotypes DHT treatment increases the rate at which the peak Ca^{2+} response is achieved. In untreated cultures, the peak Ca^{2+} concentration is reached 20-40 seconds following Ca^{2+} introduction. However, following DHT treatment, the peak concentration is reached within 15 seconds of Ca^{2+} introduction.

The nature of SOC influx is more transient in WT motoneurons than in KD motoneurons. Cytosolic Ca^{2+} does not decrease back to the level it was prior to Ca^{2+} introduction in the time frame of the experiment for either genotype, although it decreases more substantially in WT motoneurons than KD motoneurons.

Figure 3.8: Inferred Store-Operated Ca^{2+} (SOC) influx in WT and KD motoneurons.

SOC influx can be inferred by the increase in cytosolic Ca^{2+} following TG application and subsequent Ca^{2+} introduction into the recording medium. By controlling the time point at which external Ca^{2+} is available, the occurrence of SOC influx can be isolated and measured. Typical traces of the inferred SOC influx (changes in cytosolic Ca^{2+} in response to Ca^{2+} introduction to the medium) are shown in Ai) and Aii), in the absence and presence of DHT, respectively. A value for inferred SOC influx was calculated by taking an average of the Ca^{2+} concentration values at ten time points around the peak of the response. The Bar Chart (B) summarizes differences between untreated and DHT-treated WT and KD motoneurons with respect to SOC influx.

(Error Bars = standard error of mean)

Figure 3.8

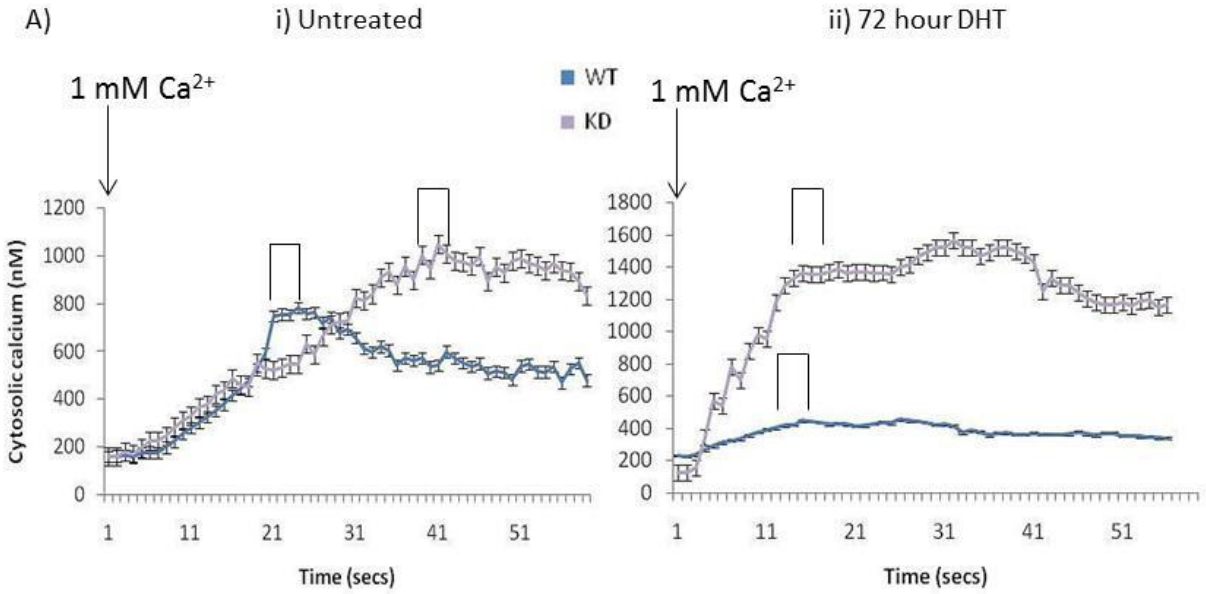

B)

Inferred SOC influx (change in cytosolic calcium in response to calcium introduction)

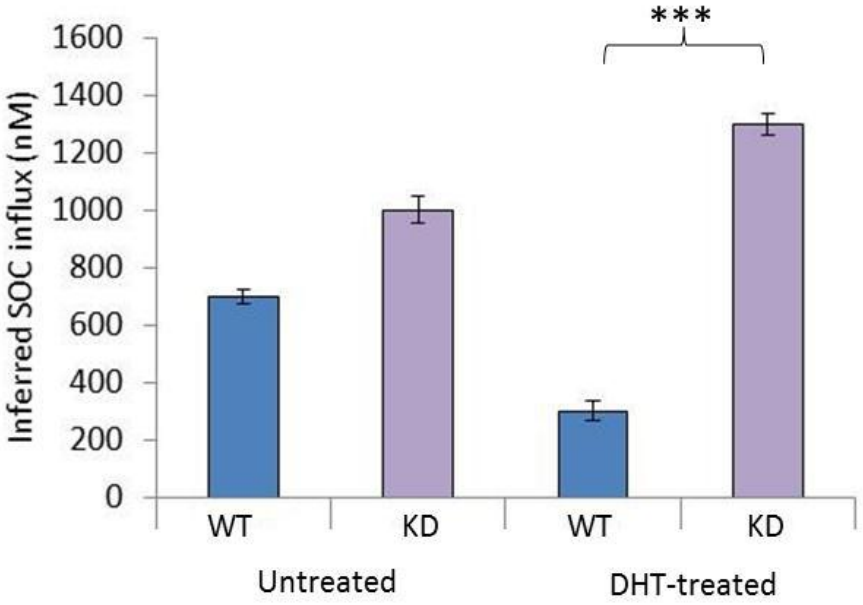

*** $p < 0.005$

3.2.5 Examination of Ca^{2+} handling in motoneurons of male and female embryos.

Because KD symptoms manifest exclusively in males, it is important to determine whether or not the differences in Ca^{2+} handling observed in motoneurons are due to androgen availability or inherent differences in AR expression in motoneurons. The same protocol was therefore carried out in DHT-treated motoneurons that had been cultured from spinal cords of identified male and female embryos (Figure 3.9).

Measurement of basal Ca^{2+}, inferred ER Ca^{2+} and inferred SOC influx showed that there is only a negligible difference in Ca^{2+} handling between motoneurons of different sex but the same genotype.

In the case of basal cytosolic Ca^{2+}, both male and female WT motoneurons have an average concentration ranging between 200-210 nM (n=25 and 29, respectively). Both male and female KD motoneurons however, have an average concentration in the range of 450-490 nM (n=22 and 26, respectively).

The same trend is apparent when measuring inferred ER Ca^{2+} (Figure 3.9B) and SOC influx (Figure 3.9C). Again, there is only a negligible difference between motoneurons of different sexes and the same genotype.

Finally, the same trend is apparent for inferred SOC influx (Figure 3.9C). In this case there appears to be a slightly greater difference between male and female KD motoneurons, although this difference is not significant.

3.2.6 Fura 2 control experiments

In order to ensure that measurements of Ca^{2+} handling determined using Fluo 4-AM as the Ca^{2+} indicator were reliable, a short series of control experiments were undertaken using Fura 2 as an alternative Ca^{2+} indicator (see Figure 3.10). When the experiment performed in Section 3.3.4 is carried out using Fura 2 as the cytosolic Ca^{2+} indicator instead of Fluo 4-AM, the same pattern of results is apparent (Figure 3.10).

Figure 3.9: Ca^{2+} handling in male and female motoneurons

Measurements of basal cytosolic Ca^{2+}, inferred ER Ca^{2+} and SOC influx were obtained in DHT-treated WT and DHT-treated KD motoneurons that had been cultured from specific male and female embryos. By comparing male and female motoneurons in the presence of DHT, any inherent differences in the AR due to the CAG repeat expansion would be revealed. Because KD symptoms manifest exclusively in males, it is important to establish whether or not this is due to an inherent difference in the AR, or due to the difference in androgen availability. The results shown in the Bar Charts reveal that there is only a negligible difference between male and female WT, and male and female KD motoneurons with respect to basal cytosolic Ca^{2+} (A), inferred ER Ca^{2+} (B) and SOC influx (C).

(Error Bars = standard error of mean)

Figure 3.9

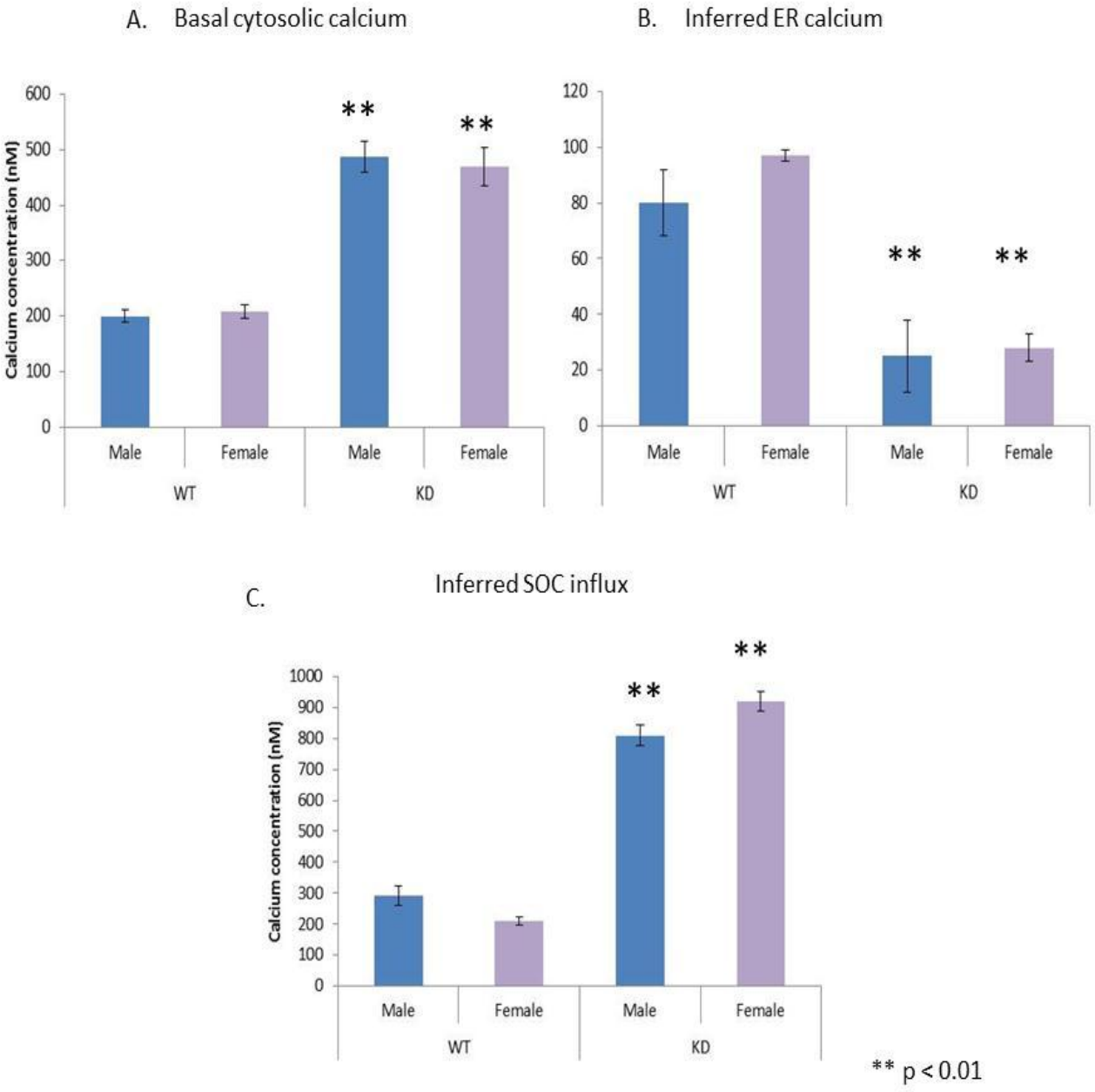
A. Basal cytosolic calcium
B. Inferred ER calcium
C. Inferred SOC influx
Calcium concentration (nM)
600
500
400
300
200
100
0
120
100
80
60
40
20
**
Male
Female
WT
KD
** p < 0.01

Fura-2 signals were quantified as the ratio between 340/380nm. It is important to note that these values are proportional to Ca^{2+}, but the function is not linear, which is why calibration is required. However, in the presence of EGTA, which is required for calibration purposes, motoneurons lose their integrity, giving rise to significant artefacts. Calibration could therefore not be performed in these experiments and so the results obtained using Fluo 4-AM and Fura-2 could not be directly compared. Instead, the *trend* in results was compared.

3.2.6.1 Basal cytosolic Ca^{2+} (Figure 3.10A)

The lowest level of basal cytosolic Ca^{2+} is still observed in DHT-treated WT motoneurons as indicated by the lowest 340/380 nm ratio of 0.5 (+/- 0.02 SEM, n=26). The highest ratio of 0.8 (+/- 0.01 SEM, n=28) is found in DHT-treated KD motoneurons indicating that cytosolic Ca^{2+} is 60% higher in KD motoneurons than in WT motoneurons. This is a greater difference than that observed using Fluo 4-AM, where the results showed that basal cytosolic Ca^{2+} in DHT-treated KD motoneurons is 20% higher than in DHT-treated WT motoneurons.

The effect of DHT treatment on cytosolic Ca^{2+} is also more pronounced when using Fura 2 as a Ca^{2+} indicator compared to Fluo 4-AM. For example, treated WT motoneurons have a basal Ca^{2+} ratio that is 20% lower than untreated WT motoneurons using Fura 2, but only 1% higher using Fluo 4-AM. Likewise, the basal level of Ca^{2+} is 42% higher in DHT- treated KD motoneurons than untreated KD motoneurons when using Fura 2, but only 17% higher when using Fluo 4-AM. These results suggest that Fura 2 is more sensitive to changes in cytosolic Ca^{2+}.

3.2.6.2 Inferred ER Ca^{2+} (Figure 3.10B)

The trend observed using Fura 2 to measure inferred ER Ca^{2+} is consistent with that obtained using Fluo 4-AM. The lowest level of inferred ER Ca^{2+} is observed in DHT-treated KD motoneurons, which respond to TG application with an increase in cytosolic Ca^{2+} with a 340/380 nm ratio of 0.03 (+/- 0.01 SEM n=28). This is significantly lower (p

< 0.001) than the increase observed in DHT-treated WT motoneurons, which was 0.18 (+/- 0.01 SEM, n=26). Thus the level of inferred ER Ca^{2+} is approximately six times lower in KD motoneurons than WT controls. This is a similar magnitude of difference to that observed using Fluo 4-AM, where the results show that DHT-treated KD motoneurons have an ER Ca^{2+} concentration that is seven times lower than that observed in DHT-treated WT motoneurons. In keeping with the Fluo 4-AM measurements, Fura 2 measurements also suggest that DHT causes a negligible increase in ER Ca^{2+} in WT motoneurons. However, Fura 2 measurements also suggest that there is a 150% decrease in ER Ca^{2+} in KD motoneurons following DHT treatment whilst a 240% increase is observed when using Fluo 4-AM. This could be because Fura 2 is more prone to compartmentalization (Thomas et al, 200), which will be discussed in more detail in the discussion (3.12.4).

3.2.6.3 Store-operated Ca^{2+} influx (Figure 3.10C)

Using Fura 2 to measure SOC influx confirmed the trend in SOC influx observed using Fluo 4-AM. The highest level of SOC influx is observed in DHT-treated KD motoneurons, which respond to external Ca^{2+} introduction with an increase in the 340/380 nm ratio of 0.045 (+/- 0.002 SEM, n=28). This ratiometric change is 22.5 times greater than that observed in DHT-treated WT motoneurons, which respond to Ca^{2+} introduction with an increase in 340/380 nm ratio of 0.002 (+/- 0.0015 SEM, n=26). This is a much greater difference than that observed using Fluo 4-AM.

3.2.7 Ca^{2+} handling in motoneurons from a mouse model of ALS

ER stress is known to play a role in the degeneration of motoneurons that occurs in the $SOD1^{G93A}$ mouse model of ALS (Saxena et al, 2009, Nishitoh et al, 2008). In this model, ER stress has been examined using biochemical approaches. In order to assess whether the changes observed in Ca^{2+} handling in KD motoneurons may be indicative of ER stress, in the next set of experiments, Ca^{2+} handling in primary

motoneurons derived from $SOD1^{G93A}$ mice were examined using the protocols described above.

Figure 3.10 Fura-2 control experiments

Some of the experiments undertaken using Fluo 4-AM as the Ca^{2+} indicator were repeated using Fura-2 in order to control for confounding factors that are known to affect single wave dyes such as Fluo 4-AM but not ratiometric dyes such as Fura 2. All variables were kept constant and primary motoneuron cultures were treated with DHT at 4 DIV and imaged at 7 DIV.

Fura 2 fluorescence ratios were obtained by dividing the fluorescence value at 340 nm (Ca^{2+}-bound) by the fluorescence value at 380 nm (Ca^{2+}-free). The ratio is proportional the level of cytosolic Ca^{2+}, although it is not linear.

The Bar Charts summarize ratios that represent basal cytosolic Ca^{2+} (A), inferred ER Ca^{2+} (B) and inferred SOC influx (C) in untreated and DHT-treated WT and KD motoneurons. With respect to all three parameters, the trends observed when using Fluo 4-AM are still apparent when using Fura 2.

(Error Bars = standard error of mean)

Figure 3.10

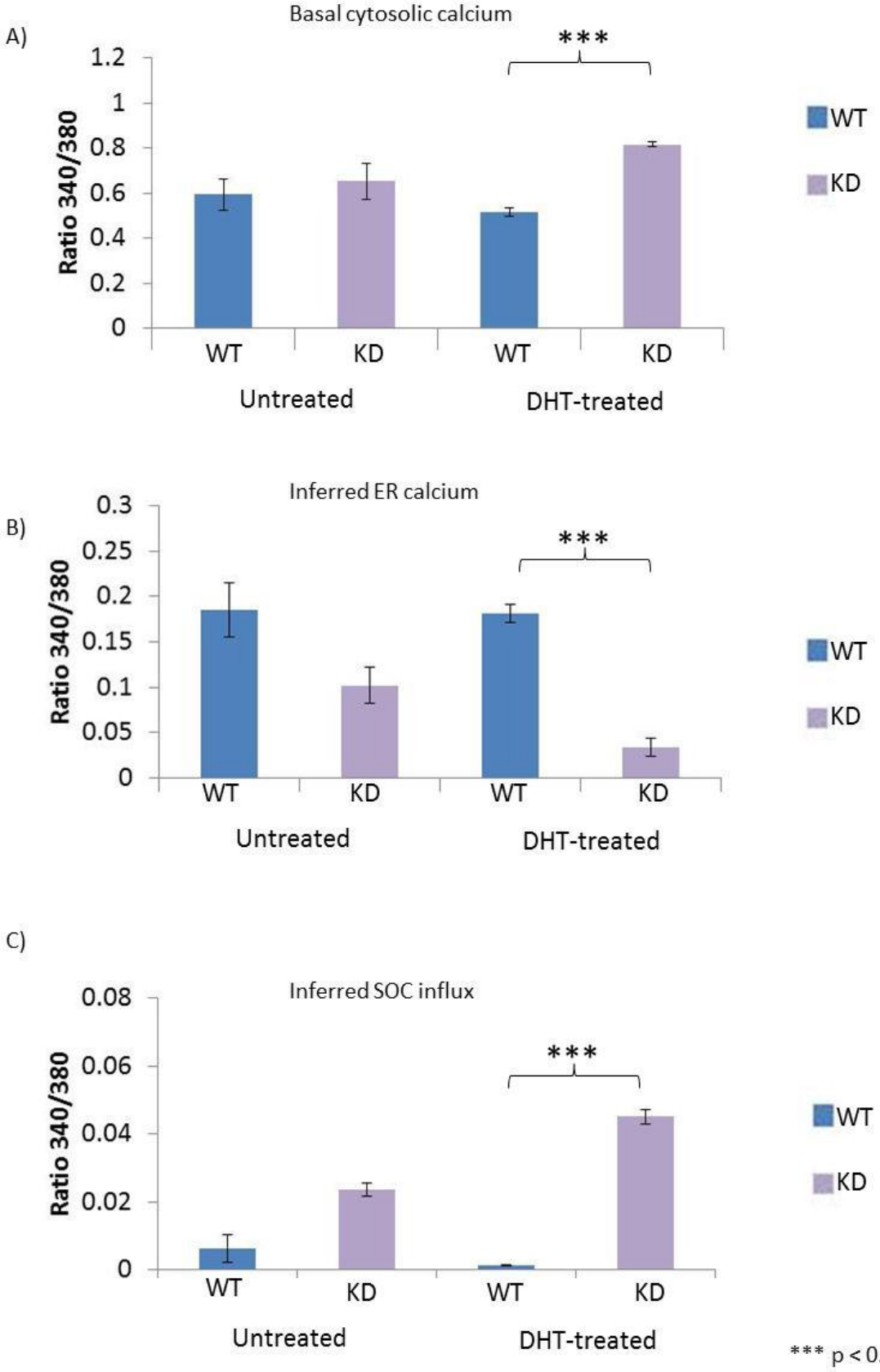
A)
Basal cytosolic calcium
***
Ratio 340/380
1.2
1
0.8
0.6
0.4
0.2
0
WT
KD
WT
KD
Untreated
DHT-treated
WT
KD
B)
Inferred ER calcium
***
Ratio 340/380
0.3
0.25
0.2
0.15
0.1
0.05
0
WT
KD
WT
KD
Untreated
DHT-treated
WT
KD
C)
Inferred SOC influx
***
Ratio 340/380
0.08
0.06
0.04
0.02
0
WT
KD
WT
KD
Untreated
DHT-treated
WT
KD
*** p < 0.005

3.2.7.1 Basal cytosolic Ca^{2+} in $SOD1^{G93A}$ motoneurons (Figure 3.11A)

The concentration of basal cytosolic Ca^{2+} is significantly higher in $SOD1^{G93A}$ motoneurons compared to WT littermate controls (p=0.02). $SOD1^{G93A}$ motoneurons have a basal Ca^{2+} concentration of 1100 nM (+/- 12.89 nM SEM, n=33), whilst motoneurons cultured from WT littermates of the $SOD1^{G93A}$ embryos have a basal Ca^{2+} concentration of 800 nM (+/- 17.99 nM SEM, n=29). Motoneurons from embryos that overexpress WT human SOD1 (SODH, which controls for overexpression of the SOD1 protein) have a basal cytosolic Ca^{2+} concentration of approximately 920 nM (+/- 16.55 nM SEM, n=27), which is approximately 120nM higher than WT basal cytosolic Ca^{2+} and 180 nM lower than the basal Ca^{2+} level observed in $SOD1^{G93A}$ motoneurons.

3.2.7.2 Inferred ER Ca^{2+} (Figure 3.11B)

Inferred ER Ca^{2+} is lowest in the $SOD1^{G93A}$ motoneurons at 52 nM (+/- 4.88 nM SEM n=33). The highest level of ER Ca^{2+} is observed in WT control motoneurons, which have a luminal Ca^{2+} concentration of 348 nM (+/- 47.54 nM SEM, n=29), which is seven times higher than that observed in $SOD1^{G93A}$ motoneurons. This difference is significant (p=0.029). An intermediate level of ER Ca^{2+} is observed in SODH motoneurons, which have an inferred ER Ca^{2+} concentration of 130nM (+/- 8.85 nM SEM, n=27). This is significantly lower than the level of inferred ER Ca^{2+} observed in WT motoneurons (p=0.047).

3.2.7.3 Store-operated Ca^{2+} influx (Figure 3.11C)

Inferred SOC influx is highest in $SOD1^{G93A}$ motoneurons, at 1400 nM (+/- 64.80 nM SEM, n=33), which is significantly higher (p=0.000) than the SOC influx observed in WT motoneurons (300nM +/- 55.71 nM SEM, n=29). SODH motoneurons respond to Ca^{2+} introduction with an increase in Ca^{2+} of 385 nM (+/- 60.62 nM SEM, n=27), which is intermediate between WT and mSOD1 motoneurons.

Figure 3.11: Cellular Ca^{2+} handling motoneurons of the $SOD1^{G93A}$ model of ALS.

Primary motoneurons were cultured from the ventral spinal cord of $SOD1^{G93A}$, WT and SODH embryos. At 7 DIV, Fluo4-AM fluorescence was measured at basal levels (A), following Thapsigargin application (thus inferring ER Ca^{2+}) (B) and following reintroduction of Ca^{2+} into the external medium (thus inferring Store-operated Ca^{2+} influx) (C). Fluorescence values were then calibrated into a Ca^{2+} concentration in nM, using the Ionomycin-induced maximum concentration as a reference point. Background fluorescence was subtracted from values throughout.

The Bar Chart (A) shows that basal cytosolic Ca^{2+} is lowest in WT motoneurons (n=29 from 3 different cultures) and highest in $SOD1^{G93A}$ motoneurons (n=33 from 3 different cultures). This increase in cytosolic Ca^{2+} is significant ($p < 0.005$). The Bar Chart (B) shows that relative to WT motoneurons there appears to be significant ER Ca^{2+} depletion in both $SOD1^{G93A}$ motoneurons and SODH motoneurons (n=27 from 3 different cultures, $p < 0.005$). In (C), the Bar Chart shows that the greatest level of SOC influx is observed in $SOD1^{G93A}$ motoneurons; whilst the level of SOC influx in WT motoneurons is significantly lower ($p < 0.005$).

(Error Bars = standard error of mean)

Figure 3.11

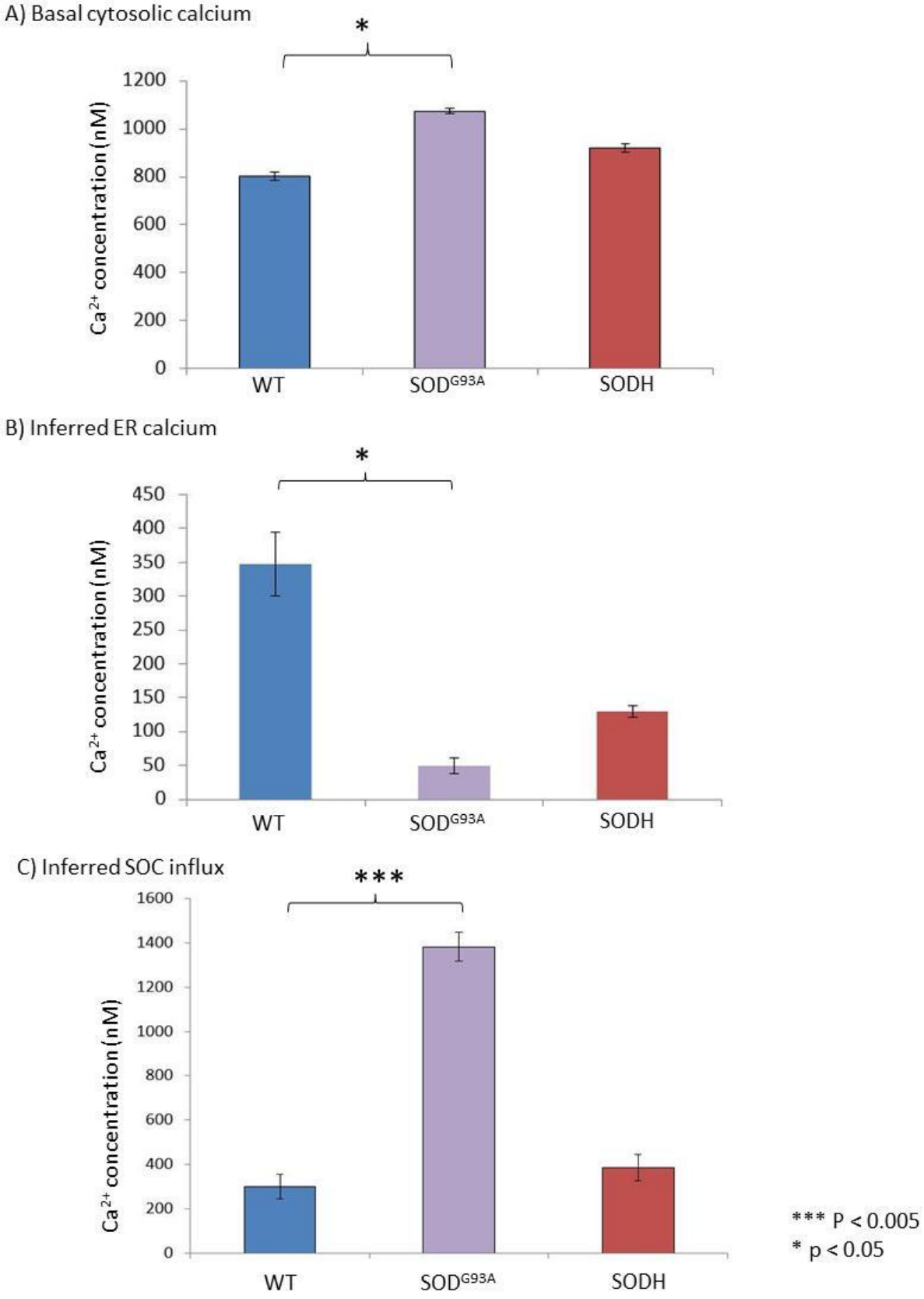
A) Basal cytosolic calcium
*
Ca2+ concentration (nM)
1200
1000
800
600
400
200
0
WT
SODG93A
SODH
B) Inferred ER calcium
*
Ca2+ concentration (nM)
450
400
350
300
250
200
150
100
50
0
WT
SODG93A
SODH
C) Inferred SOC influx
***
Ca2+ concentration (nM)
1600
1400
1200
1000
800
600
400
200
0
WT
SODG93A
SODH
*** P < 0.005
* p < 0.05

3.2.8 Analysis of markers of ER stress in KD motoneurons

In the next set of experiments, the expression of markers of ER stress in KD motoneurons was assessed and compared to that observed in WT motoneurons.

In order to reliably conclude that the level of ER stress marker expression is representative of motoneurons only, as opposed to other cell types found in mixed ventral horn cultures, the primary cultures were purified using Optiprep (Chapter 2) so that the percentage of motoneurons is as close to 100% as possible.

In both WT and KD purified motoneuron cultures, the percentage of motoneurons is consistently greater than 85% (Figure 3.12A). The average percentage of motoneurons in WT cultures is 96% (+/- 0.67% SEM, n=34 fields from 3 different cultures), and the average percentage of motoneurons in KD cultures is 92% (+/- 1.09% SEM, n=41 fields from 3 different cultures). In both WT and KD cultures, purification significantly increases in the percentage of motoneurons ($p<0.000$). In unpurified WT ventral horn cultures the average percentage of motoneurons is 42% (+/- 2.01% SEM, n = 42 fields from 3 different cultures), whilst in KD cultures the average percentage of motoneurons is approximately 30% (+/- 3.4 % SEM, n=36 fields from 3 different cultures).

However purifying motoneuron cultures drastically decreases motoneuron survival despite increasing motoneuron purity (Figure 3.12B). In unpurified WT ventral horn cultures, the average total number of cells present per field is 251 (+/- 23 SEM, n=42 fields from 3 different cultures), whilst in purified WT cultures, the total number of cells decreases to approximately 108 (+/- 11.4 SEM, n=36 fields from at least 3 different cultures). In unpurified KD ventral horn cultures, the average total cell number is approximately 221 (+/- 18.7 SEM, n=36 fields from 3 different cultures) whilst in purified KD motoneuron cultures the total number of cells decreases to just 45 (+/- 5.2 SEM, n=36 fields from 3 different cultures). Therefore, the purification process decreases cell

survival in both WT and KD cultures by approximately 57 % and 80 %, respectively. In both cases this decrease is significant (p=0.001 and 0.0003, respectively).

Figure 3.12: Purification of ventral horn cultures improves the proportion of primary motoneurons

Ventral horn cultures were purified using Optiprep – a density gradient medium that allows motoneurons to be separated from other cell types. The Bar chart (A) summarizes the percentage of motoneurons in unpurified and purified WT (n=42 and 34, respectively) and KD cultures (n=36 and 44, respectively). In unpurified ventral horn cultures the percentage of motoneurons ranges between 30 and 42%. In purified motoneuron cultures, the population of motoneurons increases to over 90%. Bar chart B) demonstrates the effects of purification on motoneuron survival. Following purification the number of motoneurons present at 7 DIV decreases significantly in both WT and KD cultures ($p < 0.001$).

(Error Bars = standard error of mean)

Figure 3.12

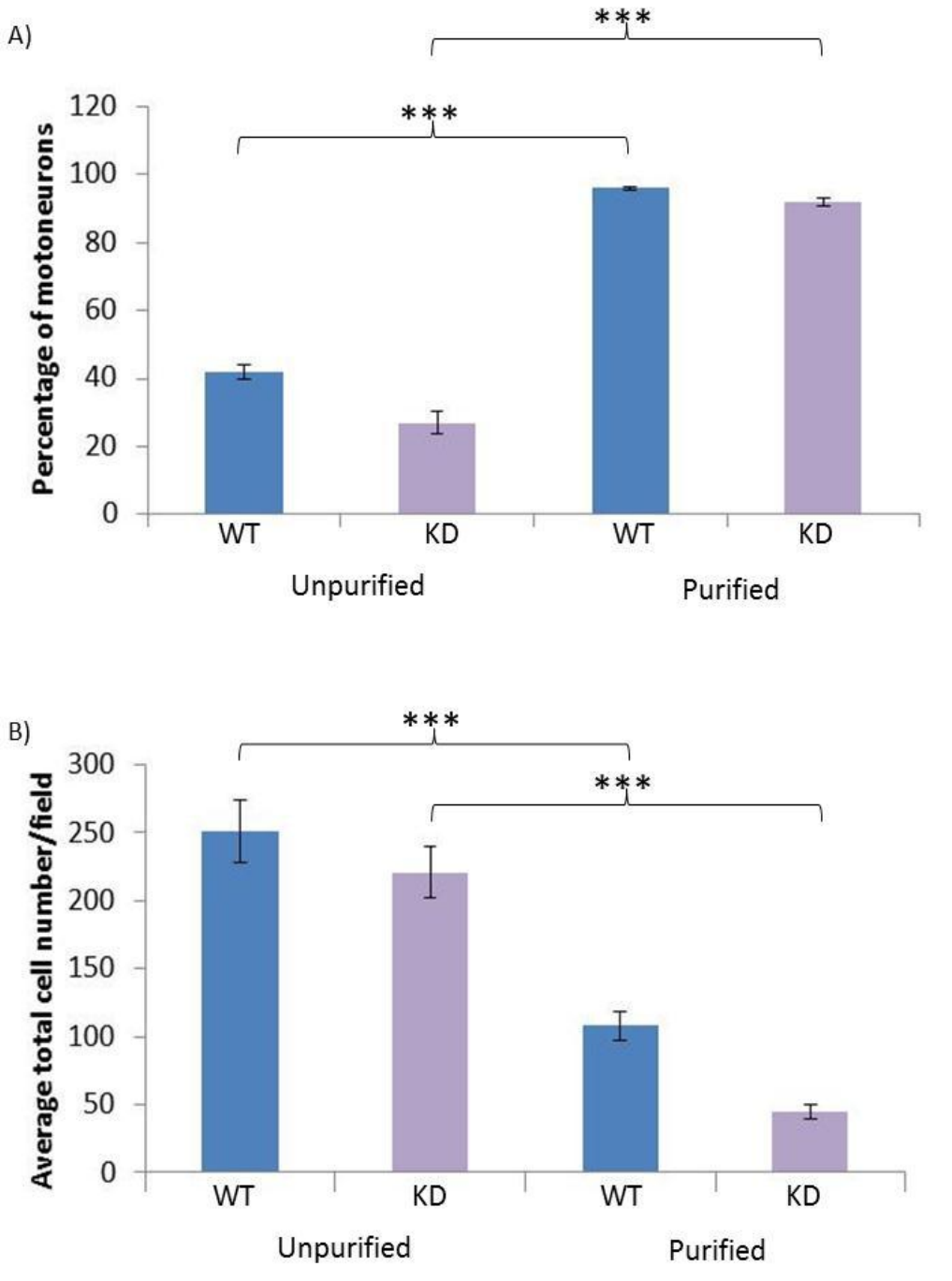

*** $p < 0.005$

3.2.9 Sarco/Endoplasmic Reticulum ATPase (SERCA) expression – the link between motoneuron genotype and ER Ca^{2+} (Figure 3.13)

As shown in Figure 3.13B, Western blot analysis of purified ventral horn motoneurons from embryonic WT and KD mice reveals that the expression level of the SERCA2b protein is significantly higher in WT motoneurons than in KD motoneurons (p=0.04). Indeed, the level of SERCA2b protein expression relative to actin (the loading control - 1.0) is 1.28 (+/- 0.2, n=6) in the case of WT motoneurons and 0.78 (+/- 0.22, n=6) in the case of KD motoneurons (Figure 3.13C).

3.2.10 Does ER Ca^{2+} depletion result in ER stress in embryonic KD motoneurons?

To assess whether or not ER stress is present in embryonic KD motoneurons, Western blot analysis and Immunohistochemistry were used to determine levels of ER stress markers in DHT-treated primary motoneuron cultures from E13 KD and WT mice.

3.2.10.1 Binding immunoglobulin Protein (BiP)

3.2.10.1.1 BiP Immunoreactivity

Primary WT and KD motoneurons were immunostained for BiP. As shown in Figure 3.14A, there is a clear increase in BiP immunoreactivity (red) in KD motoneurons particularly within the cytosol, compared to WT motoneurons (Figure 3.14A)

3.2.10.1.2 Western blot analysis of BiP

Levels of BiP were also examined by Western blot analysis. A typical blot is shown in Figure 3.14C. Assessment of the optical density of the Western blot (Figure 3.14D) reveals that the level of BiP is 39% higher in KD primary motoneurons than in WT primary motoneuron controls. In WT motoneurons, the BiP expression level relative to

Actin (1.0) is 1.13 (+/- 0.06 SEM, n=3), whereas in KD motoneurons it is 1.41 (+/- 0.12 SEM, n=3). This increase in BiP levels in KD motoneurons is significant (p= 0.05).

Figure 3.13: SERCA pump expression decreases in KD motoneurons

The SERCA2b pump sequesters Ca^{2+} from the cytosol into the ER; increasing luminal Ca^{2+} levels in motoneurons, as shown in (A). Western blot analysis of purified primary motoneurons from KD embryos and their WT littermates at 7 DIV was used to assess levels of SERCA2b expression. (B) Shows a representative Western blot. The Bar Chart (C) summarizes the optical density of each Western blot. The expression level of SERCA2b (relative to the loading control actin, which has been given a value of 1.0) is 21% lower in KD motoneurons than in WT controls (n = 6 in both cases). This decrease in expression is significant ($p < 0.05$).

(Error Bars = standard error of mean)

Figure 3.13

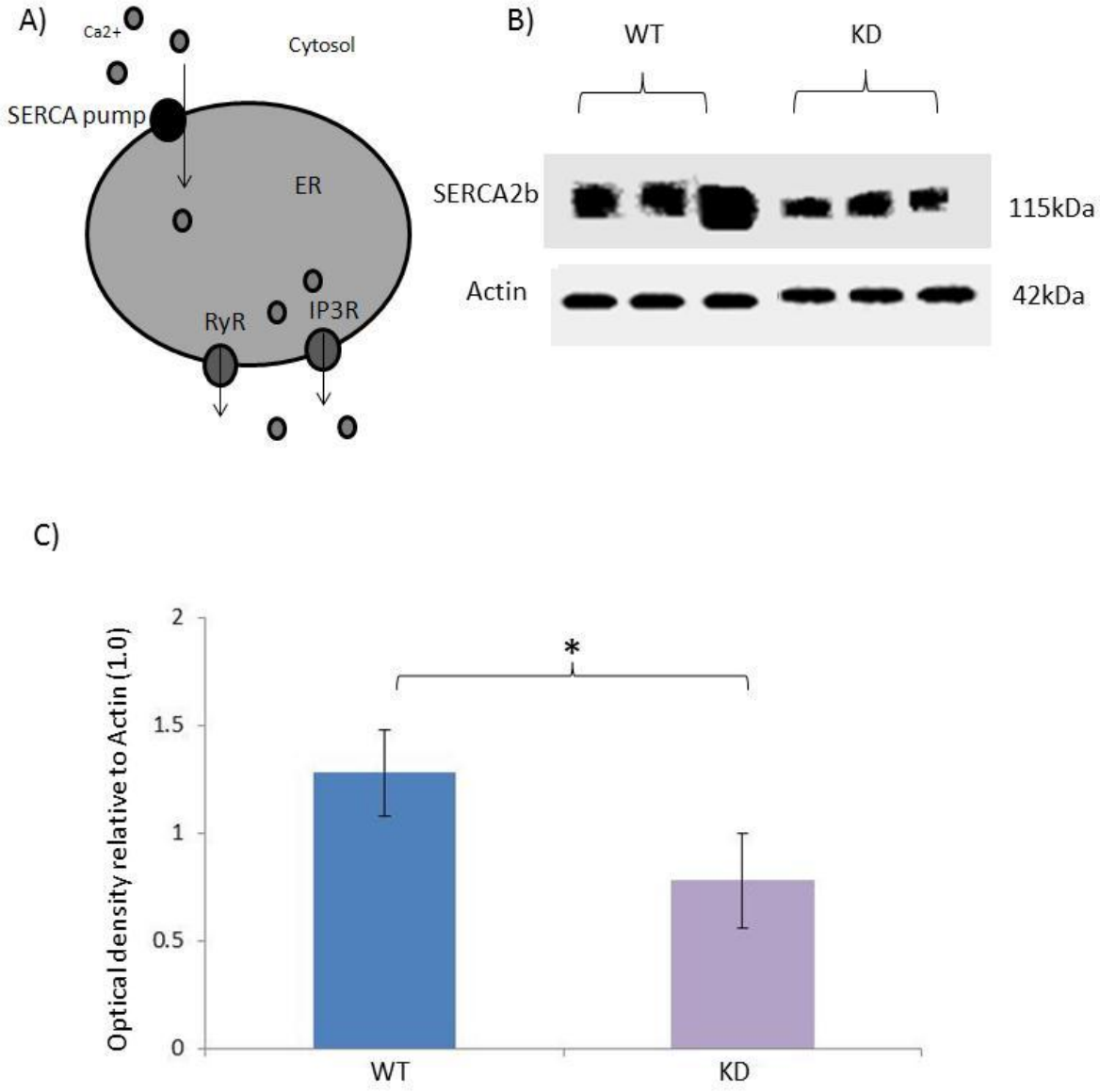
A)
Ca2+
Cytosol
SERCA pump
ER
RyR
IP3R
B)
WT
KD
SERCA2b
115kDa
Actin
42kDa
C)
Optical density relative to Actin (1.0)
2
1.5
1
0.5
0
*
WT
KD

Figure 3.14: BiP expression is elevated in embryonic KD motoneurons

WT and KD motoneuron cultures were immunostained for BiP (red) and co-stained for β-III tubulin (green, a neuronal marker) and DAPI (blue, a nuclear marker). Images showing the typical patterns of BiP immunoreactivity in WT and KD motoneuron cultures are shown in Ai) and Aii), respectively. Levels of BiP in WT and KD motoneuron cultures were also analysed by Western blot. A representative Western blot is shown in (B). Optical density analysis was performed and protein levels were expressed relative to the house-keeping protein, Actin, which was used as a loading control and given a value of 1.0. As shown in the bar chart (C), BiP expression is significantly elevated in embryonic KD motoneurons compared to WT controls ($p < 0.05$).

(Error Bars = standard error of mean, scale bars = 50 μM)

Figure 3.14

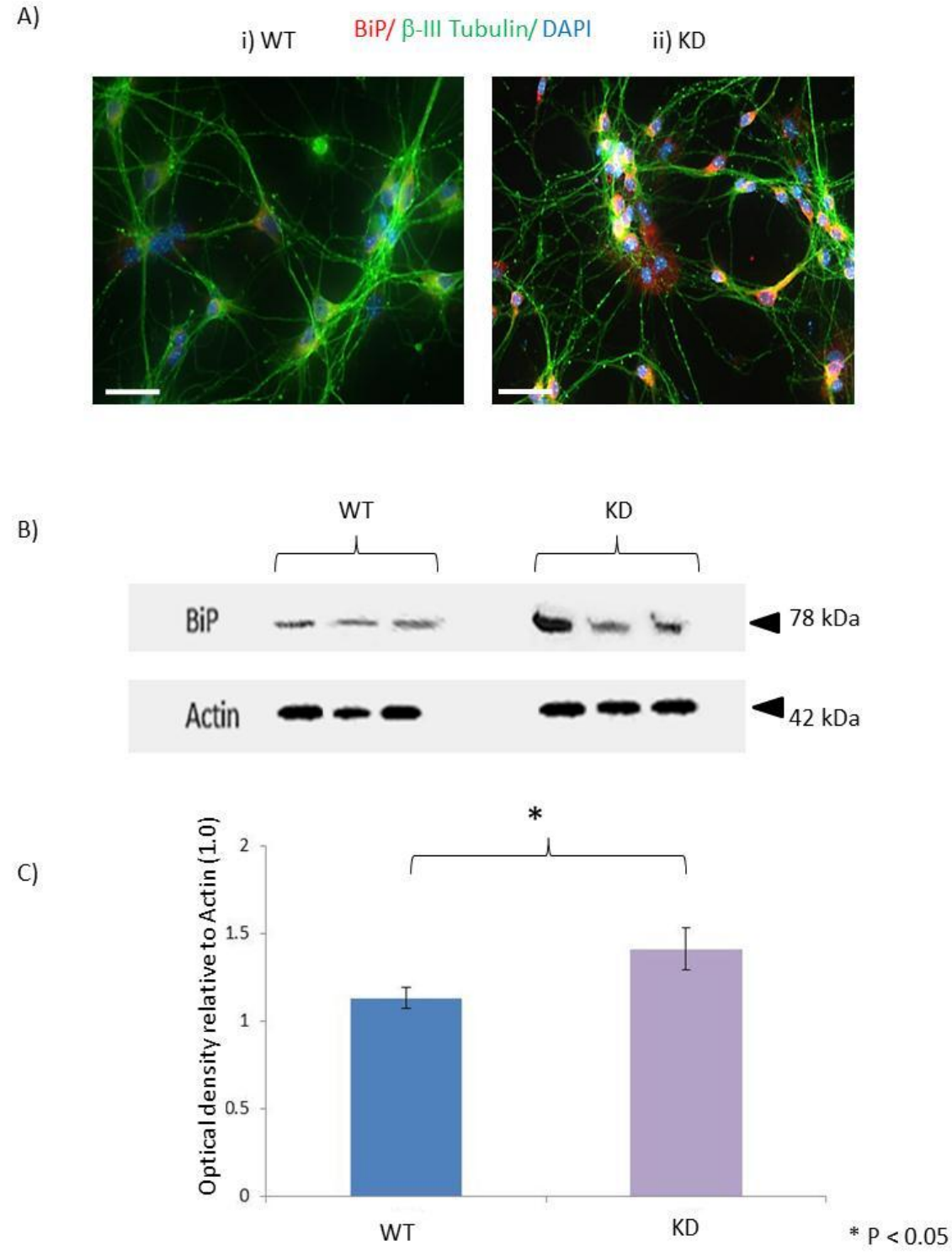
A)
i) WT
BiP/ β-III Tubulin/ DAPI
ii) KD
B)
WT
KD
BiP
78 kDa
Actin
42 kDa
C)
*
Optical density relative to Actin (1.0)
2
1.5
1
0.5
0
WT
KD
* P < 0.05

3.2.10.1.2 Eukaryotic translation initiation factor 2α (eIF2α)

As is the case with BiP, phospho-eIF2α expression appears to be slightly elevated in KD motoneurons compared to WT motoneurons (Figure 3.15). Western blot analysis reveals that the level of phospho-eIF2α in KD motoneurons, normalized to Actin is 1.25 (+/- 0.29 SEM, n=3), which is 11.2 % higher than WT motoneurons, in which the relative level of eIF2α expression is 1.11 (+/- 0.24 SEM, n=3). This difference however is not significant (p=0.07). (eIF2α immunohistochemistry was not possible as no suitable antibody is currently available).

3.2.10.1.3 Activating Transcription Factor 4 (ATF4)

The expression of ATF4, an upstream ER stress marker, was also examined in WT and KD cultures by immunohistochemistry and Western blot analysis.

3.2.10.1.3.1 ATF4 Immunoreactivity (Figure 3.16A & B)

Immunostaining of primary motoneuron cultures for ATF4 shows that ATF4 immunoreactivity is much higher in KD motoneurons (Figure 3.16A) than in WT motoneurons (Figure 3.16A) and that ATF4 immunoreactivity is largely located to motoneuron nuclei. No extra-nuclear staining for ATF4 was detected and non-motoneuron cells have a considerably lower ATF4 immunoreactivity than motoneurons.

3.2.10.1.3.2 Western blot analysis

ATF4 expression in WT and KD motoneuron cultures was also examined by Western blot analysis (Figure 3.16C). The Western blot and the data presented in the bar chart (Figure 3.16D) show that ATF4 levels are higher in KD primary motoneurons than in WT controls. Analysis of the mean optical density of ATF4 Western blots reveals that ATF4 expression is 69 % higher in KD motoneurons than WT motoneurons, which

have ATF4 expression levels of 1.55 (+/- 0.19 SEM, n = 3) and 1.01 (+/- 0.26 SEM, n = 3), respectively. This difference is significant (p=0.047).

Figure 3.15: eIF2α expression is elevated in embryonic KD motoneurons

The expression level of phospho-eIF2α, which is a marker of ER stress-induced translation arrest, in E13 WT and KD primary motoneuron homogenates was assessed by Western blot. A) shows a representative blot. The bar chart (B) summarizes the mean optical density of such blots, where results are expressed relative to the house keeping protein Actin, which was given a value of 1.0. The level of phospho-eIF2α is higher in embryonic KD motoneurons than in WT controls. This difference approaches significance (p = 0.066).

(Error Bars = standard error of mean)

Figure 3.15

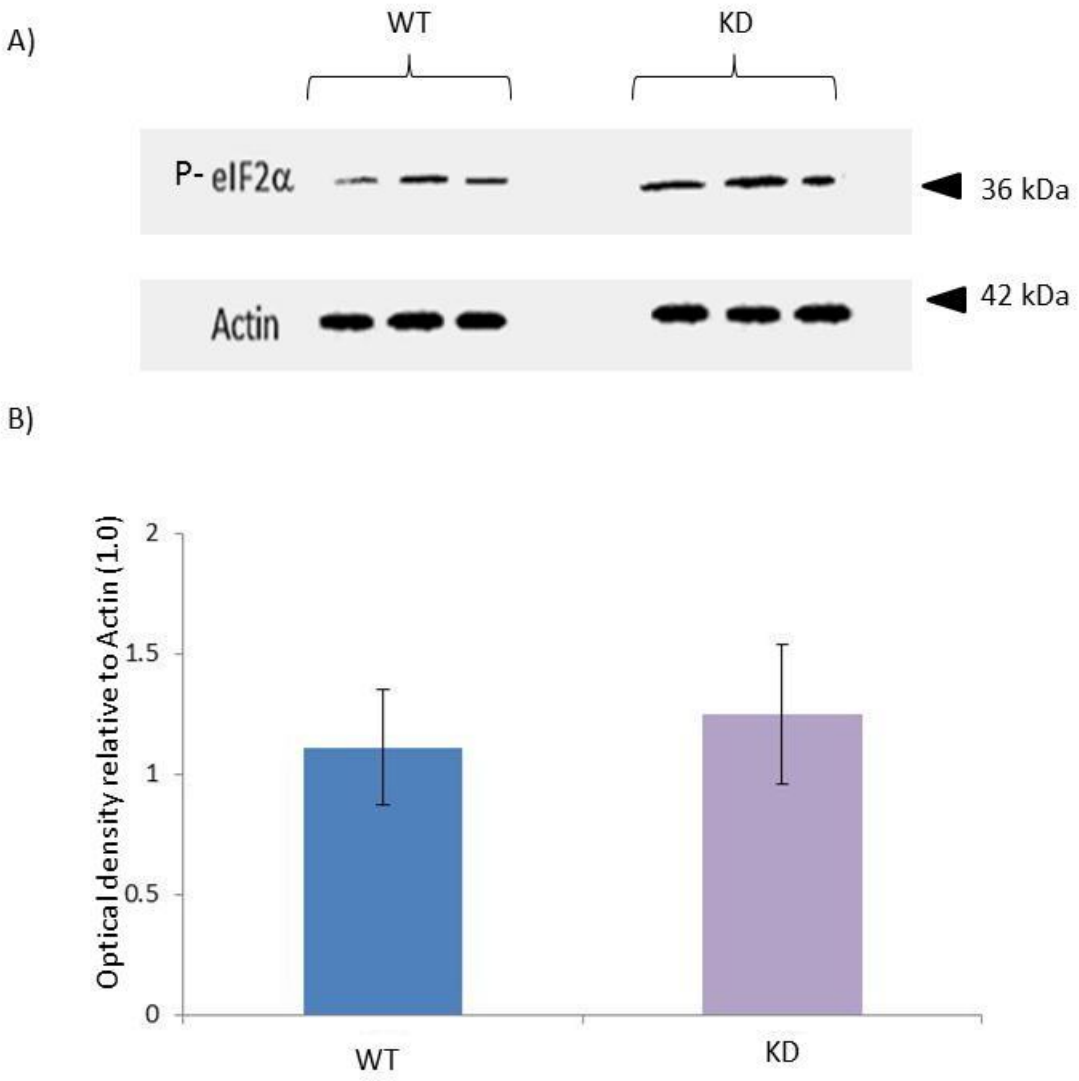
A)
WT
KD
P- eIF2α
36 kDa
Actin
42 kDa
B)
Optical density relative to Actin (1.0)
2
1.5
1
0.5
0
WT
KD

Figure 3.16: ATF4 expression is elevated in embryonic KD motoneurons

In order to assess expression levels of the ER stress marker ATF4 in embryonic WT and KD motoneurons the cultures were immunostained with a specific antibody for ATF4. Typical staining patterns observed in E13 WT and KD motoneuron cultures at 7 DIV are shown in Ai) and Aii), respectively. ATF4 immunoreactivity is shown in red. The cultures were also co-stained with β-III tubulin (green) and DAPI (blue). The images show that ATF4 immunoreactivity (red) is higher in KD motoneuron cultures than in WT controls, although WT controls still express low levels of ATF4. This increased ATF4 immunoreactivity is specific to motoneuron nuclei. Homogenates from E13 WT and KD motoneuron cultures were also processed for Western blot analysis of ATF4 expression levels. A typical Western blot is shown in B). The bar chart (C) summarizes quantification of the blot. The optical density of the blot was obtained and protein levels were normalized to the house keeping protein Actin, which was used as a loading control and given a value of 1.0. The expression of ATF4 is significantly higher in embryonic KD motoneurons than in WT controls ($p < 0.05$).

(Error Bars = standard error of mean, scale bar = 50 μM)

Figure 3.16

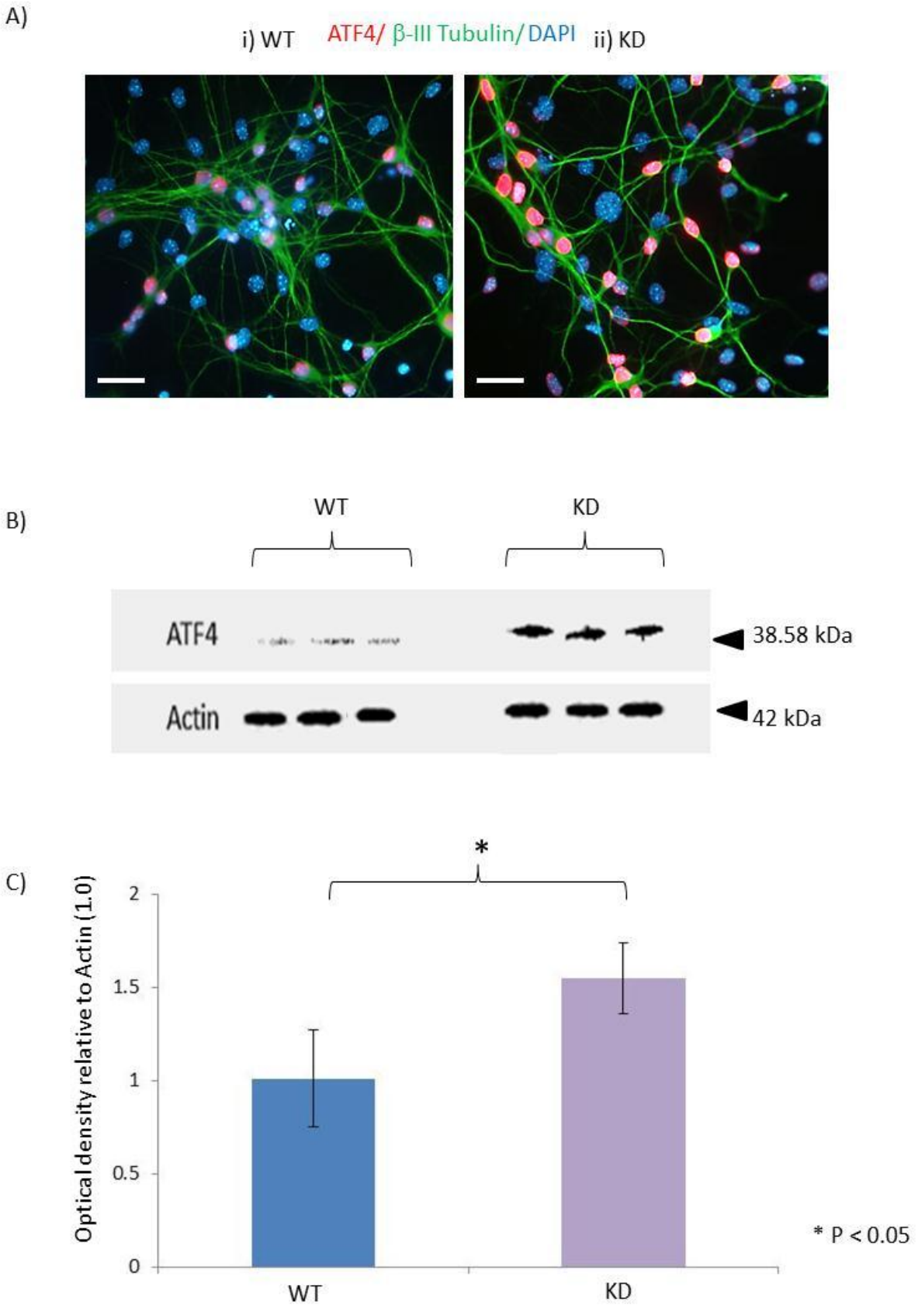
A)
i) WT
ATF4/ β-III Tubulin/ DAPI
ii) KD
B)
WT
KD
ATF4
38.58 kDa
Actin
42 kDa
C)
*
Optical density relative to Actin (1.0)
2
1.5
1
0.5
0
WT
KD
* P < 0.05

3.2.10.1.4 CCAAT/enhancer-binding protein homologous protein (CHOP)

Levels of expression of CHOP in E13 WT and KD motoneurons were examined by immunohistochemistry and Western blot analysis.

3.2.10.1.4.1 Immunoreactivity

Immunostaining of primary ventral motoneuron cultures shows that CHOP immunoreactivity is considerably higher in KD motoneurons than in WT controls, and that CHOP expression in KD cultures is specific to motoneuron nuclei (Figure 3.17B). In WT cultures there is no detectable CHOP immunoreactivity in motoneuron nuclei, and only low intensity staining is detected in non-neuronal cells. In KD cultures the staining intensity in the non-neuronal cells is similar to that in WT cultures.

3.2.10.1.4.2 Western Blot analysis

The level of expression of CHOP in E13 WT and KD motoneuron cultures at 7 DIV was also examined by Western blot. A typical Western blot is shown in Figure 3.17C, and the mean optical density measurements of such blots are summarized in the bar chart (Figure 3.17D). CHOP levels, like all previous ER stress markers, are elevated in KD ventral motoneurons compared to WT controls. The Western blot data shows that the level of CHOP expression is approximately 39% higher in KD motoneurons than WT motoneurons. Indeed, the relative level of CHOP in KD motoneurons is 1.48 (+/- 0.12 SEM, n=3), compared to 1.12 (+/- 0.10 SEM, n=3) in WT controls. This difference is significant ($p= 0.008$).

In order to assess whether or not ER stress is present in vivo in KD mice spinal cord, Western blot analysis and immunocytochemistry were used to assess the levels of ER stress markers in spinal cord homogenates and sections from both KD and WT mice at P5, 3 months, 12 months (symptom onset) and 18 months (end stage).

Figure 3.17: CHOP expression is elevated in embryonic KD motoneurons

The expression level of the ER stress-induced, pro-apoptotic protein CHOP in embryonic WT and KD motoneurons was assessed by immunohistochemistry and Western blot analysis. The pattern of CHOP immunoreactivity in E13 WT and KD motoneuron cultures at 7 DIV is shown in Ai) and Aii), respectively. Cultures were immunostained for CHOP (red) and MAP2 (green), a neuronal-specific marker, and stained with DAPI (blue), a nuclear marker. The images show that CHOP immunoreactivity is higher in KD motoneuron cultures than in WT controls and that this increase in CHOP immunoreactivity is specific to motoneuron nuclei. Although there is some CHOP-positive staining in non-neuronal cells in WT cultures there is no difference in the pattern of intensity of CHOP immunoreactivity between WT and KD cultures.

Homogenates of E13 WT and KD motoneuron cultures at 7 DIV were also analysed by Western blot. A typical CHOP Western blot is shown in B). Quantitative analysis of these blots was undertaken and the results are summarized in the bar chart (C). CHOP protein levels were expressed relative to the house keeping protein Actin, which was given a value of 1.0. It can be seen that CHOP expression is significantly elevated in embryonic KD motoneurons compared to WT controls ($p<0.05$).

Although the molecular weight of CHOP is 19 kDa, the antibody used (abcam) is detected at 31 kDa.

(Error Bars = standard error of mean, scale bar = 40 μM)

Figure 3.17

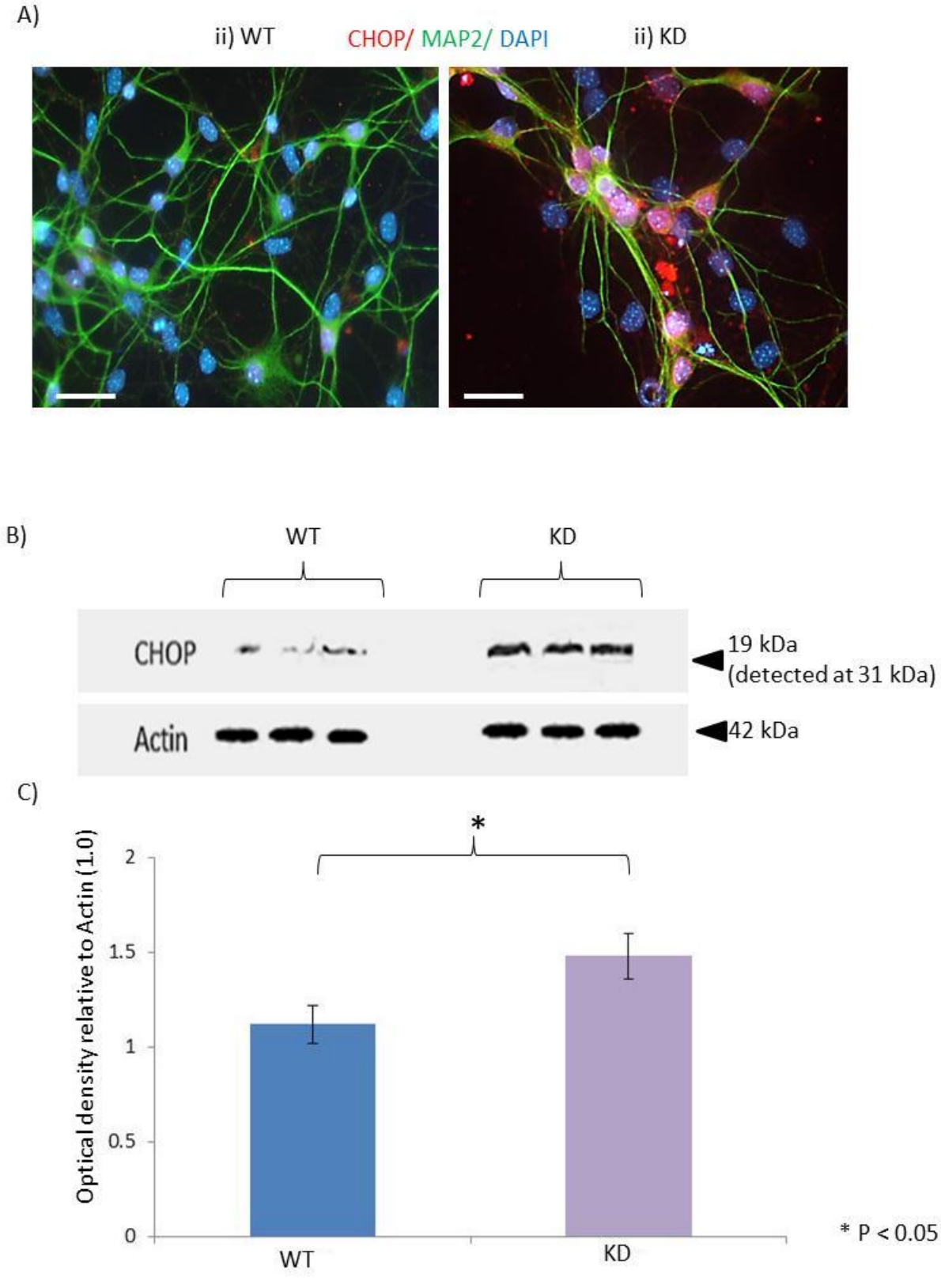
A)
ii) WT
CHOP/ MAP2/ DAPI
ii) KD
B)
WT
KD
CHOP
19 kDa
(detected at 31 kDa)
Actin
42 kDa
C)
*
Optical density relative to Actin (1.0)
2
1.5
1
0.5
0
WT
KD
* P < 0.05

3.2.11 The presence of ER stress markers in vivo in spinal cords of KD mice

3.2.11.1 BiP

3.2.11.1.1 BiP Immunoreactivity

Spinal cord sections from WT and KD mice at 3 months, 12 months and 18 months were immunostained for BiP. Examples of the pattern of BiP immunoreactivity is shown in Figure 3.18, for WT and KD mice (Figure 3.18A & B, respectively). BiP immunoreactivity is much higher in KD ventral motoneurons than in WT motoneurons at 3 months of age. However the clear difference in staining intensity between the genotypes observed at 3 months is not detected in 12 and 18 month old mice. At 12 months, BiP immunoreactivity appears to be slightly more intense in the KD spinal cord sections than in WT; however there is no observable difference in BiP staining intensity between KD and WT at 18 months.

The elevation of BiP expression that is observed in KD spinal cord sections appears to be specific to the cytosol of motoneurons and is not apparent in other cell types, which are identifiable by a positive DAPI stain but a negative β-III tubulin stain.

3.2.11.1.2 Western blot analysis

Western blot analysis of BiP expression levels (Figure 3.18 C & D) reveals that the expression levels of BiP are higher in KD spinal cord tissue than in control WT spinal cord tissue at all of the time points tested. Optical density analysis of Western blot data shows that the peak difference in BiP expression between WT and KD spinal cords occurs at P5. At this time point, the expression levels of BiP are approximately 44% higher in KD spinal cord than in WT controls. At 3 months of age, the difference between WT and KD expression is almost unchanged at 41%. The elevation of BiP expression at both P5 and 3 months is significant ($p = 0.002$ and 0.05, respectively). However, this difference between WT and KD spinal cord BiP expression diminishes as

the disease progresses. By 12 months of age the average expression level of BiP in KD spinal cord is just 5% higher than in WT spinal cord and at 18 months, the level of BiP expression is just 2% higher in KD spinal cords compared to WT controls. Differences at these stages are not significant.

3.2.11.2 phospho-eIF2α expression levels

The expression of phospho-eIF2α in WT and KD spinal cords was examined by Western blot analysis. Immunohistochemistry was not undertaken due to the lack of a suitable antibody for immunohistochemistry. As seen in Figure 3.19, Western blot analysis reveals that the expression level of phopsho-eIF2α is greater in KD spinal cord than in WT spinal cord at all ages studied apart from 18 months, when expression of eIF2α in KD spinal cord is not significantly different from WT spinal cord tissue.

The greatest elevation in phospho-eIF2α expression in KD spinal cord is observed at P5. At this age, the level of phospho-eIF2α expression is 104% greater in KD spinal cord than in WT. This difference is significant (p= 0.001). At 3 months, the difference between KD and WT spinal cord expression declines to 42 %, which is still significantly greater than WT. By 12 months of age, phospho-eIF2α expression in KD spinal cord is only 4.6% greater than in WT spinal cord, which is not a significant difference.

3.2.11.3 ATF4

ATF4 expression in KD and WT spinal cords was examined by both immunohistochemistry and Western blot analysis.

3.2.11.3.1 ATF4 Immunoreactivity (Figure 3.20A)

Immunostaining of KD and WT spinal cord sections for ATF4 reveals that at 3 and 12 months of age there is a clear increase in ATF4 immunoreactivity in KD motoneurons compared to WT controls. However by 18 months ATF4 expression is not significantly different from the pattern or intensity of ATF4 staining in WT controls.

Figure 3.18: BiP expression in spinal cords of KD mice at different stages of disease progression

BiP expression in the spinal cord of KD mice was examined at various stages of disease by immunohistochemistry and western blot analysis.

Lumbar spinal cords were removed from KD and WT littermates at P5, 3, 12 and 18 months of age. Examples of the pattern of BiP immunoreactivity in the ventral horn of WT and KD spinal cords are shown in Ai) and Aii) respectively at i) 3 months, ii) 12 months and iii) 18 months. The sections were immunostained for BiP (red) and co-stained for β-III tubulin (green), a neuronal marker, and stained with DAPI (blue), a nuclear marker. A clear increase in BiP immunoreactivity is observed in the cytoplasm of KD motoneurons at 3 months of age, but the intensity of BiP staining decreases significantly during disease progression and by 18 months is no longer detectable. No BiP staining was observed in WT motoneurons at any age examined. Western blot analysis of BiP expression in spinal cord homogenates of WT and KD mice was also undertaken. A typical Western blot for BiP is shown in B), and the quantitative analysis of such blots is summarized in the bar chart (C). The results indicate that BiP expression is already significantly increased in the spinal cord of KD mice as early as P5, compared to WT levels, and continues to be raised at 3 and 12 months. However, by 18 months BiP expression in KD spinal cords is not significantly greater than that observed in WT spinal cords.

(Error Bars = standard error of mean, scale bars = 30 μM)

Figure 3.18

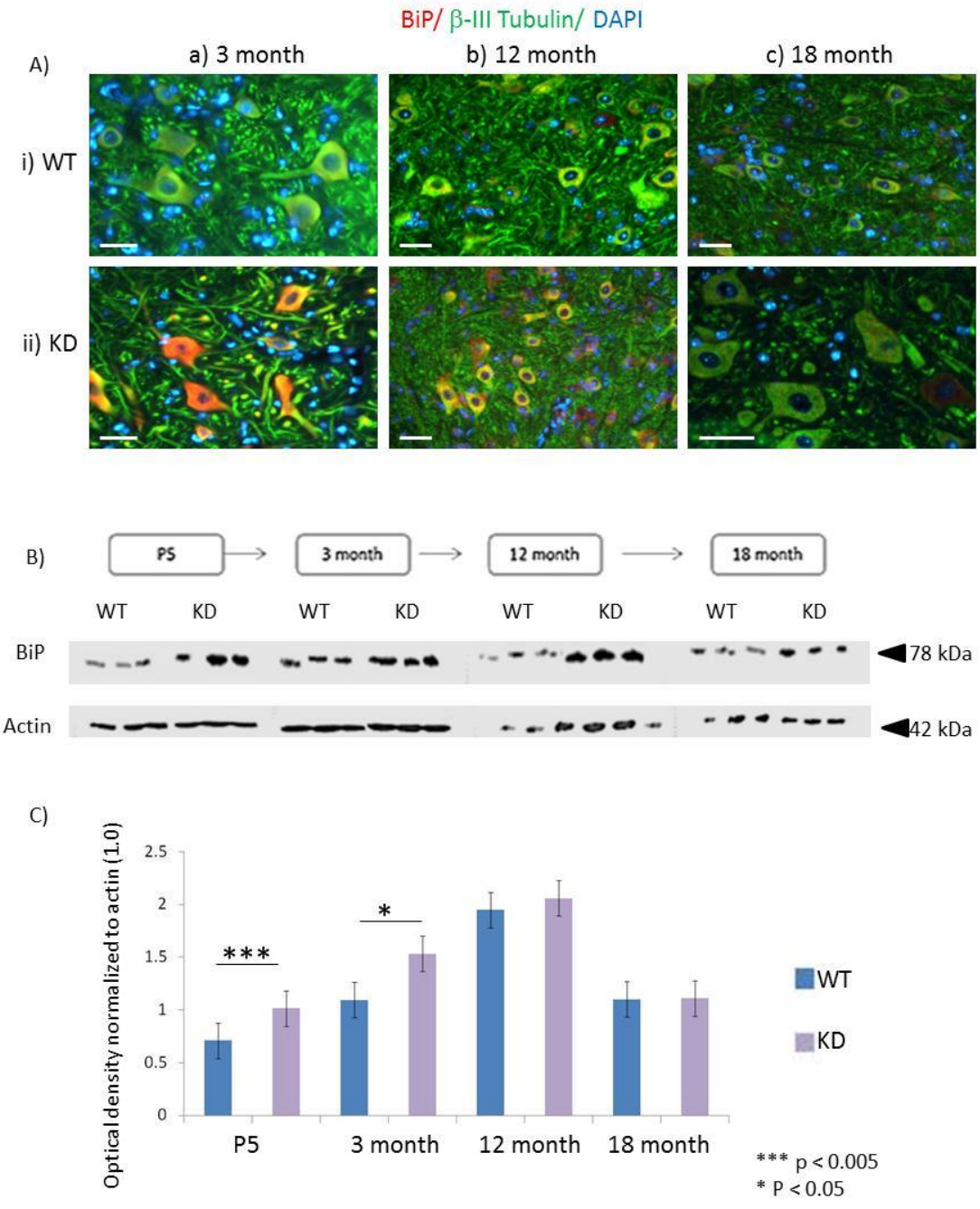
BiP/ β-III Tubulin/ DAPI
A)
a) 3 month
b) 12 month
c) 18 month
i) WT
ii) KD
B)
P5
3 month
12 month
18 month
WT
KD
BiP
78 kDa
Actin
42 kDa
C)
Optical density normalized to actin (1.0)
2.5
2
1.5
1
0.5
0
***
*
P5
3 month
12 month
18 month
WT
KD
*** p < 0.005
* P < 0.05

Figure 3.19: Phospho-eIF2α expression in spinal cord of KD mice at different stages of disease progression

Western blot analysis was used to determine the expression levels of phosho-eIF2α in WT and KD spinal cord homogenates from P5, 3, 12 and 18 month old mice. A typical blot is shown in A). For each genotype and age, 3 different mice were used and samples were run twice to test reproducibility. Quantitative analysis of the optical density of such blots is summarized in the bar chart (B) in which phospho-eIF2α levels are expressed relative to the loading control actin (given a value of 1.0). The largest increase in phospho-eIF2α expression in KD spinal cord is observed at P5, and levels remain significantly elevated at 3 months of age. From this stage on, phospho-eIF2α expression is not significantly greater in KD spinal cord than WT spinal cord.

(Error Bars = standard error of mean)

Figure 3.19

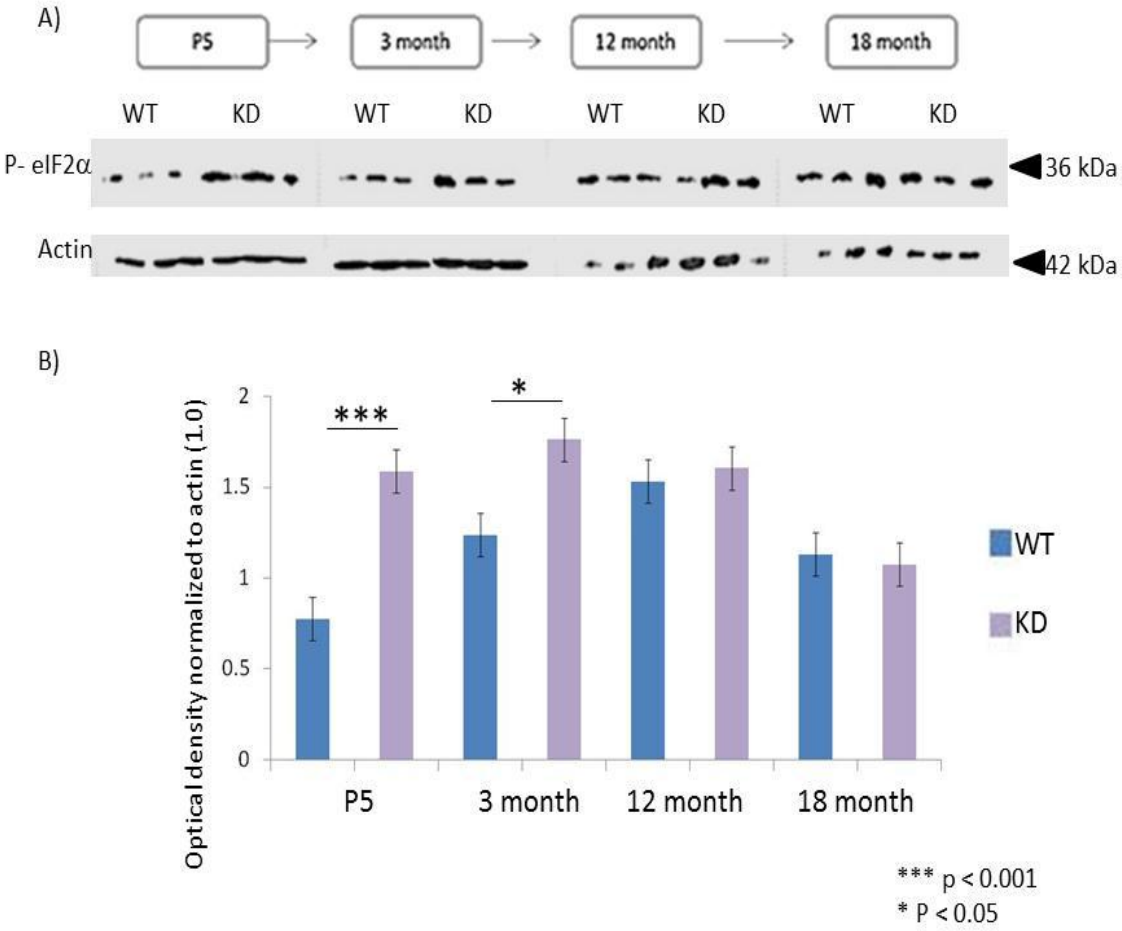
A)
P5
3 month
12 month
18 month
WT
KD
WT
KD
WT
KD
WT
KD
P- eIF2α
36 kDa
Actin
42 kDa
B)
Optical density normalized to actin (1.0)
2
1.5
1
0.5
0
***
*
P5
3 month
12 month
18 month
WT
KD
*** p < 0.001
* P < 0.05

In KD motoneurons, the expression of ATF4 appears to be exclusively nuclear in all spinal cord sections. Indeed, over exposure of the sections does not reveal any additional extra-nuclear staining. The elevated ATF4 expression in KD motoneurons is also detected in cell types other than motoneurons, although not all non-motoneuron cells display elevated ATF4 levels whereas, *all* motoneurons do.

3.2.11.3.2 Western blot analysis (Figure 3.20B)

As observed with BiP and phospho-eIF2α, the expression of ATF4 is elevated in KD spinal cords compared to WT spinal cords although the difference between the two genotypes diminishes as the disease progresses, so that by 18 months levels are no longer significantly higher in KD spinal cords than WT spinal cords.

The peak increase in ATF4 expression in KD spinal cord occurs at P5, when ATF4 expression is 80% higher in KD spinal cords than in WT control tissue. This difference in expression is significant ($p=0.015$). At 3 months of age the increased ATF4 expression in KD spinal cord is 39 % greater than in WT tissue ($p = 0.002$). At 12 months ATF4 levels are still 31% higher in KD spinal cord than in WT ($p= 0.0014$). By 18 months however the difference between the genotypes is no longer significant, and ATF4 expression is only 10% higher in KD spinal cords than in WT controls.

3.2.11.4 CHOP expression in WT and KD spinal cords

The expression of CHOP was examined by immunohistochemistry and Western blot analysis in spinal cords of WT and KD mice at various stages of disease progression.

3.2.11.4.1 CHOP Immunoreactivity (Figure 3.21A)

CHOP immunoreactivity appears to be predominantly motoneuron-specific and nuclear in spinal cord sections of both KD and WT mice.

Figure 3.20: ATF4 expression in KD spinal cord at various stages of disease progression

Sections of WT and KD lumbar spinal cords were immunostained for ATF4 at various stages of disease progression. Typical examples of the pattern of ATF4 immunoreactivity in WT and KD motoneurons are shown in Ai) and Aii), respectively at i) 3 months, ii) 12 months and iii) 18 months. Sections were immunostained for ATF4 (red), the neuronal marker MAP2 (green) and the nuclear marker DAPI (blue). A clear increase in ATF4 immunoreactivity is detected in KD motoneurons at 3 and 12 months of age, although no significant increase in staining is detected at 18 months of age. Western blot analysis of ATF4 expression was also undertaken and a typical Western blot for ATF4 is shown in B). The bar chart (C) summarizes the quantification of the optical density of such blots and shows that ATF4 levels are significantly greater in KD spinal cords at P5, 3 months and 12 months of age, but are not significantly elevated compared to WT by 18 months of age.

(Error Bars = standard error of mean, scale bars = 30 μM)

Figure 3.20

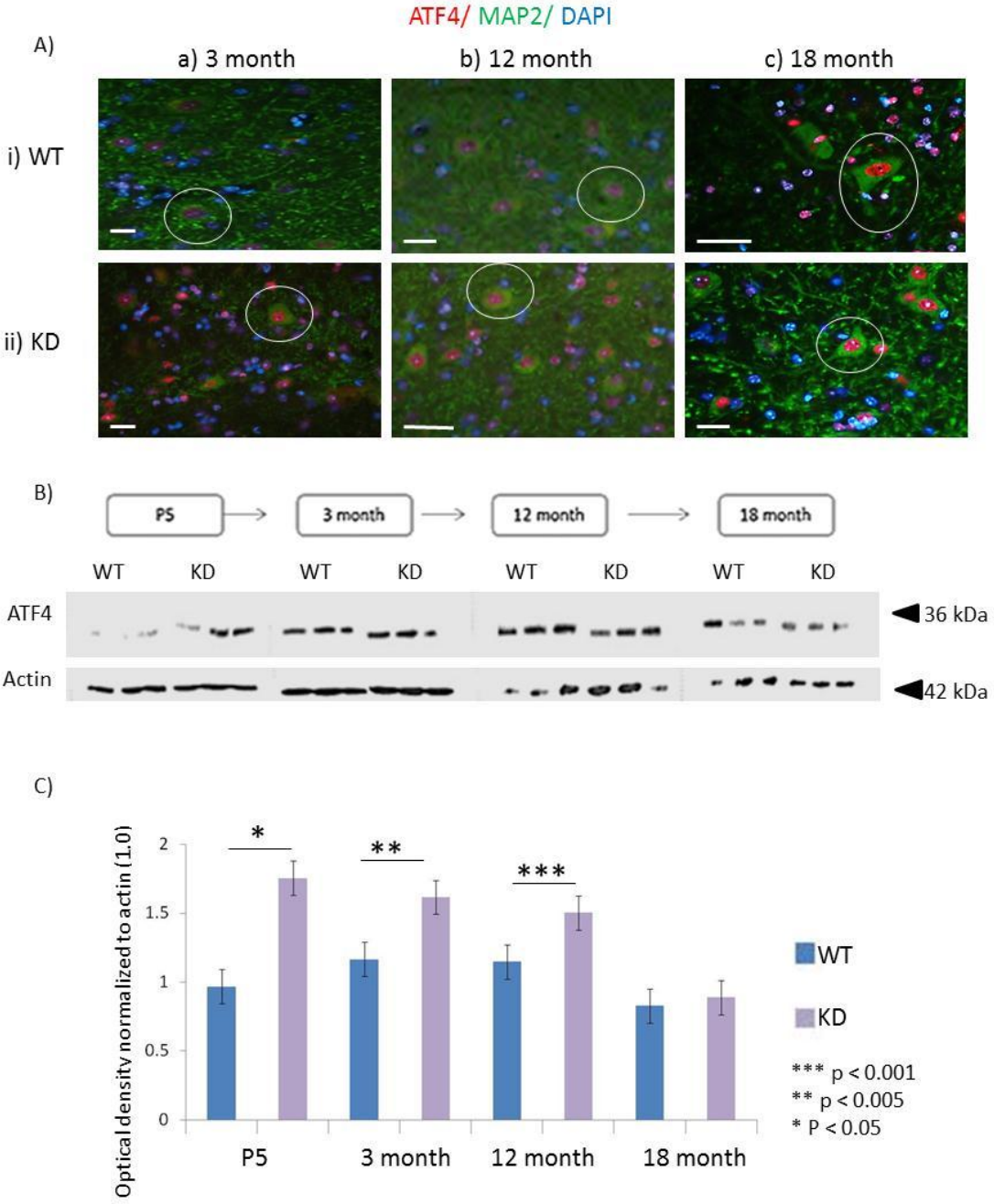
ATF4/ MAP2/ DAPI
A)
a) 3 month
b) 12 month
c) 18 month
i) WT
ii) KD
B)
P5
3 month
12 month
18 month
WT
KD
ATF4
Actin
36 kDa
42 kDa
C)
Optical density normalized to actin (1.0)
*
**
***
WT
KD
*** p < 0.001
** p < 0.005
* P < 0.05
P5
3 month
12 month
18 month

At 3 months and 12 months of age no difference in nuclear CHOP staining intensity is detected between WT and KD motoneurons and at 18 months only a slight increase in staining intensity is observed in KD motoneurons. Overall, the background staining for CHOP appears higher in the KD spinal cord sections, but CHOP-specific immunoreactivity appears to be at the same intensity in both KD and WT sections.

3.2.11.4.2 Western blot analysis (Figure 3.21C & D)

Western blot analysis reveals that CHOP expression is elevated in KD spinal cords compared to WT controls at *all* ages, and like all three of the previous ER stress markers investigated, the magnitude of the difference between KD and WT expression peaks at P5, and is lower at end stage. Indeed, at P5 CHOP expression levels are 70% higher in KD spinal cords compared to WT controls and this difference is significant ($p = 0.008$). At 18 months however, CHOP expression is not significantly higher in KD spinal cords than in WT controls. Unlike other ER stress markers examined, the difference between KD and WT expression of CHOP is higher at 12 (42%, $p < 0.001$) and 18 months (15%, not significant) than at 3 months (10%, not significant).

3.2.11.5 ER stress marker expression with disease progression (Figure 3.22)

Figure 3.22 summarizes the changes in ER stress markers observed in KD spinal cord *relative* to the changes observed in WT controls. The results show that all ER stress markers examined are elevated in KD spinal cords relative to WT controls at some stages of the disease. Furthermore, the peak ER stress marker elevation in KD spinal cords relative to WT controls mainly occurs at P5 and for most markers declines by disease end-stage. In the case of ER stress markers that are further upstream in the UPR, i.e. BiP and phospho-eIF2a, there is only a negligible difference in expression levels between KD and WT spinal cords at disease end-stage. In the case of downstream ER stress markers although there is a decline in the expression difference between WT and KD spinal cords at end-stage, the difference is not significant.

Figure 3.21: CHOP expression in KD spinal cord at various stages of disease progression

Sections of WT and KD lumbar spinal cords were immunostained for CHOP at various stages of disease progression. Typical examples of the pattern of CHOP immunoreactivity in WT and KD motoneurons are shown in Ai) and Aii), respectively at i) 3 months, ii) 12 months and iii) 18 months. Sections were immunostained for CHOP (red), the neuronal marker MAP2 (green) and the nuclear marker DAPI (blue). A modest increase in CHOP immunoreactivity is detected in KD motoneurons at 3, 12 and 18 months of age. Western blot analysis of CHOP expression was also undertaken and a typical Western blot for CHOP is shown in B). The bar chart (C) summarizes the quantification of the optical density of such blots and shows that CHOP levels are significantly greater in KD spinal cords at P5, and 12 months of age, but are not significantly elevated compared to WT at 3 months and 18 months of age.

(Error Bars = standard error of mean, scale bars = 25 μM)

Figure 3.21

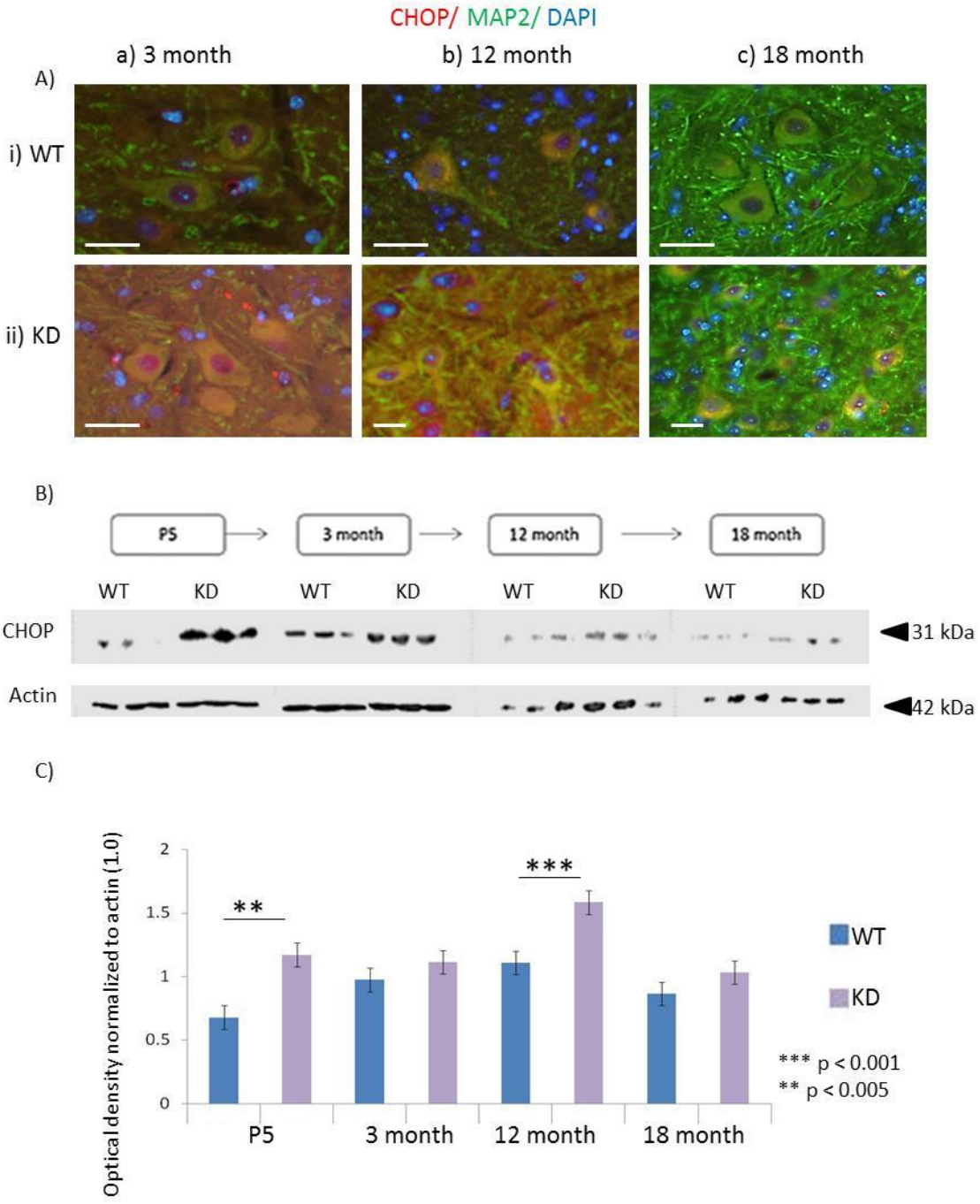
CHOP/ MAP2/ DAPI
a) 3 month
b) 12 month
c) 18 month
A)
i) WT
ii) KD
B)
P5
3 month
12 month
18 month
WT
KD
CHOP
31 kDa
Actin
42 kDa
C)
Optical density normalized to actin (1.0)
**
***
WT
KD
*** p < 0.001
** p < 0.005
P5
3 month
12 month
18 month

Figure 3.22: Summary of ER stress marker expression with disease progression

The bar chart summarizes the increase in expression of ER stress markers (BiP, phospo-eIF2α, ATF4 and CHOP) detected by Western blot in KD spinal cords relative to WT controls at all stages of disease examined. Optical density analysis was performed and protein levels were expressed relative to the house-keeping protein Actin (1.0). For each ER stress marker and time point the percentage increase in expression in KD spinal cord samples relative to corresponding WT controls was calculated. Levels of all of the ER stress markers examined are increased in KD spinal cords throughout disease progression, with a peak increase in all markers detected at P5, followed by a slow decline to WT levels by 18 months.

(Error Bars = standard error of mean)

Figure 3.22

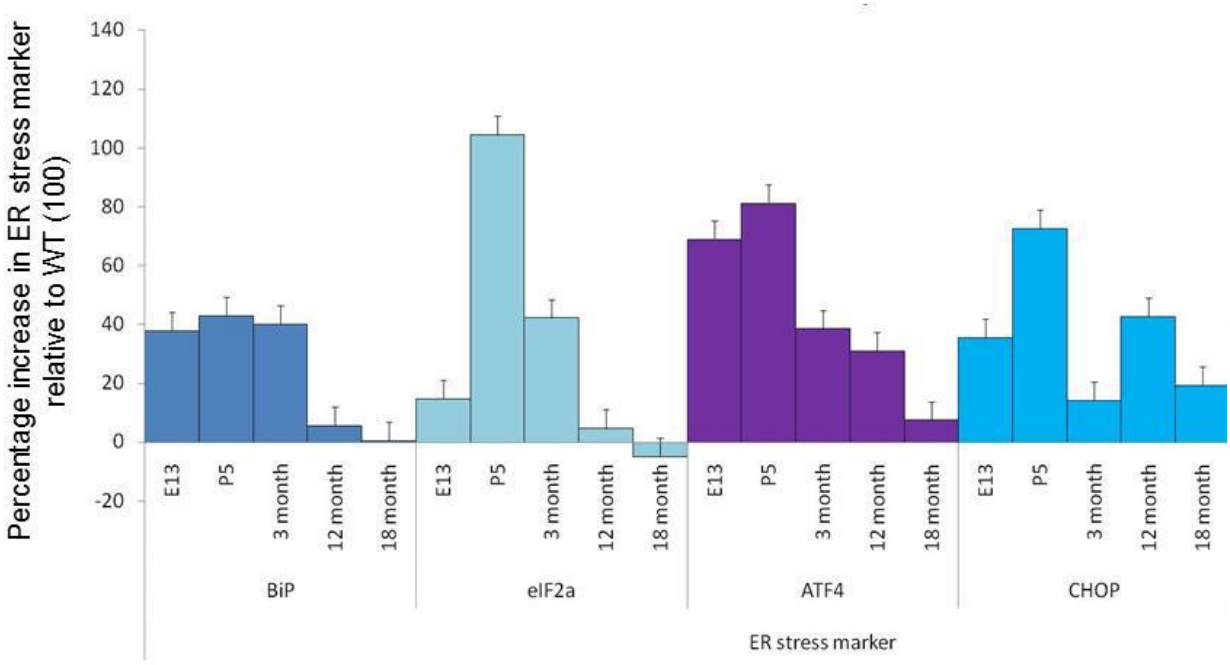
Percentage increase in ER stress marker relative to WT (100)
140
120
100
80
60
40
20
0
-20
E13
P5
3 month
12 month
18 month
BiP
eIF2a
ATF4
CHOP
ER stress marker

3.3 Discussion

3.3.1 Summary

In this study I investigated whether ER stress was a feature of Kennedy's Disease Pathogenesis using two approaches; i) Ca^{2+} imaging; and ii) Determination of ER stress marker levels using immunohistochemistry and Western blot analysis.

I have shown that Ca^{2+} handling is disrupted in primary KD motoneurons resulting in ER Ca^{2+} depletion, which is suggestive of ER stress. Furthermore, ER stress markers are elevated in KD embryonic motoneuron cultures and in spinal cords, especially at early stages of the disease. This indicates that ER stress has a potential role as an early trigger of the disease.

3.3.2 Ca^{2+} handling in KD motoneurons

3.3.2.1 Effects of DHT on cytosolic Ca^{2+} under normal conditions

Under normal circumstances, 50 nM DHT serves a protective function to motoneurons. This is confirmed by treating WT motoneurons with various DHT *final* concentrations, ranging from 0.1 nM to 50 nM, for 72 hours and then imaging them at 7 DIV to obtain readouts of Ca^{2+}.

As the concentration of DHT increases, the basal cytosolic Ca^{2+} concentration in WT motoneurons decreases. This decrease in cytosolic Ca^{2+} can be considered as being protective to cells (Ciutat et al, 1995) however it is important to note that decreases in cytosolic Ca^{2+} are not *exclusively* protective to cells (Arduino et al 2004). It is important to establish whether or not a final DHT concentration of 50 nM, which has been used previously to treat KD motoneurons (Malik et al, 2011), is detrimental to cell survival and thus would confound results obtained in this study. Because increases in DHT result in decreases in cytosolic Ca^{2+}, it can be assumed that 50 nM DHT is not detrimental to motoneurons under normal circumstances. Therefore any toxic effects of

the AR100 mutation can be attributed to the mutation specifically and not to the 50 nM DHT treatment.

Indeed, when Ca^{2+} handling is investigated in KD motoneurons and WT controls the detrimental effects of the mutation are evident.

3.3.2.2 Basal cytosolic Ca^{2+} in primary KD motoneurons

The first indication that KD motoneurons have an imbalanced Ca^{2+} homeostasis compared to WT controls is presented by their cytosolic Ca^{2+} concentration. My results show that cytosolic Ca^{2+} is significantly higher in DHT-treated KD motoneurons both in the absence and presence of external Ca^{2+}, than in WT motoneurons. The lowest level of cytosolic Ca^{2+} is detected in DHT-treated WT motoneurons. These results suggest that DHT-treated KD motoneurons may be more vulnerable, for example, to excitotoxic insult. Indeed it has been shown previously that increases in cytosolic Ca^{2+} in motoneurons makes them more vulnerable to excitotoxicity (for review see Choi, 1996). High levels of cytosolic Ca^{2+} are known to result in various pathological processes such as opening of the mitochondrial permeability transition pore and the consequential release of Cytochrome C from mitochondria, triggering apoptosis (Brustovetsky et al, 2002). Elevated cytosolic Ca^{2+} can also disturb the production of ATP thus jeopardising the energy supply to the cell. This would be detrimental to a vast number of essential cellular processes such as active transport, metabolism and DNA synthesis (et al,Phebus et al, 1995, Yu et al, 2006).

Measurement of cytosolic Ca^{2+} in both DHT-treated and untreated WT and KD cultures, reveals the toxic effect of activation of the mutant AR. In WT motoneurons, DHT treatment results in a decrease in basal cytosolic Ca^{2+} – more noticeably when Ca^{2+} is present in the recording medium. Thus DHT treatment in WT motoneurons can be considered to be protective. In KD motoneurons however, DHT treatment results in an increase in cytosolic Ca^{2+}, indicating that activation of the mutant AR has a potentially toxic effect on motoneurons.

3.3.2.3 ER Ca^{2+} in primary KD motoneurons

Unlike the cytosol, where increases in Ca^{2+} are likely to have deleterious effects, the ER has relatively high levels of Ca^{2+} under normal conditions, so that decreases in ER Ca^{2+} are detrimental to ER function.

The lowest level of ER Ca^{2+} was detected in DHT-treated cultures and the highest level was found in DHT-treated WT cultures. Since a decrease in ER Ca^{2+} is indicative of ER stress (Chami et al, 2008), these results suggest that ER stress is present in DHT-treated KD motoneurons. Under normal circumstances the concentration of Ca^{2+} in the ER is in the 0.3-1 mM range. Because DHT-treated WT cultures, despite having the highest level of ER Ca^{2+} recorded in these experiments, still have a concentration that is below the normal μM range (Narayanan et al, 2010), it is possible that the process of culturing primary motoneurons results in ER Ca^{2+} depletion even in WT motoneurons. Thus the experimental protocol used can only give an indication of *relative* levels of ER Ca^{2+}. Conclusions based on these experiments however, need to be approached with caution, as the values obtained for ER Ca^{2+} are not absolute. Indeed, following TG application, Ca^{2+} is released into the cytosol, which is a larger compartment than the ER and thus the Ca^{2+} signal is diluted. Furthermore, Ca^{2+} is pumped out of the cytosol by the plasma membrane calcium ATPase, (PMCA) so is decreasing during quantification of the signal. Thus, it is the relative levels of Ca^{2+} that are considered.

As observed with the measurement of basal cytosolic Ca^{2+}, DHT treatment appears to have opposite effects on ER Ca^{2+} in WT and KD motoneurons. In WT motoneurons, 72 hour DHT treatment results in an increase in ER Ca^{2+}, suggesting an improvement in ER function. In KD motoneurons however, DHT treatment results in a significant decrease in ER Ca^{2+}, suggesting a significant impairment of ER function. Furthermore, there is only a negligible difference between untreated WT and untreated KD motoneurons with respect to inferred ER Ca^{2+}, yet the response of WT and KD motoneurons is significantly different following DHT treatment. This finding suggests

that the presence of the mutant AR alone, in the absence of the ligand, does not cause significant ER Ca^{2+} depletion. However when the ligand i.e. the androgen, is present and the AR is activated, there is significant ER Ca^{2+} depletion. This observation reflects the clinical phenotype of KD, where the disease only manifests in males. In cases where females express the mutant AR, the absence of the ligand, i.e. androgens, means that the AR remains inactive, resulting in an asymptomatic phenotype.

3.3.2.3 Inferred Store-operated Ca^{2+} (SOC) influx in primary KD motoneurons

ER Ca^{2+} depletion results in store-operated Ca^{2+} influx (SOC influx), as discussed in detail in Section 3.1.2.1. Briefly, SOC influx involves the entry of Ca^{2+} through plasma membrane channels, resulting in elevated cytosolic Ca^{2+}. This aids ER Ca^{2+} replenishment. Thus the lower the level of ER Ca^{2+}, the higher the level of consequential SOC influx. Indeed, in the results presented in this Chapter, in keeping with the finding that DHT-treated KD motoneurons have the lowest level of inferred ER Ca^{2+}, they also possess the highest level of SOC influx. Furthermore, the level of SOC influx is significantly higher in DHT-treated KD motoneurons than in DHT-treated WT motoneurons, which have a significantly higher level of inferred ER Ca^{2+}.

The increased level of SOC influx in DHT-treated KD motoneurons could also explain the increased level of basal Ca^{2+} observed when cultures are examined in a 1 mM Ca^{2+} recording medium. If the ER is depleted of Ca^{2+} and external Ca^{2+} is available, SOC influx would already be occurring in the motoneurons and thus under basal conditions, the concentration of cytosolic Ca^{2+} would be higher.

3.3.2.3 Kinetics of the cytosolic responses of motoneurons to TG application and external Ca^{2+} introduction

As well as measuring absolute values, observation of the kinetics of Ca^{2+} handling in motoneurons in response to both Thapsigargin (TG) application and Ca^{2+} introduction can also provide information about the mechanisms responsible for disturbances in cellular Ca^{2+} handling.

Following TG application to cultures, the response onset and time-to-cytosolic Ca^{2+} peak are similar for WT and KD motoneurons. TG inhibits the SERCA pump and this prevents Ca^{2+} from being pumped from the cytosol into the ER. The elevated cytosolic Ca^{2+} that occurs as a result of TG application is therefore a result of Ca^{2+} leaving the ER without being pumped back in. Because the onset and time-to-cytosolic Ca^{2+} peak are the same in WT and KD motoneurons, it can be suggested that Ca^{2+} exit out the ER is not impaired in KD motoneurons. However, the lower steady state level of ER Ca^{2+} in KD motoneurons indicates that Ca^{2+} exit out of the ER occurs at a slower rate than in WT motoneurons. Thus a greater amount of ER Ca^{2+} is able to exit the ER in WT motoneurons in the same amount of time as a lower amount of Ca^{2+} from the ER in KD motoneurons, due to higher Ca^{2+} concentration gradient between the ER and the cytosol in the WT cells.

The duration of Ca^{2+} elevation in response to TG application also provides some useful information about cellular Ca^{2+} handling. In WT motoneurons the response to TG is relatively prolonged, but it is more transient in KD motoneurons. This could reflect the lower level of Ca^{2+} in the ER in KD motoneurons. Because the ER is depleted of Ca^{2+} in these motoneurons, the supply of ER Ca^{2+} runs out more rapidly in KD motoneurons following TG application and thus the duration of the response is shorter. These results could also suggest however that processes by which Ca^{2+} is expelled from the cytosol, for example activation of the Plasma Membrane Ca^{2+} ATPase (PMCA) pump, are heightened in KD motoneurons. The nature of SOC influx however does not support this possibility – in this case the WT response is transient whilst the KD response is relatively prolonged. Therefore it is more likely that the ER rapidly runs out of Ca^{2+} in KD motoneurons giving rise to a shorter TG-induced response. The prolonged SOC influx in KD motoneurons suggests that because the ER is depleted of Ca^{2+}, a greater amount of time and a higher level of Ca^{2+} influx are needed for ER Ca^{2+} to be replenished in KD motoneurons.

3.3.3 Activation of the mutant AR by androgens is essential for the induction of ER stress in motoneurons

Taken together, these results indicate that the presence of the mutant AR in combination with receptor activation in the presence of androgens, are detrimental to ER Ca^{2+} and thus ER function. If ER Ca^{2+} depletion does indeed play a role in KD pathogenesis, it is important to determine whether or not it would occur in KD males due to an inherent difference between male and female androgen receptors or due to differences in androgen availability. The manifestation of KD is believed to occur due to the availability of androgens rather than an inherent difference in the AR. This is because AR antagonists relieve KD symptoms, whilst the administration of androgens to female mice possessing the mutant receptor results in presentation of the disease phenotype (Katsuno et al, 2003). Therefore, in these experiments it was important to establish if the differences observed in ER Ca^{2+} in WT and KD motoneurons were the result of an intrinsic defect due to the presence of the mutant AR, or only manifest in KD motoneurons in the presence of androgens irrespective of the sex of the mouse from which they were derived. I showed that there were no differences in ER Ca^{2+} in motoneurons from male and female mice, in the presence of the androgen i.e. female KD motoneurons and male KD motoneurons showed the same deleterious changes following exposure to DHT.

With respect to basal cytosolic Ca^{2+}, there is only a negligible difference between DHT-treated male and DHT-treated female KD motoneurons. A similar trend is observed for inferred ER Ca^{2+} and inferred SOC influx. These results show that there is no difference between DHT-treated KD male and DHT-treated KD female motoneurons with respect to cytosolic and ER Ca^{2+} levels. This finding suggests there is no inherent difference in the AR. Female motoneurons treated with DHT have elevated levels of cytosolic Ca^{2+} and depleted ER Ca^{2+}, in the same way that female mice possessing the mutation present with KD symptoms when treated with androgens (Breedlove et al, 1981). It can therefore be suggested that the pattern of occurrence of depleted ER Ca^{2+}

is consistent with symptom presentation in KD motoneurons and thus it is a candidate for an underlying pathological mechanism.

3.3.4 Control experiments using Fura 2

The results discussed above were obtained using Fluo 4-AM as a Ca^{2+} indicator. Measurements obtained when using single wavelength excitation (SW) dyes such as Fluo 4-AM are often difficult to interpret because the fluorescence intensity of the dye often changes in response to factors other than Ca^{2+} concentration such as heterogeneous loading of the dye in different cells, dye leakage or bleaching of the signal by continuous illumination. Ratiometric dyes overcome this problem (Rudolf 2003). Therefore, I re-examined some of the key features of Ca^{2+} handling in WT and KD motoneurons using the ratiometric dye, Fura 2 in order to see if the trend in results is reproducible and reliable. The same trend was indeed observed for basal cytosolic Ca^{2+}, inferred ER Ca^{2+} and SOC influx using Fura 2 as had been recorded using Fluo 4-AM. DHT-treated KD motoneurons have the highest basal Ca^{2+} and SOC influx and the lowest ER Ca^{2+}. The largest discrepancy between Fluo 4-AM and Fura 2 read-outs is observed when measuring inferred ER Ca^{2+}. Fura 2 measurements suggested that there was a 150% decrease in ER Ca^{2+} in KD motoneurons following DHT treatment but a 240% increase is observed when using Fluo 4-AM as the calcium indicator. This could be because Fura 2 is more prone to compartmentalization than Fluo 4-AM (Thomas et al, 2000), which could produce a lower global cytosolic calcium concentration average. However, because the Fura 2 signal is not calibrated, the discrepancies in the results cannot be explained.

3.3.5 ER stress in a model of ALS

In order to test the reliability of ER Ca^{2+} depletion measurements to assess ER stress I undertook a similar series of recordings using a different model of MND that is known to involve ER stress in its underlying pathology (Saxena et al, 2009). If ER Ca^{2+} depletion is detected in motoneurons from the $SOD1^{G93A}$ mouse model of ALS in which

convincing evidence for ER stress has been published, the occurrence of ER Ca^{2+} depletion correlates with the occurrence if ER stress.

The $SOD1^{G93A}$ mouse model overexpresses the SOD1 enzyme and therefore in order to control for the effects of overexpression of the SOD1 protein, SODH mice, which over express the Wild-Type SOD1 protein were used as a control as they allow the effects of the mutation *per se* to be examined as opposed to over-expression of the protein.

The highest level of cytosolic Ca^{2+} was detected in $SOD1^{G93A}$ motoneurons, whilst WT motoneurons possess a significantly lower level of basal cytosolic Ca^{2+}, which may contribute to the selective vulnerability of $SOD1^{G93A}$ motoneurons to excitotoxicity (Van Den Bosch et al, 2006). SODH motoneurons however, have a basal cytosolic Ca^{2+} concentration that is intermediate between $SOD1^{G93A}$ and WT. This suggests that protein over-expression is enough to result in elevated cytosolic Ca^{2+} and has toxic effects on motoneurons.

The same trend was observed for ER Ca^{2+}. Inferred ER Ca^{2+} is highest in WT motoneurons and significantly lower in $SOD1^{G93A}$ motoneurons. ER Ca^{2+} is not as low in SODH motoneurons as it is in $SOD1^{G93A}$ motoneurons, however the level of ER Ca^{2+} is still significantly lower in SODH motoneurons than in WT motoneurons. This suggests that over-expression of the SOD1 protein alone is enough to cause ER Ca^{2+} depletion. As is the case with basal cytosolic Ca^{2+} however, $SOD1^{G93A}$ expression and protein over-expression appear to have a cumulative effect on ER Ca^{2+}.

$SOD1^{G93A}$ motoneurons not only have the lowest level of ER Ca^{2+}, but they also have the highest level of SOC influx. Furthermore, the lowest level of SOC influx is observed in WT motoneurons, which have the highest level of ER Ca^{2+}. The level of SOC influx observed in SODH motoneurons lies between the levels measured in WT and $SOD1^{G93A}$ motoneurons. This suggests that although over-expression of the SOD1

protein is detrimental for motoneuron Ca^{2+} handling, the mutation *per se* also has effects on cellular Ca^{2+}.

3.3.6 What causes ER Ca^{2+} depletion in KD motoneurons?

Although confocal microscopy reveals that the ER is depleted of Ca^{2+} in KD motoneurons, it does not reveal any information about what may be the cause of this ER Ca^{2+} depletion. Furthermore, it also only allows the presence of ER stress to be inferred and not confirmed. Western blot analysis of purified DHT-treated WT and DHT-treated KD embryonic motoneurons can provide some of the information that confocal experiments lack.

ER Ca^{2+} is controlled by the $InsP_3$ and Ryanodine receptors, which allow movement of Ca^{2+} out of the ER, and the Sarco/Endoplasmic Reticulum ATPase 2 (SERCA2 pump), which pumps Ca^{2+} into the ER against its concentration gradient. It has been shown previously that one of the downstream actions of the AR is to up-regulate expression of SERCA2 pump mRNA, leading to an increase in ER Ca^{2+} (Foradori et al, 2008). Therefore, the SERCA2 pump could be a link between mutations in the AR and ER Ca^{2+} levels.

Western blot analysis reveals that the level of SERCA2b pump protein expression is significantly lower in E13 DHT-treated KD motoneurons than in WT controls. This is very likely to contribute to the lower level of ER Ca^{2+} observed in KD motoneurons. A lower level of SERCA2b pump expression in the ER membrane would impair the capacity of the ER to sequester Ca^{2+} from the cytosol and thus could result in ER Ca^{2+} depletion. However in order to determine whether or not this could account for levels of ER Ca^{2+}, future work would need to establish expression levels and activity of the $InsP_3$ and Ryanodine receptors. If expression levels and activity of these channel receptors are impaired, it could balance out SERCA2 pump impairment and so there would be no net decrease in ER Ca^{2+}. This will be discussed in more detail in Chapter 6.

The fact the SERCA2b expression decreases in KD motoneurons is in keeping with the observed ER Ca^{2+} depletion. However, it is not in keeping with the finding that SERCA2b expression normally increases as a result of cytosolic Ca^{2+} increase and as a downstream effect of AR activation, as discussed earlier (Chapter 1, Section 1.2.2). This suggests that the AR mutation alters the transcriptional activity of the receptor. Indeed it has been suggested that the CAG-repeat expansion in the N-terminal domain of the AR results in truncated forms of the receptor being produced (Fischbeck et al, 1999). Translocation of the truncated form of the AR into the nucleus has been found to be impaired and so the transcription of downstream targets of the receptor is also likely to be impaired (Butler et al, 1998). Indeed, residues 101-370 of the N-terminal domain of the AR are required for full ligand activated transcriptional activity (Bevan et al, 1999).

3.3.7 ER Ca^{2+} depletion results in ER stress in KD motoneurons

Although ER Ca^{2+} depletion occurs in KD motoneurons, possibly as a result of reduced SERCA2b expression, these findings did not confirm that ER stress is a feature of KD motoneurons. However, examination of the expression levels of several markers of ER stress revealed that ER stress is significantly higher in embryonic KD motoneurons than in WT controls. BiP levels for example, are approximately 20 % higher in KD motoneurons than in WT controls, which is indicative of both ER stress and elevated cytosolic Ca^{2+} depletion, as BiP is transcribed as a result of these two events (Hong et al, 2005).

The expression of phospho-eIF2α is also higher in embryonic KD cultures by approximately 11.2 %, which suggests that ER stress-induced protein translation is arrested to a greater extent in KD motoneurons than in WT controls, even as early as E13. This conclusion however, would be more reliable if eIF2α expression was also measured as it is the phospho-eIF2α:eIF2α ratio of that quantifies ER stress (van

Huizen et al, 2003). This would therefore be a necessary future experiment to investigate ER stress further.

Expression levels of ER stress markers that are further downstream of the UPR such as ATF4 and CHOP are also elevated in embryonic KD motoneurons compared to WT controls. Increased expression of CHOP in KD motoneurons suggests that there is a greater amount of pro-apoptotic protein transcription in these motoneurons than in WT controls. This increases the risk of ER stress-induced apoptosis occurring in KD motoneurons. This possibility will be examined further in Chapter 4. Because ER stress occurs to a greater extent in KD motoneurons even at such an early stage of development it can be considered as a strong candidate for an underlying disease trigger for KD.

3.3.8 ER stress during disease progression in the spinal cord of KD mice

As well as identifying the earliest time point at which ER stress occurs in motoneurons of KD mice it is also useful to determine whether or not ER stress persists throughout disease progression. As discussed previously (Section 3.1.3.1), markers of ER stress are elevated throughout disease progression in the $SOD1^{G93A}$ model of ALS (Saxena et al, 2009). The earliest observed increase in the ER stress marker BiP occurs at P5 in the $SOD1^{G93A}$ mice suggesting that ER stress plays an early role in ALS pathogenesis (Saxena et al, 2009). Sharp increases in BiP in the $SOD1^{G93A}$ model also coincide with the occurrence of denervation, indicating that the occurrence of ER stress correlates with symptom manifestation (Saxena et al, 2009).

All of the markers of ER stress measured in this study appear to be elevated in KD spinal cords compared to WT controls as early as postnatal day 5 (P5) and evidence of ER stress observed throughout disease progression. However, in all cases the difference between WT and KD spinal cords with respect to ER stress marker levels diminishes with disease progression and in the case of BiP and phospho-eIF2α, there is no difference between the genotypes at disease end-stage. It is possible that at

disease end stage, a large proportion of motoneurons have already degenerated so that KD motoneurons, which would be expressing elevated levels of ER stress markers, are no longer present. The read out that is obtained at end-stage is based on surviving motoneurons only – not all disease-affected motoneurons. Furthermore, at disease end-stage, the natural effects of aging, which also occur in WT motoneurons, have also influenced levels of ER stress markers. Indeed, up until 12 months of age, the level of ER stress markers appears to be modestly increasing in WT motoneurons. These motoneurons are not made vulnerable by an underlying pathology and do not degenerate, whereas KD motoneurons are progressively lost. Thus, the overall protein levels of ER stress markers from WT 18 month spinal cords, where there is a low level of age-related ER stress in a large number of motoneurons, is similar to the overall protein levels in KD spinal cords, where there is a high amount of ER stress in very few motoneurons. Indeed, data from our lab shows that by 18 months of age only 60% of motoneurons survive in the sciatic motor pool of KD mice (Malik et al, 2011).

The levels of BiP observed at various stages of disease in KD mice reveal that ER stress may in fact be an earlier event in KD pathology than in ALS pathology. Indeed, the peak elevation in BiP in KD motoneurons is detected at P5 in KD motoneurons but at P28 $SOD1^{G93A}$ mice (Saxena et al, 2009). Furthermore, disease progress is much slower in the AR100 mouse model of KD than in the $SOD1^{G93A}$ model of ALS, with the first symptoms manifesting at approximately 440 days (Sopher et al, 2004) and 90-120 days of age (Reyes et al, 2010), respectively. Thus an earlier peak elevation of BiP in the KD mouse model suggests that ER stress is more likely to be a feature of disease pathology in KD than in ALS pathology.

As observed at E13, increased expression of BiP in spinal cords of KD mice of different ages appears to be specific to motoneurons, as demonstrated by BiP immunoreactivity in spinal cord sections. This correlation between the expression of ER stress markers and vulnerability to disease pathology further suggests that ER stress is an underlying pathological mechanism in KD.

In keeping with the results found for BiP expression levels, phospho-eIF2α expression also appears to be elevated in KD spinal cord tissue compared to WT tissue and the peak of this elevation is also at P5. This suggests that the PERK pathway of the UPR is active in KD spinal cord tissue at P5 and that translational block is occurring. However, as discussed above, conclusions regarding the expression of eIF2α need to be approached with caution until the ratio of phospho-eIF2α:eIF2α is obtained.

The expression of ATF4 and CHOP are also elevated in KD spinal cord tissue compared to WT controls and this elevation peaks at P5. However unlike BiP and phospho-eIF2α, ATF4 and CHOP remain elevated in KD spinal cord compared to WT controls at disease end-stage. Therefore, markers that are further downstream of the UPR appear to remain elevated for longer. This could be because of an imbalance between the expression of pro-survival and pro-apoptotic proteins expressed downstream of the UPR in KD motoneurons. The results suggest that this is indeed the case. Both BiP (pro-survival) and CHOP (pro-apoptotic) are transcribed downstream of the PERK pathway as discussed above. When the relative protein levels of BiP and CHOP are examined in WT and KD spinal cords at P5 – when there is peak ER stress- the imbalance between pro-survival and pro-apoptotic proteins is revealed. In WT spinal cord the relative levels of BiP and CHOP are both approximately 0.7. However in KD spinal cord tissue, the relative protein level of CHOP is 20% higher than the level of BiP. Thus there could be a skew in expression towards pro-apoptotic proteins in KD motoneurons at P5.

3.3.9 Summary

The results presented in this Chapter have shown that there is elevated basal cytosolic Ca^{2+} in embryonic motoneurons cultured from the AR100 mouse model of Kennedy's Disease (KD) compared to WT littermate controls, implying that KD motoneurons could be more vulnerable to excitotoxic insult. Embryonic KD motoneurons also possess a lower concentration of ER Ca^{2+} than WT controls and as a direct result respond to

drug-induced ER Ca^{2+} depletion and subsequent Ca^{2+} introduction with a higher level of SOC influx.

The decrease in ER Ca^{2+} that occurs in KD motoneurons is likely to be a result of a decreased expression of the SERCA2b pump in these motoneurons. A decrease in SERCA2b expression lowers the ability of the ER to sequester Ca^{2+} from the cytosol and thus Ca^{2+} that exits the ER is not replaced efficiently and there is a resultant net decrease.

All of the ER stress markers measured are elevated in primary embryonic KD motoneurons compared to embryonic WT motoneurons. The presence of ER stress at such an early stage of disease indicates that ER stress may be a causative event in KD pathology as opposed to a secondary effect. ER stress remains in motoneurons throughout disease progression in the AR100 model of KD although the difference between KD and WT motoneurons with respect to ER stress marker expression decreases over time, possibly because disease-affected motoneurons are suspected to be dying. Examination of ER stress longitudinally also reveals an imbalance between pro-survival and pro-apoptotic protein transcription downstream of the UPR in KD motoneurons, in which levels of pro-apoptotic proteins are higher.

Because ER stress is present in embryonic KD motoneurons, and the peak difference in ER stress marker expression between KD and WT spinal cord tissue is at P5, it seems likely that the role of ER stress is at its peak pre-symptomatically. This makes ER stress a strong candidate for an early, underlying disease trigger.

CHAPTER 4: RESULTS 2 – ER STRESS-INDUCED APOPTOSIS IN KD MOTONEURONS

4.1. Introduction

The Unfolded Protein Response (UPR) is a cellular response that is activated downstream of ER stress as an attempt to restore ER homeostasis. It results in the transcription of both pro-survival and pro-apoptotic proteins so when the source of ER stress cannot be resolved and the UPR is activated for a prolonged length of time, pro-apoptotic proteins accumulate and ER stress-induced apoptosis ensues (Szegezdi et al, 2007). The results presented in Chapter 3 show that ER stress is an early feature of pathology in KD motoneurons in vitro. However, it is not necessarily the case that such stress results in ER stress-induced apoptosis and therefore it cannot be concluded that the ER stress observed in embryonic KD motoneurons contributes to the death of motoneurons observed in Kennedy's Disease.

Therefore, in this Chapter in order to determine the contribution of ER stress to motoneuron death in KD, markers of ER stress-induced apoptosis were examined in WT and KD primary motoneurons and the effects of pharmacologically inhibiting ER stress on motoneuron survival investigated.

4.1.1 ER stress-induced apoptosis & the role of Caspase 12

ER stress-induced apoptosis can be considered to involve three separate stages; initiation, commitment and execution (Szegedi et al, 2003). The initiation and commitment phases occur when the UPR is initiated and pro-apoptotic proteins, such as CHOP, are consequentially transcribed, (Discussed in Chapter 3, Section 3.1.2.2). The execution of ER stress-induced apoptosis essentially involves the activation of Caspases and will be the focus of this Chapter. Although mitochondrial and death receptor-mediated apoptosis are well characterized, Caspases involved in ER stress-induced apoptosis have yet to be established with Caspases 12, 3, 6, 7, 8 and 9 being implicated in the process (Dahmer et al, 2005, Rosati et al, 2010, Szegedi et al, 2003).

Caspase 12 has been suggested to be the key mediator of ER stress-induced apoptosis and was the first Caspase to be associated with the ER (Nakagawa et al,

2000). Caspase 12 is expressed in rodents exclusively, with Caspase 4 fulfilling the same role in humans (Szegedi et al, 2003) and its activation is specific to ER stress-induced apoptosis (Yoneda et al, 2001). Indeed, Caspase-12 knock-out mice display an increased resistance to ER stress-induced apoptosis whilst vulnerability to triggers of other apoptotic mechanisms is unchanged (Nakagawa et al, 2000).

Caspase 12 is a Group 1 Caspase (Eckhart et al, 2009). These proteins consist of a long Caspase-recruitment domain (CARD domain), which interacts with various proteins such as *TNF receptor-associated factor 2 (*TRAF2) and other Caspases. Group 1 Caspases also contain two catalytic domains referred to as P10 and P20 (Eckhart et al, 2009). The proposed structure of Caspase 12 is depicted in Figure 4.1.

There are several suggested mechanisms for the activation of Caspase 12 that occurs downstream of ER stress. One such mechanism involves the protein TRAF2, which is recruited by Inositol Requiring Enzyme 1 (IRE1) during the UPR (Urano et al, 2000). Inactive pro-Caspase 12 forms a stable complex with TRAF2 in unstressed cells (Yoneda et al, 2001). Following ER stress however, pro-Caspase 12 is thought to dissociate from TRAF2 and in doing so is able to form pro-Caspase 12 oligomers (Yoneda et al, 2001). Oligomerization of pro-Caspase 12 is then thought to trigger autoprocessing of the CARD domain and as a result, active catalytic domains are cleaved and Caspase 12 is activated (Yoneda et al, 2001).

Another proposed mechanism of Caspase 12 activation, which is suggested to specifically occur downstream of ER Ca^{2+} depletion has also been suggested (Nakagawa et al, 2000). Ca^{2+} release from the ER is proposed to activate the Ca^{2+}-dependent, neutral protease Calpain, which cleaves pro-Caspase 12 (Nakagawa et al, 2000). Calpain cleavage of pro-Caspase 12 at residue D318, releases the CARD domain, leaving a 38 kDa Caspase fragment.

Figure 4.1: Proposed structure of Caspase 12

Caspase 12 consists of a long Caspase-recruitment domain (CARD domain), which is also referred to as the Pro-domain and is 2-32 kDa in size. Caspase 12 also contains two catalytic domains referred to as P10 and P20, which are 17-20 kDa and 10-13 kDa in size, respectively. Aspartate residues at the borders of the catalytic domains form the cleavage sites involved in Caspase 12 activation.

Prior to activation, Caspase 12 dimerizes and the most accepted configuration is shown in diagram B): The P20 domains are exposed to the cytosol, whilst the P10 domains are concealed.

Figure 4.1

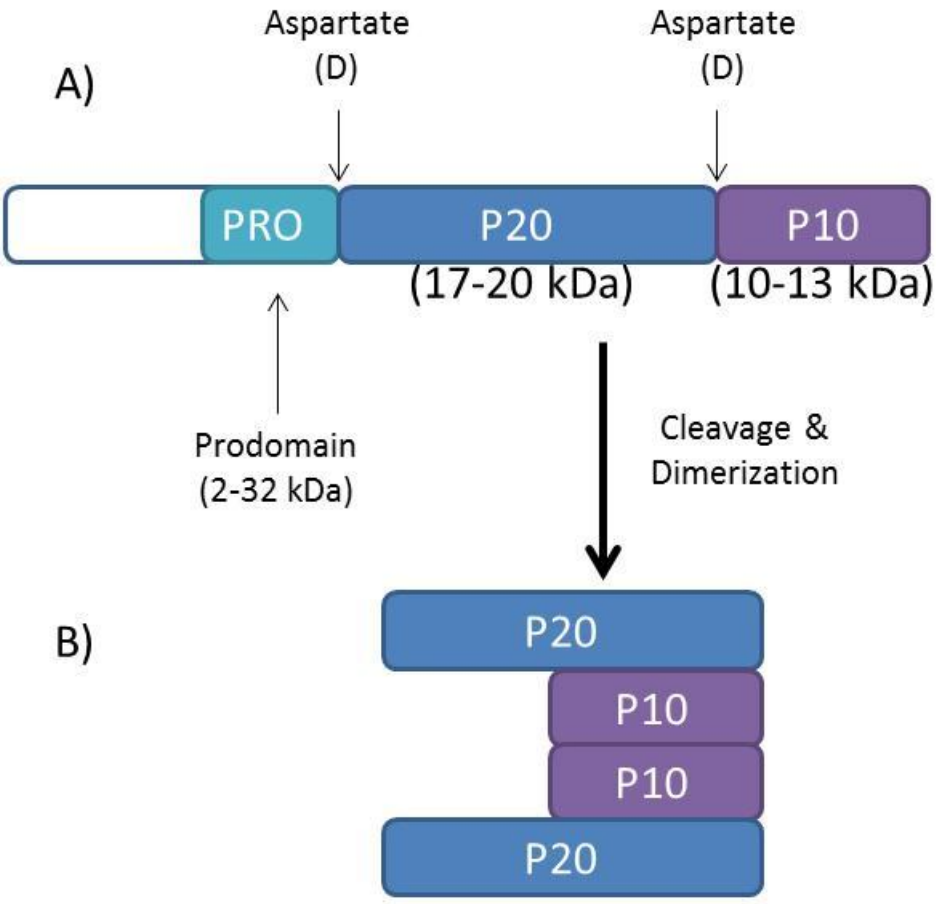

Adapted from Springer images, online resource

The P10 subunit is then cleaved, leaving a 23 kDa Caspase fragment that contains the P20 subunit and an intact catalytic residue; C298. Finally, autolytic cleavage is proposed to result in the release of the P20 fragment (Martinez et al, 2010).

As well as Calpain-mediated cleavage of pro-Caspase 12, other Caspases, such as Caspase 7 are thought to cleave and thus activate Caspase 12 (Martinez et al, 2010). Furthermore, the cleavage of pro-Caspase 12 by Caspase 7 has been suggested to play a more pivotal role than Calpain-mediated cleavage in apoptosis triggered downstream of ER Ca^{2+} depletion. Indeed, decreases in both Caspase 12 activation and Thapsigargin-induced death in PC12 cells are larger following Caspase 7 inhibition than they are following Calpain inhibition (Martinez et al, 2010).

By whatever mechanism, once Caspase 12 has been activated, apoptosis ensues. This occurs via the activation of Caspase 3, which is an ubiquitously expressed Caspase that mediates the execution of apoptosis (Kerbiriou et al, 2009). The mechanism of action by which Caspase 3 is activated downstream of Caspase 12 is summarized in Figure 4.2. The activation of Caspase 3 induces apoptosis via the cleavage of several essential cellular proteins. For example, the activation of Caspase 3 has been associated with the proteolytic cleavage of Protein Kinase C (Anantharam et al, 2002), cytoskeletal proteins (Mashima et al, 1999) and Poly-ADP ribose polymerase, or PARP (Jimenez et al, 2002).

4.1.2 ER stress-induced apoptosis in Motor Neuron Diseases

Caspase 12 activation has been found to occur in other models of Motor Neurone Diseases (MNDs) such as the $SOD1^{G93A}$ transgenic mouse model of Amyotrophic Lateral Sclerosis (ALS). For example, quantitative PCR analysis has revealed that the level of cleaved Caspase 12 is significantly higher in the spinal cord of symptomatic $SOD1^{G93A}$ ALS mice compared to WT controls (Wootz et al, 2004).

Figure 4.2: Activation of Caspase 3 downstream of Caspase 12

The schematic illustrates two mechanisms, which have been proposed for the activation of Caspase 12.

Following ER stress-induced activation of the UPR, TRAF2 dissociates from Caspase 12 and interacts with IRE1 in the ER membrane (1a). This results in Caspase 12 dimerization (1b). Alternatively, Ca^{2+}release from the ER results in the activation of Calpain, which cleaves Pro-Caspase 12 (2). Active Caspase 12 then activates Caspase 9 (3), which activates Caspase 3 (4).

Figure 4.2

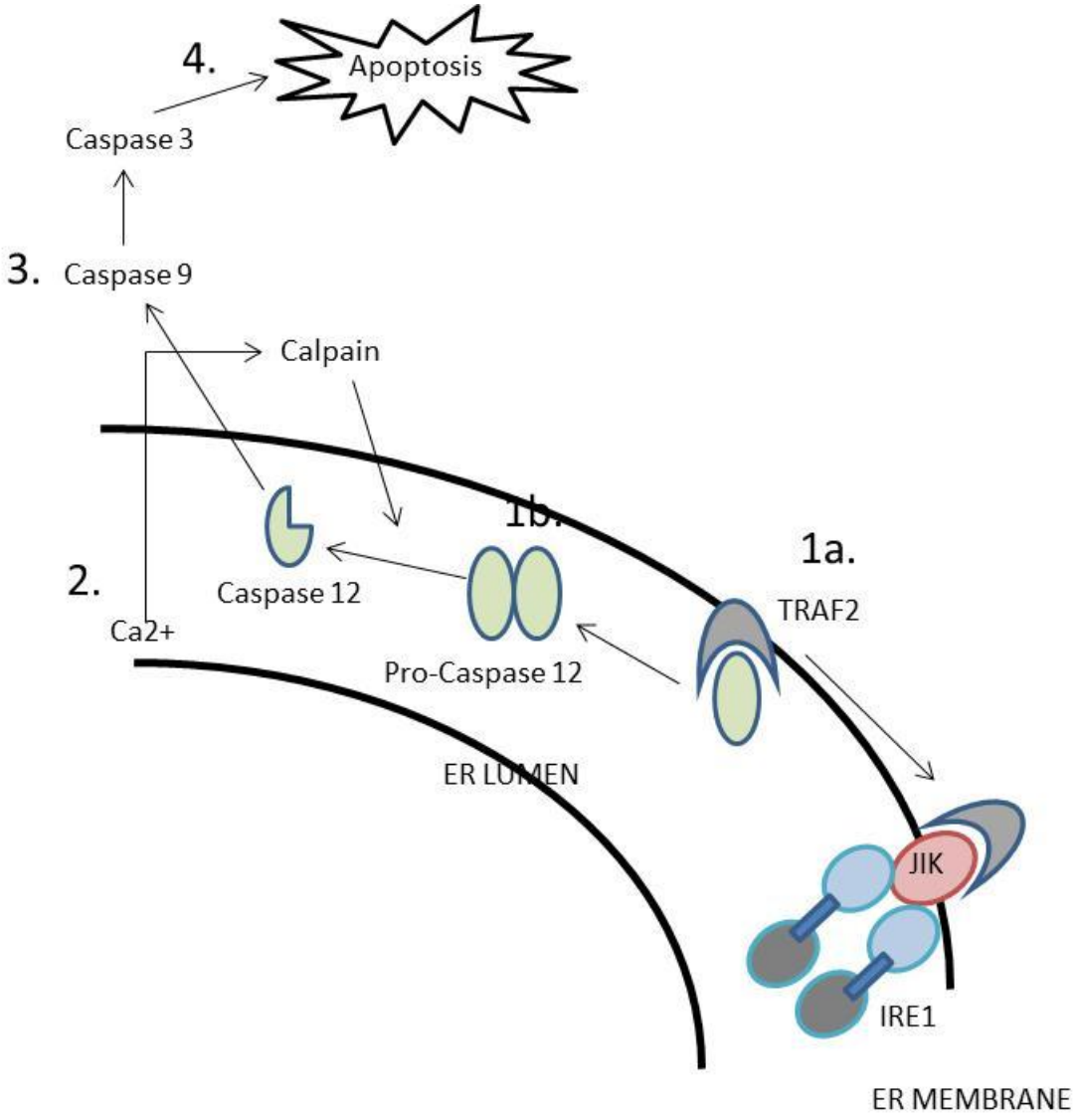
4.
Apoptosis
Caspase 3
3.
Caspase 9
Calpain
1b.
1a.
2.
Caspase 12
TRAF2
Ca2+
Pro-Caspase 12
ER LUMEN
JIK
IRE1
ER MEMBRANE

Furthermore, the level of cleaved Caspase 12 is higher in symptomatic $SOD1^{G93A}$ mice than in pre-symptomatic $SOD1^{G93A}$ mice, although these asymptomatic mice express higher levels of active Caspase 12 than WT mice (Wootz et al, 2004). This suggests that the presence of the mutant SOD1 protein alone increases levels of active Caspase 12 pre-symptomatically and that Caspase 12 activation increases further with symptom manifestation. Increased levels of Caspase 12 have also been detected in the cerebrospinal fluid (CSF) of ALS patients relative to healthy controls (Vijayalakshmi et al, 2010). Furthermore, rat spinal motoneurons exposed to CSF from ALS patients express elevated levels of Caspase 12 compared to control motoneurons that are exposed to non-ALS CSF (Vijayalakshmi et al, 2010**).** This suggests that, in the case of ALS, the causes of ER stress can be extrinsic to motoneurons.

4.1.3 ER stress-induced apoptosis in CAG-repeat disorders: the effect of repeat size

ER stress-induced apoptosis also occurs in other CAG-repeat disorders such Huntington's Disease (HD). The presence of Poly-CAG aggregates is accompanied by activation of Caspase 12 via cleavage at the D318 residue (Kouroku et al, 2002). Immunoblotting of this cleavage site reveals that the levels of active Caspase 12 following Tunicamycin treatment are higher in cells expressing a Huntingtin protein possessing 72 CAG-repeats than cells expressing a control protein with 11 CAG repeats (Kouroku et al, 2002). These findings therefore indicate that levels of active Caspase 12 increase with increasing CAG-repeat number.

4.1.4.1 Salubrinal: Pharmacological inhibition of ER stress

As well as measuring expression levels of markers of ER stress-induced apoptosis, the role of ER stress-induced apoptosis in disease pathology can also be investigated by examining the effects of pharmacological inhibition of ER stress. One such ER stress inhibitor is Salubrinal, ($C_{21}H_{17}N_4OSCl_3$), a cell-permeable inhibitor of phosphatases that normally dephosphorylate phospho-eIF2α (Boyce et al, 2005). Salubrinal maintains the

phosphorylation state of eIF2α and therefore maintains the translational block that occurs when the UPR is elicited. This effectively makes the response to ER stress more potent.

4.1.4.2 Salubrinal in MNDs and CAG-repeat diseases

Salubrinal has been used previously to investigate the role of ER stress-induced apoptosis in both MNDs and CAG-repeat disorders.

In models of MNDs such as ALS, the administration of Salubrinal has been found to decrease motoneuron death both in vitro and in vivo (Oh et al, 2008, Saxena et al, 2009). For instance, in vitro, 48 hour Salubrinal treatment of Neuro2a cells expressing the mutant SOD-1 protein (mSOD-1) prevents mSOD1-induced cell death. Salubrinal treatment also improves the viability of the remaining motoneurons as demonstrated by Propidium Iodide staining (Oh et al, 2008). The benefits of Salubrinal are also evident in animal models of ALS. In $SOD1^{G93A}$ mice, Salubrinal attenuates symptoms of disease, such as denervation, and delays disease progression (Saxena et al, 2009). These findings suggest that ER stress can be directly implicated in disease pathology in MND and is associated with disease-related motoneuron death. Thus, when ER stress is inhibited by Salubrinal, motoneuron death decreases and disease progression is delayed.

Salubrinal treatment has also been used to determine the role of ER stress in the pathology of CAG-repeat disorders. In a cell model of Huntington's Disease, in which PC6.3 cells are transfected with a mutant Huntingtin protein containing up to 120 CAG-repeats, Salubrinal treatment decreases neuronal death by 40 % (Reijonen et al, 2008). Furthermore, Salubrinal treatment also results in a decrease in Caspase 12 cleavage and thus the pharmacological prevention of ER stress correlates with both decreased Caspase 12 activation and decreased neuronal death.

Since Kennedy's Disease is both a MND and a CAG repeat disorder, and because the results presented in Chapter 3 showed that ER stress occurs in the AR100 mouse

model of the disease (see Chapter 3), it is possible that the treatment of motoneurons from AR100 mice with Salubrinal will reduce ER stress and thereby increase motoneuron survival. The experiments in this Chapter aim to determine if this is true and will also establish whether or not inhibition of ER stress alone is enough to significantly rescue KD motoneurons from death.

4.2. Results

4.2.1 KD motoneurons are less viable in culture than WT motoneurons

In these experiments, the effects of ER stress on motoneuron survival were investigated. In the first instance, in order to determine if the presence of the expanded Androgen Receptor (AR) itself increased the vulnerability of motoneurons, the level of motoneuron survival in basal culture conditions was established for WT and KD motoneurons at 7 DIV.

At 7 DIV, DHT-treated WT and DHT-treated KD primary ventral motoneuron cultures were stained with the neurofilament marker β-III tubulin. The results show that there are consistently fewer motoneurons present in KD cultures than in WT control cultures and that the motoneurons that are present in the KD cultures are more clustered than those in WT cultures (Figure 4.3A). Thus, as shown in Figure 4.3B when the number of motoneurons is expressed as a percentage of total cell number per coverslip, significantly fewer motoneurons survive in KD cultures than in WT cultures ($p<0.001$). Whilst WT cultures consist of 42% motoneurons (+/- 1.11 % SEM, n = 40 fields from 3 different cultures), KD cultures consist of only 29% motoneurons (+/- 1.27 % SEM, n = 40 fields from 3 different cultures). Thus approximately 1.5 times more motoneurons survive at 7 DIV in WT cultures than in KD cultures.

4.2.2 Treatment with an inhibitor of ER stress improves motoneuron survival in WT and KD cultures

Salubrinal is a well-established inhibitor of ER stress (Kessel et al, 2006). A range of Salubrinal concentrations was first tested on WT cultures in order to ensure that Salubrinal did not have a detrimental effect on primary motoneurons under normal conditions.

Figure 4.3: Motoneuron survival in WT and KD cultures under basal conditions

Primary motoneurons were cultured from WT and KD embryos at E13. Cultures were treated with 50 μM DHT (final concentration 500 nM) at 4 DIV and were fixed in 4% PFA at 7 DIV. Cultures were immunostained for β-III tubulin (green) and the nuclear marker DAPI (blue) to determine motoneuron number and total cell number, respectively. Typical example images of WT and KD cultures are shown in Ai) and ii), respectively. There are fewer motoneurons present in KD cultures, and the motoneurons that are present are more clustered than motoneurons in WT cultures.

When the number of motoneurons present in each culture is expressed as a percentage of total cell number (B) significantly fewer motoneurons survive in KD cultures ($p < 0.005$). Data was acquired from 40 different fields, from at least 3 different cultures for each genotype.

Error bars show the standard error of mean. Scale Bar in A) = 45 μm.

Figure 4.3

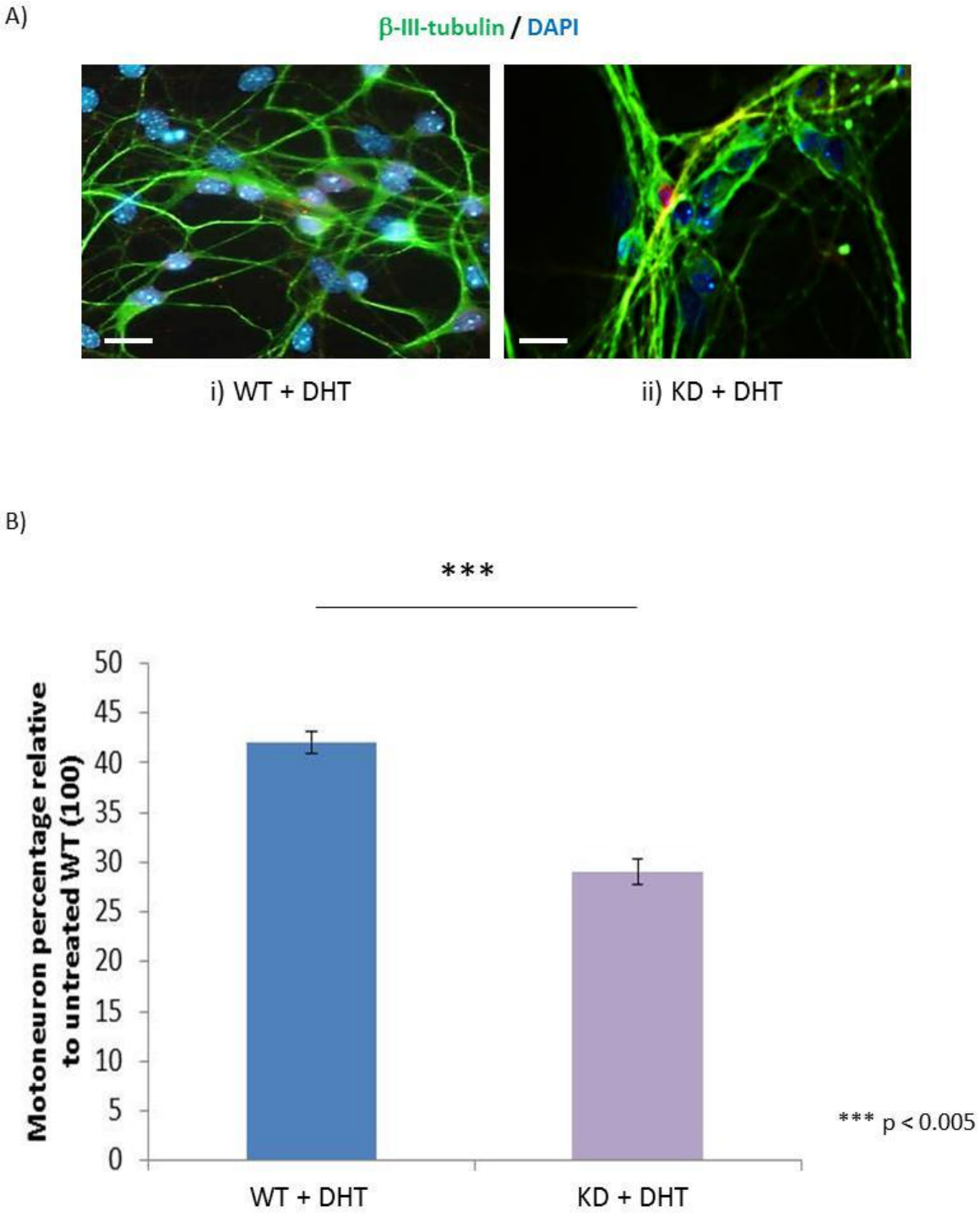
A)
β-III-tubulin / DAPI
i) WT + DHT
ii) KD + DHT
B)
***
Motoneuron percentage relative to untreated WT (100)
50
45
40
35
30
25
20
15
10
5
0
WT + DHT
KD + DHT
*** p < 0.005

The concentrations ranged between 1 μM and 100 μM (final concentrations 10 nM – 100 nM). There was no significant difference observed in motoneuron survival in cultures treated with different concentrations of Salubrinal and so 50 μM Salubrinal, which has been used previously in primary cultures, was used in the following experiments (Kessel 2006). Thus at 6 DIV, motoneurons cultures were treated with 50 μM Salubrinal (final concentration = 500 nM) for 24 hours.

Following treatment with 24 hour Salubrinal (500 nM) there was an increase in the number of motoneurons in both WT and KD cultures, with more β-III tubulin-positive cells, with 2 or more processes, in Salubrinal-treated cultures compared to untreated cultures (Figure 4.4A). Salubrinal treatment also appears to decrease motoneuron clustering in KD cultures (Figure 4.4Aii). When the percentage of β-III tubulin-positive cells, with 2 or more processes, is expressed as a percentage of total cell number, the number of motoneurons in Salubrinal-treated KD cultures is 48%, which is approx. 115% (+/- 2.85 % SEM, n=40 fields from 3 different cultures), relative to WT cultures that have not been treated with Salubrinal, and approximately 178% relative to KD cultures that have not been treated with Salubrinal (Figure 4.4B). This increase in motoneuron survival in KD cultures following Salubrinal treatment is significant ($p < 0.005$). When WT cultures were treated with Salubrinal, the percentage of motoneurons increased to 53.4%, which is 127% (+/- 1.42 % SEM, n = 40 fields from 3 different cultures) relative to WT cultures that had not been treated with Salubrinal (Figure 4.4B). This increase in survival is also significant ($p = 0.043$) Thus, Salubrinal treatment appears to be beneficial to both WT and KD motoneurons.

To summarize, 30% fewer KD motoneurons survive at 7 DIV compared to WT cultures. However, following treatment with Salubrinal there is a significant increase in motoneuron survival in WT and KD cultures so that motoneuron survival in Salubrinal-treated KD and WT cultures is not significantly different.

Figure 4.4: Treatment with Salubrinal improves the survival of KD motoneurons

Primary motoneuron cultures from WT and KD embryos were treated with 5 μM DHT at 4 DIV and fixed at 7 DIV in 4% PFA before being stained for β-III tubulin (green) and the nuclear marker DAPI (blue). In some cases cultures were also treated with 50 mM Salubrinal at 6 DIV. Example images of DHT-treated WT and KD cultures in the absence and presence of Salubrinal are shown in Ai) and ii), respectively. Salubrinal decreases motoneuron clustering and increase motoneuron number in KD cultures.

When the number of motoneurons is expressed as a percentage of total cell number (B) Salubrinal treatment results in a significant increase in motoneuron survival in both WT and KD cultures ($p < 0.05$ and < 0.005, respectively). The data is the mean from 40 different fields from at least 3 different cultures. Error bars show the standard error of mean. Scale bars in A) = 30 μm

Figure 4.4

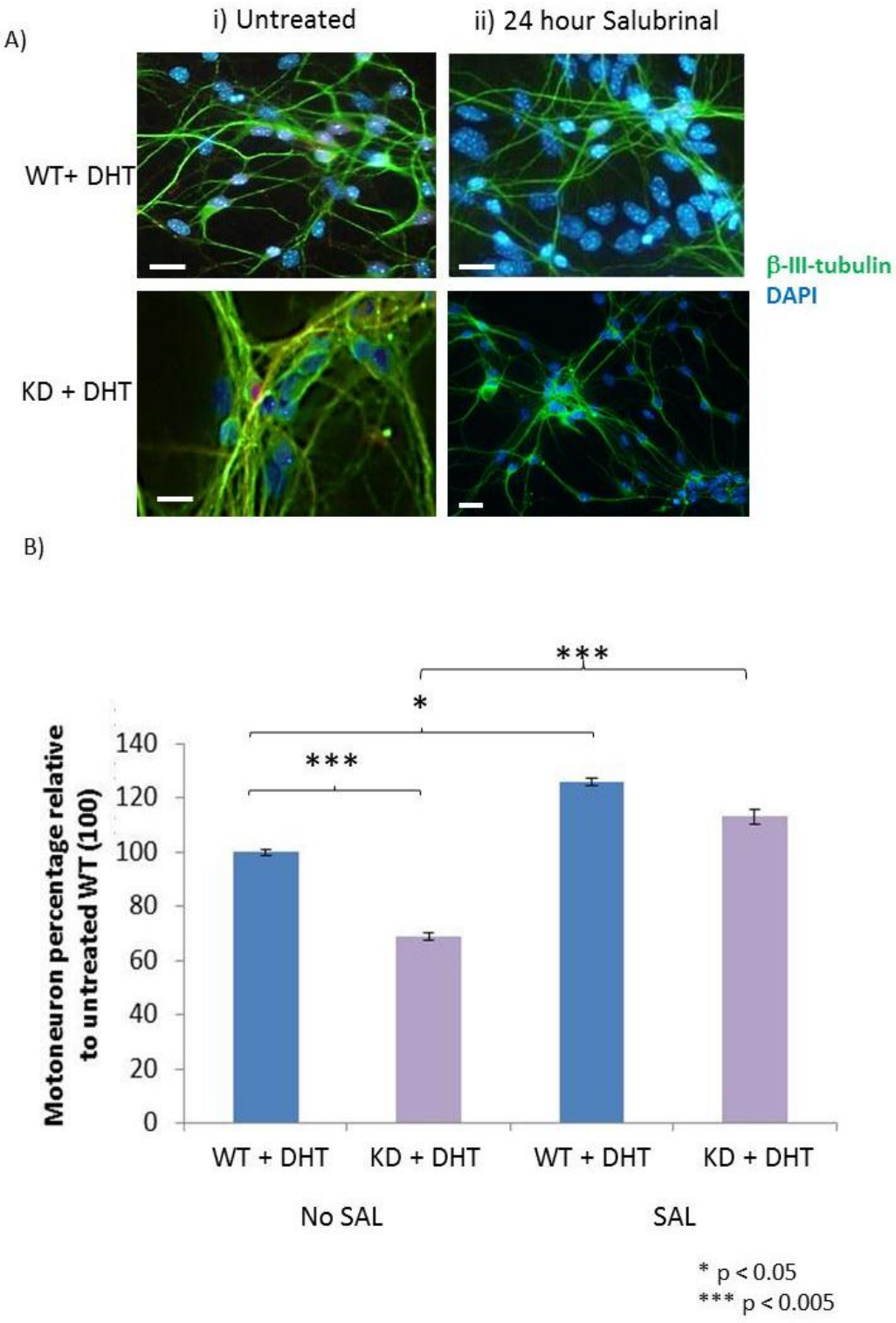
A)
i) Untreated
ii) 24 hour Salubrinal
WT+ DHT
KD + DHT
β-III-tubulin
DAPI
B)
Motoneuron percentage relative to untreated WT (100)
140
120
100
80
60
40
20
0
***
*
***
WT + DHT
KD + DHT
WT + DHT
KD + DHT
No SAL
SAL
* p < 0.05
*** p < 0.005

4.2.3 KD motoneurons have an increased vulnerability to ER stressors that deplete ER Ca^{2+} such as Thapsigargin (TG).

Primary WT and KD ventral motoneuron cultures were treated at 6 DIV for 24 hours with various concentrations of Thapsigargin (TG) ranging from 10 nM to 1 μM. The cultures were fixed at DIV 7 and stained for MAP2 and DAPI to assess motoneuron survival. In WT cultures, TG begins to have a detrimental effect on motoneuron survival at 1 μM, whereas survival of KD motoneurons decreases most noticeably at 300 nM. Therefore a concentration of 300 nM (Figure 4.5), which has been used previously in primary cultures, was used in the following experiments (Rahman et al, 1996).

Following the treatment of cultures with TG for 24 hours there are visible changes in both WT and KD motoneurons. WT motoneurons are more clustered following TG treatment whilst the number of KD motoneurons appears to decrease dramatically – as demonstrated by a lower number of β-III tubulin-positive cells (Figure 4.6A).

When the number of motoneurons in each culture is expressed as a percentage of total cell number, it shows that treatment with 300 nM TG for 24 hours results in decreased in motoneuron survival in both WT and KD cultures (Figure 4.6B). In WT cultures, TG treatment results in a decrease in motoneuron survival, from 42% in untreated cultures to 33% in TG-treated cultures i.e. the survival of TG-treated WT motoneurons, relative to WT motoneurons that are not exposed to TG, is 91% (+/- 1.11 SEM, n=40 fields from 3 different cultures). This decrease in motoneuron survival, although only 9%, is significant (p=0.05). In contrast, KD motoneuron cultures are more vulnerable to TG treatment, so that motoneuron survival decreases from 29% (+/- 1.27 % SEM, n = 40 fields from 3 different cultures) in untreated conditions to only 12% (+/-1.01% SEM, n = 40 fields from 3 different cultures) in TG-treated cultures (p=0.0008). Thus, relative to WT motoneurons that are *not* exposed to TG, TG - treated KD motoneuron survival is 71 % lower, which is a significant decrease (p= 0.0002). Furthermore, the difference in survival between TG-treated WT and KD motoneurons is significant (p=0.003).

Figure 4.5 Effects of different concentrations of Thapsigargin on ER Ca^{2+} in WT and KD primary motoneurons.

Primary ventral motoneuron cultures from WT and KD embryos were treated at 4 DIV with 5 μM DHT and were then fixed at 7 DIV in 4% PFA. The cultures were immunostained for β-III tubulin (green) and stained with DAPI (blue). In some cases, at 6 DIV, cultures were also treated with various concentrations of Thapsigargin (TG) ranging from 10 nM to 1μM.

The Bar Chart summarizes the results obtained when the number of motoneurons surviving at 7 DIV is expressed relative to the number of motoneurons present in untreated WT cultures. A significant decrease in KD motoneuron survival is observed when cultures are treated with 300 nM and 1 μM TG. A significant decrease in WT motoneuron survival is only observed following treatment of cultures with 1 μM TG ($p < 0.005$). Error bars show the standard error of mean.

Figure 4.5

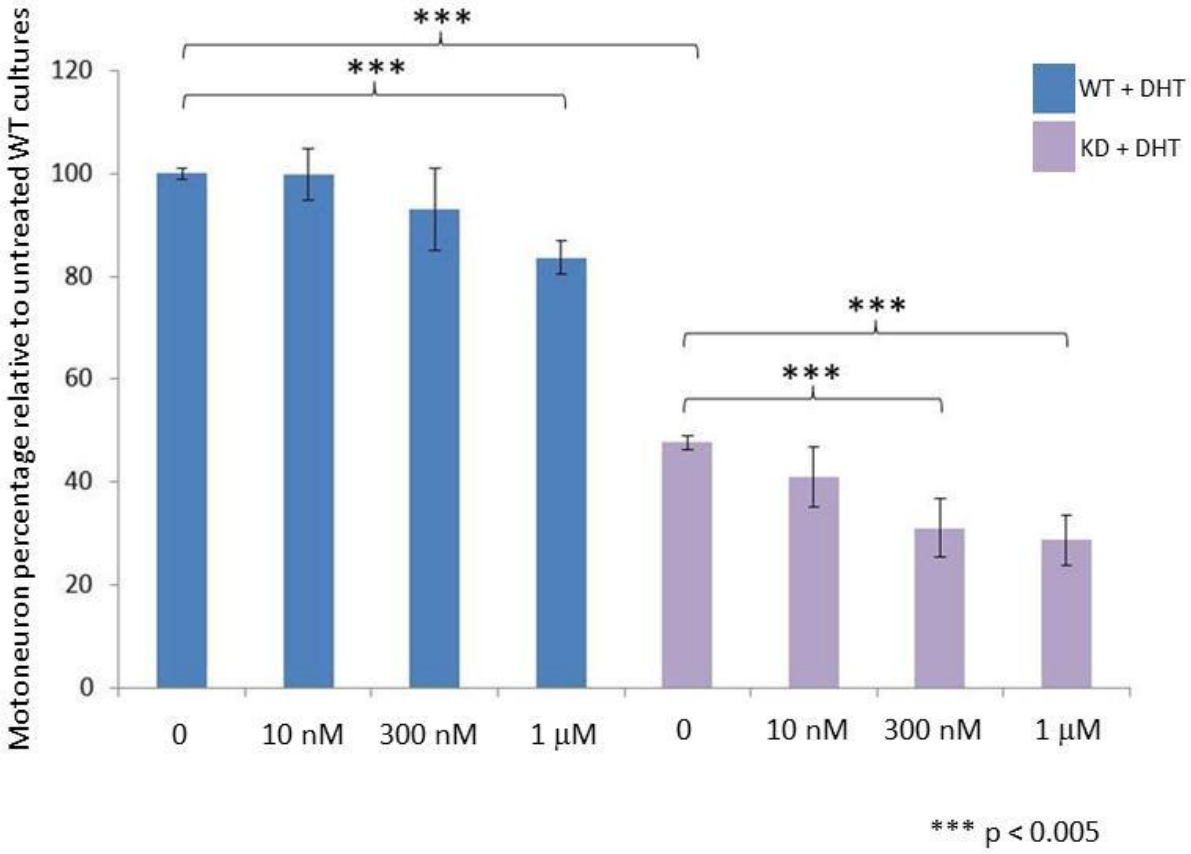
***
***
***
***
Motoneuron percentage relative to untreated WT cultures
120
100
80
60
40
20
0
0
10 nM
300 nM
1 µM
0
10 nM
300 nM
1 µM
WT + DHT
KD + DHT
*** p < 0.005

Figure 4.6: KD motoneurons are more vulnerable to ER stress than WT motoneurons: the effect of Thapsigargin

Primary motoneuron cultures from WT and KD E13 embryos were treated with 5 μM DHT at DIV 4 and fixed in 4% PFA at 7DIV before being stained for β-III tubulin (green) and the nuclear marker DAPI (blue). In some cases, at 6DIV, the cultures were also treated with 300 nM Thapsigargin (TG). Examples of immunostained DHT-treated WT and KD cultures in the absence and presence of TG are shown in Ai) and ii), respectively. TG increases motoneuron clustering in WT cultures and decreases motoneuron survival in KD cultures. The number of surviving motoneurons in each culture was expressed as a percentage of total number of cells present, which was then expressed relative to the percentage of motoneurons in untreated WT cultures. (B) TG treatment results in a significant decrease in motoneuron survival in KD cultures ($p < 0.01$). Mean motoneuron survival was determined by examining 40 different fields from at least 3 different cultures.

Error bars show the standard error of mean. Scale bars in A) = 30 μM

Figure 4.6

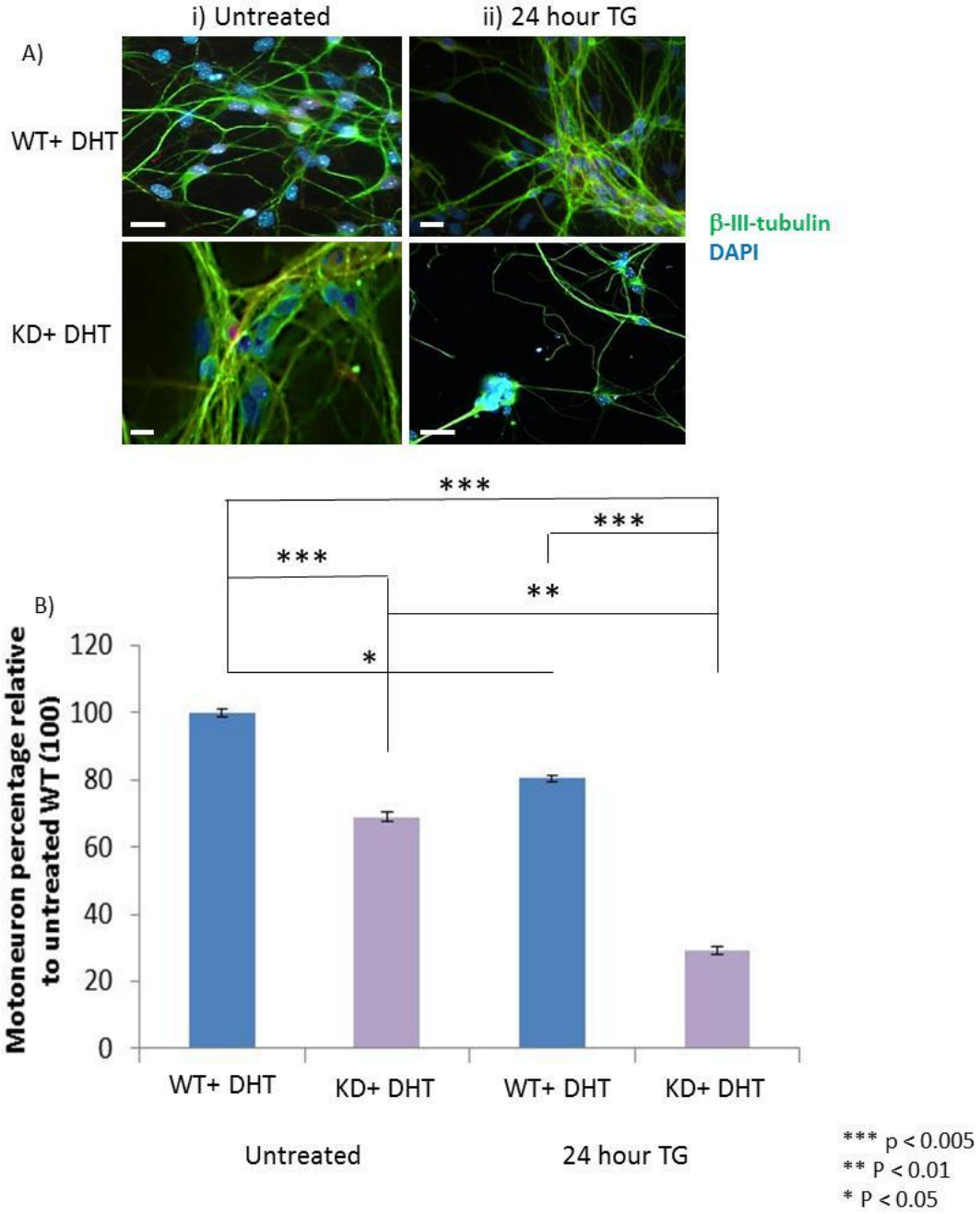
i) Untreated
ii) 24 hour TG
A)
WT+ DHT
KD+ DHT
β-III-tubulin
DAPI
B)
Motoneuron percentage relative to untreated WT (100)
120
100
80
60
40
20
0
***
***
***
**
*
WT+ DHT
KD+ DHT
WT+ DHT
KD+ DHT
Untreated
24 hour TG
*** p < 0.005
** P < 0.01
* P < 0.05

4.2.4 Treatment with an inhibitor of ER stress rescues motoneurons from TG-induced death

Treatment with Thapsigargin for 24 hours results in axonal clustering in WT cultures and a significant loss of motoneurons in KD cultures (Figure 4.6). To determine if this effect was due to the known ER stress-inducing effects of TG, the effects of Salubrinal, an ER stress inhibitor, on TG-induced stress was examined. When motoneurons were treated with Salubrinal (50 μM) as well as TG (300 nM), a decrease in motoneuron clustering was observed, although it was not eliminated (Figure 4.7A). However, a dramatic increase in motoneuron survival was observed in KD cultures treated with TG *and* Salubrinal. Thus, significantly fewer KD and WT motoneurons died in cultures treated with Salubrinal in addition to TG than TG-only treated cultures (Figure 4.7B). In TG-treated WT cultures 45.0 % (+/- 0.82 % SEM, n = 40 fields from 3 different cultures) of motoneurons survived following treatment with Salubrinal, an increase of approximately 12% compared to TG only-treated cultures ($p < 0.001$). Relative to untreated WT cultures, TG-treated WT motoneuron survival is 9 % lower, but in the presence of Salubrinal in addition to TG, survival is 7 % *higher* (Figure 4.7B). In TG-treated KD cultures however, the increase in motoneuron survival observed following treatment with Salubrinal is even greater, so that motoneuron survival increases by 37.6 % to 44.6 % (+/- 0.77 % SEM, n= 40 fields from 3 different cultures). This increase is significant ($p<0.001$). Relative to untreated WT cultures, TG-treated KD motoneuron survival is 71 % lower, but in the presence of Salubrinal in addition to TG, survival is 6% higher (Figure 4.7B). Importantly, there is no difference in survival between TG-treated WT and TG-treated KD motoneurons in the presence of Salubrinal.

4.2.5 KD motoneurons are less vulnerable to Ca^{2+}-independent ER stress

To examine whether KD motoneurons are also more vulnerable to Ca^{2+}-independent ER stress than WT motoneurons, the cultures were treated with Tunicamycin, an established inducer of Ca^{2+}-independent ER stress.

Figure 4.7: Salubrinal treatment prevents KD motoneuron vulnerability to Thapsigargin

Primary motoneuron cultures from WT and KD E13 embryos were treated with 5 μM DHT at 4 DIV and 300 nM Thapsigargin (TG) at 6 DIV. Cultures were then fixed at 7 DIV in 4% PFA and immunostained for β-III tubulin (green) and DAPI (blue). In some cases, cultures were also treated with 50 μM Salubrinal at 6 DIV. Example images of DHT and TG- treated WT and KD cultures in the absence and presence of Salubrinal are shown in Ai) and ii), respectively. There does not appear to be a noticeable difference between TG-treated WT cultures and Salubrinal + TG-treated WT cultures. However in TG-treated KD cultures there appears to be an increase in motoneuron survival following Salubrinal treatment.

When the number of motoneurons is expressed as a percentage of total cell number and then expressed relative to the percentage of motoneurons in untreated WT cultures (B), Salubrinal treatment results in significant increases in motoneuron survival in both TG-treated WT and TG-treated KD cultures ($p < 0.005$ in both cases). Motoneuron survival is based on 40 different fields from at least 3 different cultures. Error bars show the standard error of mean. Scale bars in A) = 30 μm

Figure 4.7

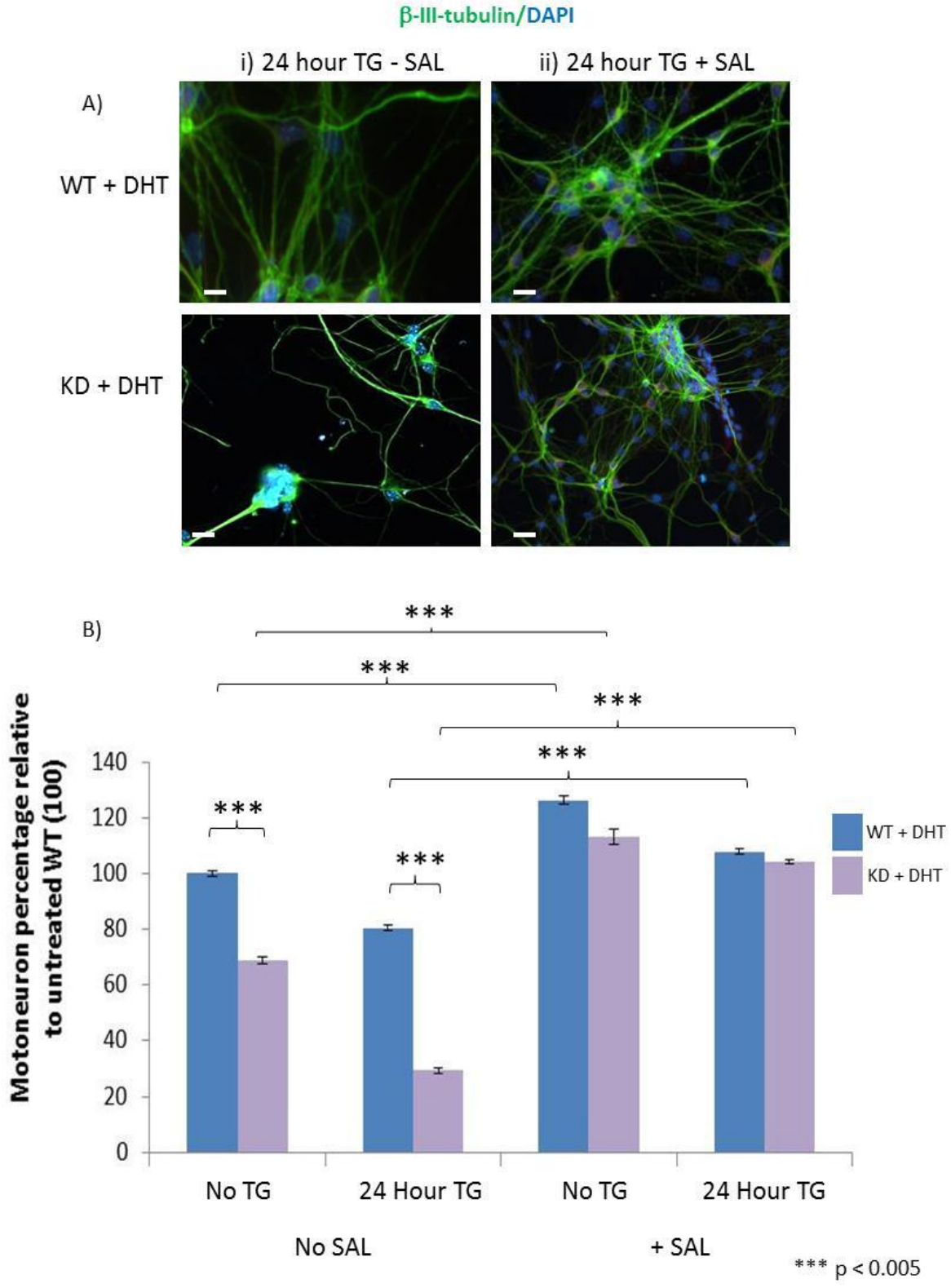
β-III-tubulin/DAPI
i) 24 hour TG - SAL
ii) 24 hour TG + SAL
A)
WT + DHT
KD + DHT
B)
Motoneuron percentage relative to untreated WT (100)
140
120
100
80
60
40
20
0
***
***
***
***
***
***
WT + DHT
KD + DHT
No TG
24 Hour TG
No TG
24 Hour TG
No SAL
+ SAL
*** p < 0.005

Following 24 hour treatment of WT and KD cultures with Tunicamycin, cultures were immunostained for β-III tubulin and the number of motoneurons surviving in WT and KD cultures was established (Figure 4.8A). As shown in Figure 4.8B, following treatment with Tunicamycin at concentrations ranging from 10 nM – 1 μM, there is a decrease in motoneuron survival in WT cultures at all concentrations used but only at 1 μM is this decrease significant. Thus following exposure to 1 μM Tunicamycin for 24 hours, WT motoneuron survival decreases by approximately 50 % compared to untreated WT cultures ($p=0.01$). However in KD cultures, motoneuron survival is not significantly different in Tunicamycin-treated cultures compared to untreated KD cultures at any concentration and is the same as that observed in WT motoneuron cultures treated with the highest concentration of Tunicamycin (1 μM).

4.2.6 KD motoneurons undergo ER stress-induced apoptosis

To examine whether the increase in ER stress that is detected in primary KD motoneurons resulted in an increase in ER stress-induced apoptosis, in KD and WT cultures, the level of Caspase 12 expression was examined by immunohistochemistry and Western Blot analysis. As shown in Figure 4.9A, Cleaved Caspase 12 immunoreactivity (red) appears to be higher in DHT-treated KD motoneurons than in DHT-treated WT controls (Figure 4.9A). Indeed, in WT cultures Caspase 12 staining is barely visible whereas there is high intensity staining in KD motoneurons.

Western Blot analysis of purified, DHT-treated WT and KD motoneuron cultures reveals that there is a significantly higher level of Caspase 12 expression in KD cultures than in WT controls ($p=0.003$). Thus the expression level of Caspase 12 relative to actin is only 0.694 (+/- 0.06 SEM, n = 3) in WT motoneurons, compared to 1.588 (+/- 0.28 SEM, n = 3) in KD motoneurons (Figure 4.9C).

Figure 4.8: KD motoneurons are resistant to Tunicamycin

Primary ventral motoneuron cultures from WT and KD embryos were treated at 4 DIV with 5 μM DHT and were then fixed at 7 DIV in 4% PFA. The cultures were immunostained for β-III tubulin (green) and stained with DAPI (blue). In some cases, at 6 DIV cultures were also treated with various concentrations of Tunicamycin (TM) ranging from 10 nM to 1μM. Examples of DHT - treated WT and KD cultures in the absence and presence of 1 μM TM are shown in Ai) and ii), respectively.

When the number of motoneurons surviving at 7 DIV is expressed relative to the number of motoneurons present in untreated WT cultures (B), only the highest concentration of TM (1 μM) results in a significant decrease in motoneuron survival in WT cultures ($p < 0.01$). However there is no significant decrease in KD motoneuron survival at any concentration tested. Motoneuron survival was measured in 40 different fields from at least 3 different cultures. Error bars show the standard error of mean. Scale bars in A) = 30 μm

Figure 4.8

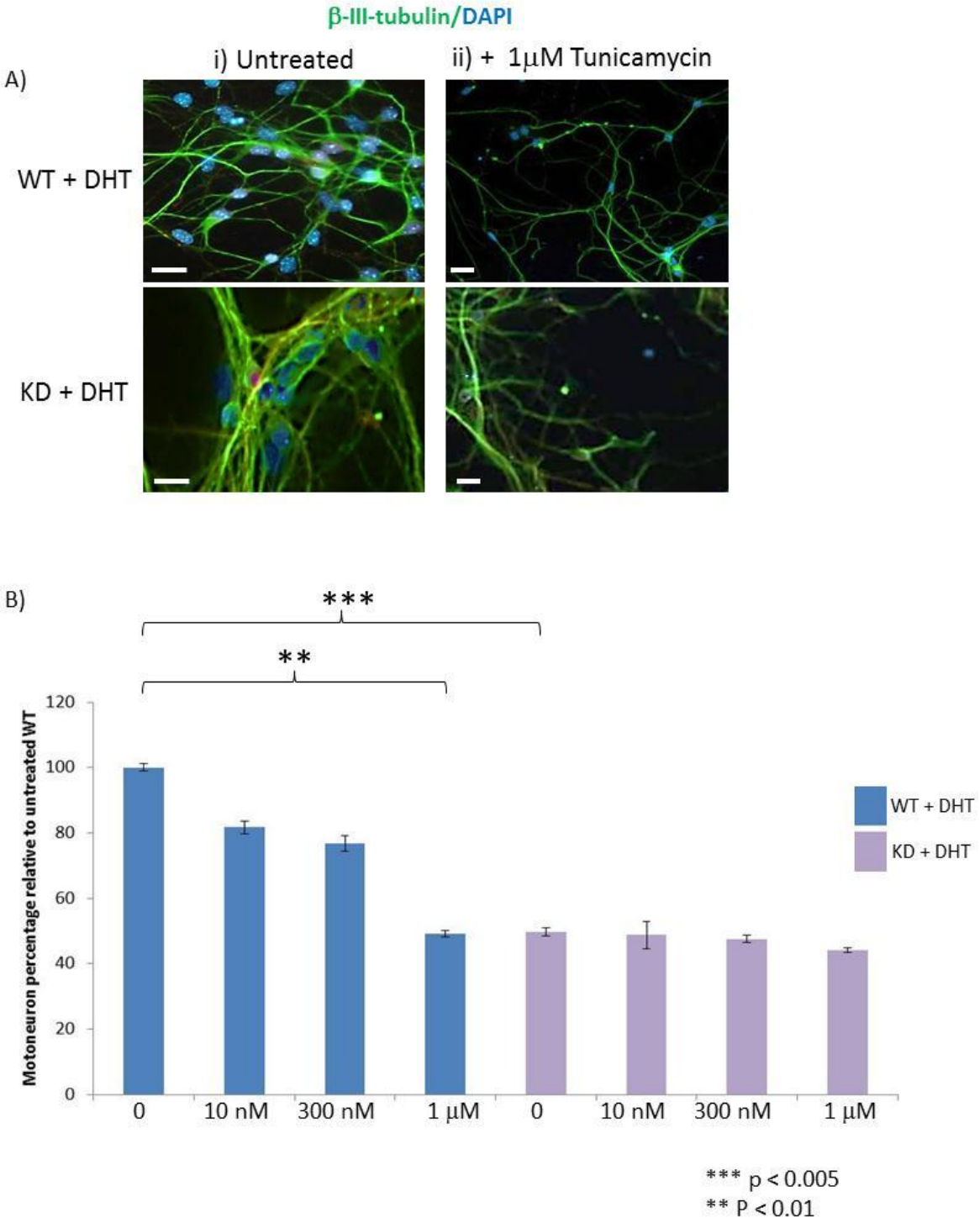
β-III-tubulin/DAPI
A)
i) Untreated
ii) + 1μM Tunicamycin
WT + DHT
KD + DHT
B)
***
**
Motoneuron percentage relative to untreated WT
120
100
80
60
40
20
0
0
10 nM
300 nM
1 μM
0
10 nM
300 nM
1 μM
WT + DHT
KD + DHT
*** p < 0.005
** P < 0.01

Figure 4.9: Caspase 12 expression is higher in KD primary motoneurons

Primary motoneuron cultures from WT and KD embryos were treated at 4 DIV with 5 μM DHT. In some cultures the cells were fixed at 7 DIV in 4% PFA before being immunostained for β-III tubulin (green), Caspase 12 (red) and DAPI (blue). Example images of WT and KD motoneuron cultures are shown in Ai) and ii), respectively. There appears to be much higher Caspase 12 immunoreactivity in KD motoneurons than in WT motoneurons.

In other cultures the cells were homogenized at 7 DIV and processed for Western blot analysis of Caspase 12. An example blot is shown in B). The blot shows that there is a higher level of expression of Caspase 12 in KD motoneurons compared to WT controls.

Quantification of the blot was achieved by expressing the optical density of the Caspase 12 bands relative to that of the corresponding Actin band, which was given a value of 1.0. The result is shown in Bar Chart C). There is a significantly higher level of Caspase 12 in KD motoneurons compared to the WT controls ($P < 0.005$). Values are based on the average of three different cultures from three different embryos. The blot was repeated twice. Error bars show the standard error of mean. Scale bars in A) = 30 μm

Figure 4.9

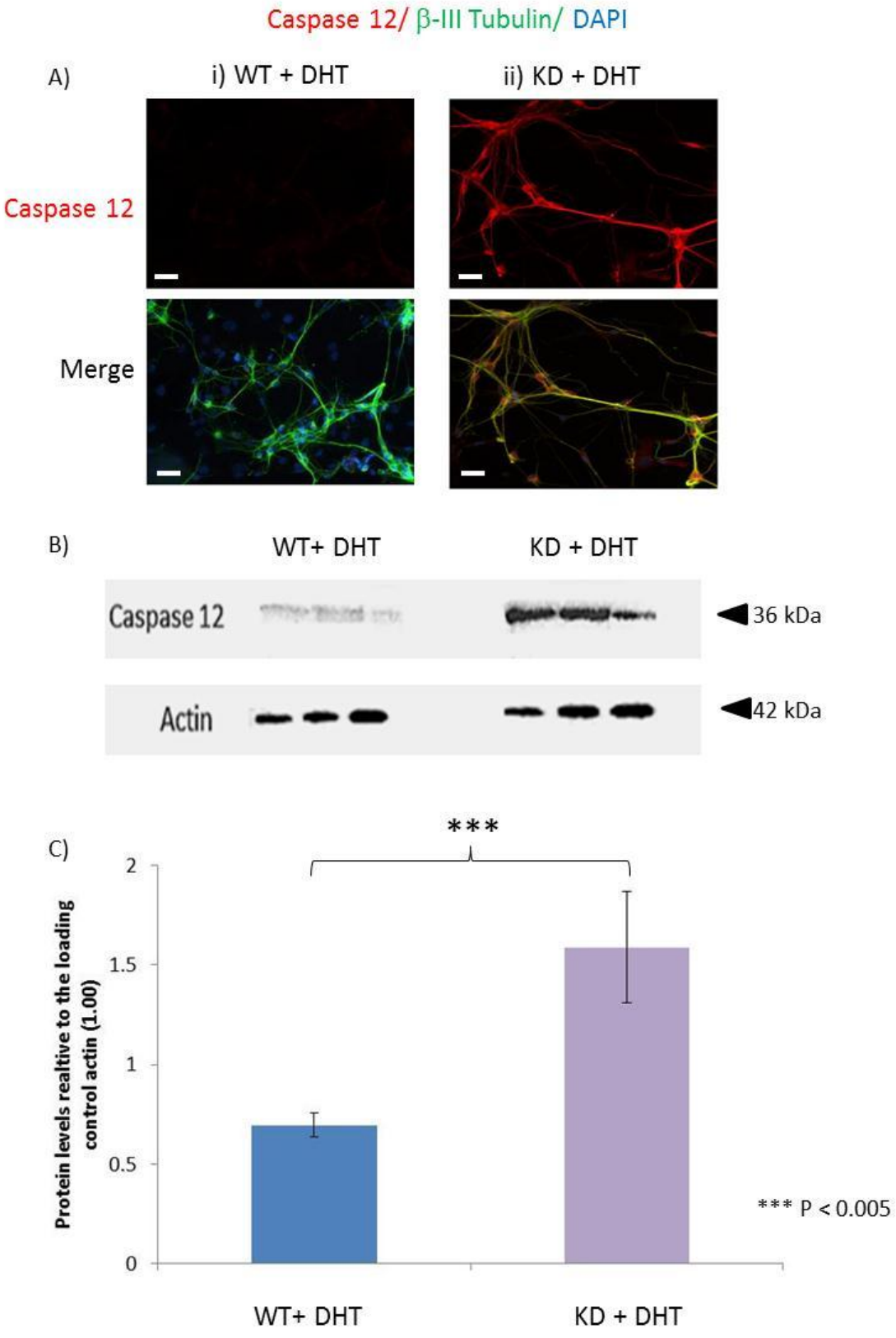
Caspase 12/ β-III Tubulin/ DAPI
A)
i) WT + DHT
ii) KD + DHT
Caspase 12
Merge
B)
WT+ DHT
KD + DHT
Caspase 12
36 kDa
Actin
42 kDa
C)
***
Protein levels realtive to the loading control actin (1.00)
2
1.5
1
0.5
0
*** P < 0.005
WT+ DHT
KD + DHT

4.2.7 Treatment with an inhibitor of ER stress reduces ER stress-induced apoptosis in KD motoneurons

To establish whether the increase in Caspase 12 expression detected in DHT-treated KD motoneurons was indeed due to ER stress, the cultures were treated with Salubrinal, an ER stress inhibitor. The level of Caspase 12 expression was determined by immunohistochemistry and Western blot analysis. Following 24 hour Salubrinal (50 μM) treatment, Caspase 12 immunoreactivity appears to decrease in primary KD ventral motoneurons (Figure 4.10A) so that a similar level of Caspase 12 immunoreactivity is observed in KD and WT Salubrinal-treated cultures.

Western blot analysis of DHT-treated purified WT and KD motoneurons reveals that following 24 hour treatment with Salubrinal there is a significant decrease in Caspase 12 expression in both WT and KD motoneurons ($p=0.042$ and 0.0004, respectively). The expression level of Caspase 12 decreases by 84.2% in WT motoneurons following Salubrinal treatment to 0.11, relative to Actin (+/- 0.18 SEM, n = 3). In KD motoneurons, there is a 85% decrease in Caspase 12 expression following Salubrinal treatment – with the relative level of Caspase 12 now being 0.24 (+/- 0.21 SEM, n =3). Although the expression of Caspase 12 is higher in KD motoneurons than in WT controls, this difference is not significant.

4.2.8 Inhibition of ER stress increases ER calcium levels in KD motoneurons

Inhibition of ER stress in KD motoneurons by treatment with Salubrinal decreases Caspase 12 expression and improves motoneuron survival in KD cultures. To examine the effect of Salubrinal on ER Ca^{2+} levels, which are depleted in untreated KD motoneurons (Chapter 3, Section 3.3.4.2), ER Ca^{2+} levels were examined using Fluo 4-AM and confocal microscopy to infer ER Ca^{2+} in primary ventral motoneurons from embryonic WT and KD cultures (as described in Chapter 3). As shown in Figure 4.11 and Chapter 3, (Section 3.3.2.1), there is a significantly lower level of ER Ca^{2+} in KD motoneurons compared to WT controls ($p< 0.005$).

Figure 4.10: Treatment with Salubrinal decreases Caspase 12 expression in KD motoneurons

Primary cultures from WT and KD embryos were treated at 4 DIV with 5 μM DHT and then fixed at 7 DIV in 4% PFA. The cultures were either immunostained for β-III tubulin (green), Caspase 12 (red) and DAPI (blue), or processed for Western blot analysis. In some cases, the cultures were also treated at 6 DIV with 50 μM Salubrinal. Example images of immunostained WT and KD cultures are shown in Ai) and ii), respectively. Western blot analysis of Caspase 12 expression (B) showed that Salubrinal treatment results in a decrease in Caspase 12 expression in both WT and KD motoneurons. The level of Caspase 12 was expressed as optical density of the Caspase 12 band relative to the optical density of the corresponding Actin band (the loading control), which was given a value of 1.0 (C). In both WT and KD motoneurons, Salubrinal results in a significant decrease in Caspase 12 expression ($p < 0.05$ and 0.005, respectively). Although Caspase 12 expression is slightly higher in KD motoneurons, this is not significant. Values are based on the average of three different cultures from three different embryos. Each blot was repeated twice.

Error bars show the standard error of mean. Scale bars in A) = 30 μm

Figure 4.10

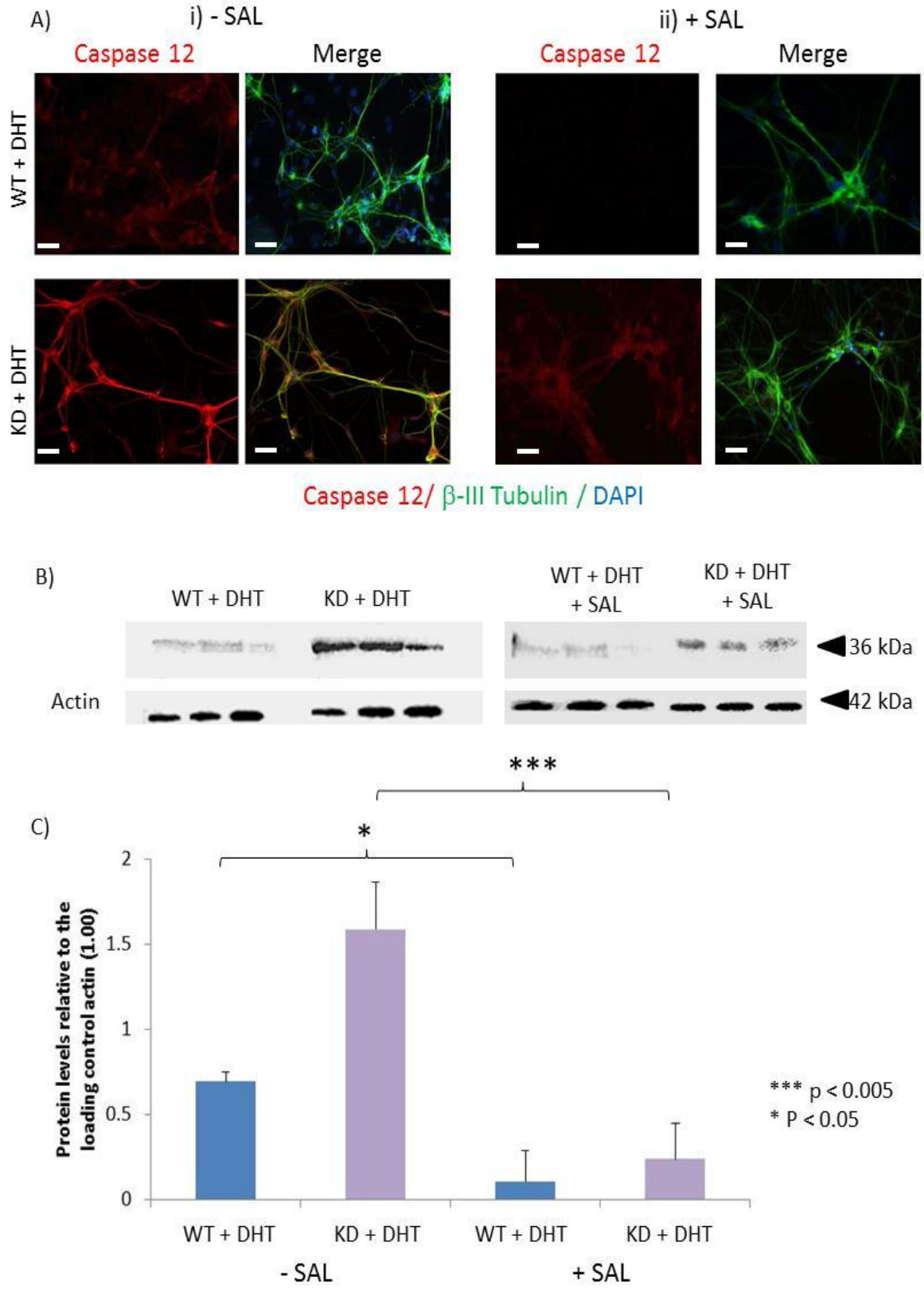
A)
i) - SAL
ii) + SAL
Caspase 12
Merge
Caspase 12
Merge
WT + DHT
KD + DHT
Caspase 12/ β-III Tubulin / DAPI
B)
WT + DHT
KD + DHT
WT + DHT + SAL
KD + DHT + SAL
36 kDa
Actin
42 kDa
C)
***
*
Protein levels relative to the loading control actin (1.00)
2
1.5
1
0.5
0
WT + DHT
KD + DHT
WT + DHT
KD + DHT
- SAL
+ SAL
*** p < 0.005
* P < 0.05

Following 24 hour treatment with Salubrinal, ER Ca^{2+} increases significantly in KD cultures (Figure 4.11). In WT cultures, although ER Ca^{2+} increases by 12 nM to 152 nM (+/- 29 nM SEM, n = 29) this is not significant. In KD motoneurons however, ER Ca^{2+} increases by 59 nM to 69 nM (+/- 11.5 nM SEM, n = 34). This increase in ER Ca^{2+} is significant (p = 0.008). Despite a significant increase in ER Ca^{2+} in KD motoneurons, ER Ca^{2+} levels in Salubrinal-treated WT motoneurons are significantly higher in than in Salubrinal treated KD motoneurons (p= 0.009).

4.2.9 Caspase 12 expression levels throughout KD progression

In order to determine whether the increase in ER stress-induced apoptosis observed in embryonic KD motoneurons in culture was also present in KD motoneurons in vivo and to establish whether ER stress-induced apoptosis was present throughout the disease, the pattern and level of Caspase 12 expression was examined in spinal cord sections of WT and KD mice at various stages of disease by immunohistochemistry and Western blot analysis.

The pattern of Caspase 12 immunoreactivity in WT and KD spinal cord sections from mice at 3, 12 and 18 months of age suggests that the increase in Caspase 12 expression observed in KD motoneurons at E13 does not persist throughout disease progression (Figure 4.12A). At 3 and 12 months of age, there is a clear increase in Caspase 12 immunoreactivity in KD motoneurons compared to WT motoneurons. However, by 18 months of age, Caspase 12 immunoreactivity in KD motoneurons has reduced, so that there is no detectable difference in Caspase 12 immunoreactivity between WT and KD motoneurons.

The expression levels of Caspase 12 in spinal cord tissue from WT and KD mice at P5, 3, 12 and 18 months of age were also assessed by Western blot analysis. A typical Western blot is shown in Figure 4.12 B, which shows that Caspase 12 expression is elevated early in disease in KD spinal cord and expression gradually declines as the disease progresses.

Figure 4.11: Salubrinal treatment increases ER Ca^{2+} in KD motoneurons

Motoneuron cultures from E13 WT and KD embryos were examined using confocal microscopy at 7 DIV. Fluo 4 AM was used to measure cytosolic Ca^{2+} following TG-induced Ca^{2+} release from the ER, giving an indication ER Ca^{2+} levels. The fluorescence signal was then calibrated using the Ionomycin-induced maximum cytosolic Ca^{2+} fluorescence as described in Chapter 2 (Section 2.6). In all cases, cultures were treated at 4 DIV with 5 μM DHT and were treated with either 50 μM Salubrinal at 6 DIV or left untreated. The Bar Chart shows the average ER Ca^{2+} in WT and KD motoneurons (+/- Salubrinal). Salubrinal significantly increases ER Ca^{2+} in KD motoneurons ($p < 0.01$), although the level of ER Ca^{2+} is still significantly higher in WT motoneurons ($p = 0.009$).

Error bars show the standard error of mean. The N number varies between 29 and 34, from at least three different cultures for each genotype.

Figure 4.11

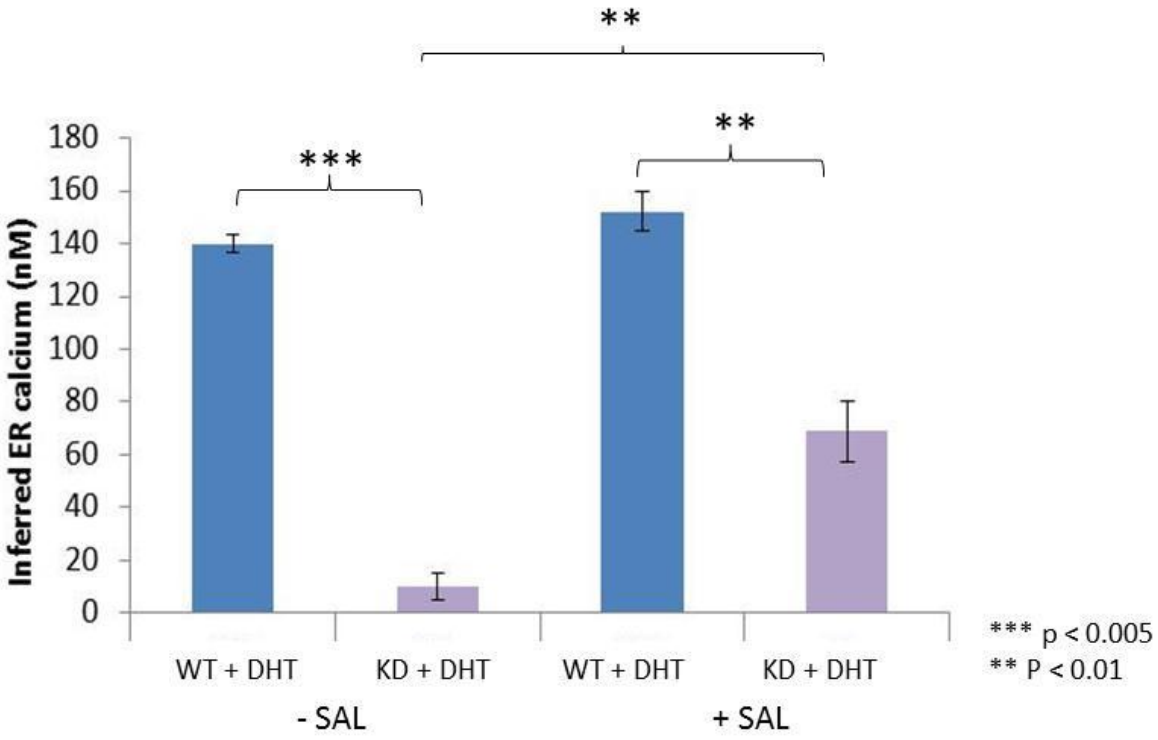
**
***
**
180
160
140
120
100
80
60
40
20
0
Inferred ER calcium (nM)
WT + DHT
KD + DHT
WT + DHT
KD + DHT
- SAL
+ SAL
*** p < 0.005
** P < 0.01

Quantification of these Western blots (Figure 4.12 C) reveals that the peak elevation of Caspase 12 in KD motoneurons relative to WT controls occurs at P5. At P5 the level of Caspase 12 in WT spinal cord tissue, relative to Actin, is 0.93 (+/- 0.17 SEM, n = 3) compared to 1.87 (+/- 0.31 SEM, n = 3) in KD spinal cord, an increase of 101% (p=0.03). Caspase 12 expression remains elevated in KD spinal cord at 3 months of age when Caspase 12 levels in WT spinal cord tissue are 1.25 (+/- 0.12 SEM, n =3) compared to 1.74 (+/- 0.18 SEM, n = 3) in KD spinal cord, a difference of 39% ($p < 0.05$).

By 12 months of age, Caspase 12 levels in KD spinal cord begin to decline, and although levels are higher than in WT spinal cord, 1.74 (+/- 0.09 SEM, n = 3) in KD spinal cord compared to 1.23 (+/- 0.10 SEM, n = 3) in WT spinal cord, this difference is not significant.

By 18 months of age, Caspase 12 expression in KD spinal cord is significantly higher than in 18 month WT spinal cord ($p < 0.01$), so that Caspase 12 levels are 1.02 (+/- 0.01 SEM, n = 3) in KD spinal cord compared to 0.70 (+/- 0.08 SEM, n =3) in WT tissue, a difference of 45%.

4.2.10 Results summary

In this Chapter, ER stress-induced apoptosis has been detected in KD motoneurons and its role in KD-associated motoneuron death has been investigated. Motoneuron counts in primary WT and KD ventral motoneuron cultures reveal that even under basal culture conditions KD motoneuron survival is reduced. Furthermore, treatment of cultures with the ER stressor Thapsigargin (TG) has a more detrimental effect on the survival of KD motoneurons than WT controls. Treatment of cultures with Salubrinal, which inhibits ER stress, rescues KD motoneurons both under basal conditions and in the presence of TG.

Figure 4.12: Expression of Caspase 12 remains elevated in KD spinal cords throughout disease progression

Transverse sections (10 μM) of spinal cords from WT and KD mice at 3 months (pre-symptomatic), 12 months (symptom onset) and 18 months (end-stage) of age were immunostained for β-III tubulin (green), Caspase 12 (red) and stained with DAPI (blue). Example images are shown in A). Caspase 12 immunoreactivity (red) appears to be higher in KD motoneurons than in WT controls at 3 and 12 months of age although there appears to be no detectable difference at 18 months of age. (Scale bars = 25 μm).

Western blot analysis was carried out to determine expression levels of Caspase 12 in WT and KD spinal cords. Spinal cord homogenates were prepared from WT and KD mice at P5 (first signs of ER stress in ALS), 3, 12 and 18 months of age. A typical blot is shown in B). The blot shows that the level of Caspase 12 expression is higher in KD spinal cords than WT controls at P5 and 3 months of age, but there is no clear difference at 12 or 18 months of age. Quantification of the blot was achieved by expressing the optical density of the Caspase 12 band relative to the optical density of the corresponding Actin band, which was given a value of 1.0. The results are summarized in the Bar Chart (C), which shows the average values based on mean data from three different spinal cords. The results show that the relative level of Caspase 12 expression is higher in KD spinal cords than in WT controls at P5, 3 months and 18 months ($p < 0.05$, 0.05 and 0.01, respectively) but not at 12 months of age. The blot was repeated twice on each set of samples. Error bars show the standard error of mean.

Figure 4.12

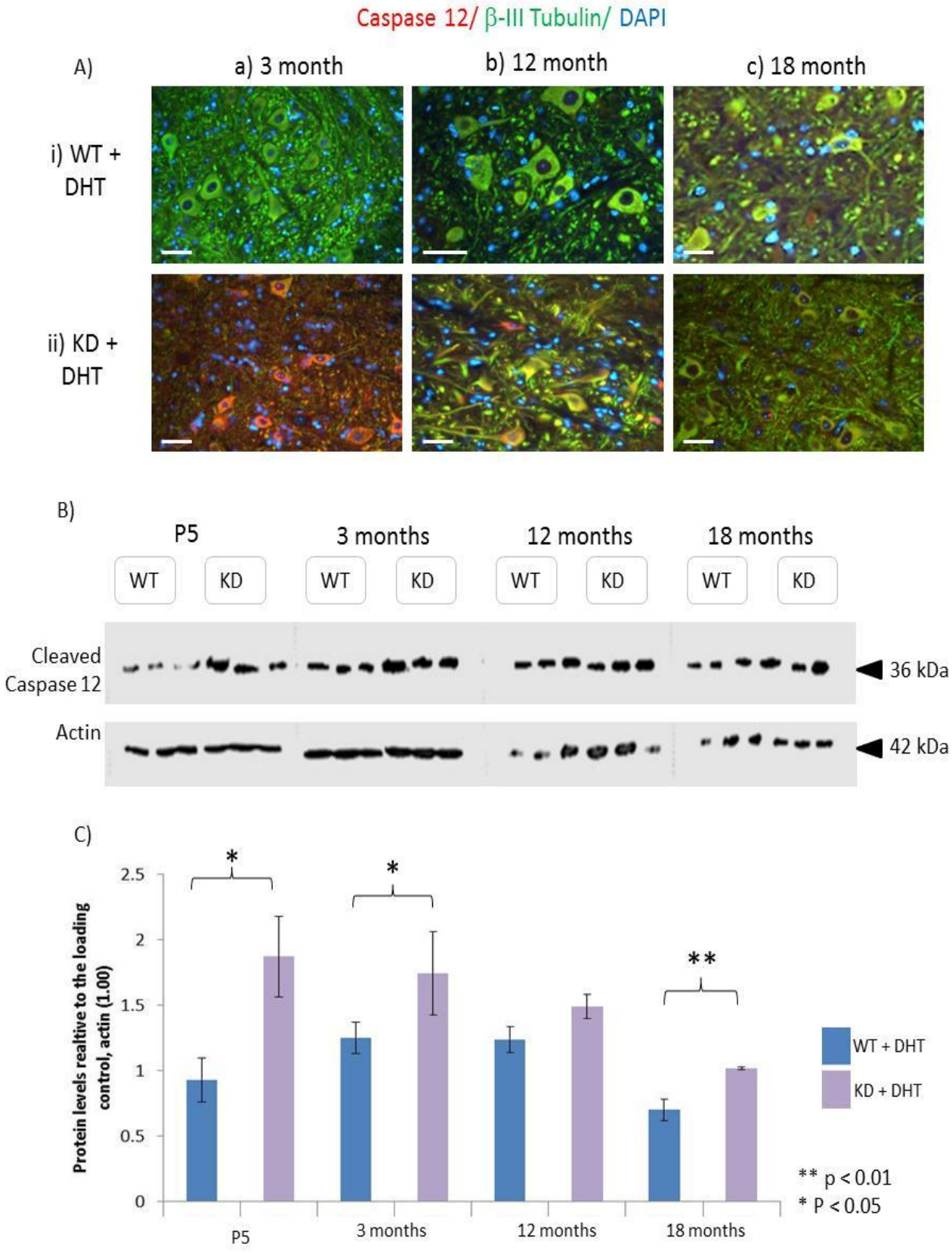
Caspase 12/ β-III Tubulin/ DAPI
A)
a) 3 month
b) 12 month
c) 18 month
i) WT + DHT
ii) KD + DHT
B)
P5
3 months
12 months
18 months
WT
KD
Cleaved Caspase 12
36 kDa
Actin
42 kDa
C)
Protein levels realtive to the loading control, actin (1.00)
2.5
2
1.5
1
0.5
0
*
*
**
P5
3 months
12 months
18 months
WT + DHT
KD + DHT
** p < 0.01
* P < 0.05

When a Ca^{2+}-independent ER stressor, Tunicamycin (TM), is applied to primary motoneuron cultures, there is no additional motoneuron death in KD cultures, highlighting the specific vulnerability of KD motoneurons to ER Ca^{2+} depletion.

When the expression of Caspase 12, a marker of ER stress-induced apoptosis, is examined in purified, primary WT and KD motoneurons, Caspase 12 expression in KD motoneurons is higher than in WT controls, indicating a higher level of ER stress-induced apoptosis. Furthermore, treatment of primary motoneurons with Salubrinal, which decreases KD motoneuron death, also reduces Caspase 12 expression, so that there is only a negligible difference in Caspase 12 expression between WT and KD motoneurons. Salubrinal treatment also appears to increase ER Ca^{2+} in both WT and KD cultures.

Finally, in KD spinal cord tissue, Caspase 12 expression remains higher than WT controls throughout disease progression. The peak elevation in Caspase 12 expression in KD spinal cord occurs pre-symptomatically, at P5, but remains significantly higher in KD spinal cord tissue at disease end-stage.

4.3. Discussion

In this Chapter I investigated whether the ER stress that was observed in KD motoneurons in Chapter 3 was associated with an increased vulnerability of KD motoneurons to ER stress-induced apoptosis. The results presented in this Chapter show that ER stress-induced apoptosis does indeed occur in KD motoneurons both in vitro and in vivo, and can be prevented by treatment with ER stress inhibitors.

4.3.1 Motoneuron death occurs in the AR100 model of Kennedy's Disease.

We have previously shown that motoneuron degeneration occurs in vivo in the AR100 mouse model of KD (Malik et al, 2011). However, the first step in establishing whether or not ER stress-induced apoptosis plays a role in the pathology of the AR100 mouse model of KD at the embryonic stage is to determine whether or not motoneuron death is significantly higher in KD primary cultures than in WT controls. Analysis of motoneuron survival reveals that significantly fewer KD motoneurons survive than WT motoneurons even under basal conditions. This finding suggests that even during embryonic development, KD motoneurons are more vulnerable to cell death and are less able to withstand the process of culturing. There also appeared to be increased axonal clustering in KD cultures. Indeed, it has been shown previously that cells cluster in culture when axonal growth is inhibited (Kimura-Kuroda et al, 2010), which may suggest that the growth of embryonic KD motoneurons is impaired and thus the reduced survival of KD motoneurons could reflect impaired development. This would be consistent with the neurotrophic support deficit discussed in Chapter 1 (Section 3.3).

4.3.2 The effects of treatment with an inhibitor of ER stress on KD motoneuron survival

In order to correlate the presence of ER stress observed in KD motoneurons (Chapter 3, Section 3.3.10) with an increased vulnerability to cell death, the effects of inhibition of ER stress on motoneuron survival was investigated, by treating the cultures with the ER stress inhibitor, Salubrinal. If motoneurons are rescued following the inhibition of

ER stress, it would indicate that ER stress is, at least in part, involved in the increased death of motoneurons observed in KD cultures. The results show that following Salubrinal treatment, motoneuron survival improved in both WT and KD cultures so that the number of motoneurons in WT and KD cultures was not significantly different. This finding has several implications. The first is that even in WT cultures, the culturing process induces a degree of ER stress since Salubrinal treatment increases motoneuron survival. The second implication is that ER stress plays a role in KD pathology and occurs in addition to ER stress associated with the culturing process, as motoneuron survival improved to a greater extent in KD cultures than in WT cultures. Indeed, treatment of KD cultures with Salubrinal significantly rescued KD motoneurons from cell death, so that there was no longer a difference in motoneuron survival between WT and KD cultures. These findings show that the inhibition of ER stress alone is enough to rescue the death of embryonic KD motoneurons, and suggests that triggers of apoptosis other than ER stress do not contribute to KD motoneuron death as much as ER stress does, at least during embryonic development. This finding, combined with the fact that ER stress is present in KD motoneurons even during embryonic development, strongly suggests that the occurrence of ER stress is an important trigger of disease pathology in KD.

4.3.3 Vulnerability of KD motoneurons to ER stressors

As well as being a trigger per se, the increased presence of ER stress in KD motoneurons may result in these cells being more vulnerable to ER stressors and not being able to restore ER homeostasis in response to further ER stress. In order to investigate this, the effects of the ER stressor, Thapsigargin (TG), on WT and KD motoneurons was examined. In both WT and KD cultures, motoneuron survival decreased following 24 hour treatment with 300 nM TG for 24 hours. However, the effects of treatment were more severe in KD cultures. This suggests that the ER stress that is present in KD motoneurons even under basal conditions increases their vulnerability to additional insults such as TG-induced ER Ca^{2+} depletion. Furthermore,

KD motoneurons appear to be more vulnerable to ER Ca^{2+} depletion than other causes of ER stress. When Tunicamycin (TM), which interferes with post-translational modification of proteins, was applied to WT and KD cultures for 24 hours there was no significant decrease in motoneuron survival in KD cultures. Indeed, at higher concentrations of TM, WT motoneurons seem to be affected to a greater extent than KD motoneurons. This may suggest that the normal site of action of TM (peptidoglycan synthesis) is affected in KD. Alternatively, it may be that the effects of TM are not as substantial in KD motoneurons because there is already a greater basal level of ER stress and apoptosis occurring and so the effects of TM are concealed by pre-existing pathology.

4.3.4 Inhibition of ER stress reduces the vulnerability of KD motoneurons

Treatment with Salubrinal, a pharmacological inhibitor of ER stress, reduced the vulnerability of KD motoneurons to ER Ca^{2+} depletion. Indeed, Salubrinal eliminated basal levels of ER stress and negated effects of TG, so that there was no difference between WT and KD motoneuron survival following Salubrinal treatment in the absence and presence of TG. Furthermore, motoneuron survival was still higher in KD cultures treated with both TG and SAL than in untreated cultures. This suggests that the inhibition of ER stress is very effective at preventing ER stress in KD motoneurons.

4.3.5 ER stress-induced apoptosis in KD motoneurons

In Chapter 3, ER Ca^{2+} depletion and ER stress were found to occur in motoneurons from the AR100 model of KD. The results presented in this Chapter established that this ER stress is associated with an increased vulnerability to motoneuron death. The increased death of KD motoneurons is likely to be downstream of ER stress, as inhibition of ER stress with Salubrinal improves motoneuron survival. The results presented in this Chapter also suggest that ER stress-induced apoptosis is a result of the ER Ca^{2+}depletion observed in KD motoneurons in Chapter 3 (Section 3.3.4.2). Whilst TG treatment caused significant motoneuron death in KD motoneurons,

Tunicamycin, which causes ER stress independently of Ca^{2+}, did not increase KD motoneuron death. In order to confirm that ER Ca^{2+}depletion is a cause of ER stress and subsequent ER stress-induced apoptosis in KD motoneurons, the expression of Caspase 12, a mediator of ER stress-induced apoptosis, which is activated downstream of Ca^{2+}release from the ER, was assessed both in embryonic KD motoneurons in vitro and in spinal cords of KD (AR100) mice at various stages of disease. Briefly, following the release of $Ca^{2+}$from the ER, the protease Calpain is activated (Nakagawa et al, 2000) and cleaves Caspase 12. Caspase 12 then activates Caspase 3 and apoptosis ensues. Western blot analysis of Caspase 12 expression in WT and KD purified ventral motoneurons, showed that Caspase 12 levels were significantly higher in KD motoneurons than in WT controls. This suggests that Caspase 12 activation increases in KD motoneurons downstream of the ER Ca^{2+} depletion observed in KD motoneurons in Chapter 3 (Section 3.3.4.2). Furthermore, following treatment with Salubrinal, which increases motoneuron survival and ER Ca^{2+}, Caspase 12 expression in both WT and KD motoneurons decreased. This finding suggests that Salubrinal increases ER Ca^{2+}, despite acting at the level of the Unfolded Protein Response (UPR). This finding suggests that there is a two-way relationship between ER Ca^{2+} and ER stress i.e. they can be both a cause and a result of each other. This possibility will be discussed in more detail in Chapter 6.

Taken together, the results presented in this Chapter show that treatment with Salubrinal increases ER Ca^{2+}, decreases ER stress and decreases ER stress-induced apoptosis in KD cultures, thereby improving KD motoneuron survival. These findings suggest that motoneuron death in KD may occur as a result of a sequence of events at the ER. Thus ER Ca^{2+}depletion leads to the activation of Caspase 12 and initiation of the UPR. This results in ER stress-induced apoptosis, due to a combination of Caspase 12 activation and pro-apoptotic proteins, which are expressed downstream of the UPR. If this proposal is correct, it suggests that prevention of ER Ca^{2+} depletion

may be an effective therapeutic target in the treatment of KD. This possibility will be discussed in more detail in Chapter 6.

4.3.6 Caspase 12 expression in spinal cord of KD mice changes during disease progression

In order to establish whether ER stress-induced apoptosis observed in KD embryonic motoneurons in vitro, was a feature of disease pathology in vivo, Caspase 12 expression in spinal cord tissue from KD mice was assessed at various stages of disease. This analysis may also indicate if elevated levels of ER stress-induced apoptosis act exclusively as an initial disease trigger, or remain with disease progression. The results showed that at all stages of the disease, from E13 until end stage, Caspase 12 expression was elevated in KD motoneurons and spinal cords compared to WT, age-matched controls. As was the case with ER stress markers examined in Chapter 3 (Section 3.3.10), the peak increase in Caspase 12 expression occurred at P5, in keeping with the possibility that ER stress acts as an early disease trigger. However, unlike previous ER stress markers, Caspase 12 was *significantly* elevated in KD spinal cord tissue compared to WT tissue at disease end-stage and the smallest difference in Caspase 12 expression between WT and KD spinal cord tissue occurred at 12 months, at symptom onset. This implies that ER stress may have different roles in KD pathology, occurring at two different stages. There appears to be an initial/early stage that occurs during embryonic development and remains until approximately 3 months of age. ER stress at this pre-symptomatic stage could be an initial disease trigger and give rise to an underlying vulnerability in KD motoneurons. The second occurrence of ER stress-induced apoptosis however, could be a combination of KD motoneuron vulnerability together with the effects of aging. Aging alone is not sufficient to cause ER stress-induced apoptosis since the level of Caspase 12 in WT spinal cord tissue does not change as dramatically with age as it does in KD spinal cord tissue. Therefore additional factors, caused by KD pathology must play a role in Caspase 12 elevation in KD motoneurons at end-stage. Thus, the AR mutation

associated with KD may cause early changes that have subsequent, long term, negative effects on the vulnerability of motoneurons to other factors that accumulate with age and which have been implicated in the pathogenesis of other neurodegenerative disorders. Such factors include mitochondrial dysfunction, impaired axonal transport and protein aggregation (Paradies et al, 2011, Tashiro & Komiya 1994, Lindner and Demarez 2009). Mitochondrial dysfunction is strongly implicated in the process of aging. It has been suggested that reactive oxygen species (ROS), which are produced downstream of respiratory chain activity, have been shown to attack protein and lipid constituents of the mitochondrial membrane as well as mitochondrial DNA (Pak et al, 2003). With age, ROS-associated mitochondrial mutations are suggested to increase, resulting in impairment in respiratory chain function and a consequential increase in ROS production and mitochondrial DNA mutations (Larsson et al, 2010). This has been shown to occur during the aging process in various tissue types including the brain and skeletal muscle (Larsson 2010). An underlying pathological mechanism such as ER stress could render motoneurons more vulnerable to this natural phenomenon of aging.

Impairments in axonal transport have also been shown to occur with age (Tahsiro & Komiya 1994). For example, a longitudinal study of the rat sciatic nerve revealed that as rats aged, the rate of slow axonal transport decreased and the proteolysis of retarded proteins, particularly neurofilament proteins, was found to accelerate (Tashiro & Komiya 1994). In another set of experiments the expression of Dynein, which is an essential motor protein involved in axonal transport (Carter et al, 2011), was found to decrease over time in neuroblastoma cells and result in the accumulation of Tau (Kimura et al, 2007). The impairment of axonal transport can result in other pathological features of aging such as protein aggregation (Lindner and Demarez 2009). Such protein aggregation would increase the demand on the ER and thus the presence of ER stress could result in vulnerability to causes of protein aggregation, such as axonal transport impairment.

As well as factors that accumulate with age, the early occurrence of ER stress may also affect the vulnerability of KD motoneurons to factors that occur downstream of the Androgen Receptor (AR) mutation. For example, nuclear inclusions of the AR, which have been found to occur in KD but are not necessarily associated with pathology (Adachi et al, 2007), could also result in degeneration of motoneurons. Nuclear inclusions have been found to occur in KD, but are not restricted to cell types that are affected by the disease (Adachi et al, 2007). It could therefore be the case that only cell types with an underlying vulnerability are affected by the presence of nuclear inclusions. Such vulnerability could be triggered by ER stress. Therefore, as well as acting as an initial disease trigger, ER stress may also serve as a mechanism by which motoneurons are rendered more vulnerable to deleterious age-related factors as the disease progresses.

CHAPTER 5: RESULTS 3 – MITOCHONDRIAL DYSFUNCTION IN KD MOTONEURONS

5.1. Introduction

In Chapters 3 and 4, the presence of ER Ca^{2+} depletion, ER stress and ER stress-induced apoptosis in primary KD motoneurons was confirmed, suggesting that ER stress makes a contribution to motoneuron degeneration associated with Kennedy's Disease. Changes in the ER such as ER Ca^{2+} depletion have been shown previously to have downstream effects on mitochondrial function (Romagnoli et al, 2008). In this Chapter, mitochondrial function and biogenesis in primary KD motoneurons are therefore investigated in order to determine downstream effects of ER stress in KD as well as the role of mitochondrial dysfunction *per se*.

5.1 Mitochondrial structure & function

5.1.1.1 Structure

Mitochondria are dynamic organelles that are constantly being transported around the cell, changing in size, shape and number (Hollenbeck et al, 2005). Depending on the cell type they can appear as spheres, rod-like structures or filamentous bodies (Krauss et al, 2001). Their general function in all cells is to produce energy via the electron transport chain (ETC) and to play an essential role in programmed cell death (Krauss et al, 2001). Mitochondria also have several other cell-specific functions including; steroid synthesis, neuronal signalling, membrane potential regulation, monitoring cell differentiation and building and breaking down products (Krauss et al, 2001), some of which will be discussed in more detail below

The hallmark structure of mitochondria, which was first identified in the 1950s using electron microscopy (Palade 1953) is depicted in Figure 5.1. The outer membrane consists of a phospholipid bilayer that contains protein structures referred to as Porins. Porins are permeable to molecules that are less than or equal to 10 kDa in size, which is the maximum size of ions, adenosine triphosphate (ATP), adenosine diphosphate (ADP) and nutrient molecules (Schirmer et al, 1998). The protein-to-lipid ratio of the outer membrane is approximately 50:50 (Krauss 2001). The inner membrane however

has a protein-to-lipid ratio of approximately 80:20 (Krauss 2001). It consists of folds that convolute into the mitochondrial matrix and are referred to as cristae. These cristae increase the membrane surface area and are permeable to O_2, CO_2 and H_2O only (Mannella 2006).

The inner membrane acts as an electrical insulator and chemical barrier and is the site of the ETC and ATP synthetase (Krauss et al, 2001). The ETC is a group of complexes at which separate redox reactions occur. It couples the transfer of electrons between electron donors (reduced Nicotinamide Adenine Dinucleotide - NADH) and acceptors (for example, O_2) to the transfer of H+ ions across the mitochondrial membrane from the matrix into the mitochondrial intermembrane space. This creates a proton gradient that generates chemical energy in the form of ATP (Dimroth et al, 2000).

The matrix, which is the internal space of mitochondria, contains a mixture of different enzymes such as those involved in the synthesis of ATP as well as mitochondrial ribosomes, tRNAs and mitochondrial DNA (Krauss et al, 2001). Enzymes in the mitochondrial matrix are also major components of pathways required for carbohydrate, lipid and amino acid oxidation as well as urea and haem biosynthesis (Krauss 2001).

5.1.1.2 Function

Mitochondria have a wide variety of functions contributing to normal cell function and death. A major function of mitochondria is energy conversion, which is achieved via several processes occurring in the mitochondrial inner membrane and matrix.

One of these processes is the coupling of aerobic respiration to the production of ATP - the vital energy unit of cells (Knowles 1980). H+ ions are generated as a product of oxidative reactions in ETC complexes in the mitochondrial inner membrane (Dimroth et al, 2000).

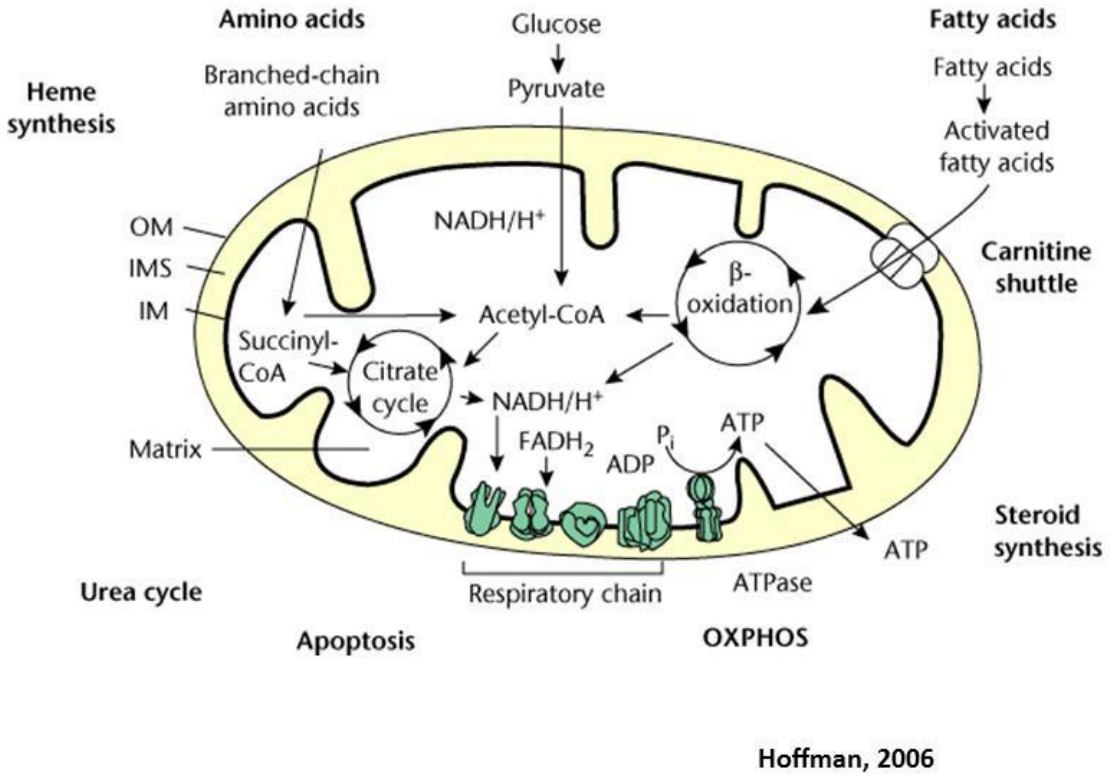

Figure 5.1 Hallmark mitochondrial structure

In general terms mitochondria consist of a double phospholipid membrane (outer and inner) enclosing a matrix that contains mitochondrial DNA as well as enzymes involved in various essential processes such as ATP synthesis and carbohydrate, lipid and amino acid oxidation. The inner membrane contains protein complexes that form the electron transport chain (ETC) and convolutes into the matrix, forming cristae that increase the membrane surface area.

The release of H+ ions into the mitochondrial intermembrane space creates an H+ electrochemical gradient, which drives the return of H+ ions into the mitochondrial matrix (Dimroth et al, 2000). This transportation of H+ into the matrix occurs via ATPsynthetase, which uses the potential energy of the transport to synthesize ATP (Dimroth et al, 2000). In addition to aerobic respiration, mitochondria utilize other processes to produce energy. For example, pyruvate, which is a product of glycolysis, is transported into the mitochondrial matrix where it is then oxidized by the pyruvate dehydrogenase complex and combined with Co-enzyme A (CoA) to produce CO_2, acetyl CoA and NADH (Reed 2001). Acetyl-CoA is the primary substrate for the Citric Acid Cycle in the matrix, which generates electrons for the ETC as well as GTP, which is readily converted into ATP by nucleoside diphospho-kinase (Weiland et al, 1991). Thus mitochondria have a vital role in the conversion of metabolic by-products into units of energy.

As well as energy conversion, mitochondria also have an important role in the regulation of cellular Ca^{2+} signalling. Mitochondria act as a Ca^{2+} buffer when the intracellular Ca^{2+} concentration exceeds 1 μM (Krauss et al, 2001). Ca^{2+} enters mitochondria through a uniporter, whilst Ca^{2+} efflux from the mitochondria is regulated by an electroneutral antiport with either H+ or Na+, depending on the cell type (Krauss et al, 2001). Under stable conditions, both of these Ca^{2+} transporters have a low level of activity and act together to produce a balanced mitochondrial Ca^{2+} cycle (Saris 2005). In the event that the level of cytosolic Ca^{2+} increases, the uniporter becomes more active and the uptake of Ca^{2+} into the mitochondrial matrix exceeds the expulsion of Ca^{2+}, resulting in a net uptake of Ca^{2+} (Saris 2005). An increase in Ca^{2+} in mitochondria has several effects. For example, the permeability transition pore is activated, followed by a decrease in mitochondrial membrane potential, resulting in transient stimulation of the proton pumping respiratory chain (Huser & Davies 2007). This process is known as the uncoupling effect and causes an increase in pH in the matrix. As well as being detrimental to mitochondrial function, Ca^{2+} is also essential for

various mitochondrial enzymes such as pyruvate dehydrogenase phosphatase (Behal et al, 1993) and isocitrate dehydrogenase (Denton 2009), thus the uptake of Ca^{2+} has both extra-mitochondrial and intra-mitochondrial effects.

Since mitochondria act as Ca^{2+} buffers, they also play a vital role in the synchronicity of neuronal signalling (Talbot et al, 2003). Indeed, the inhibition of mitochondrial Ca^{2+} uptake and subsequent mitochondrial membrane depolarization in motoneurons, results in an increase in asynchronous neurotransmitter release during low frequency stimulation. This occurs in parallel with a greater increase in intracellular Ca^{2+} concentration (Talbot et al, 2003). These results suggest that mitochondria are therefore also able to sequester Ca^{2+} in order to prevent asynchronous neurotransmitter release.

Mitochondria also have an essential role in apoptosis as well as processes that are required for cell survival. Mitochondrial permeablization and the consequential release of pro-apoptotic factors have been shown to precede or accompany the execution of apoptosis (Gulbins et al, 2003). The increase in mitochondrial permeability is caused by the opening of the mitochondrial permeability transition pore (PTP), which is a protein complex in the mitochondrial membranes (Gulbins et al, 2003). The PTP consists of a voltage-dependent anion channel (VDAC) and an adenine nucleotide translocase (ANT) in the inner mitochondrial membrane (Zamzani & Kroemer 2001). It has been suggested that following pro-apoptotic stimuli, B-cell CLL/lymphoma 2 (Bcl-2) proteins, such as Bcl2-associated X protein (Bax), interact with the VDAC and ANT, resulting in the formation of a large pore that allows mitochondrial pro-apoptotic proteins, such as Cytochrome C, to be released into the cytoplasm (Narita et al, 1998). Conversely, anti-apoptotic signals prevent opening of the pore and thus prevent the release of pro-apoptotic proteins (Marzo et al, 1998). Once pro-apoptotic proteins are released into the cytosol they initiate apoptosis, block anti-apoptotic proteins and cleave nuclear DNA (Gulbins et al, 2003). As well as the release of proteins, opening of the PTP also results in the influx of ions and water into the mitochondria, which results

in the swelling and eventual rupturing of mitochondria that is associated with apoptosis (Van der Heiden et al, 1997). The release of pro-apoptotic proteins from the mitochondria as well as interactions with regulatory proteins such as Bcl-2, place the mitochondria in a prime position to regulate apoptosis. As well as the removal of physiologically unwanted cells, apoptosis also plays a vital role in development (Naruse & Keino 1995). Thus mitochondrial regulation of apoptosis is also a vital component of embryonic development.

As well as general functions, mitochondria also have functions that are cell - or tissue-specific. In brown adipose tissue for example, mitochondria produce heat, which is an essential event in thermogenesis (Mozo et al, 2005). Mitochondria are able to produce heat due to the fact that H+ has a pathway through which it can enter the matrix without resulting in the production of ATP (Mozo et al, 2005). This is known as a proton 'leak' or mitochondrial uncoupling and the unharnessed potential energy that is created by this process is released as heat. This H+ - facilitated diffusion pathway is mediated by a proton channel called Thermogenin, or UCP1 (Mozo et al, 2005). UCP1 is expressed primarily in brown adipose tissue (Ricquier & Bouillaud 2000), which is why this heat-producing function is specific to this tissue type.

Mitochondria also have a tissue-specific role in steroid synthesis in the adrenal cortex. The synthesis of steroids requires the activation of various oxidative enzymes located in the mitochondria and ER in cells that constitute the adrenal cortex (Chung et al, 1997). In the mitochondria, Cytochrome P450 Cholesterol side chain cleavage enzyme (CYP11A1) converts cholesterol into pregnenolone, which is then processed further in the ER (Hall 1985).

5.1.2 Mitochondrial biogenesis

In general terms, mitochondrial biogenesis is the process by which mitochondrial content, turnover and number are regulated in order to maintain homeostatic demands. The process requires communication between the nuclear genome and the

mitochondrial genome as mitochondrial proteins are encoded by both genomes (for review see Hock & Kralli 2009). Such 'inter-genome' communication is carried out by various proteins including Nuclear Respiratory Factors (NRF) 1 and 2, cyclic-AMP response element binding protein (CREB) and Transcription Factor A of Mitochondria (TFAM). These proteins regulate transcription of essential mitochondrial proteins that are encoded by genes in the nuclear genome, such as those that comprise the electron transport chain (ETC), (Herzig et al, 2000, Li et al, 1999, Scarpulla 2002). Upstream of these regulatory proteins is the transcriptional co-activator; Peroxisome Proliferator-activated receptor γ co-activator 1, or PGC1, which will be used as an indicator of mitochondrial biogenesis in this Chapter (for review see Ventura-Clapier 2008).

5.1.2.1 PGC1α

There are three PGC1 isoforms, namely α, β and γ, however PGC1α will be the focus of this Chapter as it has been frequently associated with health and disease (Frink & Kelly 2006). The PGC1α gene is located on chromosome 5 in mice and chromosome 4 in humans (Puigserver et al, 1998). The murine gene encodes a protein that is 797 amino acids in length and is located within the nucleus (Puigserver et al, 1998). PGC1α is highly expressed in tissues that have a high demand for oxidative metabolism, such as skeletal and cardiac smooth muscle (Puigserver et al, 1998). However, relatively high levels of PGC1α are also found in the central nervous system (Puigserver et al, 1998).

5.1.2.2 Regulation of PGC1α expression and activity

A large number of signalling pathways have been found to regulate the expression and activity of PGC1α (for review see Ventura-Clapier et al, 2008). Ca^{2+} and other second messengers for example, have been found to exert transcriptional control over the PGC1α gene. For example, in skeletal muscle a prolonged period of contraction results in a prolonged elevation of cytosolic Ca^{2+}, which activates the Ca^{2+}-dependent

phosphatase, Calcineurin (CaN) as well as the Ca^{2+}-calmodulin-dependent kinase CaMK (Heineke & Molkentin 2006). CaN has been shown to control the expression of PGC1α in muscle (Handschin et al, 2003). CaN-mediated activation of the PGC1α promoter is dependent on Myocyte Enhancer Factor 2 (MEF2) as well as Histone Deacetylases (HDAC). Resistance to HDAC in mice has been shown to result in a decrease in the number of mitochondria (Czubryt et al, 2003), whilst deletion of MEF2 in mice is also accompanied by a reduction in mitochondrial number (Naya et al, 2002). These results indicate that CaN and MEF2 play a major role in the regulation of PGC1α. However they are not sufficient to regulate the expression of PGC1α as their disruption does not completely eliminate PGC1α expression. As described above, prolonged Ca^{2+} elevation also results in the activation of CaMK. CaMK activation requires the presence of cAMP response element binding protein (CREB), which has also been suggested to regulate the expression of PGC1α (Wu et al, 2006). For example, a strong positive correlation between CREB activation, PGC1α expression and mitochondrial protein content has been observed in murine cardiac tissue (Wu et al, 2006, Watson et al, 2007).

As well as Ca^{2+}, other second messengers such as those involved in the p38 mitogen-activated protein kinase (MAPK) pathway have also been suggested to regulate PGC1α expression. However, unlike the downstream effects of elevated Ca^{2+}, MAPK activation has been suggested to have a negative regulatory effect over PGC1α transcription (Wall et al, 2006). Indeed, the overexpression of the MAPK upstream Kinase 6 (MKK6) is accompanied by a reduction in oxidative respiration, which is indicative of compromised mitochondrial function and/or number (Wall et al, 2006).

In addition to second messenger regulation, PGC1α transcription has also been suggested to be controlled indirectly by thyroid hormones (Wrutniak-Cabello et al, 2001). The precise effect that thyroid hormones have on PGC1α expression however remains unclear. In some cases, the treatment of rats with thyroid hormone appears to

result in increased cardiac oxygen consumption and elevated PGC1α expression (Goldenthal et al, 2004). However other studies report that thyroid hormone treatment has no effect on the level of PGC1α expression (Irrcher et al, 2003).

Cyclin-dependent kinases (CDKs), which are involved in the cell cycle, have also been found to regulate PGC1α transcription (for review see Ventura-Clapier et al, 2008). Gene expression profiling studies have shown that CDK9 (a RNA polymerase kinase) for example, decreases the expression of PGC1α and some of its downstream effectors (Sano et al, 2004).

As well as transcriptional regulation, PGC1α is also subject to post-translational modification, which alters its activity. There are various forms of post-translational modification. For example, PGC1α has been shown to undergo p38MAPK-induced phosphorylation, which is thought to be a mechanism by which the effects of cytokines are regulated (Knutti et al, 2001). The activity of PGC1α has also been suggested to be positively regulated by deacetylation, which is catalysed by the NAD+-dependent SIRT1 deacetylase (Rodgers et al, 2005). The third post-translational modification that is thought to regulate PGC1α activity is arginine methylation, which is catalysed by the protein arginine methyl transferase-1, or PRMT1 (Teyssier et al, 2005). This proposed mechanism of modification has been supported by the fact that mutations of arginine residues in the c-terminal of the PGC1α protein result in reduced expression of various PGC1α target genes (Teyssier et al, 2005).

Thus PGC1α regulation is both complex and varied, making its level of expression and activity vulnerable to a wide range of pathological mechanisms.

5.1.3 Pharmacological manipulation of mitochondrial biogenesis

In order to establish the role that disturbances in mitochondrial biogenesis have in neurodegenerative disease pathology, the effects of pharmacological induction of biogenesis have been examined. There are various drugs that can be used to induce

biogenesis, including Resveratrol and Bezafibrate, which are used in the experiments described in this Chapter.

5.1.3.1 Resveratrol

Resveratrol is a naturally occurring polyphenol that is found in red wine, peanuts and grapes (Sanders et al, 2000, Siemann et al, 1992). It has been shown to increase levels of PGC1α thereby increasing mitochondrial biogenesis (Lagouge et al, 2006). Resveratrol has therefore often been considered as a potentially useful therapeutic tool for neurodegenerative disorders in which mitochondrial biogenesis is impaired (see below Section 5.1.3.2). One of the suggested mechanisms by which Resveratrol is able to increase the activity of PGC1α is via its interaction with the protein Silent Mating Type Information Regulation 2 Homolog 1, or SIRT1 (Lagouge et al, 2006). Under normal circumstances SIRT1 physically interacts with and deacetylates PGC1α and multiple lysine sites, which results in an increase in PGC1α activity (Rodgers et al, 2005). Resveratrol is thought to increase SIRT1 activity (Borra et al, 2005) and in doing so is also thought to increase the deacetylation and hence activity of PGC1α. However this finding is controversial in light of recent evidence, which suggests that Resveratrol may not affect SIRT1 activity (Pacholec et al 2010). Indeed, when the level of native SIRT1 substrates such as p53 were measured using ELISA and Western Blot analysis, the level of SIRT1 activity appeared to be unaffected by the presence of Resveratrol (Pacholec et al 2010). Interestingly, Reseveratrol did increase the levels of fluophore-tagged substrates, which explains previous findings (Pacholec et al 2010).

Resveratrol has also been found to increase the expression of PGC1α (Bastin et al, 2011). In human fibroblasts for example, exposure to 75 μM Resveratrol results in a significant increase in PGC1α expression, compared to fibroblasts treated with a vehicle drug, as revealed by Western blot analysis (Bastin et al, 2011).

However, the effects of Resveratrol appear to vary substantially, with studies reporting both protective and toxic effects of the drug. For example, treatment of obese and insulin-resistant mice with Resveratrol results in increased mitochondrial biogenesis and appears to protect mice against the metabolic disease (Lagouge et al, 2006). In another study, Resveratrol treatment appears to protect neurons and improve functional recovery in a rat model of spinal cord injury (Liu et al, 2010). However, in some studies, Resveratrol treatment results in apoptosis. For example, when a hormone-sensitive prostate cancer cell line is treated with Resveratrol, viability is reduced and cells appear to have apoptotic morphology (Morris et al, 2002). The effect of Resveratrol on KD motoneurons is therefore difficult to predict. Whilst neuronal cells appear to benefit from Resveratrol treatment, treatment of cells in which the Androgen Receptor is affected, may be detrimental to survival.

5.1.3.2 Bezafibrate

Another pharmacological agent that has been previously used to induce mitochondrial biogenesis is Bezafibrate. Bezafibrate (2-[4-[2-(4-chlorobenzamido)ethyl]phenoxy]-2-methylpropanoic acid) is a synthetic ligand for peroxisome proliferator-activated α-receptors (PPARs) that is commonly used for the treatment of hyperlipidaemia, since it can lower levels of low-density lipoproteins (LDLs) and triglycerides, whilst increasing high-density lipoproteins (HDLs) in the blood (Goldenberg et al, 2008). Like Resveratrol, Bezafibrate has been shown to increase PGC1α activity (Goldenberg et al, 2008). The increase in activity occurs as a result of PPAR activation, which increases deacetylation of PGC1α (for review see Goldenberg et al, 2008). The effect of Bezafibrate exposure on PGC1α expression levels is currently unclear.

5.1.4 Mitochondrial dysfunction and Neurodegenerative Diseases

Mitochondrial dysfunction has been found to play a role in the pathogenesis of various neurodegenerative disorders such as Motor Neuron Diseases (MNDs) and Poly-CAG repeat Disorders (Afifi et al, 1966, Browne 2008). Since KD is both an MND and Poly-

CAG repeat disorder, it can therefore be suggested that mitochondrial dysfunction is also likely to occur in KD.

5.1.4.1 Mitochondrial dysfunction in Motor Neurone Diseases (MNDs)

Mitochondrial dysfunction has been suggested to play a role in the pathogenesis of MNDs such as Amyotrophic Lateral Sclerosis (ALS). The first indications of mitochondrial disruption in ALS came from post-mortem skeletal muscle tissue of sporadic ALS (sALS) patients in the 1960s (Afifi et al, 1966). These autopsies revealed subsarcolemmal aggregations of mitochondria in both skeletal muscle and intramuscular nerves, which are not present in healthy individuals (Afifi et al, 1966, Atsumi et al, 1981). Mitochondrial morphological abnormalities were also later observed in anterior horn post-mortem samples from sALS patients (Sasaki & Iwata 1996).

Consistent with the presence of abnormal morphology, evidence suggests that mitochondrial function appears to be disrupted in ALS. Abnormalities in respiratory function for example, have been implicated by mitochondrial DNA (mtDNA) frame-shift mutations that decrease the activity of complexes I and IV of the mitochondrial respiratory chain in the spinal cord and skeletal muscle of sALS patients (Wiedemann et al, 2000). Although this strongly suggests that changes in ETC complex activities play a role in ALS pathology, it does not confirm whether or not mitochondrial dysfunction is a disease trigger or a secondary effect of other pathological mechanisms. In order to establish the time point at which mitochondrial dysfunction occurs, cell lines and mouse models of ALS, which over-express a mutant SOD1 G93A protein ($SOD1^{G93A}$) have been investigated. Several studies have found that not only is the expression of $SOD1^{G93A}$ associated with morphological changes in mitochondria, but also with the disruption of mitochondrial function. For example, in neuroblastoma cells transfected with $SOD1^{G93A}$ cytosolic Ca^{2+} levels are increased, which could be indicative of disrupted mitochondrial Ca^{2+} buffering, and mitochondrial depolarization,

which is an indicator of increased mitochondrial membrane permeability (Carri et al, 1997). This finding has been replicated in the $SOD1^{G93A}$ model of ALS (Bilsland et al, 2008) and thus is a consistent effect of the over-expression of $SOD1^{G93A}$.

In keeping with findings from patient post-mortem tissue, reductions in ETC complex activity have also been found in $SOD1^{G93A}$ mice. The magnitude of the reduction in complex activity also appears to increase with disease progression (Jung et al, 2002, Mattiazzi et al, 2002). This decrease in activity of the ETC results in an impairment in mitochondrial Ca^{2+} loading and a sustained decreased capacity to consume oxygen and synthesize ATP (Mattiazzi et al, 2002). Importantly, these defects appear in $SOD1^{G93A}$ mice pre-symptomatically, indicating that mitochondrial dysfunction has an early and therefore potentially causal role in ALS pathogenesis.

As well as functional impairment, mitochondrial biogenesis is also likely to be disrupted in ALS. Although the levels of PGC1α expression and activity have yet to be extensively studied in ALS pathology, the various mechanisms of PGC1α regulation, such as Ca^{2+} signalling in skeletal muscle (Handschin et al, 2003) have been found to be affected in ALS (for review see Appel 2011)

The mechanism by which expression of mutant SOD1 results in mitochondrial dysfunction has yet to be fully established. However several theories have been proposed based on the fact that SOD1 is localized to the mitochondria (Higgins et al, 2002). Under normal circumstances, SOD1 is thought to localize to the mitochondrial intermembrane space (Mattiazzi et al, 2002). Mutant SOD1 is thought to remain localized to the mitochondrial matrix where it forms large aggregates (Vijayvergiya et al, 2005). One of the suggested mechanisms by which mSOD1 aggregates result in mitochondrial abnormalities is based on observations made during early stages of mitochondrial vacuolization is ALS. Mutant SOD1 fragments have been observed within the vacuoles and peroxisomes appear to fuse with these vacuolated mitochondria, which are thought to result in expansion of the mitochondrial outer

membrane (Higgins et al, 2003). A possible outcome of this event is that mitochondria become porous and allow Cytochrome C and other pro-apoptotic proteins to leak out of the mitochondria and into the cytosol (Higgins et al, 2003). Alternatively, it has been suggested that mSOD1 accumulates progressively on the outer membrane of the mitochondria and results in 'blockage' of the mitochondrial translational machinery, leading to mitochondrial dysfunction (Liu et al, 2004). This theory remains controversial however, since Wild-Type SOD1 also appears to localize to mitochondria as part of its normal function (Higgins et al, 2002).

5.1.4.2 Mitochondrial dysfunction in CAG-repeat disorders

The first indications that mitochondrial and energetic impairment are present in Huntington's Disease (HD) have come from the significant weight loss observed in HD patients despite a maintained caloric intake (for review see Browne 2008). Indeed, PET scans of these patients reveal that there is pre-symptomatic decrease in glucose utilization, which is suggestive of mitochondrial disturbances (Browne 2008).

Extensive studies have revealed that there are indeed several aspects of mitochondrial function that are disturbed in HD. For example, post-mortem striatum samples from HD patients in advanced stages of the disease reveal that complexes II, III and IV of the respiratory chain have a lower level of in vitro activity compared to healthy controls (Gu et al, 1996, Browne et al, 1997). This decrease in activity however is not replicated in samples of striatum (which is affected in HD) from pre-symptomatic patients, suggesting that respiratory chain impairment is not a trigger of HD (Guidetti et al, 2001). Indeed, there appears to be no difference in levels of activity of these complexes in mice expressing the full length mutant Huntingtin protein or in primary motoneurons from HD mice in vitro (Guidetti et al, 2001, Oliveria et al, 2007). The disturbance of complex activity only appears to emerge when primary neurons are challenged with Ca^{2+}-induced stress indicating that respiratory chain disturbances

could give rise to an underlying vulnerability as opposed to directly triggering HD (Oliveria et al, 2007).

Mitochondrial Ca^{2+} handling has also been suggested to be affected in HD. For example, in striatal neurons from HD rats there appears to be a susceptibility to cellular Ca^{2+} loads that is indicative of diminished mitochondrial Ca^{2+} buffering capacity (Panov et al, 1999). Furthermore, the extent of this susceptibility appears to increase with an increasing number of Huntingtin CAG repeats, which is positively correlated with symptom severity (Panov et al, 1999).

Another function of mitochondria that is disturbed in HD is ATP production. However, the role of changes in ATP production in HD is controversial, with both increases and decreases being reported. For example, in synaptossomal fractions from the HdH150 mouse model of HD, ATP levels are lower than in WT controls (Orr et al, 2008). However, this decrease has been explained by disturbances in mitochondrial trafficking as opposed to disruption of ATP synthesis *per se* (Orr et al, 2008). In contrast, ATP levels are higher in the N171-82Q model of HD, which is likely to be due to a higher level of glycolysis that is observed in this model (Olah et al, 2008). Therefore the exact effect of the CAG-repeat mutation on ATP production in mitochondria remains unclear.

The mechanism by which the CAG expansion in the Huntingtin gene can disrupt mitochondrial function has yet to be determined however several proposals have been made that include both direct and indirect effects of the mutation on mitochondria.

Evidence for a direct effect includes the fact that the mutant Huntingtin protein physically associates with mitochondria (Panov et al, 2002). The site of association is not clear however, with some groups reporting association of the protein with the outer membrane of mitochondria (Choo et al, 2004), whilst other groups report the presence of mutant Huntingtin fragments *inside* the mitochondria (Yu et al, 2003). A key process that is thought to be affected downstream of this interaction is mitochondrial trafficking (Trushina et al, 2004). It has been suggested that the presence of mutant Huntingtin

aggregates physically blocks the mitochondrial trafficking pathway (Chang et al, 2006). Alternatively, the aggregates have been proposed to sequester the trafficking machinery that is required for the normal trafficking of mitochondria (Trushina et al, 2004). Consequences of impaired mitochondrial trafficking include a disruption of cellular ATP supply, which is of particular significance in long neuronal cells, which require high amounts of energy to traffic cargo over long distances (Wang et al, 2008).

As well as mitochondrial function being disrupted, mitochondrial number also appears to decrease in HD, suggesting that mitochondrial biogenesis is also impaired (McGill & Beal 2006). Indeed in the N171-82Q mouse model of HD, there is reduced PGC1α expression in the striatum compared to WT control mice (Weydt et al, 2006). Furthermore, in HD patient post-mortem brain tissue, microarray expression analysis reveals that the expression of 24 out of 26 PGC1α target genes are reduced (Weydt et al, 2006). PGC1α activity has also been found to be reduced in muscle tissue from HD mice and myoblasts from HD patients (Chaturvedi et al, 2009). Furthermore, adenoviral-mediated delivery of PGC1α to murine muscle tissue increased expression of oxidative muscle fibre markers and heightened b-guanidinopropionic acid (GPA – a catabolic stressor) – induced responses (Chaturvedi et al, 2009). Thus the interference of PGC1α expression and activity could play a pivotal role in HD pathology.

5.1.5 Mitochondrial dysfunction in Kennedy's Disease

In view of the involvement of mitochondrial disturbances in MNDs and CAG-repeat disorders, it is not surprising that mitochondrial dysfunction has also been suggested to contribute to KD pathogenesis. At present however, the vast majority of evidence for the involvement of mitochondrial dysfunction in KD pathology has been obtained from in vitro experiments from the use of mutant AR-transfected cell lines as opposed to transgenic models and patient spinal cord biopsy tissue. In the motoneuron-derived cell line MN-1 for example, the expression of a mutant AR protein containing 65 CAG repeats results in mitochondrial membrane depolarization and decreases PGC1α

expression (Ranganathan et al, 2009). Mitochondrial-dependent apoptosis was also found to accompany the mitochondrial dysfunction observed in these cells (Ranganathan et al, 2009). For instance, activation of the mitochondrial-dependent apoptotic pathway, which can be inferred by measuring levels of active Caspase 9, is elevated by approximately 50% in these cells compared to control cells containing a AR protein with a normal number of CAG-repeats (Ranganathan et al, 2009). Furthermore, MN-1 cells containing the mutant AR protein appear to be protected by the application of the mitochondrial modulator; cyclosporine A, which prevents opening of the mitochondrial membrane transition pore, confirming further that mitochondrial dysfunction is a cause of apoptosis in these cells (Ranganathan et al, 2009).

The experiments described in this Chapter will expand on the above findings and measure mitochondrial membrane potential and PGC1α expression in primary motoneurons from the AR100 model of KD. The effects of pharmacologically-induced increases in mitochondrial biogenesis on motoneuron survival will also be examined. This will allow the magnitude of the effect of inhibiting ER stress and increasing mitochondrial biogenesis on KD motoneurons to be compared and thus to establish which is more likely to form the basis of a successful therapeutic strategy.

5.1.6 Hypothesis & Aims

Since mitochondrial dysfunction has been shown to play a role in the pathogenesis of various neurodegenerative disorders and ER Ca^{2+} depletion has also been shown previously to jeopardize mitochondrial function (Romagnoli et al, 2008), mitochondrial dysfunction is likely to play a role in the pathogenesis of KD.

In this Chapter, mitochondrial function and biogenesis in primary KD motoneurons will be investigated. In the event that mitochondrial biogenesis is impaired in primary KD motoneurons, the effect of pharmacological induction on primary KD motoneuron survival will be investigated in order to further establish the role of mitochondrial impairment in KD pathogenesis.

5.2. Results

The possibility that mitochondrial dysfunction was a feature of KD pathology at early stages of disease progression was investigated by measuring mitochondrial membrane potential in embryonic primary KD motoneurons.

5.2.1 TMRM reliably measures mitochondrial membrane potential

In order to determine whether or not TMRM reliably measures mitochondrial membrane potential, 1 μM carbonyl cyanide-trifluoromethoxyphenyl hydrazone (FCCP) is applied to cultures and the average mitochondrial fluorescence in motoneurons is measured (see Chapter 2, Section 2.6.7 for details). In untreated WT primary motoneurons the mean arbitrary TMRM fluorescence intensity is 1387.75 (+/- 83.2 SEM, n = 25). However in FCCP-treated WT primary motoneurons the average fluorescence intensity decreases by 80% (+/- 5.4% SEM, n = 15). This decrease is significant ($p < 0.001$) and is indicative of mitochondrial membrane depolarization (Figure 5.2B).

5.2.2 The mitochondrial membrane potential is depolarised in primary KD motoneurons

The mitochondrial membrane potential is depolarized in primary KD motoneurons compared to WT controls. Indeed confocal images reveal that TMRM fluorescence is stronger in WT primary motoneurons than in KD motoneurons (Figure 5.2A). When this fluorescence is quantified, the average TMRM fluorescence value in KD motoneurons is 36.1% lower (+/- 12% SEM, n = 26) than the average mitochondrial fluorescence in WT motoneurons, which is indicative of mitochondrial membrane depolarization. This is not as low as the fluorescence in FCCP-treated WT motoneurons, but is still significantly lower than the value for untreated WT motoneurons ($p = 0.003$).

Figure 5.2 Mitochondria are depolarized in KD ventral horn motoneurons compared to WT controls

Primary WT and KD motoneuron cultures were imaged at 7 DIV. Cultures were treated with 5 μM DHT (final concentration 50 nM) at 4 DIV. Cultures were incubated at 37^{o}C with TMRM, diluted in a 1 μM Ca^{2+} recording medium, prior to imaging. After 30 minutes of incubation, cultures were washed with, and subsequently imaged in, fresh TMRM-containing recording medium. Cultures were kept at 37^{o}C throughout the protocol. Ai) and Aii) show example fluorescent images taken from the experiment. TMRM is shown in red. The Bar chart (B) summarizes TMRM fluorescence in DHT-treated WT and KD motoneuron cultures, as well as FCCP-treated WT cultures, which are a positive control for mitochondrial depolarization. Values are expressed relative to the average TMRM fluorescence in WT motoneurons (100.00).

Error bars = standard error of mean, scale bars = 35 μm

Figure 5.2

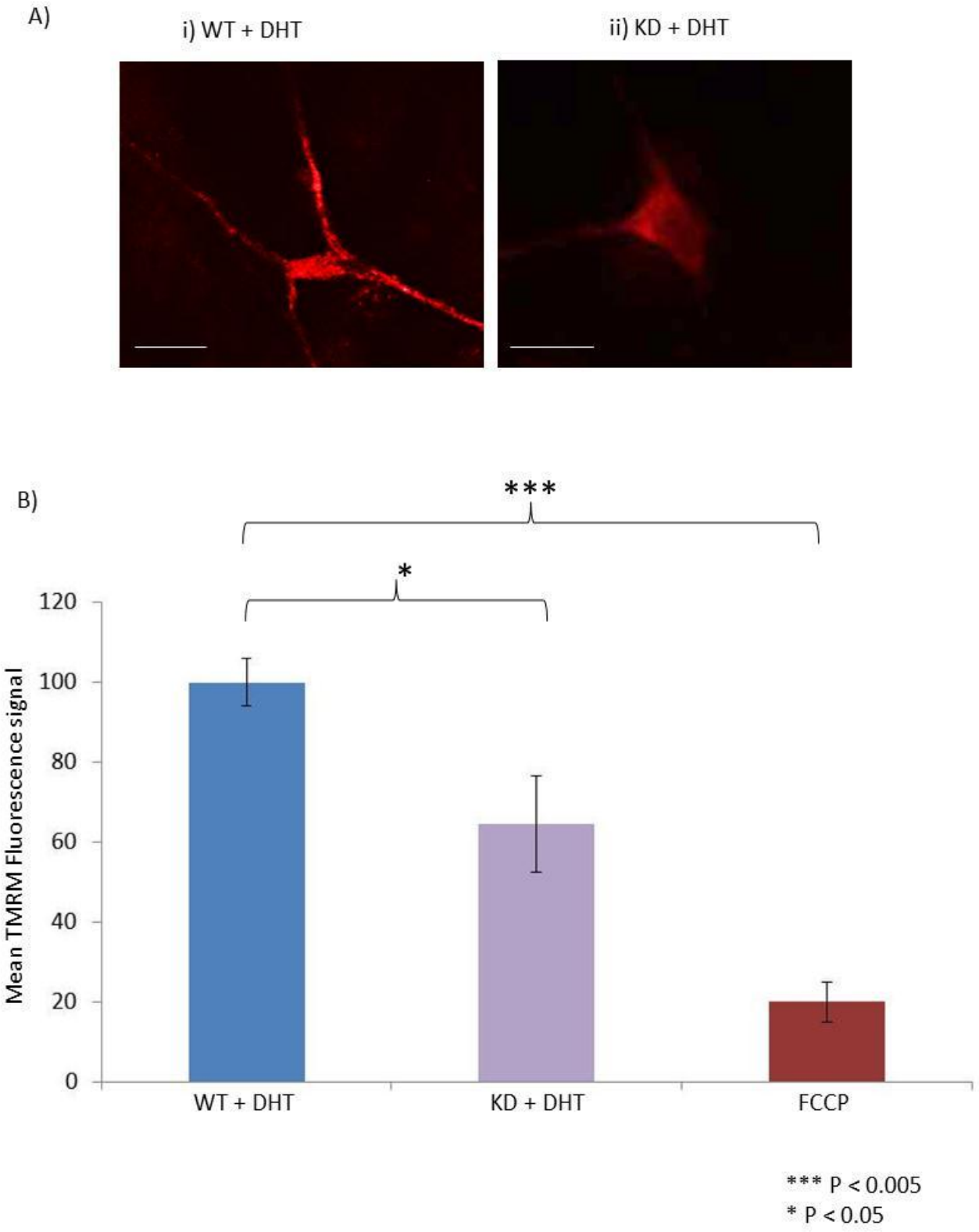
A)
i) WT + DHT
ii) KD + DHT
B)
***
*
Mean TMRM Fluorescence signal
120
100
80
60
40
20
0
WT + DHT
KD + DHT
FCCP
*** P < 0.005
* P < 0.05

5.2.3 PGC1α expression is lower in primary KD motoneurons than in WT controls

The expression of PGC1α, an inducer of mitochondrial biogenesis, was examined in WT and KD cultures by immunohistochemistry and Western blot analysis. Mitochondrial biogenesis was investigated in KD motoneurons following previous findings that mitochondrial biogenesis is impaired in other MNDs and Poly-CAG repeat disorders (Handschin 2003, McGill & Beal)

Immunostaining of WT and KD primary motoneuron cultures for PGC1α at 7 DIV reveals that PGC1α immunoreactivity is stronger in WT primary motoneurons than in KD motoneurons (Figure 5.3A). This suggests that PGC1α expression is higher in WT motoneurons.

The level of expression of PGC1α was also quantified by Western blot analysis. A typical blot is shown in Figure 5.3B.

Assessment of the optical density of the Western blot (Figure 5.3C) reveals that the level of PGC1α is 155% lower in KD primary motoneurons than in WT controls. In WT motoneurons, the PGC1α expression level relative to the loading control, Actin (1.0), is 1.25 (+/- 0.06 SEM, n=3), whereas in KD motoneurons it is 0.49 (+/- 0.02 SEM, n=3). This reduction in PGC1α levels in KD motoneurons is significant (p= 0.034).

5.2.4 The effects of pharmacological induction of mitochondrial biogenesis on PGC1α expression in KD primary motoneurons

Since the results show that mitochondrial biogenesis is reduced in KD motoneurons, the effects of pharmacological induction of mitochondrial biogenesis, using Resveratrol, were investigated.

Figure 5.3 PGC1α expression in WT and KD ventral horn motoneurons

WT and KD motoneuron cultures were immunostained for PGC1α (red) and co-stained for β-III tubulin (green – a neuronal marker) and DAPI (blue, a nuclear marker). Images showing the typical patterns of PGC1α immunoreactivity in DHT-treated WT and KD motoneuron cultures are shown in Ai) and ii), respectively. Levels of PGC1α in WT and KD motoneuron cultures were also analysed by Western blot. A representative Western blot is shown in (B). Optical density analysis was performed and protein levels were expressed relative to the house-keeping protein, Actin, which was used as a loading control and given a value of 1.0. As shown in the bar chart (C), PGC1α expression is significantly reduced in embryonic KD motoneurons compared to WT controls ($p < 0.05$).

(Error Bars = standard error of mean, scale bars = 50 μm)

Figure 5.3

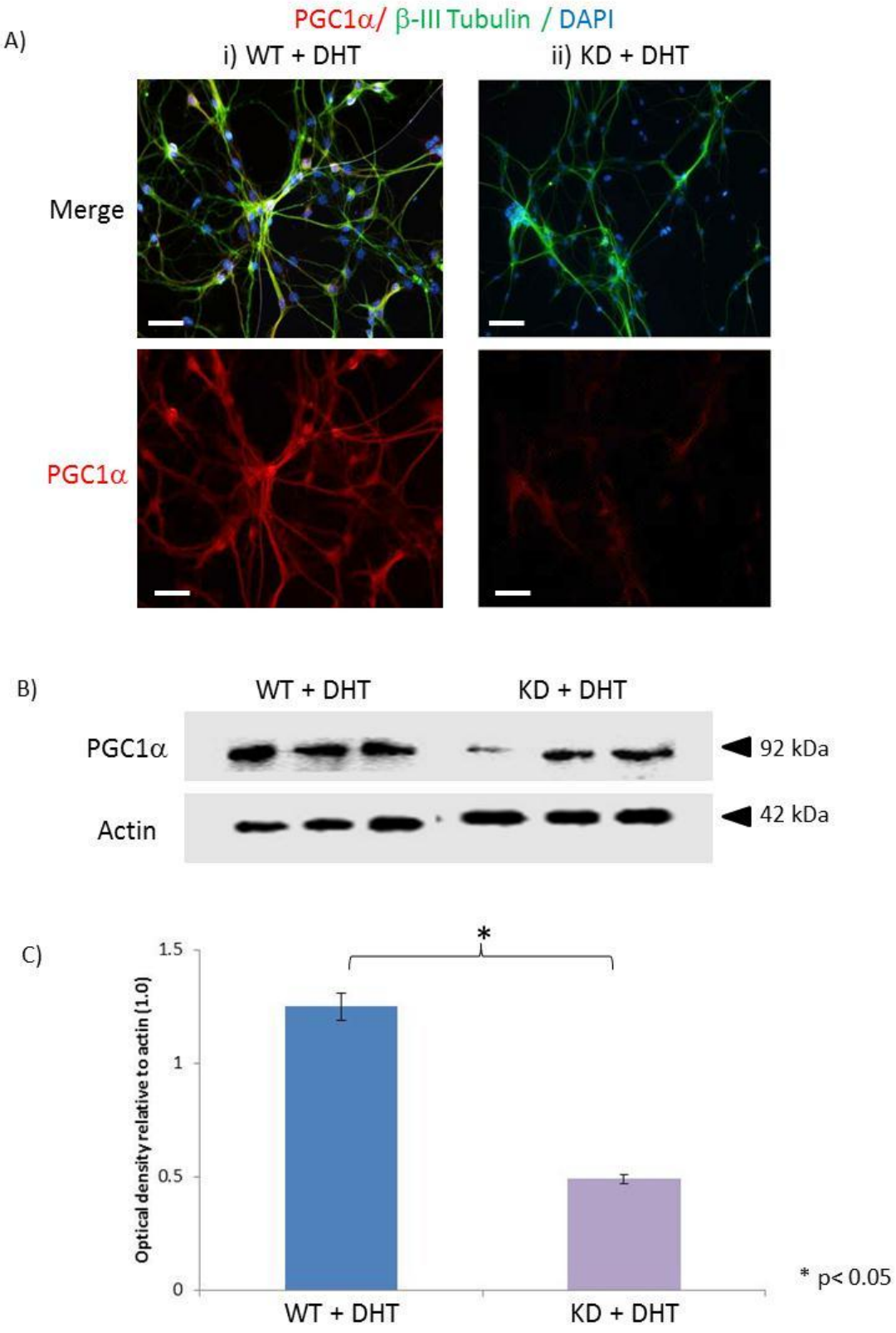
A)
PGC1α/ β-III Tubulin / DAPI
i) WT + DHT
ii) KD + DHT
Merge
PGC1α
B)
WT + DHT
KD + DHT
PGC1α
92 kDa
Actin
42 kDa
C)
*
1.5
1
0.5
0
Optical density relative to actin (1.0)
WT + DHT
KD + DHT
* p< 0.05

The expression of PGC1α, was examined in WT and KD cultures in the absence and presence of 50 μM Resveratrol by immunohistochemistry and Western blot analysis.

Immunohistochemistry reveals that following treatment of cultures with Resveratrol PGC1α immunoreactivity increases in KD motoneurons (Figure 5.4A) in contrast to WT motoneurons in which there is no noticeable change in PGC1α immunoreactivity following Resveratrol treatment.

Levels of PGC1α after 50 μM Resveratrol exposure were also examined by Western blot analysis. A typical blot is shown in Figure 5.4B. Assessment of the optical density of the Western blot (Figure 5.4C) reveals that the level of PGC1α is 15% lower in KD primary motoneurons than in WT controls compared to 155% lower in KD motoneurons that had not been exposed to Resveratrol (see Figure 5.3). In WT motoneurons, the PGC1α expression level relative to Actin (1.0) is 1.37 (+/- 0.08 SEM, n=3), whereas in KD motoneurons it is 1.165 (+/- 0.09 SEM, n=3). This difference is not significant.

5.2.5 Pharmacological induction of mitochondrial biogenesis increases motoneuron survival in KD ventral horn cultures

When motoneuron survival is calculated by expressing the number of β-III tubulin positive cells with more than two processes as a percentage of total cell number (DAPI-positive), the results show that treatment with Resveratrol increases motoneuron survival in both WT and KD cultures (Figure 5.5B). Following 24 hour Resveratrol exposure (50 μM), the percentage of motoneurons in WT cultures increases from approximately 42% to 49.6 % (+/- 1.47% SEM, n =40), an increase of almost 8%. In KD cultures however, the percentage of motoneurons increases by approximately 19% following Resveratrol treatment to 47.9% (+/- 1.32% SEM, n = 40). This increase is significant (p=0.023). Following Resveratrol treatment there is no longer a significant difference in motoneuron survival between WT and KD cultures.

Figure 5.4 The effect of Resveratrol on PGC1α expression in WT and KD ventral horn cultures

DHT-treated WT and KD motoneuron cultures were immunostained at 7 DIV for PGC1α (red) and co-stained for β-III tubulin (green – a neuronal marker) and DAPI (blue, a nuclear marker). In some cases cultures were treated at 6 DIV with Resveratrol. Images showing the typical patterns of PGC1α immunoreactivity in the absence and presence of Resveratrol in WT and KD motoneuron cultures are shown in Ai) and ii), respectively. Levels of PGC1α in WT and KD motoneuron cultures in the absence and presence of resveratrol were also analysed by Western blot. A representative Western blot is shown in (B). Optical density analysis was performed and protein levels were expressed relative to the house-keeping protein, Actin, which was used as a loading control and given a value of 1.0. As shown in the Bar chart (C), PGC1α expression is significantly reduced in embryonic KD motoneurons compared to WT controls ($p < 0.05$) but there is no significant difference in expression following Resveratrol exposure.

(Error Bars = standard error of mean, scale bars = 50 μm)

Figure 5.4

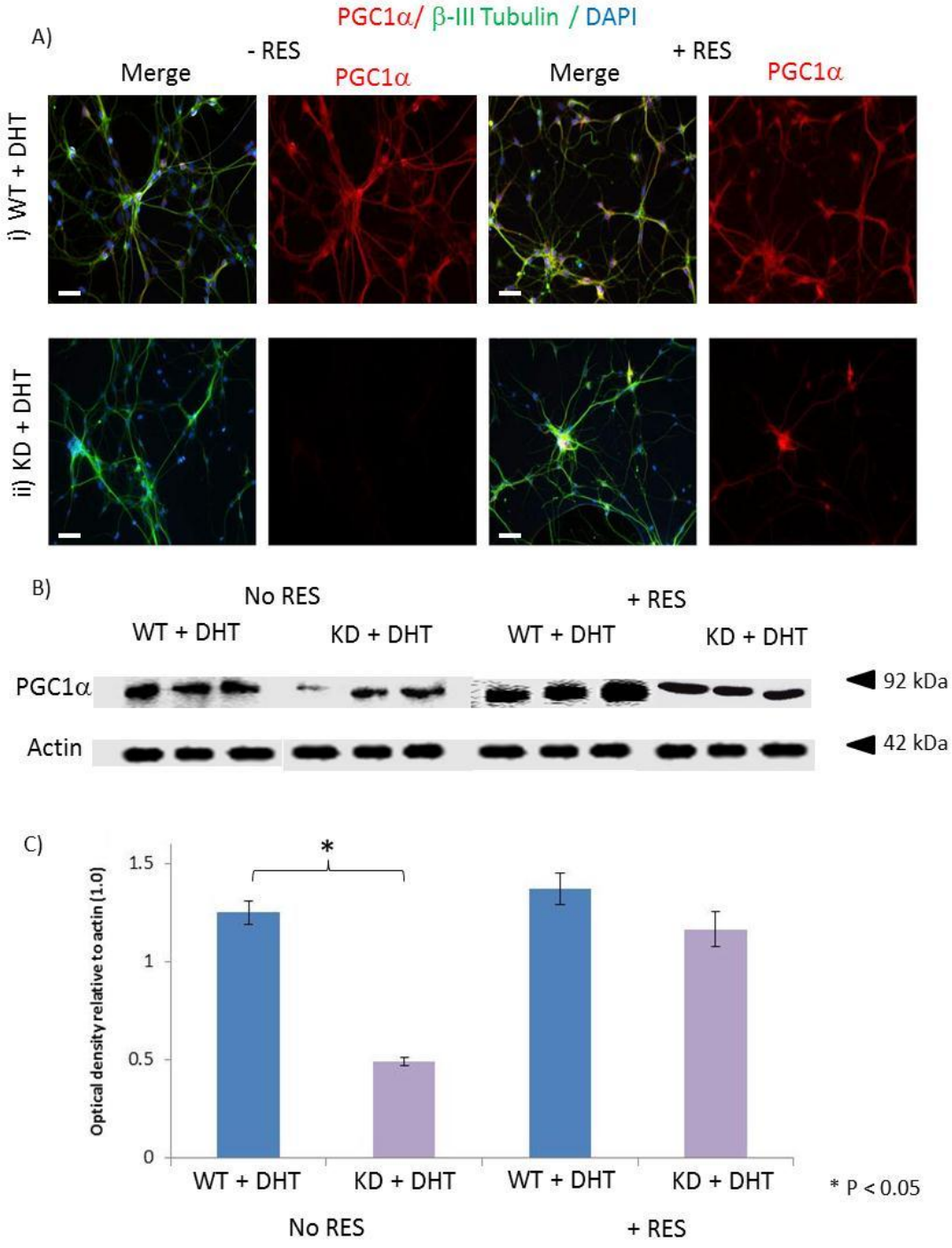
A)
PGC1α/ β-III Tubulin / DAPI
- RES
+ RES
Merge
PGC1α
Merge
PGC1α
i) WT + DHT
ii) KD + DHT
B)
No RES
+ RES
WT + DHT
KD + DHT
WT + DHT
KD + DHT
PGC1α
92 kDa
Actin
42 kDa
C)
Optical density relative to actin (1.0)
1.5
1
0.5
0
*
WT + DHT
KD + DHT
WT + DHT
KD + DHT
No RES
+ RES
* P < 0.05

Figure 5.5 The effect of Resveratrol on motoneuron survival in WT and KD ventral horn cultures

DHT-treated WT and KD motoneuron cultures were immunostained at 7 DIV for PGC1α (red) and co-stained for β-III tubulin (green – a neuronal marker) and DAPI (blue, a nuclear marker). The motoneuron survival was calculated by expressing the number of β-III tubulin-positive cells, with more than 2 processes, as a percentage of total cell number (DAPI-positive). The Bar chart shows motoneuron survival in DHT-treated WT and KD ventral horn cultures in the absence and presence of Resveratrol. Motoneuron survival is significantly lower in KD cultures compared to WT cultures in the absence of Resveratrol ($p < 0.01$), however after Resveratrol exposure the difference in survival of motoneurons between WT and KD cultures is negligible.

Figure 5.5

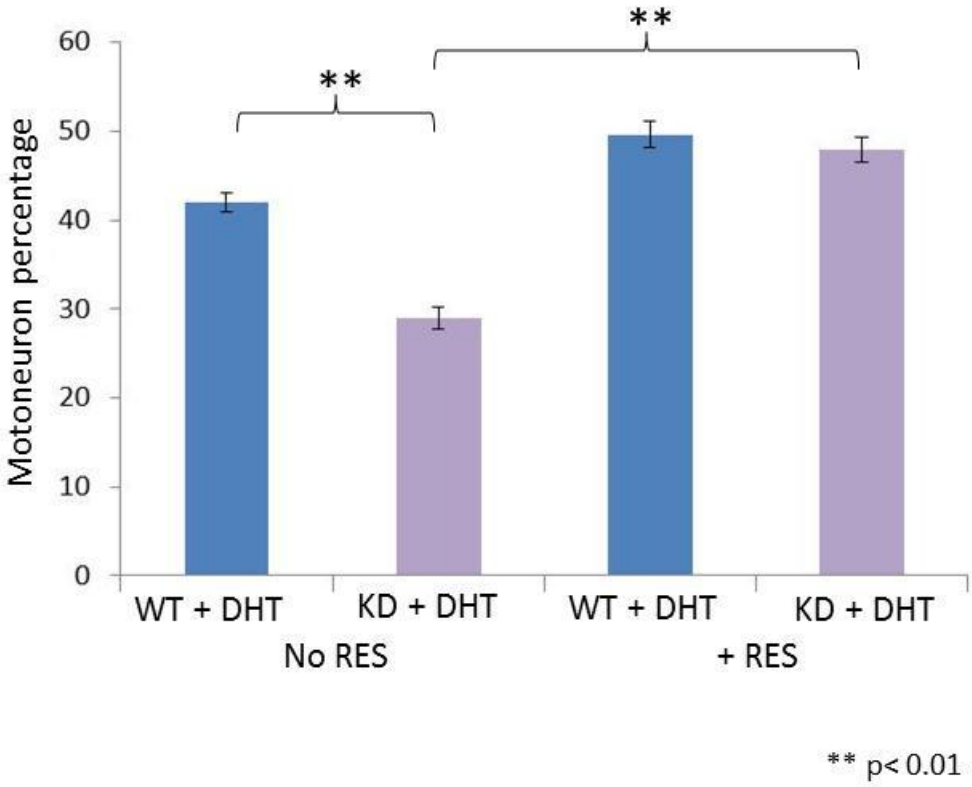

** p< 0.01

5.2.6 Resveratrol treatment decreases total cell number in WT and KD cultures

When the total number of DAPI-positive cells (blue) is counted in WT and KD ventral horn cultures in the absence and presence of Resveratrol, it appears that Resveratrol treatment decreases the total cell number in both WT and KD cultures (Figure 5.6). In DHT-treated WT cultures *not* treated with Resveratrol, the average total cell number per field is 260 (+/- 15 SEM, n = 40), however, following Resveratrol treatment, this decreases to 201 (+/- 11 SEM, n = 40), which, although a decrease of approximately 23%, is not a significant decrease. In DHT-treated KD cultures *not* treated with Resveratrol, the average total cell number per field is 231 (+/- 17 SEM, n = 40). Following Resveratrol treatment, this decreases by 54% to 105 (+/- 7 SEM, n = 40). This decrease is significant (p = 0.008). In the absence of Resveratrol treatment, there is only a negligible difference in total cell number between WT and KD cultures. However, following Resveratrol treatment, the difference in total cell number between WT and KD cultures becomes significant (p=0.01).

5.2.7 The effects of induction of mitochondrial biogenesis on mitochondrial function: Resveratrol treatment depolarizes mitochondrial membrane potential in KD motoneurons

The effects of treatment with Resveratrol on mitochondrial function were examined next by assessment of mitochondrial membrane potential. Measurements of TMRM fluorescence in DHT-treated WT and KD primary motoneuron cultures that are either treated at 6 DIV with Resveratrol or left untreated, showed that Resveratrol exposure depolarizes the mitochondrial membrane in both WT and KD motoneurons (Figure 5.7). In WT cultures the average TMRM fluorescence in motoneurons decreases to 1267, which is 91% (+/- 23% SEM, n = 28) of the average value for untreated WT motoneurons.

Figure 5.6 The effect of Resveratrol on total cell number in KD and WT ventral horn cultures.

DHT-treated WT and KD motoneuron cultures were immunostained at 7 DIV for PGC1α (red) and co-stained for β-III tubulin (green – a neuronal marker) and DAPI (blue, a nuclear marker). In some cases cultures were treated at 6 DIV for 24 hours with Resveratrol. The total cell number (DAPI-positive) was then counted for each field used in the motoneuron survival assessment in Figure 5.4. The bar chart summarizes the total number of cells in each culture. The total number of cells is significantly lower in DHT-treated KD cultures than in DHT-treated WT cultures ($p < 0.01$). This difference becomes greater after 24 hours exposure of cultures to Resveratrol ($p < 0.01$).

(Error Bars = standard error of mean)

Figure 5.6

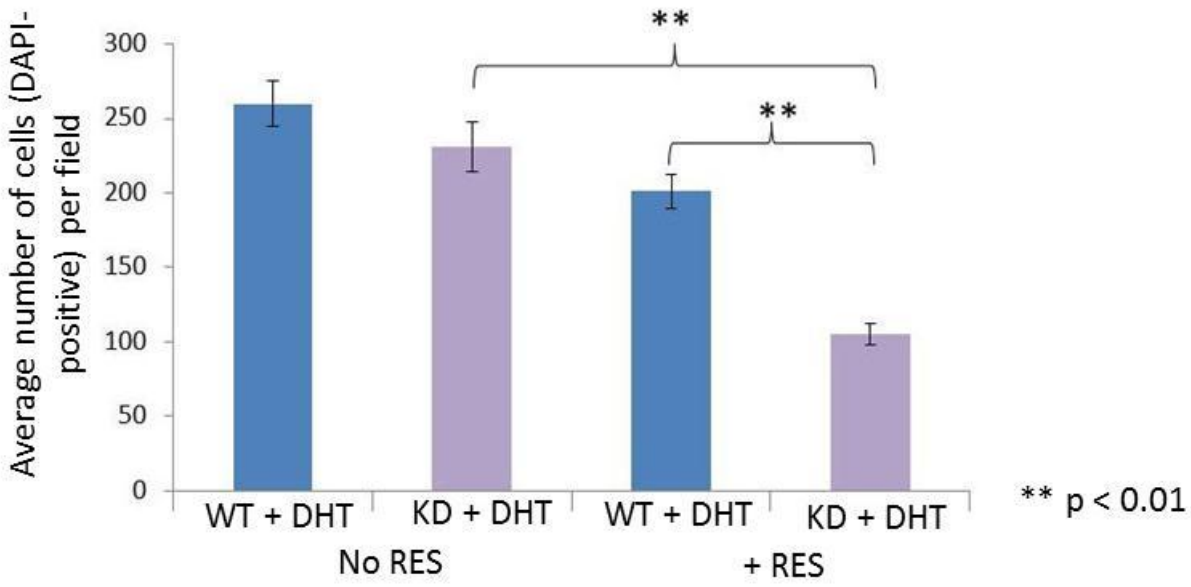
Average number of cells (DAPI-positive) per field
300
250
200
150
100
50
0
**
**
WT + DHT
KD + DHT
WT + DHT
KD + DHT
No RES
+ RES
** p < 0.01

Figure 5.7 The effect of Resveratrol on mitochondrial membrane potential in WT and KD ventral horn motoneurons

Primary WT and KD motoneuron cultures were examined at 7 DIV. All cultures were treated with 5 μM DHT (final concentration 50 nM) at 4 DIV and some were treated at 6 DIV with 50 μM Resveratrol. Cultures were incubated at 37 ^{o}C with TMRM, diluted in a 1 μM Ca^{2+} recording medium, prior to imaging. After 30 minutes of incubation cultures were washed with, and subsequently imaged in, fresh TMRM-containing recording medium. Cultures were kept at 37^{o}C throughout the protocol. The Bar chart summarizes TMRM fluorescence in DHT- treated WT and KD motoneuron cultures in the absence and presence of Resveratrol, as well as FCCP-treated WT cultures, which are a positive control for mitochondrial depolarization. Values are expressed relative to the average TMRM fluorescence in WT motoneurons (100.00). Treatment with Resveratrol decreases TMRM fluorescence in WT and KD motoneurons although the decease is not significant in either genotype.

Error bars = standard error of mean

Figure 5.7

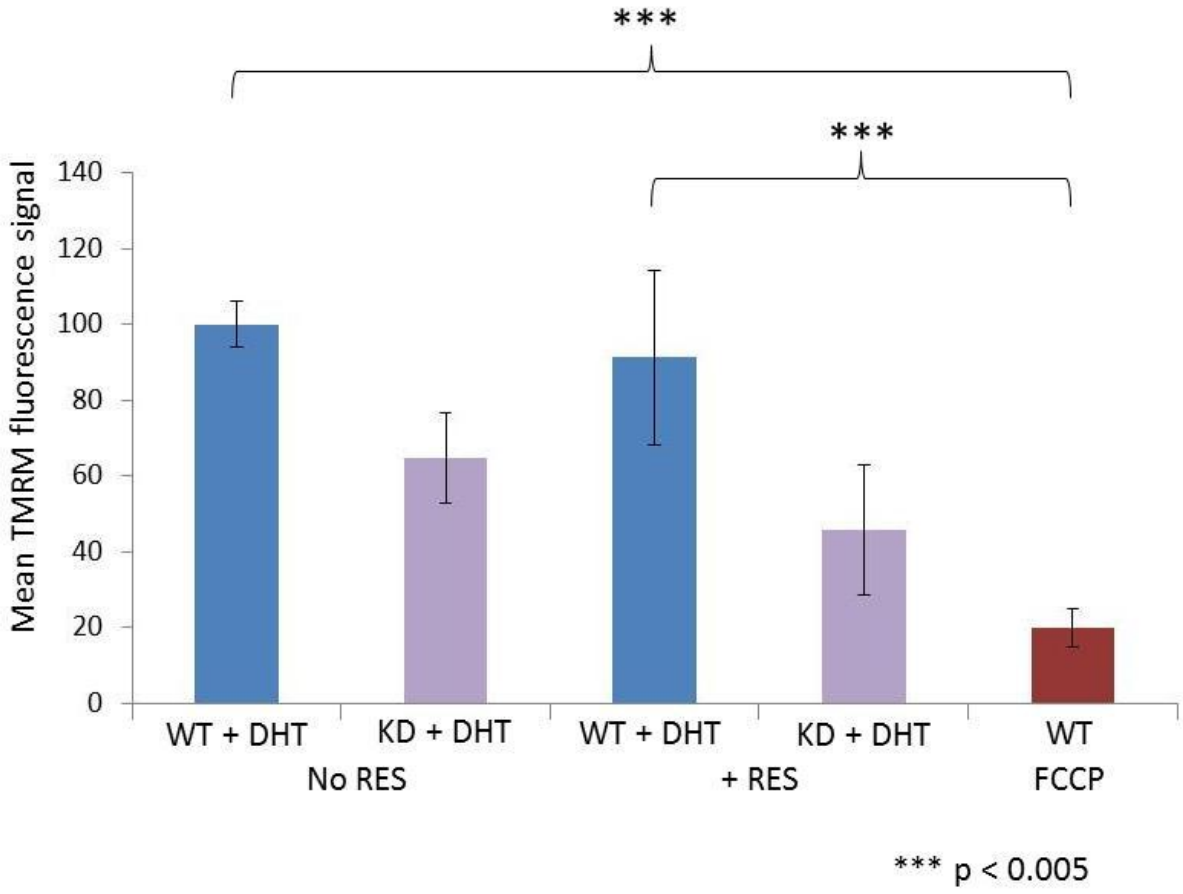
***
***
Mean TMRM fluorescence signal
140
120
100
80
60
40
20
0
WT + DHT
KD + DHT
WT + DHT
KD + DHT
WT
No RES
+ RES
FCCP
*** p < 0.005

In KD cultures however, the average TMRM fluorescence value decreases to 634 after Resveratrol exposure, which is 70% (+/- 17% SEM, n =23) of the average value for untreated KD motoneurons. The decrease in TMRM fluorescence in Resveratrol-treated KD cultures compared to KD cultures that are *not* exposed to Resveratrol is significant (p=0.05).

5.2.8 Resveratrol causes nuclear condensation and fragmentation in KD motoneurons

Treatment with Resveratrol results in nuclear condensation and fragmentation in primary KD motoneurons. When WT cultures are treated with Resveratrol, there is no noticeable change in nuclear morphology, size or DAPI staining density (Figure 5.8A). However, in KD cultures, motoneuron nuclei have a more fragmented appearance following Resveratrol treatment and DAPI staining is more intense (Figure 5.8B).

5.2.9 The effects of Bezafibrate – an alternative inducer of mitochondrial biogenesis on KD motoneurons

In view of the complicated effects of Resveratrol on KD motoneuron survival and viability, an alternative pharmacological inducer of mitochondrial biogenesis was examined next by treatment of WT and KD motoneuron cultures with Bezafibrate.

The expression of PGC1α and motoneuron survival were examined in WT and KD cultures in the absence and presence of 50 μM Bezafibrate using immunohistochemistry. Western blot analysis was not undertaken as a suitable antibody was not available.

When WT and KD primary motoneuron cultures are immunostained for PGC1α at 7 DIV, PGC1α immunoreactivity (red) increases in KD motoneurons following 24 hour Bezafibrate treatment (Figure 5.9A). In WT motoneurons Bezafibrate treatment does not result in a noticeable change in PGC1α immunoreactivity.

Figure 5.8 The effect of Resveratrol on nuclear morphology in KD and WT ventral horn motoneurons

DHT-treated WT and KD motoneuron cultures were immunostained at 7 DIV for PGC1α (red) and co-stained for β-III tubulin (green – a neuronal marker) and DAPI (blue, a nuclear marker). In some cases cultures were treated at 6 DIV with Resveratrol. The images Ai) and ii), show typical examples of WT and KD motoneurons, respectively. Image B) shows nuclear morphology in KD motoneurons in more detail.

(Scale bars = 45 μm)

Figure 5.8

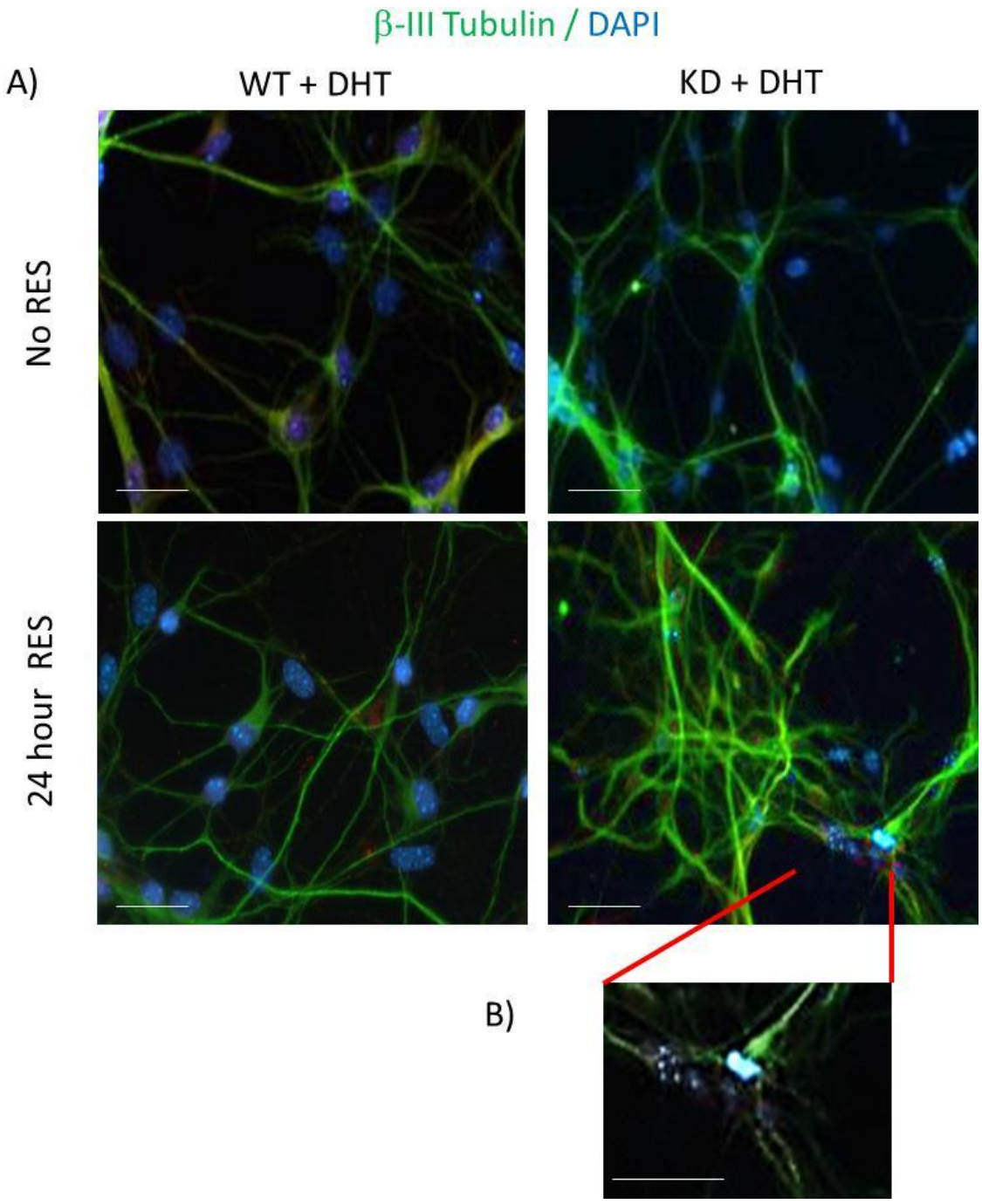

5.2.9.2 Motoneuron counts

The effects of treatment with Bezafibrate on motoneuron survival were examined. Motoneuron survival was determined by counting the number of β-III tubulin positive cells, with more than two processes, as a percentage of total cell number (DAPI-positive). The results show that 24 hour Bezafibrate treatment increases motoneuron survival in KD cultures (Figure 5.9B). Following Bezafibrate treatment, the percentage of motoneurons in WT cultures is 40.6 % (+/- 2.3% SEM, n =40),. In KD cultures however, the percentage of motoneurons in culture increases by approximately 16% following Bezafibrate treatment to 34.62% (+/- 4.6% SEM, n = 40). This increase is significant (p=0.04). Following Bezafibrate treatment there is no longer a significant difference in motoneuron survival between WT and KD cultures.

5.2.10 Results summary

The results in this Chapter strongly suggest that mitochondrial dysfunction is present in motoneurons from the AR100 mouse model of Kennedy's Disease from an early stage of development. Functional impairment of mitochondria is indicated by mitochondrial membrane depolarization, whilst a decrease in mitochondrial biogenesis is inferred by a decrease in PGC1α expression in primary KD motoneurons. When primary motoneuron cultures are treated with Resveratrol, which increases PGC1α expression and hence mitochondrial biogenesis, motoneuron survival is increased in KD cultures although the total cell number decreases and the mitochondrial membrane is depolarized. When cultures are treated with an alternative inducer of mitochondrial biogenesis, Bezafibrate, KD motoneuron survival significantly improves, however not to the extent observed following treatment with Resveratrol.

Figure 5.9 The effect of Bezafibrate on PGC1α expression and motoneuron survival in WT and KD ventral horn cultures

DHT-treated WT and KD motoneuron cultures were immunostained at 7 DIV for PGC1α (red) and co-stained for β-III tubulin (green – a neuronal marker) and DAPI (blue, a nuclear marker). In some cases cultures were treated at 6 DIV with Bezafibrate (50 μM) for 24 hours. Images showing the typical patterns of PGC1α immunoreactivity in the absence and presence of Bezafibrate exposure in WT and KD motoneuron cultures are shown in Ai) and ii), respectively. The bar chart (B) shows the percentage of motoneurons in DHT-treated WT and KD ventral horn cultures in the absence and presence of Bezafibrate. The percentage of motoneurons is significantly lower in KD cultures compared to WT cultures in the absence of Bezafibrate ($p < 0.01$), however in cultures treated with Bezafibrate there is a significant increase in KD motoneuron survival, so that there is no significant difference in motoneuron survival between KD and WT cultures.

(Error Bars = standard error of mean, scale bars = 50 μm)

Figure 5.9

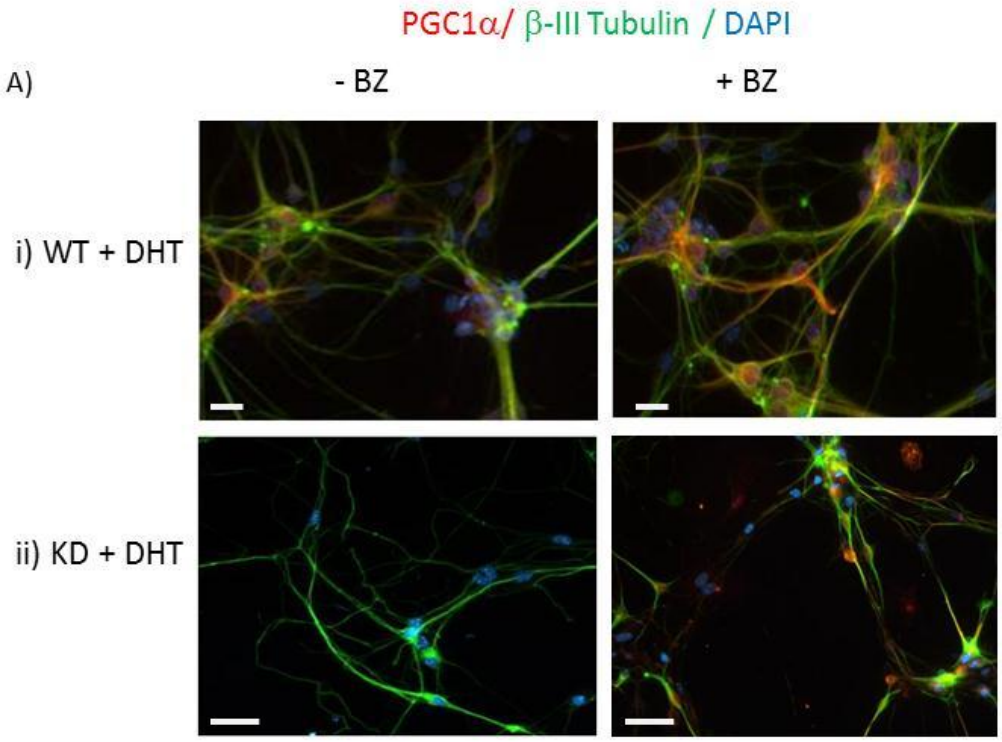
PGC1α/ β-III Tubulin / DAPI
A)
- BZ
+ BZ
i) WT + DHT
ii) KD + DHT

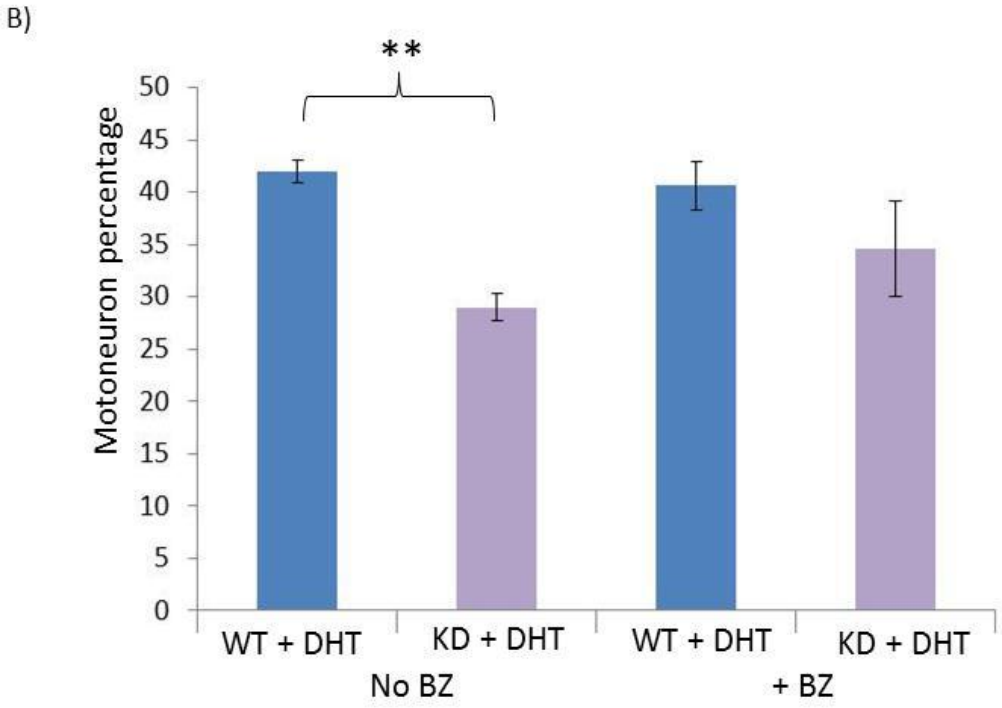
B)
**
Motoneuron percentage
50
45
40
35
30
25
20
15
10
5
0
WT + DHT
KD + DHT
WT + DHT
KD + DHT
No BZ
+ BZ

5.3. Discussion

5.3.1 Mitochondria in KD primary motoneurons are depolarized relative to WT controls

When DHT-treated WT and KD primary embryonic motoneurons were imaged using TMRM at 7 DIV, the results revealed that the level of mitochondrial fluorescence in KD motoneurons was significantly lower than in WT motoneurons. This indicates that, relative to WT motoneurons, the mitochondria in KD motoneurons are depolarized. In order to ensure that the protocol and conditions used in this study reliably measure mitochondrial membrane potential, 1 μM FCCP, which fully depolarizes mitochondria, was applied to motoneurons as a control. Following application of FCCP, mitochondrial fluorescence decreased significantly, indicating that fluorescence decreases as the mitochondrial membrane becomes depolarized. The finding that mitochondria in KD motoneurons were depolarized compliments present findings of mitochondrial dysfunction in both Motor Neuron Diseases, such as ALS, and CAG-repeat disorders, such as Huntington's disease (Mattiazzi et al, 2002, Guidetti et al, 2001). Furthermore, previous studies that have investigated mitochondrial function in KD have shown that mitochondria become depolarized in MN-1 cell lines expressing a mutant Androgen Receptor (AR) gene (Ranganathan et al, 2009).

Mitochondrial depolarization in KD motoneurons is indicative of mitochondrial dysfunction and increased permeability of the mitochondrial membrane and thus is associated with an increased risk of apoptosis (for review see Green & Reed 1998). There are several possible causes of mitochondrial depolarization. The most interesting cause in the context of this Thesis is ER stress. It has been suggested that ER stress results in the accumulation of intracellular Ca^{2+}, which is then buffered by the mitochondria, resulting in increased Ca^{2+} levels in the mitochondrial matrix (Deniaud et al, 2007). Increased levels of Ca^{2+} in the mitochondrial matrix can subsequently lead to increased permeability of the mitochondrial outer membrane, which can lead to

depolarization and the release of pro-apoptotic proteins such as Cytochrome C (Utt 2002). Thus it is possible that ER stress, which occurs in KD motoneurons as shown in Chapter 3, occurs upstream of the mitochondrial depolarization shown in this Chapter.

5.3.2 PGC1α expression is lower in KD motoneurons, indicative of decreased mitochondrial biogenesis

The level of expression of peroxisome proliferator-activated receptor γ co-activator 1 α (PGC1α) has been shown to be a useful indicator of levels of mitochondrial biogenesis (Knutti and Kralli 2001). In order to determine PGC1α expression levels in KD motoneurons, primary DHT-treated WT and KD motoneuron cultures were immunostained with an antibody against PGC1α at 7 DIV. The results show that the level of PGC1α immunoreactivity in primary KD motoneurons was lower than in WT motoneurons. In addition, in order to confirm the decreased expression quantitatively, the level of PGC1α was measured in purified DHT-treated WT and KD motoneurons at 7 DIV using Western blot analysis. Optical density analysis of the blot reveals that, relative to the control protein Actin, PGC1α expression was significantly lower in DHT-treated KD motoneurons than in DHT-treated WT motoneurons. This reduced PGC1α expression in KD motoneurons strongly suggests that mitochondrial biogenesis is impaired in KD motoneurons. Indeed, it has already been shown that in cell lines expressing the mutant AR protein, mitochondrial biogenesis is impaired as indicated by reduced PGC1α expression (Ranganathan et al, 2009).

5.3.3 Resveratrol increases PGC1α expression and improves KD motoneuron survival but has variable effects on total cell survival

In order to assess the consequence of impaired mitochondrial biogenesis in KD pathogenesis the effects of pharmacological induction of mitochondrial biogenesis were examined. One such pharmacological inducer, which has been considered previously as a possible tool for increasing mitochondrial biogenesis in Huntington's Disease, is

Resveratrol (Ho et al, 2010). Primary DHT-treated WT and KD motoneuron cultures were therefore treated for 24 hours with 50 μM Resveratrol and both PGC1α expression and motoneuron survival were determined. The results showed that Resveratrol treatment significantly increased the level of expression of PGC1α in KD motoneurons so that there was no longer a difference in PGC1α expression between WT and KD motoneurons. This suggests that increasing the expression of PGC1α by treatment with Resveratrol is sufficient to overcome the reduction of mitochondrial biogenesis induced by expression of the mutant AR in KD motoneurons.

Analysis of motoneuron survival in WT and KD cultures exposed to Resveratrol showed that there was a significant increase in the percentage of motoneurons in culture so that the level of motoneuron survival in KD cultures was the same as that observed in WT cultures. This dramatic improvement in survival is inconsistent with the modest increase in PGC1α expression observed in KD motoneurons. In order to address this issue, the total number of cells present in each culture was determined. The results show that Resveratrol treatment significantly decreased total cell survival in KD cultures. This result, in combination with the fact that motoneuron percentage increases, suggests that the decrease in total cell number in KD cultures is a result of a greater level of non-motoneuron cell death than motoneuron death. This suggests that Resveratrol could also have toxic effects over cells. Indeed, it has been shown previously that treatment of prostate cancer cells with Resveratrol resulted in cell death (Morris et al, 2002).

5.3.4 Effects of resveratrol on mitochondrial membrane potential

Although Resveratrol treatment appears to increase the survival of KD motoneurons, despite only modestly increasing PGC1α expression, it is important to determine the viability of the surviving motoneurons. In order to do this, mitochondrial membrane potential was assessed in DHT-treated WT and KD motoneurons that were exposed to Resveratrol for 24 hours. It appears that Resveratrol treatment decreases

mitochondrial membrane potential in DHT-treated WT and KD motoneurons, although the magnitude of the decrease in both genotypes is not significant. Since Resveratrol treatment does not improve the deficits in mitochondrial membrane potential in KD motoneurons, it is possible that the quantity of mitochondria as opposed to their function is a more potent determinant of motoneuron survival, since Resveratrol treatment did increase KD motoneuron survival.

5.3.5 Resveratrol treatment results in nuclear condensation and fragmentation in KD primary motoneurons

In keeping with the finding that Resveratrol treatment increases KD motoneuron survival without improving the deficits in mitochondrial function, the nuclei of surviving KD motoneurons were condensed and fragmented following Resveratrol treatment, which is indicative of apoptosis (Skalka et al, 1976). This effect is not observed in WT cultures. Resveratrol has been shown previously to depolarize the mitochondrial membrane in prostate cancer cells (Aziz et al, 2006). As is the case with KD, prostate cancer involves changes in AR function (Culig et al, 2001). This could suggest that AR function influences the effects of Resveratrol. Indeed, an interaction between Resveratrol and the Androgen Receptor has been suggested previously. For example, Resveratrol treatment was found to suppress AR transcriptional activity in HeLa cells (Shi et al, 2009).

5.3.6 Bezafibrate increases PGC1α expression and improves KD motoneuron survival

The effects of Resveratrol on primary KD motoneuron survival and mitochondrial function were complicated and the role of mitochondrial dysfunction in KD pathogenesis is difficult to determine on the basis of these results. Therefore the effects of an alternative inducer of mitochondrial biogenesis, Bezafibrate, on primary KD motoneurons were investigated. When DHT-treated WT and KD motoneurons were treated for 24 hours with Bezafibrate, both PGC1α expression and motoneuron survival

increased in KD cultures, with no observable effect in DHT- treated WT cultures. As was the case with Resveratrol treatment, Bezafibrate significantly increased the level of PGC1α expression in primary KD motoneurons, but had only a modest effect on motoneuron survival. This result, in combination with the fact that improving mitochondrial biogenesis does not appear to improve mitochondrial function in KD motoneurons, suggests that mitochondrial biogenesis does not play as significant a role as ER stress does in KD pathogenesis (Chapter 4), although comparisons between ER and mitochondrial deficits need to be approached with caution. This will be discussed further in Chapter 6.

CHAPTER 6: DISCUSSION

ER stress has been previously shown to play a major role in the pathogenesis of both Motor Neuron Diseases (MNDs), such as Amyotrophic Lateral Sclerosis (ALS), and Poly-Q repeat disorders, such as Huntington's Disease (HD) (Saxena et al, 2009, Reijonen et al, 2008). In the case of ALS, markers of ER stress including BiP and CHOP, have been found to be elevated in motoneurons in $SOD1^{G93A}$ mice that model the disease (Saxena et al, 2009) as well as in patient spinal cord autopsy tissue (Atkin 2008). Furthermore, inhibition of ER stress with Salubrinal, significantly improves $SOD1^{G93A}$ motoneuron survival in SOD1 mice and in vitro (Saxena et al, 2008). Likewise, BiP and CHOP have also been found to be elevated in cell lines transfected with a mutant Huntingtin protein compared to cell lines that had been transfected with a control protein (Reijonen 2009). Salubrinal treatment was also found to improve the survival of these cells, suggesting that ER stress, at least in part, accounts for the observed cell death.

Despite the strong evidence to suggest that ER stress is likely to play a major, causal role in the pathogenesis of both MNDs and Poly-Q disorders, the role of ER stress in the pathogenesis of Kennedy's Disease (KD), has yet to be established.

In the experiments described in this Thesis, I have shown that both ER Ca^{2+} depletion and ER stress are present in embryonic, primary motoneurons from the AR100 mouse model of KD. I have also monitored the presence of ER stress in KD spinal cord tissue at various stages of disease progression. The results here have shown the presence of ER stress in KD motoneurons even during early embryonic development. These findings suggest that ER stress may play a causal role, as opposed to a secondary effect, in KD pathogenesis. Indeed, the relative magnitude of ER stress was at its greatest in pre-symptomatic KD mice at early stages of disease, indicating that ER stress is more likely to have an early role in disease pathology and is less likely to be a secondary effect of alternative pathological mechanisms.

When cellular Ca^{2+} handling in Wild-Type (WT) and KD primary motoneurons was investigated, it was found that the highest level of cytosolic Ca^{2+} was present in DHT-treated KD primary motoneurons, whilst the lowest level of basal cytosolic Ca^{2+} was present in DHT-treated WT motoneurons. This suggests that KD motoneurons are potentially more vulnerable to excitotoxic insults than WT motoneurons, which has been found to be the case in other Motor Neuron Disorders. In the case of ALS, for example, an elevation in cytosolic Ca^{2+} has been shown to render motoneurons more vulnerable to stimuli that increase intracellular Ca^{2+} (Appel et al, 2001). This increased vulnerability arises from the fact that elevated cytosolic Ca^{2+} is associated with the activation of apoptotic pathways (Demaurex et al, 2003, Dykens 1994, Lang et al, 2002). Indeed, increases in cytosolic Ca^{2+} have been found to result in self-propagating cycles that increase cytosolic Ca^{2+} levels further and thus trigger apoptosis. For instance, elevated cytosolic Ca^{2+} in neurons appears to be accompanied by an increased production of free radicals (Dykens 1994), which results in the activation of several pathways that converge and result in further elevation of cytosolic Ca^{2+} . For example, free radical production alters glial cell-mediated removal of glutamate and in doing so, activates glutamatergic receptors, which act as Ca^{2+} channels and consequentially increase cytosolic Ca^{2+}. In addition, the production of free radicals also results in increased lipid peroxidation (Kakkar et al, 1992), increasing cytosolic Ca^{2+} as a by-product. Cytosolic Ca^{2+} triggers apoptosis when sequestered by mitochondria, which is discussed in detail below (Vindis 2005). Thus any underlying pathology which elevates cytosolic Ca^{2+} renders cells vulnerable to stimuli that increase Ca^{2+} further. The fact that the embryonic KD motoneurons examined in this study had a higher level of cytosolic Ca^{2+} than their WT counterparts, could suggest that embryonic KD motoneurons are more vulnerable to increases in Ca^{2+}.

The level of ER Ca^{2+} in untreated and DHT-treated WT and KD primary motoneurons was inferred by measuring the Thapsigargin-induced increase in cytosolic Ca^{2+} that occurred when motoneurons were imaged in a Ca^{2+}-free recording medium. The

results showed that the lowest level of inferred ER Ca^{2+} was present in DHT-treated KD motoneurons, whilst the highest level of ER Ca^{2+} was present in DHT-treated WT motoneurons. These findings suggest that ER stress is more likely to occur in KD motoneurons than WT controls since ER function is dependent on ER Ca^{2+} (Paschen & Doutheil 1999). Furthermore, DHT treatment had different effects on WT and KD primary motoneurons. Whilst exposure to DHT slightly increased ER Ca^{2+} in WT motoneurons, it significantly reduced ER Ca^{2+} in KD motoneurons. Thus DHT treatment appeared to be detrimental to KD motoneurons in as much as it appears to deplete the ER of Ca^{2+}. Reduced ER Ca^{2+} can be detrimental to cell survival since ER function is Ca^{2+}-dependent and the release of Ca^{2+} from the ER is one of the triggers of apoptosis (Demaurex 2003). Indeed, it has been shown that the release of Ca^{2+} from the ER activates pro-apoptotic proteins, such as Bcl-2-associated X protein (BAX) and Bcl-2 homologous antagonist killer (BAK), that initiate mitochondrial dysfunction, which in turn triggers apoptosis (Scorrano et al, 2003). The pattern of the effect of DHT treatment on ER Ca^{2+} observed in this study reflects the pattern of KD symptom manifestation observed in patients i.e. symptoms only occur in males who possess high levels of the AR ligand testosterone (Katsuno et al, 2006). These findings, together with the fact that ER Ca^{2+} depletion occurs in KD motoneurons at such an early time point, suggest that ER dysfunction may be a trigger of KD, or at the very least, is one of the very earliest manifestations of KD pathology.

Store-operated Ca^{2+} (SOC) influx occurs following ER Ca^{2+} depletion as an attempt to restore ER Ca^{2+} homeostasis. This process was therefore examined in untreated and DHT-treated WT and KD motoneurons. I found that the highest level of SOC influx was detected in DHT-treated KD motoneurons, whilst the lowest level was observed in DHT-treated WT motoneurons. This is consistent with the trends observed for ER Ca^{2+} since a lower level of ER Ca^{2+} is accompanied by a higher level of SOC influx in order to compensate for the deficit in ER Ca^{2+} (Smani et al, 2004). Furthermore, I observed that DHT treatment had opposing effects on SOC influx in WT and KD primary

motoneurons. In WT motoneurons, DHT treatment decreased SOC influx whilst DHT treatment increased SOC influx in KD motoneurons, again suggesting that DHT is detrimental to KD motoneurons. An increase in SOC influx can be considered to represent a detrimental change to cells for two reasons. The first is that increases in SOC influx are associated with ER Ca^{2+} depletion (Zhang 2004) and, as discussed above, the release of Ca^{2+} from the ER is one of many triggers of apoptosis (Scorrano et al, 2003). Secondly, increases in SOC influx result in an increase in cytosolic Ca^{2+} in an attempt to facilitate re-filling of ER Ca^{2+} (Smani 2004). However, if a pre-existing, underlying pathology is present, which depletes the ER of Ca^{2+} then it is possible that as a result an increased SOC influx, cytosolic Ca^{2+} remains elevated in diseased motoneurons. As discussed above, elevated cytosolic Ca^{2+} is detrimental to the survival of cells.

The kinetics of the responses in cytosolic Ca^{2+} to both Thapsigargin application and Ca^{2+} introduction into the medium was also examined in order to reveal more about the disruption in cellular Ca^{2+} handling observed in primary KD motoneurons. I found that in the case of the Thapsigargin-induced increase in cytosolic Ca^{2+}, the peak of the increase in cytosolic Ca^{2+} in WT and KD motoneurons was reached within a similar time frame. However, the response to Thapsigargin was of a more transient nature in KD motoneurons than in WT controls. This could suggest that the mechanism by which calcium is expelled from the cytosol, for example, the plasma membrane calcium pump (PMCA) is more active in KD primary motoneurons than in WT controls. The nature of the response to Ca^{2+} introduction however, suggests that increased PMCA activity is unlikely. In KD motoneurons the cytosolic Ca^{2+} response to Ca^{2+} introduction was more prolonged than in WT controls. It is therefore more likely that the transient nature of the cytosolic Ca^{2+} increase in KD motoneurons in response to Thapsigargin was due to the fact that there is a lower starting level of Ca^{2+} in the ER, so that it is depleted of Ca^{2+} more rapidly and the response duration is therefore shorter.

Experiments were also undertaken in primary motoneurons from mice of each sex, since KD manifests exclusively in males, and female carriers of the mutation remain asymptomatic (Katsuno et al, 2006). It was therefore important to determine whether or not the differences observed in ER Ca^{2+} handling were due to differences in ligand availability (i.e. DHT) or inherent differences between male and female AR proteins. Under the same treatment conditions, there appeared to be very little difference in basal Ca^{2+}, ER Ca^{2+} or SOC influx between male and female primary KD motoneurons. This finding suggests that the differences in Ca^{2+} handling that were observed between WT and KD motoneurons were not determined by sex differences. These results strongly suggest that the manifestation of KD is not dependent on inherent differences in the AR protein between the sexes, but the availability of the AR ligand and thus AR activation.

It was also important to establish whether or not alterations in ER Ca^{2+} were directly linked to mutant AR activation in the KD mice. The expression of the Sarco/Endoplasmic Reticulum ATPase (SERCA) pump is controlled downstream of AR activation and is the route by which Ca^{2+} enters the ER lumen (Foradori et al, 2008). It could therefore provide a link between mutations in the AR receptor and changes in ER Ca^{2+}. I found that the level of expression of the SERCA2b pump was significantly lower in primary KD motoneurons than in WT controls. A lower level of expression of the SERCA pump could mean that there is reduced sequestration of Ca^{2+} from the cytosol into the ER lumen, giving rise to increased cytosolic Ca^{2+} level and lower ER Ca^{2+}. However this was not enough to attribute ER Ca^{2+} depletion to reduced SERCA2b expression in DHT-treated KD primary motoneurons because the activity of the SERCA2b pump had not been determined and the expression and activity of proteins involved in Ca^{2+} release from the ER, such as the Inositol trisphosphate (IP_3) and Ryanodine receptor had not been examined. Future experiments should therefore aim to investigate the expression and activity levels of such proteins.

These experiments establish the presence of ER Ca^{2+} depletion in KD motoneurons, suggesting that ER stress is an early feature of KD pathogenesis. To assess whether or not ER stress was occurring in DHT-treated KD motoneurons as a result of ER Ca^{2+} depletion, I examined various markers of the Unfolded Protein Response (UPR). Western blot analysis and immunohistochemistry revealed that all of the ER stress markers examined, including Binding immunoglobulin protein (BiP), Activating Transcription Factor (ATF4) and C/EBP Homologous Protein (CHOP), were all significantly elevated in DHT-treated KD motoneurons compared to DHT-treated WT controls. These findings therefore suggest that the extent of ER stress was greater in KD embryonic primary motoneurons in culture than in WT controls. WT motoneurons did not appear to be completely free of ER stress however, possibly due to the effects of the culturing process. Indeed, all ER stress markers were also present at detectable levels in DHT-treated WT motoneurons. Importantly however, the expression of ER stress markers in KD motoneurons was *significantly* higher than in WT motoneurons. KD motoneurons can therefore be considered to have either a higher level of basal ER stress, or may be more vulnerable to ER stress-induced by the culturing process.

The fact that ER stress appeared to be elevated in primary KD motoneurons at such an early stage of development, suggested that ER stress was more likely to play a causal role in KD pathogenesis as opposed to being a secondary effect of another pathogenic mechanism. KD is a multifactorial, progressive disease (Katsuno et al, 2006) and so as the disease progresses, it becomes difficult to identify and differentiate between pathological triggers and secondary effects. The fact that ER stress was found to occur in KD motoneurons prior to birth makes it a strong candidate as an early disease trigger.

Although ER stress was present in KD motoneurons during embryonic development, whether it remained a feature of disease at later stages of disease progression was also examined. The time points investigated included postnatal day 5 (P5), 3, 12, and 18 months of age. P5 was selected on the basis that it is the earliest time point at

which ER stress was found to occur in the $SOD1^{G93A}$ mouse model of ALS (Saxena et al, 2009). Three months of age represents a pre-symptomatic stage of disease in AR100 mice, whilst 12 months and 18 months of age are the median time points of symptom onset and disease end-stage, respectively (Sopher et al, 2004).

Examination of markers of ER stress in spinal cord tissue revealed that the expression of each ER stress marker measured i.e. BiP, ATF4 and CHOP, was higher in KD spinal cord tissue than in WT control tissue at all disease stages, although significant differences were predominantly observed at pre-symptomatic disease stages. This suggests that the predominant role of ER stress in KD pathogenesis is as an early pathological event, although its presence appears to persist throughout the disease. The fact that the difference in expression of ER stress markers between WT and KD spinal cord tissue decreased with disease progression could be due to the fact that the survival of KD motoneurons was lower than the survival of WT motoneurons. Western blot analysis did not give an indication of the level of expression in individual motoneurons, but the tissue sample as a whole. Therefore, if there are fewer KD motoneurons expressing a high level of ER stress marker, the total level of expression could be the same as the level of expression from a larger number of WT motoneurons expressing a lower level of ER stress marker. Alternatively, the level of ER stress markers may increase in WT spinal cord tissue as a natural effect of aging, which has previously been suggested to occur (Naidoo et al, 2009). Indeed, at such a late stage in mice, it could be the case that aging-induced ER stress conceals underlying pathological effects in KD mice.

Although all of the ER stress markers examined in this study were elevated in KD spinal cords compared to WT controls, subtle differences in the expression pattern of the markers revealed more about the role of ER stress in KD pathogenesis. For example, whilst there was no difference in the expression of BiP between WT and KD spinal cord tissue and 12 months and 18 months of age, the difference in the expression levels of CHOP between WT and KD spinal cord tissue still appeared to be

significant at 12 months of age and substantial (although not significant) at 18 months of age. These findings therefore suggest that pro-apoptotic, or downstream markers of the UPR remain elevated later into disease progression. Whether or not this means that there is a skew in transcription towards pro-apoptotic factors at later disease stages however, requires further investigation of the expression of other UPR mediators.

Establishing the presence of ER stress however, does not confirm its role in motoneuron degeneration. I therefore attempted to clarify this role by examining the relationship between ER stress and motoneuron survival in KD motoneurons. Firstly, whether embryonic motoneuron survival was lower in basal culture conditions in KD cultures than that of WT controls was examined. Motoneuron counts indicated that the survival of KD motoneurons was significantly lower than that of WT motoneurons. This suggests that KD motoneuron survival was indeed reduced in the model of KD used in this lab.

These experiments establish that embryonic KD motoneuron survival was significantly reduced and that markers of ER stress are significantly elevated in embryonic KD motoneurons. In order to determine whether or not ER stress results in motoneuron degeneration in the AR100 mouse model of KD, the expression level of Caspase 12, a marker of ER stress-induced apoptosis (Nakagawa et al, 2000), was examined. In addition, the effects of inhibiting ER stress on Caspase 12 expression, ER Ca^{2+} and motoneuron survival was determined. The results showed that the level of expression of Caspase 12 was significantly higher in embryonic, purified KD motoneurons than in WT controls. This suggests that there was a greater amount of ER stress-induced apoptosis occurring in KD motoneurons and indicates that KD motoneurons are not able to overcome ER stress. This could be due to the fact that the UPR is disturbed, or that the cause of ER stress, i.e. the presence of the mutated CAG-repeat expansion in the AR gene, is fervent, or a combination of the two.

Examination of spinal cord tissue revealed that the expression of active Caspase 12 remains elevated in KD spinal cord relative to WT control tissue at all stages of disease progression. The peak increase in Caspase 12 expression was observed in pre-symptomatic spinal cord tissue, which then declined with disease progression. Interestingly, even at disease end-stage, there was a significantly higher level of expression of Caspase 12 in KD spinal cord tissue relative to WT control tissue. This could suggest that as the disease progresses transcription is skewed towards pro-apoptotic factors, possibly as a result of the combined effects of KD pathogenesis and aging.

These findings do not however *confirm* that ER stress-induced apoptosis results in KD motoneuron degeneration. The occurrence of ER stress-induced apoptosis can only be correlated with decreased motoneuron survival at this point. Therefore the possibility that ER stress-induced apoptosis plays a key role in KD motoneuron degeneration was investigated by studying the effects of ER stress inhibitors on motoneuron survival.

In order to inhibit ER stress, motoneuron cultures were treated with Salubrinal, which prevents dephosphorylation of eIF2α (Boyce et al, 2005). I found that Salubrinal improved the survival of both WT and KD motoneurons, with the percentage of motoneurons in culture increasing significantly. Following Salubrinal exposure, there was no longer a significant difference in the survival of motoneurons in WT and KD cultures. These findings not only suggest that ER stress-induced apoptosis plays a key role in KD motoneuron death, but that the inhibition of this pathway is sufficient to rescue motoneurons; ER stress therefore plays a major role in KD motoneuron degeneration. In keeping with the improvement in KD motoneuron survival, the level of expression of Caspase 12 in KD motoneurons was also significantly reduced by Salubrinal, confirming that inhibition of ER stress rescues motoneurons, possibly through the prevention of ER stress-induced apoptosis.

At this point it is important to acknowledge that the relationship between ER Ca^{2+} depletion and ER stress can be a two-way interaction. Thus, as well as ER Ca^{2+} depletion resulting in ER stress, ER stress can result in ER Ca^{2+} depletion. Inhibition of ER stress was also found to result in an increase in inferred ER Ca^{2+} in WT and KD motoneurons. Given that Salubrinal treatment also decreased Caspase 12 expression, it appears that there is a cycle between ER Ca^{2+}, ER stress and ER stress-induced apoptosis. Whilst ER Ca^{2+} depletion can result in ER stress and therefore ER stress-induced apoptosis, ER stress can also result in ER Ca^{2+} depletion which can in turn result in activation of Caspase 12 and hence ER stress-induced apoptosis. This toxic, propagative cycle appears to be broken by treatment with Salubrinal.

Another possibility examined in this Thesis was whether or not KD motoneurons are inherently more vulnerable to triggers of ER stress. This possibility was examined by treating WT and KD cultures with two pharmacological agents that induce ER stress via different mechanisms. The first agent was Thapsigargin, and the second agent was Tunicamycin, which interferes with post-translational modification of proteins, specifically N-glycosylation (Brandish et al, 1996). Interestingly, DHT-treated KD motoneuron survival was significantly reduced following exposure to Thapsigargin but not following exposure to Tunicamycin at any concentration. This finding suggests that KD motoneurons are more vulnerable to ER Ca^{2+} depletion than to other triggers of ER stress, such as alterations in protein structure. However, whether or not ER Ca^{2+} depletion is the major cause of ER stress in KD cannot be determined without investigating the role of other causes of ER stress such as ATP and glucose depletion (Xu 2005).

Simultaneous treatment of motoneuron cultures with Thapsigargin and Salubrinal revealed that the vulnerability of KD motoneurons to ER Ca^{2+} depletion was prevented by the inhibition of ER stress. Following treatment of DHT- and Thapsigargin-treated KD motoneuron cultures with Salubrinal, the survival of KD motoneurons was similar to the level of survival observed in DHT-treated WT cultures. This result suggests that

treatment of KD motoneurons with Salubrinal is sufficient to eliminate the increased vulnerability of KD motoneurons to Thapsigargin treatment

As well as ER stress, mitochondrial dysfunction has also been found to play a major role in the pathogenesis of ALS (Manfredi et al, 2005, Shi et al, 2010) and Huntington's Disease (Oliveira et al, 2010). In the case of ALS for example, both morphological and biochemical abnormalities have been found in ALS patient forebrain biopsy tissue and the mutant SOD1 mouse model of ALS (Manfredi et al, 2005). Likewise, various aspects of mitochondrial function have been found to be disturbed in several mouse models of HD. For example, in the R6/2 and YAC128 models of HD, the Ca^{2+} loading capacity of mitochondria in forebrain neurons appeared to be reduced under basal conditions, whilst the Ca^{2+} loading capacity of forebrain mitochondria from the Hdh 150 knock-in model of HD appeared to be vulnerable to NMDA receptor activation, thus cytosolic Ca^{2+}elevation (Oliveira et al, 2007). This strongly suggests that mitochondrial deficits play an important role in the pathology of several mouse models of HD. Activity of essential mitochondrial proteins such as Complex IV/Cytochrome C Oxidase and Aconitase, have also been found to be reduced in the R6/2 mouse model of HD, thus the respiratory chain and the Citric Acid cycle also appear to be impaired in HD (Tabrizi et al, 2000).

However, as is the case with ER stress, the role of mitochondrial dysfunction in animal models of KD has not been established and evidence of mitochondrial dysfunction in KD is predominantly restricted to mutant AR-transfected cell lines (Ranganathan et al, 2009). In another set of experiments I therefore aimed to determine whether or not mitochondrial dysfunction occurred in primary DHT-treated KD motoneurons and whether or not mitochondrial dysfunction played a more dominant role than ER stress in KD pathogenesis. TMRM fluorescence and PGC1α expression analysis suggested that mitochondrial depolarization and impaired mitochondrial biogenesis were present in embryonic DHT-treated KD primary motoneurons, respectively. The effects of pharmacologically inducing mitochondrial biogenesis on DHT-treated KD primary

motoneuron survival were examined next to determine the importance of impaired biogenesis in KD pathology. Although treatment with the mitochondrial biogenesis inducer, Resveratrol, appeared to improve DHT-treated KD motoneuron survival, the morphology of surviving motoneurons and TMRM fluorescence suggested that there was no improvement in motoneuron viability. For instance, following 24 hour Resveratrol exposure, KD motoneuron nuclei appeared condensed and fragmented and mitochondria remained depolarized. This could suggest that the number of mitochondria is a more dominant determinant of motoneuron survival than mitochondrial dysfunction in KD motoneurons. It could also suggest however that mitochondrial dysfunction does not play a major role in KD pathogenesis. Indeed it has been suggested that such mitochondrial dysfunction occurs downstream of ER Ca^{2+} depletion (Arduino et al, 2004) and thus targeting such depletion and consequential ER stress could form the basis of a more effective therapy than improving mitochondrial biogenesis. It could also be suggested that the most effective therapy for KD would be a therapy that targets *both* ER stress and mitochondrial dysfunction.

The results presented in this Thesis provide evidence for the presence of ER Ca^{2+} depletion and ER stress in embryonic motoneurons from the AR100 mouse model of KD. This early presence of ER stress strongly suggests that ER stress plays an early, key role in KD pathology and is not a secondary effect of the disease process. The beneficial effects of inhibition of ER stress on KD motoneuron survival also suggest that ER stress plays a direct role in the degeneration of motoneurons in KD. Furthermore, following treatment of cultures with Salubrinal, there was no longer a difference in the survival between WT and KD motoneurons. This suggests that the occurrence of ER stress almost completely accounts for the motoneuron degeneration that occurs in embryonic KD motoneurons.

With respect to the initial aims of this Thesis, the above experiments have:

1. Established an early, potentially causative role of ER stress in the pathogenesis of KD.
2. Established an early elevation of markers of ER stress in the spinal cord of KD mice that decreases with disease progression.
3. Confirmed that ER stress is related to the motoneuron degeneration observed in KD.
4. Confirmed that mitochondrial dysfunction is an early pathological feature of KD.

It is therefore possible that therapeutic approaches that aim to target ER stress, for example, treatment with Salubrinal, may be a possible therapeutic approach for the treatment of KD. Such an approach may be particularly effective if used in combination with other agents that target additional pathological mechanisms that are likely to be involved in this progressive neurodegenerative disease.

APPENDIX

Solutions & Reagents

1.1Primary ventral horn motoneuron culture solutions

1.1.1 Complete Neurobasal Medium (per 150 ml)

143.75 ml Neurobasal medium (Gibco)

3 ml B27 supplement (Gibco BRL)

3 ml Heat-activated Horse Serum (Sigma)

1.5 ml Penicillin/Streptomycin (0.6g Penicillin and 1g Streptomycin in 1 litre)

125 μl 0.5mM L-glutamine

75 μl 25uM 2-mercaptoethanol (Sigma)

1.5 μl 10ng/ml CNTF (R&D systems)

0.5 μl 100pg/ml GDNF (R&D systems)

0.5 μl BDNF (R&D systems)

1.1.2 0.25 %Trypsin

Preparation: 2.5 % w/v solution

- 25 mg trypsin powder (Sigma) in 1 ml Phosphate-Buffered Saline (PBS). Stored at -20^{o}C, defrosted and used at 37^{o}C.

1.1.3 Bovine serum albumin (BSA)

4% BSA

Preparation: BSA powder (Sigma) in l L15 medium (Gibco). Stored at -20^{o}C, used at room temperature

1.1.4 Deoxyribonuclease 1 (DNAse 1)

DNAse 1 is an enzyme that catalyzes the hydrolytic cleavage of phosphodiester linkages in the DNA backbone thus degrading unwanted single- and double-stranded DNA (Vitolo et al, 1999).

Preparation: 1 mg of DNase powder (Sigma) in 1 ml Neurobasal medium (Gibco BRL). Aliquoted and stored at -20^{o}C, used at room temperature.

1.1.5 Optiprep

Optiprep is a density gradient medium that has been used previously to purify primary ventral motoneurons (Gingras et al, 2007). The high density of Optiprep facilitates the fractionation of motoneurons by encouraging flotation from an area of relatively high density through either a continuous or discontinuous gradient.

Preparation: 10.4% Optiprep solution in 10 mM Trycine and 4% Glucose w/v (Nycomed) in clear L15 (Gibco) medium

1.1.6 Polyornithine

Polyornithine is used to coat the coverslips with a negative charge prior to culturing thus attracting the positively charged phospholipid membranes of cells growing in culture.

Preparation: 1.5mg/ml in sterile water. Used at 1 in 1000 in sterile water (Baxter)

1.1.7 Laminin (already prepared by Sigma – 1mg/ml)

Coverslips are coated with Laminin prior to culturing. Laminin is an extracellular matrix glycoprotein, which guides and promotes the growth and differentiation of neuronal cells (Luckenbill-Edds1997).

Preparation: Dilute in L15 medium at 1 in 200

1.2 Genotyping Solutions & Reagents

1.2.1 Rapid Digestion Buffer (RDB); for the digestion of embryonic tail biopsies

10 mM Tris-HCl (pH 8.3)

50 mM KCl

0.1 mg/ml Gelatin

0.45% NP40

0.45% Tween-20

1.2.2 10 X Electrophoresis Buffer (10X TBE)

1 L double distilled water

108 g Tris Base

40 mls 0.5M EDTA (pH8.0)

1.3 Confocal microscopy solutions

1.3.1 Confocal recording medium

Table 1 summarizes the recipe for confocal recording medium. The amounts given are in grams per litre of distilled water. In addition to the components below, 50 μl of 1 M $CaCl_2$ is added to 50 ml of recording medium when a 1 mM Ca^{2+} recording medium is required.

Table 1

	Molecular Weight	Grams/Litre	Final conc.
NaCl	58.44	7.305	125 mM
KCl	74.55	0.372	5 mM
Na3PO4.12H2O	380.12	0.380	1 mM
MgSO4.7H2O	246.48	0.246	1 mM
D-Glucose	180.16	1.000	1g/L
Hepes	238.3	4.766	20 mM

1.3.2 Fluo 4-AM – non-ratiometric/single wave calcium indicator

Per 1 ml of 1 mM Ca^{2+} confocal recording medium: 5 μl 1μM Fluo 4-AM (Invitrogen) + 2 μl of 10% Pluronic acid.

1.3.3 Fura 2–ratiometric calcium indicator

Per 1 ml of Ca^{2+} confocal recording medium: 5 μl 1mM Fura 2 (Invitrogen) + 2 μl of 10% Pluronic acid

1.3.4 Thapsigargin

10 μl of 1mM Thapsigargin (in DMSO) per 1 ml of *calcium-free* recording medium (to produce a final concentration of 1 μM in the imaging chamber)

1.3.5 Ionomycin

50 μl of per 1 ml of 1 mM Ca^{2+} recording medium (to produce a final concentration of 5 μM in the imaging chamber

1.3.6 10 mM Ca2+ recording medium

10 ml of 1mM Ca^{2+} per 1 ml of calcium-free recording medium (producing a final concentration of 1 μM in the imaging chamber

1.4 Western blot solutions

1.4.1 Bovine serum albumin (BSA) standard solutions

BSA controls are used to obtain protein standards to which samples of interest are calibrated.

Preparation: 2, 1, 0.5, 0.25 and 0.125 mg of BSA in 1 ml homogenizing buffer to make control solutions of 2, 1, 0.5, 0.25 and 0.125 mg/ml

1.4.2 Culture tissue and P5 spinal cord homogenising buffer

500 ml Tris buffer:

- 0.302g Tris Base (5 mM in 500 mls), and 0.394g Tris HCl (5 mM in 500 mls)

-400 ml distilled water

-Make up to a pH of 6.8 by adding NaOH

2% SDS (10g)

2 mM EDTA (0.372g)

2 mM EGTA (0.468g)

1.4.3 Resolving gel

For the purposes of the proteins being identified, 7.5 % and 10.5 % gels were made, which are suitable for detecting proteins in the range of 25-200 kDa and 15-100 kDa, respectively (according to manufacturer's instructions).

In the case of the 7.5% gel the preparation was as follows:

2.5 ml Protogel resolving buffer (stored at room temperature)

4.935 ml dH_2O (stored at room temperature)

2.5 ml 30 % acrylamide (stored at room temperature)

50 μl 10 % ammonium persulphate (stored at -20^oC)

5 μl TEMED (stored at room temperature)

1.4.4 Stacking gel

4.137 ml Protogel stacking buffer (stored at room temperature)

833 μl 30% acrylamide

25 μl 10% ammonium persulphate

5 μl Tetramethylethylenediamine (TEMED)

The stacking gel sets very quickly following the addition of ammonium persulphate and TEMED, and therefore care was taken to add these reagents to the gel solution just prior to it being poured into the combs (see section 2.7.3).

1.4.5 Running buffer

100 ml Stock running buffer (National diagnostic, stored at room temperature)

- *0.25 M Tris*
- *1.92 M Glycine*
- *1% SDS*

900 ml dH_2O

1.4.6 Transfer buffer

100 ml Stock transfer buffer (National diagnostic, stored at room temperature), per litre dH2O:

-Glycine *29.3 g*

-TRIS base *58.1 g*

-SDS *3.75 g*

200 ml Methanol

700 ml dH_2O

1.4.7 Blocking solution

Approximately 10 ml of blocking solution is required per blot

95% PBS + 0.1% Tween

5% milk

1.5 Immunohistochemistry

1.5.1 Blocking solution

92% PBS + 0.1% Triton X

5% Milk

3% Animal serum (depending on host of secondary antibody)

1.6 Immunostaining and Western Blot Antibodies (Table 2)

The antibodies used in this study for immunohistochemistry (IHC) and western blot analysis (WB) are summarized in Table 2.

Table 2: Antibodies

Antibody	IHC concentration	WB concentration	Purpose	Supplier	Reference
Neuronal Antibodies					
β-III tubulin anti-rabbit	1 in 1000	N/A	Neuronal marker	Abcam 18207	Chen et al, 2010
MAP2 anti-mouse	1 in 1000	N/A	Neuronal marker	Abcam 11267	Orlova et al, 2010
Chicken Peripherin	1 in 1000	N/A	Ventral motoneuron marker	EnCor	Errante et al, 1994
Nuclear Stain					
DAPI	1 in 2000	N/A	Nuclear stain	Sigma D8417	Collins, 1997
UPR/ER stress markers					
BiP anti-rabbit	1 in 500-1000	1 in 1000	ER chaperone protein	Abcam 21685	Chai et al, 2010
Phospho-eIF2α anti-rabbit	1 in 100	1 in 1000	UPR activation	Abcam 19288	Not available
ATF4 anti-mouse	1 in 500	1 in 1500	UPR activation	Abcam 50546	Ouyang et al, 2011
CHOP anti-mouse	1 in 500	1 in 500	Pro-apoptotic protein downstream of UPR	Abcam 11419	Nishina et al, 2010
Caspase 12 anti-rabbit	1 in 500	1 in 1000	ER stress-induced apoptosis	Abcam 62484	Chen et al, 2010
ER calcium pump					
SERCA anti-rabbit	1 in 400	1 in 1000	ER calcium pump	Abcam 3625	Babai et al, 2010
Mitochondrial Biogenesis					
PGC1α anti -mouse	1 in 500	1 in 1000	Inducer of mitochondrial biogenesis	Abcam 54481	Kim et al, 2010
Loading control					
β Actin anti-mouse	N/A	1 in 5000	Western blot loading control	Abcam 8226	Xu et al, 2011

REFERENCES

1. Abel A, Walcott J, Woods J, Duda J and Merry D. Expression of expanded repeat androgen receptor produces neurological disease in transgenic mice. Hum Mol Genet. 19, 107-116 (2001)
2. Adachi H, et al,. CHIP overexpression reduces mutant androgen receptor protein and ameliorates phenotypes of the spinal and bulbar muscular atrophy transgenic mouse model. J. Neurosci. 27(19), 5115-5126 (2007)
3. Afifi A, Aleu F, Goodgold J and MacKay B. Ultrastructure of atrophic muscle in amyotrophic lateral sclerosis. Neurology 16(5), 475-481 (1966)
4. Anantharam V, et al,. Caspase-3-dependent proteolytic cleavage of protein kinase Cdelta is essential for oxidative stress-mediated dopaminergic cell death after exposure to methylcyclopentadienyl manganese tricarbonyl. J. Neurosci. 22(5), 1738-1751 (2002).
5. Antonini G et al,. Sensory involvement in spinal-bulbar muscular atrophy (Kennedy's Disease). Muscle Nerve 23, 252-258 (2000)
6. Appel S, et al,. Calcium: the Darth Vader of ALS. Amyotroph Lateral Scler Other Motor Neuron Disord. 2, Suppl 4:27-32 (2001)
7. Arduino D, Esteves A and Cardoso S. Endoplasmic reticulum and mitochondrial interplay mediates apoptotic cell death: Relevance to Parkinson's Disease. Neurochemistry International 5, 341-348 (2004)
8. Atkin, J.D. et al,. Endoplasmic reticulum stress and induction of the unfolded protein response in human sporadic amyotrophic lateral sclerosis. Neurobiol. Dis. 30, 400–407 (2008).
9. Atsumi T. The ultrastructure of intramuscular nerves in amyotrophic lateral sclerosis. Acta. Neuropathol. 55(3), 193-198 (1981)
10. Atsuta N, et al,. Natural history of spinal and bulbar muscular atrophy (SBMA): a study of 223 Japanese patients. Brain 129, 1446-1455 (2006)

11. Authi K. Orai1: A channel to safer antithrobotic therapy. Blood 113, 1872-1873 (2009)
12. Aziz M, Nihal M, Fu V, Jarrard D and Ahmad N. Resveratrol-caused apoptosis of human prostate carcinoma LNCaP cells is mediated via modulation of phosphatidylinositol 3'-kinase/Akt pathway and Bcl-2 family proteins. Mol. Cancer Ther. 5(5), 1335-1341 (2006)
13. Baek S, et al,. Ligand-specific allosteric regulation of coactivator functions of androgen receptor in prostate cancer cells. Proc. Natl. Acad. Sci. U S A. 103, 3100-3105 (2006)
14. Barreto-Chang O and Dolmetsch R. Calcium imaging of cortical neurons using Fura-2 AM. J. Vis. Exp. 23, 1067 (2009)
15. Bastin J, Lopes-Costa A and Djouadi F. Exposure to resveratrol triggers pharmacological correction of fatty acid utilization in human fatty acid oxidation-deficient fibroblasts. Hum. Mol. Genet. 20(10), 2048-2057 (2011)
16. Behal R, Buxton D, Robertson J and Olson M. Regulation of the pyruvate dehydrogenase multienzyme complex. Annu. Rev. Nutr. 13, 497-520 (1993)
17. Berridge M. Inositol trisphosphate and calcium signalling mechanisms. Biochem. Biophys. Acta. 1793(6), 933-940 (2008)
18. Bevan C and Parker M. The role of coactivators in steroid hormone action. Exp. Cell. Res. 253(2), 349-356 (1999)
19. Bilsland L, et al,. Deficits in axonal transport precede ALS symptoms in vivo. Proc. Natl. Acad. Sci. U S A. 107, 20523-20528 (2008)
20. Bingham P, et al,. Stability of an expanded trinucleotide repeat in the androgen receptor gene in transgenic mice. Nat. Genet. 9(2), 191-196 (1995)
21. Bingol B and Schuman E. Activity-dependent dynamics and sequestration of proteasomes in dendritic spines. Nature 441, 1144-1148 (2006)
22. Borra M, Smith B and Denu J. Mechanism of human SIRT1 activation by Resveratrol. J. Biol. Chem. 280(17). 17187-17195 (2005)

23. Boyce, M. et al,. A selective inhibitor of eIF2a dephosphorylation protects cells from ER stress. Science 307, 935–939 (2005).
24. Brandish P, et al,. Modes of action of tunicamycin, liposidomycin B, and mureidomycin A: inhibition of phosphor-N-acetylmuramyl-pentapeptide translocates from Escherichia coli. Antimicrob. Agents. Chemother. 40, 1640-1644 (1996)
25. Breckenridge D, et al, Regulation of apoptosis by endoplasmic reticulum pathways. Oncogene 22(53), 8608-8618 (2003)
26. Breedlove S and Arnold A. Sexually dimorphic motor nucleus in the rat lumbar spinal cord: response to adult hormone manipulation, absence in androgen-insensitive rats. Brain Res. 225, 297-307 (1981)
27. Browne S. Mitochondria and Huntington's disease pathogenesis: insight from genetic and chemical models. Ann. N Y Acad. Sci. 1147, 358-382 (2008)
28. Brustovetsky N, Brustovetsky T and Dubinsky J. On the mechanism of neuroprotection by creatine and phosphocreatine. J. Neurochem. 76(2), 425-434 (2002)
29. Burgdorf S, Leister P and Schedtmann KH. TSG101 interacts with apoptosis-antagonizing transcription factor and enhances androgen receptor-mediated transcription by promoting its monoubiquitination. J Biol Chem 279, 17524 – 17534 (2004).
30. Burklen TS et al,. The Creatine Kinase/Creatine Connection to Alzheimer's Disease: CK inactivation, APP-CK complexes and Focal Creatine Deposits. J Biomed Biotechnol, 35936 (2006)
31. Butler R, Leigh P, McPhaul and Gallo J. Truncated forms of the androgen receptor are associated with polyglutamine expansion in X-linked spinal and bulbar muscular atrophy. Hum. Mol. Genet. 7(1), 121-127 (1998)
32. Cai X. Molecular evolution and functional divergence of the Ca(2+) sensor protein in store-operated Ca(2+) entry: stromal interaction molecule. PLoS One. 2, e609 (2007)

33. Callewaert L, Van Tilborgh N and Claessens F. Interplay between two hormone-independent activation domains in the androgen receptor. Cancer Res. 66, 543-553 (2006)
34. Carri M, et al,. Expression of a Cu,Zn superoxide dismutase typical of familial amyotrophic lateral sclerosis induces mitochondrial alteration and increase of cytosolic Ca2+ concentration in transfected neuroblastoma SH-SY5Y cells. FEBS Lett. 414(2), 365-368 (1997).
35. Cary G and La Spada. Androgen receptor function in motor neuron survival and degeneration. Phys. Med. Rehabil. Clin. N. Am. 19(3), 479-494 (2008)
36. Centenera M, Harris J, Tilley W and Butler L. The contribution of different androgen receptor doamins to receptor dimerization and signalling. Mol. Endocrinol. 22(11), 2373-2382 (2008)
37. Chamberlain N, Driver E and Miesfeld R. The length and location of CAG trinucleotide repeats in the androgen receptor N-terminal domain affect transactivation function. Nucleic. Acids Res. 22(15), 3181-3186 (1994)
38. Chami M, Oulès B, Szabadkai G, Tacine R, Rizzuto R, Paterlini-Bréchot P. Role of SERCA1 truncated isoform in the proapoptotic calcium transfer from ER to mitochondria during ER stress. Mol Cell 32, 641-651 (2008).
39. Chang D, Rintoul G, Pandipati S and Reynolds I. Mutant huntingtin aggregates impair mitochondrial movement and trafficking in cortical neurons. Neurobiol. Dis. 22(2), 388-400 (2006).
40. Chaturvedi R, et al,. Impaired PGC1-alpha function in muscle in Huntington's Disease. Hum. Mol. Genet. 18(16), 3048-3065 (2009)
41. Chen CM. Mitochondrial dysfunction, metabolic deficits, and increased oxidative stress in Huntington's disease. Chnag Gung Med 34, 135-152 (2011)
42. Chevalier M, King L and Blond S. Purification and properties of BiP. Methods Enzymol. 290, 26827-26835 (1998).
43. Chilton J and Guthrie S. Development of oculomotor axon projections in the chick embryo. J Comp. Neurol. 472, 308-317 (2004)

44. Choi D. Ischemia-induced neuronal apoptosis. Curr Opin. Neurobiol 6(5), 667-672 (1996)
45. Choo Y, et al,. Mutant huntingtin directly increases susceptibility of mitochondria to the calcium-induced permeability transition and cytochrome c release. Hum. Mol. Genet. 13(14), 1407-1420 (2004)
46. Chung J, Semelka R and Martin D. Adrenal adenomas: characteristics postgadolinium capillary blush on dynamic MR imaging. J. Magn. Reson. Imaging 13(2), 242-248 (1997)
47. Ciechanover A and Brundin P. The ubiquitin proteasome system in neurodegenerative diseases: sometimes the chicken, sometimes the egg. Neuron 40, 427-446 (2003)
48. Ciutat D, Esquerda J and Caldero J. Evidence for calcium regulation of spinal cord motoneuron death in the chick embryo in vivo. Brain Res. Dev. 86, 167-179 (1995)
49. Claessens F, et al,. Diverse roles of androgen receptor (AR) domains in AR-mediated signaling. Nucl. Recept. Signal. 6, e008 (2008).
50. Collier M, Ji G, Wang Y and Kotlikoff M. Calcium-induced calcium release in smooth muscle: loose coupling between the action potential and calcium release. J Gen Physiol 115(5), 653-663 (2000).
51. Culig Z, Klocker H, Bartsch G and Hobisch A. Androgen receptor mutations in carcinoma of the prostate: significance for endocrine therapy. Am. J. Pharmacogenomics 1(4), 241-249 (2001)
52. Czubryt M, McAnally J, Fishman G and Olson E. Regulation of peroxisome proliferator-activated receptor gamma coactivator 1 alpha (PGC-1 alpha) and mitochondrial function by MEF2 and HDAC5. Proc. Natl. Acad. Sci. USA 100(4), 1711-1716 (2003)
53. Dahmer M. Caspases-2, -3, and -7 are involved in thapsigargin-induced apoptosis of SH-SY5Y neuroblastoma cells. J. Neurosci. Res. 80, 576-583 (2005)

54. Dedeoglu A, et al,. Therapeutic effects of cystamine in a murine model of Huntington's Disease. J. Neurosci. 22(20), 8942-8950 (2002)
55. Deepa P, et al,. Down regulation of trophic factors in neonatal rat spinal cord after administration of cerebrospinal fluid from sporadic amyotrophic lateral sclerosis patients. J. Neural. Transm. 118(4), 531-538 (2010)
56. Dejager S et al,. A comprehensive endocrine description of KD revealing androgen insensitivity to CAG repeat length. J Clin Endocrinol. Metab. 87, 3893-3901 (2002)
57. Deniaud A, et al,. Endoplasmic reticulum stress induces calcium-dependent permeability transition, mitochondrial outer membrane permeabilization and apoptosis.Oncogene 27, 285-299 (2007)
58. Denton R. Regulation of mitochondrial dehydrogenases by calcium ions. Biochim. Biophys. Acta. 1787(11), 1309-1316 (2009)
59. DeVos K et al. Familial amyotrophic lateral sclerosis-linked SOD1 mutants perturb fast axonal transport to reduce axonal mitochondria content. Hum Mol Genet 16, 2720-2728 (2007)
60. Diaz-Hernandez M, et al,. Neuronal induction of the immunoproteasome in Huntington's Disease. J. Neurosci. 23, 11653-11661 (2003)
61. Dimroth P, Kaim G and Matthey U. Crucial role of the membrane potential for ATP synthesis by F(1)F(o) ATP synthases. J. Exp. Biol. 203, 51-59 (2000)
62. Ding Y, et al,. Comparative studies of intracellular Ca2+ in strongly and weakly metastatic rat prostate cancer cell lines. Int. J. Biochem. Cell Biol. 38, 366-375 (2005)
63. Dobson C and Ellis R. Protein folding and misfolding inside and outside the cell. EMBO J 17, 5251-5254 (1998)
64. Domiano M et al,. Neural mitochondrial Ca2+ capacity impairment precedes the onset of motor symptoms in G93A Cu/Zn-superoxide dismutase mutant mice. J Neurochem 96, 1349-1361 (2006)

65. Domitrz I, et al,. Kennedy's Disease: expansion of the CAG trinucleotide. Neurol. Neurochir Pol. 35, 107-114 (2001)
66. Duennwald M and Lindquist S. Impaired ERAD and ER stress are early and specific events in polyglutamine toxicity. Genes Dev. 22(23), 3308-3319 (2008)
67. Dupuis L and Echaniz-Laguna A. Skeletal muscle in motor neuron diseases: therapeutic target and delivery route for potential treatments. Curr Drug Targets 11, 1250-1261 (2010)
68. Dykens JA. Isolated cerebral and cerebellar mitochondria produce free radicals when exposed to elevated Ca2+ and Na+: implications for neurodegeneration. J. Neurochem 63, 584-591 (1994)
69. Eckhart L, et al,. Duplication of the caspase-12 prodomain and inactivation of NLRC4/IPAF in the dog. Biochem. Biophys. Res. Commun. 384(2), 226-230 (2009)
70. Eisen J. Genetic and molecular analyses of motoneuron development. Curr. Opin. Neurobiol. 8(6), 697-704 Review (1998)
71. Endo M. Calcium-induced calcium release in skeletal muscle. Physiol Rev. 89(4), 1153-1176 (2009).
72. Englehardt J, Siklos L and Appel S. Altered calcium homeostasis and ultrastructure in motoneurons of mice caused by passively transferred anti-motoneuronal IgG. J. Neuropathol Exp. Neurol 56, 21-39 (1997)
73. Fargo K, Foecking E, Jones J and Sengelaub D. Neuroprotective actions of androgens on motoneurons. Front Neuroendocrinol. 30, 130-141 (2009)
74. Faus H and Haendler B. Post-translational Modification of Steroid Receptors. Biomedicine & Pharmacotherapy 60, 520-528 (2006)
75. Fels D and Koumenis C. The PERK/eIF2alpha/ATF4 module of the UPR in hypoxia resistance and tumor growth. Cancer Biol. Ther. 5(7), 723-728 (2006)

76. Feng J, Cai X, Zhao J and Yan Z. Serotonin receptors modulate GABA(A) receptor channels through activation of anchored protein kinase C in prefrontal cortical neurons. J. Neurosci 21, 6502-6511 (2001)
77. Fernandez de Sevilla D, Nunez A, Borde M, Malinow R and Buno W. Cholinergic-mediated IP3-receptor activation induces long-lasting synaptic enhancement in CA1 pyramidal neuorns. J. Neurosci. 28, 1469-1478 (2008)
78. Feske S, et al,. A mutation in Orai1 causes immune deficiency by abrogating CRAC channel function. Nature 441, 179-185 (2006)
79. Fischbeck K, et al,. Localization of the gene for X-linked spinal muscular atrophy. Neurology 36(12), 1595-1598 (1986).
80. Foradori C, et al,. Activation of the androgen receptor alters the intracellular calcium response to glutamate in primary hippocampal neurons and modulates sarco/endoplasmic reticulum calcium ATPase 2 transcription. Neuroscience 149, 155-164 (2008).
81. Fotakis G and Timbrell J. In vitro cytotoxicity assays: comparison of LDH, neutral red, MTT and protein assay in hepatoma cell lines following exposure to cadmium chloride. Toxicol. Lett. 160, 171-177 (2006)
82. Foyouzi-Youssefi R, et al,. Bcl-2 decreases the free Ca2+ concentration within the endoplasmic reticulum. Proc. Natl. Acad. Sci, USA 97(11), 5723-5728 (2000).
83. Freiden P, Gaut J and Hendershot M. Interconversion of three differentially modified and assembled forms of BiP. EMBO J. 11(1), 63-70 (1992).
84. Fu M et al. p300 and p300/cAMP-response element-binding protein-associated factor acetylate the androgen receptor at sites governing hormone-dependent transactivation. J Biol Chem 275, 20853-20860 (2000)
85. Fu M et al Androgen receptor acetylation governs trans activation and MEKK1-induced apoptosis without affecting in vitro sumoylation and trans-repression function. J Biol Chem. 32, 3373-3388 (2002).

86. Gallo J. Kennedy's Disease: a triplet repeat disorder or a motor neuron disease? Brain. Res. Bull. 56, 209-214 (2001)
87. Gao W and Dalton J. Expanding the therapeutic use of androgens via selective androgen receptor modulators (SARMs). Drug Discovery Today 12, 241-248 (2007)
88. Georgiou I, et al,. Preimplantation genetic diagnosis for spinal and bulbar muscular atrophy (SBMA). Hum. Genet. 108(6), 494-498 (2001)
89. Gines S et al,. Specific progressive cAMP reduction implicates energy deficit in presymptomatic Huntington's disease knock-in mice. Hum Mol Genet 12, 497-508 (2003)
90. Gingras M, Gangon V, Minotti S, Durham H and Berthod F. Optimized protocols for isolation of primary motor neurons, astrocytes and microglia from embryonic mouse spinal cord. J. Neurosci. Methods 163(1), 111-118 (2007).
91. Glass A. Gynecomastia. Endocrinol. Metab. Clin. North. Am. 23(4), 825-837 (1994).
92. Goldenberg I, Benderly M, Goldbourt U. Update on the use of fibrates: focus on bezafibrate. Vasc. Health Risk Manag. 4(1), 131-141 Review (2008)
93. Goldenthal M, Weiss H, Marin-Garcia J. Bioenergetic remodelling of heart mitochondria by thyroid hormone. Mol. Cell. Biochem. 265(1-2), 97-106 (2004).
94. Greenland K and Zajac J. Kennedy's Disease: pathogenesis and clinical approaches. Intern Med J 34, 279-286 (2004)
95. Grigoriev I, et al,. STIM1 is a MT-plus-end-tracking protein involved in remodeling of the ER. Curr. Biol. 18(3), 177-182 (2008)
96. Gu M, et al,. Mitochondrial defect in Huntington's disease caudate nucleus. Ann. Neurol. 39(3), 385-389 (1996).
97. Guidetti P, et al,. Early degenerative changes in transgenic mice expressing mutant huntingtin involve dendritic abnormalities but no impairment of mitochondrial energy production. Exp. Neurol 169(2), 340-350 (2001).

98. Gulbins E, Dreschers S and Bock J. Role of mitochondria in apoptosis. Exp. Physiol. 88(1), 85-90 Review (2003).

99. Gurney M, et al,. Motor neuron degeneration in mice that express a human Cu,Zn superoxide dismutase mutation. Science 264, 1772-1775 (1994).

100. Handschin C, Rhee J, Lin J, Tarr P and Spiegelman B. An autoregulatory loop controls peroxisome proliferator-activated receptor gamma coactivator 1alplha expression in muscle. Proc. Natl. Acad. Sci. USA 100(12), 7111-7116 (2003)

101. He B et al. An androgen receptor NH_2-terminal conserved motif interacts with the COOH terminus of the Hsp70-interacting protein (CHIP). J Biol Chem (279), 30643 - 30653 (2004)

102. Hegedua J, Putman C, Tyreman N and Gordon T. Preferential motor unit loss in the SODG93A transgenic mouse model of ALS. J Physiol 586, 3337-3351 (2008)

103. Heineke J and Molkentin J. Regulation of cardiac hypertrophy by intracellular signalling pathways. Nat. Rev. Mol. Cell. Biol 7(8), 589-600 review (2006)

104. Heinlein C and Chang C. The roles of androgen receptors and androgen-binding proteins in nongenomic androgen actions. Mol. Endocrinol. 16(10), 2181-2187 (2002)

105. Her L and Goldstein L. Enhanced sensitivity of striatal neurons to axonal transport defects induced by mutant huntingtin. J Neurosci. 28(50), 13662-13672 (2008)

106. Herzig R, Scacco S and Scarpulla R. Sequential serum-dependent activation of CREB and NRF-1 leads to enhanced mitochondrial respiration through the induction of cytochrome C. J. Biol. Chem. 275(17), 13134-13141 (2000)

107. Higgins C, Jung C and Xu Z. ALS-associated mutant SOD1G93A causes mitochondrial vacuolation by expansion of the intermembrane space and by involvement of SOD1 aggregation and peroxisomes. BMC Neurosci. 15, 4-16 (2003)

108. Ho D, et al,. Resveratrol protects against peripheral deficits in a mouse model of Huntington's disease. Exp. Neurol. 225(1), 74-84 (2010)

109. Ho S and Levin V. Induction of progesterone receptor by androgens in the mouse uterus. Mol. Cell. Endocrinol.

110. Hock M and Kralli A. Transcriptional control of mitochondrial biogenesis and function. Annu. Rev. Physiol. 71, 177-203 (2009)

111. Hoffman 2006 mito structure figure

112. Hollenbeck P and Saxton W. The axonal transport of mitochondria. J. Cell Sci. 118, 5411-5419 (2005)

113. Hong M et al,. Transcriptional regulation of the Grp78 promoter by endoplasmic reticulum stress: role of TFII-I and its tyrosine phosphorylation. J Biol Chem 280, 16821-16828 (2005)

114. Huser C and Davies M. Calcium signaling leads to mitochondrial depolarization in impact-induced chondrocyte death in equine articular cartilage explants. Arthritis. Rheum. 56(7), 2322-2334 (2007)

115. Gioeli D et al. Androgen receptor phosphorylation. Regulation and identification of the phosphorylation sites. J Biol Chem (277), 29304-29314 (2002)

116. Igarashi S, et al,. Strong correlation between the number of CAG repeats in androgen receptor genes and the clinical onset of features of spinal and bulbar muscular atrophy. Neurology 42(12), 2300-2302 (1992)

117. Igarashi S, et al,. Suppression of aggregate formation and apoptosis by transglutaminase inhibitors in cells expressing truncated DRPLA protein with an expanded polyglutamine stretch. Nat. Genet. 18(2), 111-117 (1998)

118. Ikesugi K, et al,. Induction of endoplasmic reticulum stress in retinal pericytes by glucose deprivation. Curr. Eye Res. 31(11), 947-953 (2006)

119. Ilieva E, et al,. Oxidative and endoplasmic reticulum stress interplay in sporadic amyotrophic lateral sclerosis. Brain 130, 3111-3123 (2007)

120. Irrcher I, Adhihetty P, Sheehan T, Joseph A and Hood D. PPARgamma coactivator-1aplha expression during thyroid hormone-and contractile activity-induced mitochondrial adaptations. Am. J. Physiol. Cell Physiol. 284(6), 1669-1677 (2003)

121. Ito Y, et al,. Involvement of CHOP, an ER stress apoptotic mediator, in both human sporadic ALS and ALS model mice. Neurosci Res 66, 124-130 (2009)

122. Ivessa N, et al,. The Brefeldin A-induced retrograde transport from the Golgi apparatus to the endoplasmic reticulum depends on calcium sequestered to intracellular stores. J. Biol. Chem. 270(43), 25960-25967 (1995)

123. Jafri M and Gillo B. A membrane potential model with counterions for cytosolic calcium oscillations. Cell Calcium 16(1), 9-19 (1994)

124. Janczewski A and Lakatta E. Thapsigargin inhibits Ca2+ uptake, and Ca2+ depletes sarcoplasmic reticulum in intact cardiac myocytes. Am J Physiol 265, (517-522 (1993).

125. Jenster G, Korput H, Trapman and Brinkman A. Identification of two transcription activation units in the N-terminal domain of the human androgen receptor. J. Biol. Chem. 270(13), 7341-7346 (1995)

126. Jimenez F, et al,. Activated caspase 3 and cleaved poly(ADP-ribose)polymerase in salivary epithelium suggest a pathogenetic mechanism for Sjögren's syndrome. Rheumatology (Oxford) 41(3), 338-342 (2002)

127. Jordan C, Padgett B, Hershey J, Prins G and Arnold A. Ontogeny of androgen receptor immunoreactivity in lumbar motoneurons and in the

sexually dimorphic levator ani muscle of male rats. J. Comp. Neurol. 379, 88-89 (1997)

128. Jung C, Higgins C and Xu Z. A quantitative histochemical assay for activities of mitochondrial electron transport chain complexes in mouse spinal cord sections. J Neurosci. Methods 114(2), 165-172 (2002)

129. Kabashi E, Agar J, Taylor D, Minotti S and Durham H. Focal dysfunction of the proteasome: a pathogenic factor in a mouse model of amyotrophic lateral sclerosis. J. Neurochem. 89, 1325-1335 (2004)

130. Kakkar P, Mehrotra A and Viswanathan PN. Interrelation of active oxygen species, membrane damage and altered calcium functions. Mol Cell Biochem 111, 11-15 (1992)

131. Katsuno M, et al,. Leuprorelin rescues polyglutamine-dependent phenotypes in a transgenic mouse model of spinal and bulbar muscular atrophy. Mat. Med. 9(6), 768-773 (2003)

132. Katsuno M, Adachi H, Tanaka F and Sobue G. Spinal and bulbar muscular atrophy: ligand-dependent pathogenesis and therapeutic perspectives. J Mol. Med 82(5) 298-307 (2004).

133. Katsuno M, et al,. reversible disruption of Dynactin 1-mediated retrograde axonal transport in polyglutamine-induced motor neuron degeneration. Journal Neurosci 26, 12106-12117 (2006).

134. Keller E, Ershler W and Chang C. The androgen receptor: a mediator of diverse responses. Front BioSci 1, 59-71 Review (1996)

135. Kemp M et al,. Impaired motoneuronal retrograde transport in two models of SBMA. Hum Mol Genet 22, 4475-4490 (2011)

136. Kemppainen J, et al,. Distinguishing androgen receptor agonists and antagonists: distinct mechanisms of activation by medroxyprogesterone acetate and dihydrotestosterone. Mol. Endocrinol 13(3), 440-454 (1999)

137. Kerbiriou M, Teng L, Benz N, Trouve P and Ferec C. The calpain, caspase 12, caspase 3 cascade leading to apoptosis is altered in F508del-CFTR expressing cells. PloS One 4(12), e8436 (2009)

138. Kieran D, Kalmar B, Dick J, Riddoch-Contreras J, Burnstock G and Greensmith L. Treatment with arimoclomol, a coinducer of heat shock proteins, delays disease progression in ALS mice. Nat. Med. 10(4), 402-405 (2004)

139. Kimura N, Imamura O, Ono F and Terao K. Aging attenuates dynactin-dynein interaction: down-regulation of dynein causes accumulation of endogenous tau and amyloid precursor protein in human neuroblastoma cells. J. Neurosci. Res. 85(13), 2909-2916 (2007)

140. Kiviluoto S, et al,. STIM1 as a key regulator for Ca2+ homeostasis in skeletal-muscle development and function. Skeletal Muscle 1, 1-16 (2011)

141. Knowles A and Kaplan N. Oxidative phosphorylation and ATPase activities of human tumor mitochondria. Biochim. Biophys. Acta 590(2), 170-181 (1980)

142. Knutti D, Kressler D and Kralli A. Regulation of the transcriptional coactivator PGC-1 via MAPK-sensitive interaction with a repressor. Proc. Natl. Acad. Sci. USA 98(17), 9713-9718 (2001)

143. Koochekpour S. Androgen receptor signaling and mutations in prostate cancer. Asian J Androl 5, 639-657 (2010)

144. Kouroku Y, et al,. Polyglutamine aggregates stimulate ER stress signals and caspase-12 activation. Hum. Mol. Genet. 11(13), 1505-1515 (2002)

145. Kousteni S, Kockar F, Sweeney G and Ramji D. Characterization and developmental regulation of the xenopus laevis CCAT-enhancer binding protein beta gene. Mech. Dev. 77(2), 143-148 (1998)

146. Kruman I, Pedersen W, Springer and Mattson M. ALS-linked Cu/Zn SOD mutation increases vulnerability of motor neurons to excitotoxicity by a mechanism involving increased oxidative stress and perturbed calcium homeostasis. Exp. Neurol. 160(1), 28-39 (1999)

147. Krauss S, Zhang C and Lowell BB. A significant portion of mitochondrial proton leak in intact thymocytes depends on expression of UCP2. Proc. Natl. Acad. Sci USA 99(1), 118-122 (2001)

148. Kurz E, Brewer R and Sengelaub D. Hormonally mediated plasticity of motoneuron morphology in the adult rat spinal cord: a cholera toxin-HRP study. J. Neurobiol 22(9), 976-988 (1991)

149. Kuznetsov et al, 1996 glucose deprivation

150. Lagouge M, et al,. Resveratrol improves mitochondrial function and protects against metabolic disease by activating SIRT1 and PCG1-aplha. Cell. 127(6), 1109-1122 (2006)

151. Lai T, et al,. Multimodal evoked potentials of Kennedy's disease. Can J Neurol Sci 34(3), 328-332 (2007)

152. Lang K et al,. Enhanced erythrocyte apoptosis in sickle cell anemia, thalassemia and glucose-6-phosphate dehydrogenase deficiency. Cell Physiol Biochem 12, 365-372 (2002)

153. La Spada A. et al,. Androgen receptor gene mutations in X-linked spinal and bulbar muscular atrophy. Nature 352, 77-79 (1991).

154. Larsen A, Frandsen A and Treiman M. Upregulation of the SERCA-type Ca2+ pump activity in response to endoplasmic reticulum stress in PC12 cells. BMC Biochem. 2:4 (2001)

155. Larsen K and Smith T. "Jaw drop" as an atypical manifestation of Kennedy's disease. Ugeskr Laeger 167, 3310-3311 (2005)

156. Larsson N. Somatic mitochondrial DNA mutations in mammalian aging. Annu Rev. Biochem. 79, 683-706 (2010)

157. Lecoeur H. Nuclear apoptosis detection by flow cytometry: influence of endogenous endonucleases. Exp. Cell. Res 277(1), 1-14 (2002)

158. Lee J et al,. Phenotypic variability in Kennedy's Disease: implication of the early diagnostic features. Acta Neurol Scand. 112, 57-63 (2005)

159. Lee Y, et al,. Activation of PERK signaling attenuates Abeta-mediated ER stress. PLoS One 5(5), e10489 (2010)

160. Li B, Holloszy J and Semenkovich C. Respiratory uncoupling induces delta-aminolevulinate synthase expression through a nuclear respiratory factor-1-dependent mechanism in HeLa cells. J. Biol. Chem. 274(25), 17534-17540 (1999)

161. Li X et al,. Clinical manifestations and molecular genetics of spinal bulbar muscular atrophy: report of 5 cases. ZYXZZ 87, 1611-1615 (2007)

162. Lin T and Chang C. Cloning and characterization of TDD5, an androgen target gene that is differentially repressed by testosterone and dihydrotestosterone. Proc. Natl. Acad. Sci. USA 94(10), 4988-4993 (1997)

163. Lindner A and Demerez A. Protein aggregation as a paradigm of aging. Biochim Biophys Acta 1790, 980-996 (2009)

164. Liu C, et al,. Depletion of mitochondrial DNA in leukocytes of patients with poly-Q diseases. J. Neurol Sci 264, 18-21 (2007)

165. Liu C, Shi Z, Fan L, Zhang C, Wang K and Wang B. Resveratrol improves neuron protection and functional recovery in rat model of spinal cord injury. Brain Res. 1374, 100-109 (2011)

166. Luckenbill-edds L. Laminin and the mechanism of neuronal outgrowth. Brain Res. Brain Res. Rev. 23, 1-27 (1997)

167. Ma Y, Brewer J, Diehl J and Hendershot L. Two distinct stress signalling pathways converge upon the CHOP promoter during the mammalian unfolded protein response. J. Mol. Biol 318, 1351-1365 (2001)

168. Maclean H and Handlesman D. Unraveling androgen action in muscle: genetic tools probing cellular mechanisms.Endocrinology 150, 3437-3439 (2009)

169. MacLean J and Wilkinson M. The Rhox genes. Reproduction 140(2), 195-213 (2010)

170. Magrane J and Manfredi G. Mitochondrial function, morphology, and axonal transport in amyotrophic lateral sclerosis. Antioxid Redox Signal 11, 1615-1626 (2009)

171. Malik B, et al,. Absence of disturbed axonal transport in spinal and bulbar muscular atrophy. Hum. Mol. Genet. 20, 1776-1786 (2011)

172. Mandrusiak L, et al,. Transglutaminase potentiates ligand-dependent proteasome dysfunction induced by polyglutamine-expanded androgen receptor. Hum. Mol. Genet. 12(13), 1497-1506 (2003).

173. Manfredi G and Xu Z. Mitochondrial dysfunction and its role in motor neuron degeneration in ALS. Mitochondrion 5(2), 77-87 Review (2005)

174. Mannella C. Structure and dynamics of the mitochondrial inner membrane cristae. Biochim. Biophys. Acta. 1763(5-6), 542-548 (2006)

175. Maravall M, Mainen Z, Sabatini B and Svoboda K. Estimating intracellular calcium concentrations and buffering without wavelength ratioing. Biophys. J 78(5), 2655-2667 (2000)

176. Marciniak S, et al,. CHOP induces death by promoting protein synthesis and oxidation in the stressed endoplasmic reticulum. Genes Dev. 18(24), 3066-3077 (2004)

177. Mariotti C et al,. Phenotypic manifestations associated with CAG-repeat expansion in the androgen receptor gene in male patients and heterozygous females: a clinical and molecular study of 30 families. Neuromuscul Disord 10, 391-397 (2000)

178. Martin G, Sabido O, Durand P and Levy R. Cryopreservation induces an apoptosis-like mechanism in bull sperm. Biol. Reprod 71(1), 28-37 (2004)

179. Marzo I, et al,. Bax and adenine nucleotide translocator cooperate in the mitochondrial control of apoptosis. Science 281, 2027-2031 (1998)

180. Martinez J, et al,. Calpain and caspase processing of caspase 12 contribute to the ER stress-induced cell death pathway in differentiated PC12 cells. Apoptosis 15, 1480-1493 (2010)

181. Mashima T, Naito M, Tsuruo T. Caspase-mediated cleavage of cytoskeletal actin plays a positive role in the process of morphological apoptosis. Oncogene 18(15), 2423-2430 (1999).

182. Matias P, et al,. Structural basis for the glucocorticoid response in a mutant human androgen receptor (AR(ccr)) derived from an androgen-independent prostate cancer. J Med. Chem. 45(7), 1439-1446 (2002).

183. Matsumoto A, Arai Y, Urano A and Hyodo S. Androgen regulates gene expression of cytoskeletal proteins in adult rat motoneurons. Horm. Behav. 28(4), 357-366 (1994)

184. Mattiazzi M, et al,. Mutated human SOD1 causes dysfunction of oxidative phosphorylation in mitochondria of transgenic mice. J. Biol. Chem. 277(33), 29626-29633 (2002)

185. Mayor T. A cryptic protease couples deubiquitination and degradation by the proteasome. Med. Sci (Paris) 278(39), 37545-37552 (2003)

186. Merry D, McCampbell A, Taye A, Winston R, Fischbeck K. Toward a mouse model for SBMA: effect of neuronal expression of androgen receptor in transgenic mice. Am J Hum 59, A271 (1996)

187. Merry D. Animal models of KD. NeuroRx 2, 471-479 (2005)

188. Meusser B, Hirsch C, Jarosch E and Sommer T. ERAD: the long road to destruction. Nat. Cell Biol. 7(8), 766-772 (2005)

189. McGill J and Beal M. PGC1-alpha, a new therapeutic target in Huntington's Disease? Cell 127(3), 465-468 (2006)

190. McEwan I, Lavery D, Fischer K and Watt K. Natural disordered sequences in the amino terminal domain of nuclear receptors: lessons from the androgen and glucocorticoid receptors. Nucl. Recept. Signal 5, e001 Review (2007)

191. Michels G and Hoppe U. Rapid actions of androgens. Front Neuroendocrinol. 29(2), 182-198 (2008)

192. Milner A, Johnson G and Gregory C. Prevention of programmed cell death in Burkitt lymphoma cell lines by bcl-2-dependent and -independent mechanisms. Int. J. Cancer 52(4), 636-644 (1992)

193. Mo K, et al,. Microarray analysis of gene expression by skeletal muscle of three mouse models of Kennedy disease/spinal bulbar muscular atrophy. PLoS One 5(9), e12922 (2010)

194. Mochel F and Haller R. Energy deficit in Huntington's Disease: why it matters. J. Clin. Invest. 121(2), 493-499 (2011)

195. Moore A, Donahue C, Bauer K and Mather J. Simultaneous measurement of cell cycle and apoptotic cell death. Methods Cell Biol. 57, 265-278 (1998)

196. Moras D and Gronemeyer H. The nuclear receptor ligand-binding domain: structure and function. Curr. Opin. Cell. Biol. 10(3), 384-391 (1998)

197. Morfini G, et al,. Axonal transport defects in neurodegenerative diseases. J. Neurosci. 29(41), 12776-12786 (2009)

198. Morris G, Williams R, Elliot M and Beebe S. Resveratrol induces apoptosis in LNCaP cells and requires hydroxyl groups to decrease viability in LNCaP and DU 145 cells. Prostate 52(4), 319-329 (2002)

199. Mosbah B, et al,. Endoplasmic reticulum stress inhibition protects steatotic and non-steatotic livers in partial hepatectomy under ischemia-reperfusion. Cell Death Dis. 1, e52 (2010).

200. Mozo J, et al,. Thermoregulation: what role for UCPs in mammals and birds. Biosci. Rep. 25(3-4), 227-249 (2005)

201. Murphy AN. In a flurry of PINK, mitochondrial bioenergetics takes a leading role in Parkinson's disease. EMBO Mol Med 1, 81-84 (2009).

202. Naidoo N. The endoplasmic reticulum stress response and aging. Rev. Neurosci. 20, 23-37 (2009)

203. Nakagawa T and Yuan J. Cross-talk between two cysteine protease families. Activation of caspase-12 by calpain in apoptosis. J. Cell. Biol. 150(4), 887-894 (2000)

204. Nakano T, et al,. Endoplasmic reticulum Ca2+ depletion induces endothelial cell apoptosisindependently of caspase-12. Cardiovasc. Res. 69, 908-915 (2006)

205. Narayanan R, Dougherty K and Johnson D. Calcium store depletion induces persistent perisomatic increases in the functional density of h channels in hippocampal pyramidal neurons. Neuron 68(5), 921-935 (2010)

206. Narita M, et al,. Bax interacts with the permeability transition pore to induce permeability transition and cytochrome c release in isolated mitochondria. Proc. Natl. Acad. Sci. USA 95(25), 14681-14686 (1998)

207. Naruse I and Keino H. Apoptosis in the developing CNS. Prog Neurobiol 47(2), 135-155 (1995)

208. Naya F, et al,. Mitochondrial deficiency and cardiac sudden death in mice lacking the MEF2A transcription factor. Nat. Med. 8(11), 1303-1309 (2002)

209. Nishitoh H, et al,. ALS-linked mutant SOD1 induces ER stress- and ASK1-dependent motor neuron death by targeting Derlin-1. Genes Dev. 22, 1451-1464 (2008)

210. Novoa I, Zeng H, Harding H and Ron D. Feedback inhibition of the unfolded protein response by GADD34-mediated dephosphorylation of eIF2alpha. J. Cell. Biol. 153(5), 1011-1022 (2001)

211. Oliveria S, Dell'Acqua M and Sather W. AKAP79/150 anchoring of calcineurin controls neuronal L-type Ca2+ channel activity and nuclear signalling. Neuron 55(2), 261-275 (2007)

212. Oh Y, Shin K, Yuan J and Kang S. Superoxide dismutase 1 mutants related to amyotrophic lateral sclerosis induce endoplasmic stress in neuro2a cells. J Neurochem. 104(4), 993-1005 (2008)

213. Ohoka N, et al,. TRB3, a novel ER stress-inducible gene, is induced via ATF4-CHOP pathway and is involved in cell death. EMBO J. 24, 1243-1255 (2005)

214. Olah J, et al,. Increased glucose metabolism and ATP level in brain tissue of Huntington's disease transgenic mice. FEBS J. 275(19) 4740-4755 (2008)

215. Orr H. Unstable nucleotide repeat minireview series: a molecular biography of unstable repeat disorders. J. Biol. Chem. 284(12), 7405 (2008)

216. Ostwald T and MacLennan D. Isolation of a high affinity calcium-binding protein from sarcoplasmic reticulum. J. Biol. Chem. 3, 974-979 (1974)

217. Pachatz C, et al,. Upper motoneuron involvement in X-linked recessive bulbospinal muscular atrophy. Clin. Neurophysiol 118, 262-268 (2007)

218. Pacholec M, et al. SRT1720, SRT2183, SRT1460, and Resveratrol Are Not Direct Activators of SIRT1. J. Biol. Chem 285 (11), 8340-8351 (2004).

219. Pak K, Chan S and Mattson M. Presenilin-1 mutation sensitizes oligodendrocytes to glutamate and amyloid toxicities, and exacerbates white matter damage and memory impairment in mice. Neuromolecular Med. 3(1), 53-64 (2003)

220. Palade G. An electron microscope study of the mitochondrial structure. J. Histochem. Cytochem. 1(4), 188-211 (1953)

221. Palazzolo I, et al,. The role of the polyglutamine tract in androgen receptor. J Steroid Biochem Mol Biol 108, 245-253 (2008)

222. Panov A, Obertone T, Bennett-Desmelik J and Greenamyre J. Ca(2+)-dependent permeability transition and complex I activity in lymphoblast mitochondria from normal individuals and patients with Huntington's or Alzheimer's disease. Ann. N Y Acad. Sci 893, 365-368 (1999)

223. Paradas C, et al,. Highly skewed inactivation of the wild-type X-chromosome in asymptomatic female carriers of spinal and bulbar muscular atrophy (Kennedy's disease). J. Neurol. 255(6), 853-857 (2008)

224. Paradies G, Petrosillo G, Paradies V and Ruggiero F. Mitochondrial dysfunction in brain aging: role of oxidative stress and cardiolipin. Neurochem. Int. 58(4), 447-457 (2011)

225. Parekh A and Penner R. Store depletion and calcium influx. Physiol. Rev. 77, 901-930 (1997)

226. Paschen W and Doutheil J. disturbance of endoplasmic reticulum functions: a key mechanism underlying cell damage? Acta. Neurochir. Suppl. 73, 1-5. Review (1999)

227. Peinelt C, et al,. Amplification of CRAC current by STIM1 and CRACM1 (Orai1). Nat. Cell. Biol. 8(7), 771-773 (2006)

228. Perez C, Margolskee R, Kinnamon S and Ogura T. Making sense with TRP channels: store-operated calcium entry and the ion channel Trpm5 in taste receptor cells. Cell Calcium 33, 541-549 (2003)

229. Periasamy M and Kalyanasundaram A. SERCA pump isoforms: their role in calcium transport and disease. Muscle Nerve. 35, 430-442 (2007)

230. Phebus L, Mincy R and Clemens J. Ischemia increases tissue and decreases extracellular levels of acid dopamine metabolites in the rat striatum:

further evidence for active transport of metabolites. Life Sci. 13 1135-1341 (1995)

231. Polo A et al,. Sensory involvement in X-linked spino-bulbar muscular atrophy: an electrophysiological study. J Neurol 243, 388-392 (1996)

232. Potier M, et al,. Evidence for STIM1- and Orai1-dependent store-operated calcium influx through ICRAC in vascular smooth muscle cells: role in proliferation and migration. FASEB J. 23, 2425-2437 (2009)

233. Poulsen J, et al,. Thapsigargin-sensitive Ca(2+)-ATPases account for Ca2+ uptake to inositol 1,4,5-trisphosphate-sensitive and caffeine-sensitive Ca2+ stores in adrenal chromaffin cells. Biochem J. 307, 749-758 (1995)

234. Prakriya M, et al,. Orai1 is an essential pore subunit of the CRAC channel. Nature 443 (7108), 230-233 (2006)

235. Puigserver P, et al,. Involvement of the retinoblastoma protein in brown and white adipocyte cell differentiation: functional and physical association with the adipogenic transcription factor C/EBPalpha. Eur. J. Cell Biol. 77(2), 117-123 (1998)

236. Puttaparthi K, Van Kaer L and Elliot J. Assessing the role of immuno-proteasomes in a mouse model of familial ALS. Exp. Neurol. 206(1), 53-58 (2007).

237. Puttaparthi K and Elliot J. Non-neuronal induction of immunoproteasome subunits in an ALS model: possible mediation by cytokines. Exp. Neurol. 196(2), 441-451 (2005)

238. Rahman S and Neuman R. Action of 5-hydroxytryptamine in facilitating N-methyl-D-aspartate depolarization of cortical neurones mimicked by calcimycin, cyclopiazonic acid and thapsigargin. Br. J. Pharmacol. 119(5), 877-884 (1996)

239. Ranganathan S, et al,. Mitochondrial abnormalities in spinal and bulbar muscular atrophy. Hum. Mol. Genet. 18(1), 27-42 (2009)

240. Rao J, et al,. STIM1 translocation to the plasma membrane enhances intestinal epithelial restitution by inducing TRPC1-mediated Ca2+ signaling after wounding. Am. J. Physiol. Cell. Physiol. 299, 579-588 (2010)

241. Rawlings N and Barrett A. Families of serine peptidases. Methods Enzymol 244, 19-61 (1994)

242. Reed J and Kroemer G. Mechanisms of mitochondrial membrane permeabilization. Cell Death Differ. 7(12), 1145 Review (2001)

243. Reijonen S. et al,. Inhibition of endoplasmic reticulum stress counteracts neuronal cell death and protein aggregation caused by N-terminal mutant huntingtin proteins. Exp. Cell. Res. 314, 950-960 (2008)

244. Reimertz C, et al,. Gene expression during ER stress-induced apoptosis in neurons: induction of the BH3-only protein Bbc3/PUMA and activation of the mitochondrial apoptosis pathway. J. Cell. Biol. 162, 587-597 (2003)

245. Reyes N, et al,. Blocking the mitochondrial apoptotic pathway preserves motor neuron viability and function in a mouse model of ALS. J. Clin. Invest. 120(10), 3673-3679 (2010)

246. Ricote M, et al,. The p38 transduction pathway in prostatic neoplasia. J. Pathol. 208(3), 401-407 (2006)

247. Ricquier D and Bouillaud F. Mitochondrial uncoupling proteins: from mitochondria to the regulation of energy balance. J Physiol 529, 3-10 (2000)

248. Rodgers J, et al,. Nutrient control of glucose homeostasis through a complex of PGC1alpha and SIRT1. Nautre 434(7029), 113-118 (2005)

249. Rodriguez-Enriquez S, He L and Lemasters J**.** Role of mitochondrial permeability transition pores in mitochondrial autophagy. Int. J. Biochem. Cell Biol. 36(12), 2463-2472 (2004)

250. Romagnoli A, et al,. Endoplasmic reticulum/mitochondria calcium cross-talk. Novartis Found Symp. 287, 122-131 (2007).

251. Romero G, et al,. Protective effects of calcium channel blockers in carbon tetrachloride-induced liver toxicity. Life Sci. 55(13), 981-990 (1994)

252. Ron D and Walter P. Signal integration in the endoplasmic reticulum unfolded protein response. Nat. Rev. Mol. Cell Biol. 8(7), 519-529 (2007)

253. Rossi A and Dirksen R. Sarcoplasmic reticulum: the dynamic calcium governor of muscle. Muscle Nerve 33(6), 715-731 (2006)

254. Roy B, Li W and Lee A. Calcium-sensitive transcriptional activation of the proximal CCAAT regulatory element of the grp78/BiP promoter by the human nuclear factor CBF/NF-Y. J. Biol. Chem 271(46), 28995-29002 (1996)

255. Rudolf R, Mongillo M, Rizzuto R and Pozzan T. Looking forward to seeing calcium. Nat Rev Mol Cell Biol 4(7), 579-586 (2003).

256. Sanchez I, Mahlke C and Yuan J. Pivotal role of oligomerization in expanded polyglutamine neurodegenerative disorders. Nature 421, 373-379 (2003)

257. Sanders T, McMichael R and Hendrix K. Occurrence of resveratrol in edible peanuts. J. Agric. Food Chem. 48(4), 1243-1246 (2000)

258. Sano M and Schneider M. Cyclin-dependent kinase-9: an RNAPII kinase at the nexus of cardiac growth and death cascades. Circ. Res. 95(9), 867-876 (2004)

259. Saris N and Carafoli E. A historical review of cellular calcium handling, with emphasis on mitochondria. Biochemistry 70(2), 187-194 (2005)

260. Sasaki S and Iwata M. Impairment of fast axonal transport in the proximal axons of anterior horn neurons in amyotrophic lateral sclerosis. Neurology 47(2), 535-540 (1996)

261. Sasaki S, Warita H, Abe K and Iwata M. Impairment of axonal transport in the axon hillock and the initial segment of anterior horn neurons

in transgenic mice with a G93A mutant SOD1 gene. Acta. Neuropathol. 110(1), 355-362 (2005)

262. Saxena S, Cabuy E & Caroni P. A role for motoneuron subtype-selective ER stress in disease manifestations of FALS mice. Nat. Neurosci. 12, 627-636 (2009).

263. Scarpulla R. Nuclear activators and coactivators in mammalian mitochondrial biogenesis. BioChim. Biophys. Acta. 1576(1-2), 1-14 (2002)

264. Schirmer E, et al,. The ATPase activity of HSP104, effects on environmental conditions and mutations. J. Biol. Chem 273(25), 15546-15552 (1998).

265. Schmidt B, Greenberg C, Allingham-Hawkins D and Spriggs E. Expression of X-linked bulbospinal muscular atrophy (Kennedy disease) in two homozygous women. Neurology 59, 770-772 (2002)

266. Schoenmakers I, Nap R, Mol J and Hazewinkel H. Calcium metabolism: an overview of its hormonal regulation and interrelation with skeletal integrity. Vet Q 21(4), 147-153 (1999)

267. Scorrano L et al,. BAX and BAK regulation of endoplasmic reticulum Ca2+: a control point for apoptosis. Science 300, 135-139 (2003)

268. Seo H, Sonntag K, Kim W, Cattaneo E and Isacson O. Proteasome activator enhances survival of Huntington's disease neuronal model cells. PLoS One 2(2), e238 (2007)

269. Shi T, et al,. Novel alpha1-adrenergic receptor signaling pathways: secreted factors and interactions with the extracellular matrix. Mol Pharmacol 70(1), 129-142 (2006)

270. Shi W, et al,. Repressive effects of resveratrol on androgen receptor transcriptional activity. PLoS One. 4(10), e7398 (2009)

271. Siemann D. Tissue oxygen manipulation and tumor blood flow. Int. J. Radiat. Oncol. Biol. Phys. 22, 393 – 395 (1992)

272. Sinclair R, et al,. Men with Kennedy's Disease have a reduced risk of androgenetic alopecia. Br. J. Dermatol 157, 290-294 (2007)

273. Skalka H. Diabetic retinopathy: an overview. J. Med. Assoc. State Ala. 45(7), 25-29 (1976)

274. Slagsvold T, Kraus I, Bentzen T, Palvimo J and Saatcioglu F. Mutational analysis of the androgen receptor AF-2 core domain reveals functional and mechanistic differences of conserved residues compared with other nuclear receptors. Mol Endocrinol 14, 1603-1617 (2000)

275. Sobue G, et al,. X-linked recessive bulbospinal neuronopathy. A clinicopathological study. Brain 112, 209-232 (1989)

276. Sopher B, et al,. Androgen Receptor YAC transgenic mice recapitulate SBMA motor neuronopathy and implicate VEGF164 in the motor neuron degeneration. Neuron 41, 687-699 (2004).

277. Soraru G, et al,. Spinal and bulbar muscular atrophy: skeletal muscle pathology in male patients and heterozygous females. J. Neurol. Sci. 264, 100-105 (2007).

278. Sorenson E and Klein C. Elevated creatine kinase and transaminases in asymptomatic SBMA. Amyotroph. Lateral Scler. 8(1), 62-64 (2007)

279. Steiger J, Bandyopadhyay S, Farb D and Russek S. cAMP response element-binding protein, activating transcription factor-4, and upstream stimulatory factor differentially control hippocampal GABABR1a and GABABR1b subunit gene expression through alternative promoters. J. Neurosci. 24, 6115-6126 (2004)

280. Stenoien D et al,. Polyglutamine-expanded androgen receptors form aggregates that sequester heat shock proteins, proteasome components and SRC-1, and are suppressed by the HDJ-2 chaperone. Hum Mol Genet 8, 731-741 (1999)

281. Strand A, et al,. Expression profiling of Huntington's disease models suggests that brain-derived neurotrophic factor depletion plays a major role in striatal degeneration. J. Neurosci. 27, 11758-11768 (2007).

282. Sulek A, et al,. CAG repeat polymorphism in the androgen receptor (AR) gene of SBMApatients and a control group. J. Appl. Genet. 46(2), 237-239 (2005).

283. Sundaram K, Kumar N, Monder C and Bardin C. Different patterns of metabolism determine the relative anabolic activity of 19-norandrogens. J. Steroid Biochem. Mol. Biol. 53, 253-257 (1995)

284. Suzuki K, et al,. CAG repeat size correlates to electrophysiological motor and sensory phenotypes in SBMA. Brain 131, 229-239 (2007)

285. Szegezdi E, Logue SE, Gorman AM, Samali A. Mediators of endoplasmic reticulum stress-induced apoptosis. EMBO Rep. 9, 880-885 (2006)

286. Tabrizi SJ et al,. Mitochondrial dysfunction and free radial damage in the Huntington R6/2 transgenic mouse. Ann Neurol 47, 80-86 (2000)

287. Tahiri B, Auzou G, Nicolas J, Sultan C and Lupo B. Participation of critical residues from the extreme C-terminal end of the human androgen receptor in the ligand binding function. Biochemistry 40(29), 8431-8437 (2001).

288. Tai H and Schuman E. Ubiquitin, the proteasome and protein degradation in neuronal function and dysfunction. Nat Rev Neurosci 9, 826-838 (2008)

289. Talbot J, David G and Barrett E. Inhibition of mitochondrial Ca2+ uptake affects phasic release from motor terminals differently depending on external [Ca2+]. J. Neurophysiol. 90(1), 491-502 (2003)

290. Tanner T, Claessens F amd Haelens A. The hinge region of the androgen receptor plays a role in proteasome-mediated transcriptional activation. Ann N Y Acad. Sci. 1030, 587-592 (2004)

291. Tashiro T and Komiya Y. Impairment of cytoskeletal protein transport due to aging or beta,beta'-iminodipropionitrile intoxication in the rat sciatic nerve. Gerontology 20 Suppl 2: 36-45 (1994)

292. Tee J and Peppelenbosch M. Anchoring skeletal muscle development and disease: the role of ankyrin repeat domain containing proteins in muscle physiology. Crit Rev Biochem Mol Bio 45(4), 318-330 (2010)

293. Teyssier C, Ou C, Khetchoumian L, Losson R and Stallcup M. Transcriptional intermediary factor 1alpha mediates physical interaction and functional synergy between the coactivator-associated arginine methyltransferase 1 and glucocorticoid receptor-interacting protein 1 nuclear receptor coactivators. Mol. Endocrinol. 20(6) 1276-1286

294. Thomas D, et al,. A comparison of fluorescent Ca2+ indicator properties and their use in measuring elementary and global Ca2+ signals. Cell Calcium 28, 213-223 (2000)

295. Trushina E, et al,. Mutant huntingtin impairs axonal trafficking in mammalian neurons in vivo and in vitro. Mol. Cell. Biol. 24(18), 8195-8209 (2004)

296. Tovey S, Sun Y and Taylor C. Rapid functional assays of intracellular Ca2+ channels. Nat. Protoc. 1, 259-263

297. Tsai E, Hirsch I, Brunzell J and Cahit A. Reduced plasma peroxyl radical trapping capacity and increased susceptibility of LDL to oxidation in poorly controlled IDDM. Diabetes 43(8), 1010-1014 (1994)

298. Urano F, Bertolotti A and Ron D. IRE1 and efferent signalling from the endoplasmic reticulum. J. Cell. Sci. 113, 3697-3702 (2000)

299. Urushitani M, Kurisu J, Tsukita K and Takahashi R. Proteasomal inhibition by misfolded mutant superoxide dismutase 1 induces selective motor neuron death in familial amyotrophic lateral sclerosis. J. Neurochem 83(5), 1030-1042 (2002).

300. Yamada M, Tsuji S and Takahashi H. Pathology of CAG repeat diseases. Neuropathology 20(4), 319-325 (2000).

301. Yang L and Arnold P. Interaction of BDNF and testosterone in the regulation of adult perineal motoneurons. J. Neurobiol 44(3), 308-319 (2000).

302. Van den Bosch L, et al,. Calcium handling proteins in isolated spinal motoneurons. Life Sci. 65, 1597-1606 (1999).

303. Van Huizen R, Martindale J, Gorospe M and Holbrook N. P58IPK, a novel endoplasmic reticulum stress-inducible protein and potential negative regulator of eIF2alpha signalling. J. Biol. Chem. 278(18), 15558-15564 (2003).

304. Vassilakos P, Michalak M, Lehrman M and Williams D. Oligosaccaride binding characteristics of the molecular chaperones calnexin and calreticulin. Biochemistry 37, 3480-3490 (1998)

305. Ventura-Clapier R, Garnier A and Veksler V. Transcriptional control of mitochondrial biogenesis: the central role of PGC-1alpha. Cardiovasc. Res. 79(2), 208-217 (2008)

306. Verkhratsky A. Endoplasmic reticulum calcium signalling in nerve cells. Biol. Res. 27, 693-699 Review (2004)

307. Verma A, et al,. Inositol trisphopsphate and thapsigragin discriminate endoplasmic reticulum stores of calcium in rat brain. Biochem. Biophys. Res. Commun. 172(2). 811-816 (1990).

308. Verrijdt G, Haelens A and Claessens F. Selective DNA recognition by the androgen receptor as a mechanism for hormone-specific regulation of gene expression. Mol. Genet. Metab. 78(3), 175-185 (2003)

309. Vijayalakshmi K, et al,. Evidence of endoplasmic reticular stress in the spinal motor neurons exposed to CSF from sporadic amyotrophic lateral sclerosis patients. Neurobiol. Dis. 41(3), 695-705 (2010)

310. Vijayvergiya C, Beal M, Buck J, Manfredi G. Mutant superoxide dismutase 1 forms aggregates in the brain mitochondrial matrix of amyotrophic lateral sclerosis mice. J Neurosci. 25(10), 2463-2470 (2005)

311. Vitolo O, et al,. Adenosine and ADP prevent apoptosis in cultured rat cerebellar granule cells. Brain Res. 809(2), 297-301 (1998)

312. Voster and Shafer 1996 BAPTA

313. Wall J, et al,. Alterations in oxidative phosphorylation complex proteins in the hearts of transgenic mice that overexpress the p38 MAP kinase activator, MAP kinasekinase 6. Am. J. Physiol. Heart Circ. Physiol. 291(5), H2462-2472 (2006)

314. Wang H, Lim P, Karbowski M and Monteiro M. Effects of overexpression of huntingtin proteins on mitochondrial integrity. Hum. Mol. Genet. 18(4), 732-752 (2009).

315. Watson P, et al,. Restoration of CREB function is linked to completion and stabilization of adaptive cardiac hypertrophy in response to exercise. Am. J. Physiol. Heart Circ. Physiol. 293(1), 246-259 (2007).

316. Weydt P, et al,. Thermoregulatory and metabolic defects in Huntington's Disease transgenic mice implicate PGC1-alpha in Huntington's disease neurodegeneration. Cell Metab 4(5), 349-362 (2006)

317. Weiland J, Schonfeld W, Menke K and Repke K. Interaction of progesterone derivatives with the digitalis target enzyme: impact of glycosidation on inhibitory potency.Pharmacol Res. 23(1), 27-32 (1991).

318. Williams R, et al,. Identification and characterization of the STIM (stromal interaction molecule) gene family: coding for a novel class of transmembrane proteins. Biochem J. 357, 673-685 (2001)

319. Wootz H, Hansson I, Korhonen L, Napankangas U and Lindholm D. Caspase 12 cleavage and increased oxidative stress during motoneuron degeneration in transgenic mouse model of ALS. Biochem. Biophys. Res. Commun. 322(1), 281-286 (2004).

320. Wozniak A. Requirement of biphasic calcium release from the endoplasmic reticulum for Fas-mediated apoptosis. J. Cell. Biol. 172, 709-714 (2006)

321. Wrutniak-Cabello C, Casas F and Cabello G. Thyroid hormone action in mitochondria. J. Mol. Endocrinol 26(1), 67-77 (2001)

322. Wu K, Bungard D and Lytton J. Regulation of SERCA Ca2+ pump expression by cytoplasmic Ca2+ in vascular smooth muscle cells. Am. J. Physiol. 280(4), 843-851 (2001)

323. Wu Z, et al,. Transducer of regulated CREB-binding proteins (TORCs) induce PGC-1alpha transcription and mitochondrial biogenesis in muscle cells. Proc. Natl. Acad. Sci. USA 103(39), 14379-14384 (2006).

324. Yamamoto M, et al,. Expression of GDNF and GDNFR-alpha mRNAs in muscles of patients with motor neuron diseases. Neurochem. Res. 24(6), 785-790 (1999)

325. Yang Y, Turner R and Gaut J. The chaperone BiP/GRP78 binds to amyloid precursor protein and decreases Abeta40 and Abeta42 secretion. J. Biol. Chem. 273(40) 25552-25555 (1998)

326. Yang CS, et al. Simian virus 40 small t antigen mediates conformation-dependent transfer of protein phosphatase 2A onto the androgen receptor. Mol Cell Biol (25), 1298 – 1308 (2005)

327. Yeromin A. Molecular identification of the CRAC channel by altered ion selectivity in a mutant of Orai. Nature 443, 226-229 (2006)

328. Yoneda T, et al,. Activation of caspase-12, an endoplastic reticulum (ER) resident caspase, through tumor necrosis factor receptor-associated factor

2-dependent mechanism in response to the ER stress. J. Biol. Chem. 276(17) 13935-13940 (2001).

329. Yu S, Wang H, Dawson T and Dawson V. Poly(ADP-ribose) polymerase-1 and apoptosis inducing factor in neurotoxicity. Neurobiol. Dis. 14(3), 303-317 (2003).

330. Yu J, Kim K and Kim H. Role of NADPH oxidase and calcium in cerulein-induced apoptosis: involvement of apoptosis-inducing factor. Ann N Y Acad. Sci. 1090, 292-297 (2006).

331. Yuan Z, et al,. Na/K-ATPase thethers phospholipase C and IP3 receptor into a calcium-regulatory complex. Mol. Biol. Cell. 16(9), 4034-4045 (2005)

332. Zhang S, et al,. STIM1 is a Ca2+ sensor that activates CRAC channels and migrates from the Ca2+ store to the plasma membrane. Nature 437, 902-905 (2005)

333. Zhou X, Kudo A, Kawakami H and Hirano H. Immunohistochemical localization of androgen receptor in mouse testicular germ cells during fetal and postnatal development. Anat. Rec. 245(3), 509-518 (1996).

334. Zhu X, et al,. trp, a novel mammalian gene family essential for agonist-activated capacitative Ca2+ entry. Cell 90(1), 9-12 (1996)

335. Zu K, et al,. Enhanced selenium effect on growth arrest by BiP/GRP78 knockdown in p53-null human prostate cancer cells. Oncogene 25(4), 546-554 (2006)

336. Zamzani N and Kroemer G. The mitochondrion in apoptosis: how Pandora's box opens. Nat. Rev. Mol. Cell Biol. 2(1) 67-71 (2001)

337. Zuber M, Simpson E, Hall P and Waterman M. Effects of adrenocorticotropin on 17 alpha-hydroxylase activity and cytochrome P-450(17 alpha) synthesis in bovine adrenocortical cells. J. Biol. Chem. 260(3), 1842-1848 (1985)

338. Zylinska L, Kowalska I and Ferenc B. Calmodulin effects on steroids-regulated plasma membrane calcium pump activity. Cell Biochem. Funct. 27(2), 111-117 (2009).